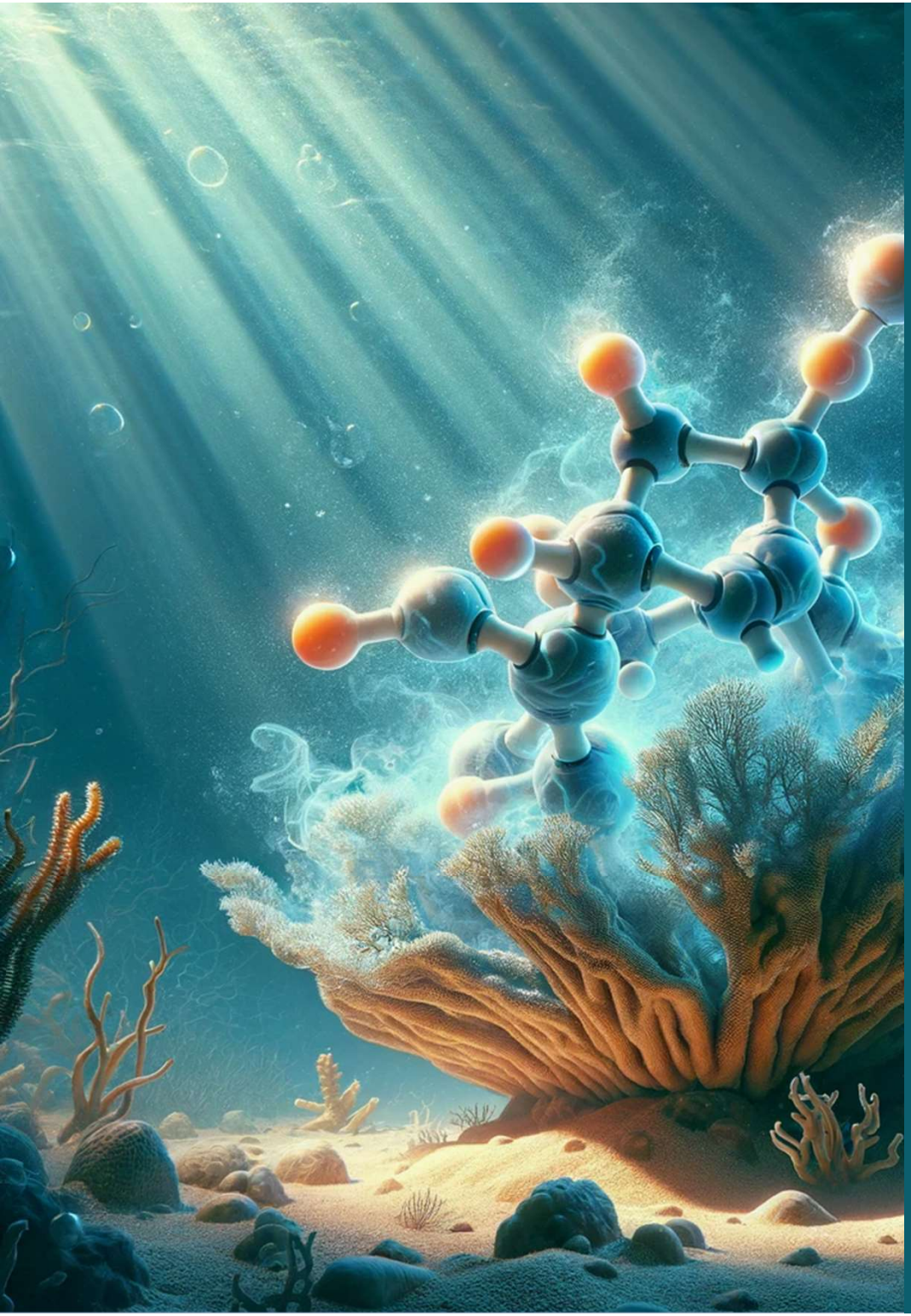

Cristina Porras Alcalá

Synthesis of new bengamide analogues and encapsulation into thermo-responsive magnetic nanoparticles

TESIS DOCTORAL

Año 2024

Universidad de Málaga

Programa de Doctorado en Química y Tecnologías Químicas, Materiales y Nanotecnología

TESIS DOCTORAL
2024

Synthesis of new bengamide analogues and encapsulation into thermo-responsive magnetic nanoparticles

Cristina Porras Alcalá

Directores:
Juan Manuel López Romero
Francisco Sarabia García

UNIVERSIDAD DE MÁLAGA

FACULTAD DE CIENCIAS

DEPARTAMENTO DE QUÍMICA ORGÁNICA

Programa de Doctorado en Química y Tecnologías Químicas. Materiales y Nanotecnología

TESIS DOCTORAL

Synthesis of new bengamide analogues and encapsulation into thermo-responsive magnetic nanoparticles

Memoria para optar al grado de

Doctor

(Mención Internacional)

por la Universidad de Málaga,

que presenta en 2024

Cristina Porras Alcalá

dirigida por

Prof. Dr. Juan Manuel López Romero

Prof. Dr. Francisco Sarabia García

UNIVERSIDAD DE MÁLAGA

AUTORA: Cristina Porras Alcalá

https://orcid.org/0000-0002-8332-8882

EDITA: Publicaciones y Divulgación Científica. Universidad de Málaga

DECLARACIÓN DE AUTORÍA Y ORIGINALIDAD DE LA TESIS PRESENTADA PARA OBTENER EL TÍTULO DE DOCTOR

Dña **Cristina Porras Alcalá**, estudiante del programa de doctorado en **Química y Tecnologías Químicas, Materiales y Nanotecnología** de la Universidad de Málaga, autor de la Tesis Doctoral presentada para la obtención del título de Doctor por la Universidad de Málaga y titulada: "**Synthesis of new bengamide analogues and encapsulation into thermo-responsive magnetic nanoparticles**". Dicha Tesis Doctoral ha sido realizada bajo la tutorización del Profesor Dr. **Juan Manuel López Romero** y dirección de los Profesores Dr. **Juan Manuel López Romero** y Dr. **Francisco Sarabia García.**

Declaro que:

La Tesis Doctoral presentada es una obra original que no infringe los derechos de propiedad intelectual, ni los derechos de propiedad industrial u otros, conforme al ordenamiento jurídico vigente (Real Decreto Legislativo 1/1996, de 12 de abril, por el que se aprueba el texto refundido de la Ley de Propiedad Intelectual, regularizando, aclarando y armonizando las disposiciones legales vigentes sobre la materia), modificado por la Ley 2/2019, de 1 de marzo. Igualmente asumo, ante a la Universidad de Málaga y ante cualquier otra instancia, la responsabilidad que pudiera derivarse en caso de plagio de contenidos en la Tesis presentada, conforme al ordenamiento jurídico vigente.

En Málaga, a 23 de Diciembre de 2023

Fdo.: **Cristina Porras Alcalá** Doctoranda	Fdo.: **Juan Manuel López Romero** Tutor
Fdo.: **Juan Manuel López Romero** y **Francisco Sarabia García** Directores de tesis	

Prof. Dr. **Juan Manuel López Romero** y Prof. Dr. **Francisco Sarabia García**, ambos Profesores Catedráticos de Universidad del Departamento de Química Orgánica de la Universidad de Málaga.

Certifican:

Que la memoria presentada por **Cristina Porras Alcalá** bajo el título "**Synthesis of new bengamide analogues and encapsulation into thermo-responsive magnetic nanoparticles**" para optar al título de Doctor en Ciencias Químicas por la Universidad de Málaga, ha sido realizada bajo nuestra dirección en los laboratorios del Departamento de Química Orgánica.

Considerando que constituye una investigación de alta calidad en el campo de la Química Fundamental, se autoriza mediante este escrito su presentación y defensa como Tesis Doctoral en la Facultad de Ciencias de la Universidad de Málaga.

Y para que así conste, firman el presente documento en Málaga a 23 de Diciembre de 2023.

Fdo.: **Juan Manuel López Romero** Fdo.: **Francisco Sarabia García**

D. **Juan Manuel López Romero** y D. **Francisco Sarabia García**, ambos como Profesores Titulares del Departamento de Química Orgánica de la Universidad de Málaga y directores de la tesis doctoral de **Cristina Porras Alcalá** bajo el título "**Synthesis of new bengamide analogues and encapsulation into thermo-responsive magnetic nanoparticles**" para optar al título de Doctor en Ciencias Químicas por la Universidad de Málaga.

Certifican:

Que los artículos que avalan la Tesis Doctoral de **Cristina Porras Alcalá**:

García-Pinel, B., **Porras-Alcalá, C**., Ortega-Rodríguez, A., Sarabia, F., Prados, J., Melguizo, C., & López-Romero, J. M. (2019). *Lipid-based nanoparticles: application and recent advances in cancer treatment.* Nanomaterials 2019, *9*(4), 638. 638; **https://doi.org/10.3390/nano9040638**

García-Pinel, B.; **Porras-Alcalá, C**.; Cabeza, L.; Ortiz, R.; Prados, J.; Melguizo, C.; Cheng-Sánchez, I.; López-Romero, J.M.; Sarabia, F. *Bengamide Analogues Show A Potent Antitumor Activity against Colon Cancer Cells: A Preliminary Study*. Mar. Drugs 2020, 18, 240. **https://doi.org/10.3390/md18050240**

Ortigosa-Palomo, A.; **Porras-Alcalá, C.**; Quiñonero, F.; Moya-Utrera, F.; Ortiz, R.; López-Romero, J. M.; Melguizo, C.; Sarabia, F.; Prados, J. *Antitumor Activity of Bengamide ii in a Panel of Human and Murine Tumor Cell Lines: In Vitro and in Vivo Determination of Effectiveness against Lung Cancer***.** Biomedicine & Pharmacotherapy 2023, 168, 115789**. https://doi.org/10.1016/j.biopha.2023.115789**

Porras-Alcalá, C.; Moya-Utrera, F.; García-Castro, M.; Sánchez-Ruiz, A.; López-Romero, J.M.; Pino-González, M.S.; Díaz-Morilla, A.; Kitamura, S.; Wolan, D.W.; Prados, J.; et al. *The Development of the Bengamides as New Antibiotics against Drug-Resistant Bacteria. Mar. Drugs* 2022, *20*, 373. **https://doi.org/10.3390/md20060373**

no han sido utilizados en Tesis Doctorales anteriores, ni serán utilizados en ocasiones venideras con el mismo fin.

Y para que así conste, firman el presente documento en Málaga a 23 de diciembre de 2023.

Fdo.: **Juan Manuel López Romero**

Fdo.: **Francisco Sarabia García**

Agradecimientos

Esta Tesis Doctoral ha sido fruto de mucha entrega, dedicación, paciencia y, sobre todo, ayuda recibida por parte de muchas personas, a las que quiero agradecer a continuación.

En primer lugar, quiero agradecer a mis directores de Tesis Doctoral, el **Prof. Dr. Manuel López Romero** y el **Prof. Dr. Francisco Sarabia García**, gracias por toda vuestra ayuda y por ofrecerme la oportunidad de iniciarme en el mundo de la investigación, en el que hoy tengo más claro que nunca que quiero seguir formando parte de él.

Gracias a todos los profesores del departamento de Química Orgánica de la Universidad de Málaga, en especial a las profesoras **Marisol**, **María**, **Amelia** y **Yolanda**. Gracias por vuestra comprensión y por escucharme, sois inspiración.

Gracias a todos aquellos compañeros de departamento y de laboratorio (**Iván**, **Ana, Cris**, y **Tina**) que durante este proceso han mostrado un apoyo incondicional hacia mí. Gracias de corazón.

Gracias a todos los estudiantes de grado que han estado en el laboratorio (**Raúl**, **Marcos**, **Alicia** y **Laura**) enseñándome a enseñar y motivándome a seguir trabajando día a día. En especial, a **Julia**, gracias por escucharme cuando más lo necesitaba, por confiar en mí y por empujarme a acabar este gran proyecto.

Gracias a mis amigos, a aquellos que no tienen nada que ver con el mundo de la química (**Alberto**, **Elena**, **María**, **Cristi**, **Bea** e **Irene**). Gracias por tantos momentos de risa cuando más lo necesitaba.

En mi última etapa de laboratorio, quizá la más dura, no puedo dejar de agradecer a mis chicas del fondo (**Yasmin**, **Desi**, **Irene** y **Esther**), no sé ni cómo agradeceros todo vuestro apoyo ese último año. Gracias por hacer que me sienta acompañada y valorada. Os deseo lo mejor en vuestro futuro.

Y en esta etapa de escritura no puedo olvidarme de mis compañeros de Villapharma (**Isrra**, **Sebas**, **Miriam**, **María**, **Cande** y **Otti**) por estos últimos meses en los que no habéis dejado de preguntarme por la Tesis. En especial a mis compañeros del S5N (**Ana**, **Lel**, **Adri** y **Anderson**) no sabéis lo afortunada que me siento de trabajar cada día a vuestro lado, hacéis que la ciencia sea divertida, muchas gracias por aguantar que hablase una y otra vez de mi libro, que finalmente aquí lo tenéis entre manos. Gracias a **Ana**, por aconsejarme y escucharme, eres la mejor compi de lab que jamás he podido tener. Gracias a mi queridísimo junior, **José Mari**, por transmitirme esa pasión por la investigación, ayudarme a creer en mí misma y motivarme para seguir en este mundo de síntesis muchos años más. Por último, gracias a mi senior **Dr. Mourad Daoubi Khamlichi**, por confiar en mí, por enseñarme tantísima química y, lo más importante, enseñarme a disfrutar de mi trabajo cada día.

A **Emi**, mi compañero de vida, gracias por estar estos años a mi lado, en los buenos y malos momentos. Gracias por tus dotes informáticas, por estar ahí para escucharme, animarme e impulsarme a cumplir mis sueños, sin ti hubiese sido imposible.

A mi hermana, **Paloma**, por enseñarme a relativizar, por enseñarme lo que verdaderamente es importante en la vida. Gracias por tu apoyo y comprensión.

A mi padre, **Manolo**, por ser la persona que más ha creído en mi durante todo este proceso. Gracias por estar a mi lado cuando más lo necesitaba, por animarme y escucharme.

A mi madre, **María José**, por ayudarme en la etapa más difícil de mi vida. Gracias, mamá, por enseñarme a priorizar mi salud mental, eres todo un ejemplo a seguir. Gracias por enseñarme que todo tiene solución en esta vida, a luchar por lo que quiero y a descansar cuando lo necesito. Te quiero muchísimo.

A Araceli

Table of contents

Abstract

The synthesis of bioactive compounds inspired by natural products represents an important and valid strategy for the development of new drugs. Thus, here we study the synthesis and development of bioactive compounds based on natural products, which may constitute promising agents for cancer treatment. Specifically, this research is focused on the family of the bengamides, which are antitumoral natural products isolated from the *Jaspidae* sponge. Additionally, bengamides occupy a preference position in pharmaceutical research based on their broad spectrum of biological activities, including antitumor, antibiotic and anthelmintics, being particularly important their antiproliferative properties. Interestingly, the antiproliferative activities of these compounds are due to an interaction between the bengamides and methionine aminopeptidase (MetAPs) which is an enzyme involved in the growth of the tumour. Thus, here is studied a structure-activity relationship (SAR) to identify analogues with more potent antitumoral activity as well as improved pharmacological properties such as the solubility in water and selectivity.

On the other hand, this research work is also focused on the nanomedicine field due to benefits nanoparticles may provide small size which allows to enter the tumour, the ease of functionalization in such a way that the nanoparticles could respond to an external or internal stimulation, which become a delivery system more selective and the biocompatibility. Thus, among all kind of nanoparticles, this Thesis is focused on a thermoresponsive magnetic nanoparticles to increase the selectivity of the drugs to the target.

Finally, to combine and unify the two fields of knowledge corresponding to Organic Synthesis and Nanomedicine, different drugs have been encapsulated into the nanosystem and biologically studied.

***Key words**: natural product, antitumoral, bengamide, analogue, synthesis, pNIPAM nanoparticle, magnetic nanoparticle.*

Resumen

La síntesis de compuestos bioactivos inspirados en productos naturales representa una estrategia importante y válida para el desarrollo de nuevos fármacos. Así, esta Tesis Doctoral estudia la síntesis y desarrollo de productos naturales bioactivos, los cuales son un prometedor tratamiento del cáncer. En concreto, esta investigación se centra en la familia de las bengamidas, productos naturales antitumorales extraídos de la esponja *Jaspidae*. Además, las bengamidas ocupan un lugar preferente en la investigación farmacéutica debido a la propiedades antitumorales, antibióticas y antihelmínticas que presentan, siendo particularmente importantes sus propiedades antiproliferativas. Así, la actividad de estos compuestos se debe a la interacción de la bengamida y la metionina aminopeptidasa (MetAPs), que es una enzima implicada en el crecimiento del tumor. Así, aquí se estudia una relación estructura-actividad (SAR) con el objetico de incrementar la actividad antitumoral de estos compuestos, así como la solubilidad en agua.

Por otro lado, este trabajo de investigación también está enfocado al campo de la nanomedicina debido a las características generales que presentan las nanopartículas: pequeño tamaño que permite la entrada al tumor, la facilidad de funcionalización de estas de manera que las nanopartículas puedan responder a un estimulación externa o interna que se convierten en un sistema de entrega más selectivo y la biocompatibilidad. Así, entre todo tipo de nanopartículas, esta Tesis se centra en nanopartículas magnéticas termosensibles para aumentar la selectividad de los fármacos hacia la enzima diana.

Finalmente, para unir los dos campos de conocimiento, la síntesis orgánica y la nanomedicina, se han encapsulado en el nanosistema y estudiado biológicamente diferentes fármacos.

***Palabras claves**: producto natural, antitumoral, bengamida, análogo, síntesis, pNIPAM y nanopartícula magnética.*

List of Abbreviations

A

AA	Acrylic Acid
Ac	acetyl
Al	Allylamine
aq	Aqueous

B

3-BA	3-Butenoic Acid
BAIB	(Diacetoxy)iodobencene
Bn	Benzyl
BOP	(Benzotriazol-1-yloxytris(dimethylamino)phosphonium hexafluorophosphate)
Bu	Butyl

C

^{o}C	Degree Celsius
^{13}C NMR	Carbon nuclear magnetic resonance
CRC	Colorectal Cancer
CTC	2-Chlrotrityl chloride
CSA	Camphorsulfonic acid

D

δ	NMR chemical shift in parts per million
DBU	1,8-Diazabicyclo[5.4.0]undec-7-ene
DCM	Dichloromethane
D-(-)DET	Diethyl D-Tartrate
DIBAL-H	Diisobutylaluminium hydride

DIC	*N,N'*-diisopropylcarbodiimide
DIPEA	Diisopropyl ethyl amine
DMAP	4-Dimethylaminopyridine
DMF	Dimethylformamide
DMSO	Dimethyl sulfoxide

E

EDC	1-Ethyl-3-(3-dimethylaminopropyl)carbodiimide
equiv	Equivalent
Et	Ethyl

F

FDA	Food and Drug Administration
FITC	Fluorescein isothiocyanate
5-Fu	5-Fluorouracil

G

g	Gram (s)

H

h	Hour (s)
^{1}H NMR	Proton nuclear magnetic resonance
HOBt	Hydroxybenzotriazole
Hz	Hertz

I

IC_{50}	Half maximal inhibitory concentration

J

J	Coupling constant

L

L	Liter
LHMDS	Lithium bis(trimethylsilyl)amide

M

m	Multiplet
µ	Micro
m-CPBA	meta-Chloroperoxybenzoic acid
MDR	Multiple Drug Resistence
MHz	Megahertz
min	Minute(s)
mol	Mol(s)

N

NaHMDS	Sodium bis(trimethylsilyl)amide
NMR	Nuclear magnetic resonance

O

OXA	Oxaliplatin

P

pNIPAM	Poly(N-isopropylacrylamide)
ppm	Parts per million
pyr	Pyridine
pTSA	p-Toluenesulfonic acid

Q

q	Quartet

R

Rf	Retention factor

S

S	Singlet
SAE	Sharpless asymmetric epoxidation

T

t	Triplet
TBAF	Tetrabutylammonium fluorite
TBDS	*Tert*-butyldimethylsilyl
TBHP	*Tert*-butylhydroperoxide
TEA	Triethylamine
TEM	Transmission electron microscopy
TEMPO	2,2,6,6-Tetramethyl-1-pyperidimeiloxy
TFA	Triflouroacetic acid
THF	Tetrahydrofuran

CHAPTER 1. INTRODUCTION

1.1. A novel family of active natural products isolated from a marine origin: the bengamides family

1.1.1. The importance of the search for new anticancer treatments

After cardiovascular diseases, cancer is the most common cause of death in the developed world. Cause of this terrible fact, the synthesis of new drugs against this disease is an urgent line of research. Specifically, Colorectal Cancer (CRC) is the third most common cancer worldwide[1] Moreover, this disease increased its incidence over the last year as result of the population aging, sedentary lifestyle, and nutrition.[2]

During the last years, different therapies have been developed for the cancer treatment such as CRC chemotherapy (colorectal cancer treatment) which is essentially based on 5-fluorouracil (5-FU), oxaliplatin (OXA) and irinotecan (IRI). Furthermore, a combined therapy of the above-mentioned drugs is commonly used as a first-line treatment because provides a better progression-free survival data compared to monotherapy. Additionally, monoclonal antibodies and multi-kinase inhibitors have been recently introduced in CRC treatment (cetuximab, panitumumab, bevacizumab).[3,4] However, all these treatments result in several side effects. Moreover, it is important to mention that colorectal cancer has moved from fourth place among cancers with the highest mortality to second place after lung cancer.[5] Due to the increase in the mortality rate, side effects of the current treatments and drug resistance make the development of new strategies an urgent and priority need.

In this search, many natural products have been explored as new anticancer drugs to avoid the side effects of the conventional therapies. A relevant example of bioactive natural product is taxol, which is used in the treatment of breast, ovarian non-small cell cancer and Kaposi's sarcoma.[6] Among all these compounds, the bengamides, which are a family of natural products isolated from marine origin, were discovered and emerged as promising anticancer compounds in virtue of their impressive

antitumoral activities and intriguing biological mechanism of action. These compounds are featured by the inhibition of the angiogenic process through their inhibition of the enzymes methionine aminopeptidases. In this context, here we explore the potential of these compounds for the treatment of cancer.

1.1.2. The Jaspidae family sponge: an interesting source of bioactive compounds

The bengamides are isolated from the *Jaspisdae* family sponges. This class of sponges has been mainly collected from the Indian Ocean and has provided a wide array of natural compounds in terms of structural diversity and biological properties. Among all these compounds, three classes of natural products stand out over the rest: the bengamides,[7] the bengazoles[8] and the jaspamides[9] (**Figure 1**).

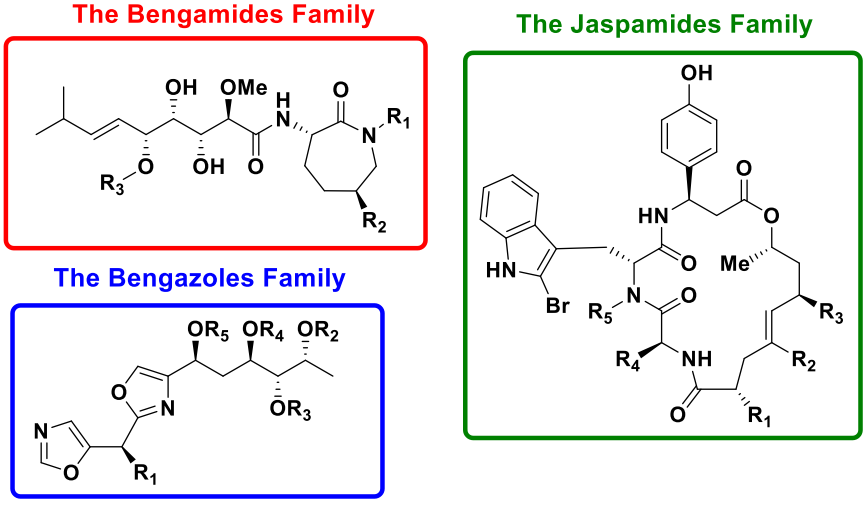

Figure 1. Natural products isolated from the *Jaspidae* family.

In addition to these compounds, others natural products were isolated from the *Jaspidae* sp. with interesting biological properties such as diketopiperazines,[9] the jaspiferals[10] and the stelliferins[11] as well as much more others which are summarized in **Table 1**.

Table 1. Summary of metabolites from Jaspis sponges.

Taxonomic Identification	Collection Site	Isolated Compounds
Jaspis cf. coriacea	Fiji Island, Solomon Island, Papua, New Guinea, Indonesia	Jasplakinolide11a, Bengamides A-F, Isobengamide E, Bengazoles A and B[b] Diketopiperazine cyclo (*L*-*trans*(4-hydroxyprolinyl)-*L*-Phe) and *N*-acetyl-*L*-phynylalanine,[12] Bengamides M-R[13c]
Jaspis carteri	New Caledonia	Bengamides A-B, G-J, K[14]
Jaspis digonoxea	Indo-Pacific region, South Africa	Digonazole[15]
Jaspis stellifera	Okinawa	Jaspiferals A-G,[10] Stellifer-ins A-F[11d]
Jaspis splendans	Vanuatu Islands	Jaspamides B-C,[13,a] Jaspamides B-G,[16] Jaspamides H-L,[9,a] Jaspamides M-P[16,a]
Jaspis cf. johnstoni	Fiji Island	Jaspamide,[17,a] Toyokamycin, 5-(Methoxycarbonyl)tubercidin
Jaspis sp.	Northern Great Barrier Reef	Bengazoles A-G and B[18,b]
Jaspis sp.	Okinawa	Jaspisamides A-C[19]
Jaspis sp.	Izu Peninsula	3,4-Dihydroxystyrene *E* and *Z*; (*E*) and (*Z*)-narains[20]
Jaspis sp.	Okino-shima Island	Isojaspisin[21]
Jaspis sp.	Indo-Pacific region	Bengazoles A-B, C-G[22,b]
Jaspis sp.	Djibouti (Red Sea, Gull of Aden)	Jaspines A-B[23,e]

[a]Jaspamides have been also isolated from the marine *Cymbastela* sp.[24]
[b]Bengazoles Z, C-4 and C-6 were additionally isolated from the sponge *Stelleta* sp.[25]
[c]Bengamides E, E' and F' were found in *Myxococcus virescens*,[26] bengamides A, F, N and Y from the sponge *Stelleta* sp. [25] and bengamide L from *Pachastrissa*[27]
[d]Stelliferins J-N were also isolated from marine sponges from Okinawan *Rhabdastrella* cf. *globostellata*,[28] *Stellata globostellata*[29] and *Geodia globostellifera*[30]
[e]Jaspines were also described from *Pachastrissa* sp.[31]

1.1.3. The bengamides: structure and classification

All over these natural products collected from the *Jaspidae sponges*, the bengamides family stand out over the rest due to their interesting biological activity. The general structure of these natural products is characterized by the presence of a side chain with 10 carbon atoms which contains three hydroxyl groups, a methoxyl group and a disubstituted olefin with a configuration *trans.* Moreover, this C-10 side chain is linked through an amide group with a caprolactam ring. The bengamides are classified according to the different side chains as well as the caprolactam ring (**Figure 2**).

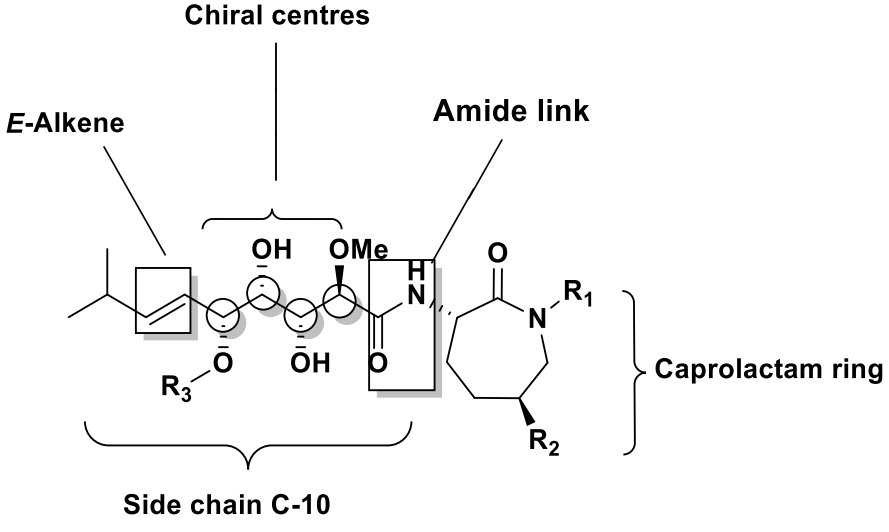

Figure 2. General structure of the bengamides.

The bengamides have been classified in two structural classes: **type I** with a caprolactam ring derived from hydroxylysine, containing or not a lipidic chain linked with this caprolactam ring (bengamides A-D (**1**-**4**), G-J (**7**-**10**), L-O (**12**-**15**), Y (**19**), Z (**20**)) and **type II** with a caprolactam ring derived from lysine (bengamides E (**5**) , F (**6**),E' (**22**), F' (**23**) , P-R (**16**-**18**)) (**Figure 3**).

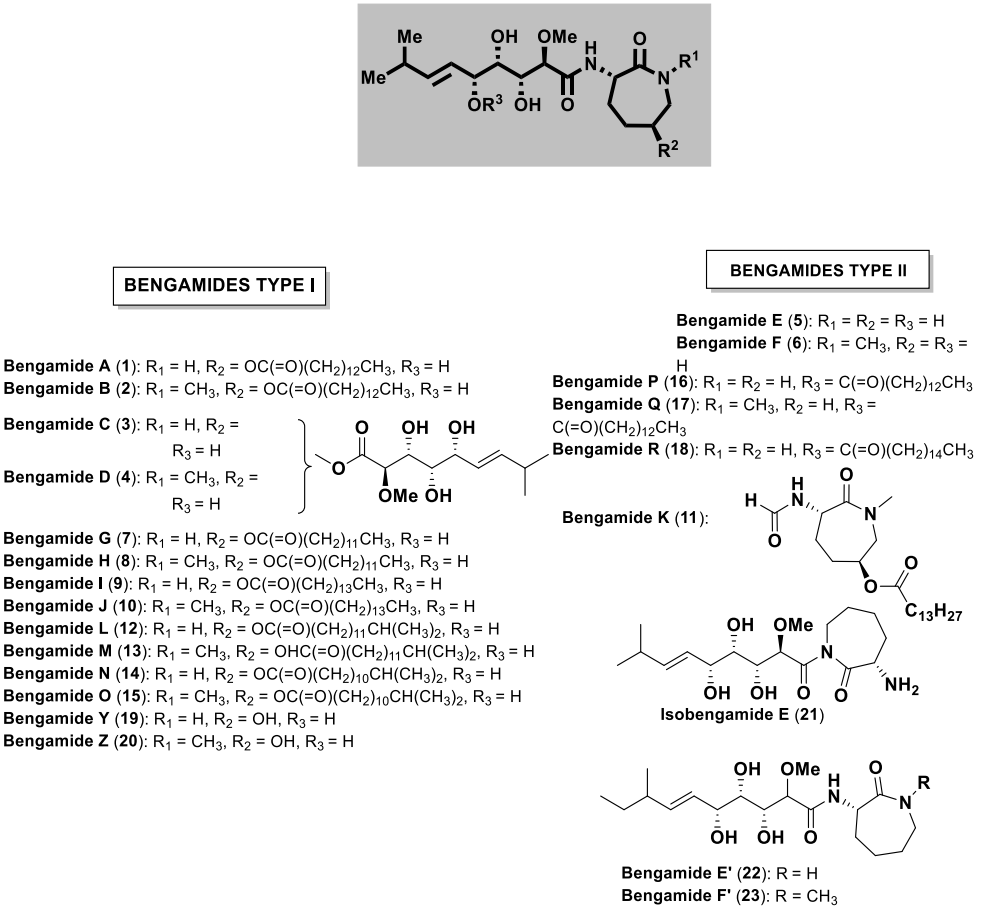

Figure 3. Structural classification of the bengamides: type I and type II.

The isolation and structural determination of these compounds was a long process as will be explained bellow. The first members discovered were the bengamides A-F (**1**-**6**) by the research group of Professor Crews (California University, USA) in 1989 from an orange sponge belonging to the *Jaspidae* family which was collected in Began Lagoon (Fiji Islands).[12]

A spectroscopic analysis allowed to Crews *et al.* to determine the structure of the principal components from that crude, corresponding to the bengamides A (**1**) and B (**2**).

A third compound (bengamide C (**3**)) was also identified from the extracted crude. However, the structural elucidation was not possible due to the low purity with which was obtained. Two years later, Crews *et al.* collected a large amount of this marine sponge and was possible to characterize bengamides C-F (**3**-**6**), together with an isomeric product (isobengamide E (**21**)) and different oxazoles denominated bengazoles.[12,32]

After these discoveries, bengamides A (**1**) and B (**2**) were isolated and identified by D'Auria *et al*. from the purified and analysed extracts of the *Jaspis Carteri* sponge which were collected in New Caledonia, together with a range of new bengamides members G-J (**7**-**10**) and truncated derived bengamide K (**11**).[14] In 1999, Groweiss *et al.*[8] isolated from a specie *Jaspis sp*. two new members of bengamides: bengamide Y (**19**) and bengamide Z (**20**), the non-acetylated bengamide B (**2**). In this year, Letourneu *et al.*[27] isolated from *Pachastrissa sp*. bengamide L (**12**), together with different new members of bengazoles. More recently, in 2001, *Crews et al*. discovered six new bengamide members: the bengamides M-R (**13**-**18**) in addition to the known bengamides A (**1**), B (**2**), E(**5**), F (**6**), G (**7**), H (**8**), I (**9**), L (**12**), Y (**19**) and Z (**20**) (**Figure 3**) from a collection of *Jaspis cf. Coriácea.*[13]

The last contribution to this family of natural product was reported by Crews[26] in 2012, who identified bacterium *Myxococcus Virescens* as a new source of bengamide E (**5**), and two new members: bengamides E' (**22**) and F' (**23**). These two new products were isolated as a mixture of diastereoisomers. Furthermore, bengamide E' (**22**) was synthetized before the isolation from the natural source.[33] Finally, 23 members of the bengamide's family have been reported and their structures determinate by spectroscopic methods (**Figure 3**).

The structural determination of these products was carried out by Crews *et al.*,[34] as well as it was previously indicated. Thus, the establishment of the absolute stereochemistry was possible by ^{1}H-NMR spectroscopic studies of the (*R*)- and (*S*)-mandelate ester of lactone **24**, a product obtained during the isolation process. Those esters, compounds **26a** and **26b**, which were prepared by reaction of lactone **24** with O-methyl mandelic acid **25a** and **25b**, respectively, showed significant differences in their respective ^{1}H-NMR spectra, particularly in high-field chemical shifts of H-4, H-5, H-6 and H-7 and low-field chemical shift of H-2 and methoxy group for the *S* **26b** derivative compared to *R* **26a** (**Scheme 1**).

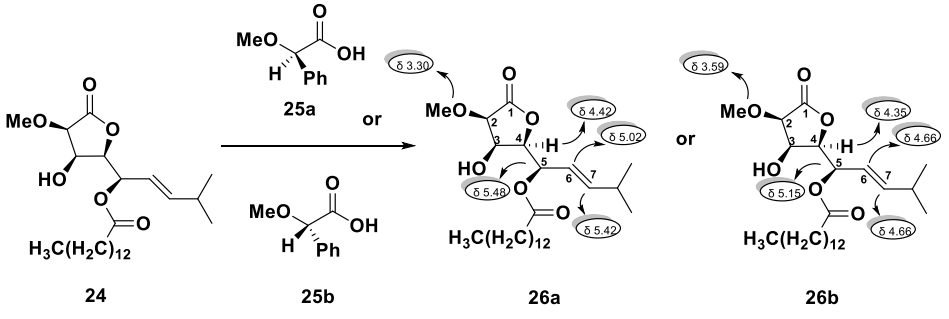

Scheme 1. Abasolute configurational determination of the bengamides.

The validation of this method was checked by the preparation of the corresponding (-)-menthol ester, with similar effects in the chemical shifts of the key protons (**Scheme 1**).[35]

Few years later, total synthesis of the bengamides A (**1**),[36] B (**2**)[37] and E (**5**)[38] confirmed the absolute configuration for the side chain C-10 and the caprolactam ring derived from hydroxylysine.

1.1.4. *The biosynthetic origin of the bengamides*

On the other hand, the biosynthetic origin of the bengamides seems to be a symbiotic interaction between the *Jaspidae* sp. sponge and bacteriums. In fact, the bengamide's structure contains a side chain C-10 with an isopropyl termination, which is characteristic of fat acid bacterium.[39]

Interestingly, the research carried out by Crews[26] and later by Brönstrup *et al.*[40] concluded that the natural origin of bengamides E (**5**), F (**6**), E' (**22**) and F' (**23**) was a result of interaction between the terrestrial myxobacteria *Myxococcus Virescens* and the natural source. Recently, bengamide R (**18**) was isolated and characterized from the *Jaspis Splendens* sponges together with new antimycobacterial agents.[41] Consequently, the structure of the bengamides could be a result of link between a diketide with *L*-leucine to establish the side chain and *L*-lysine cycled to form the amino ε-caprolactam (**Figure 4**).[12]

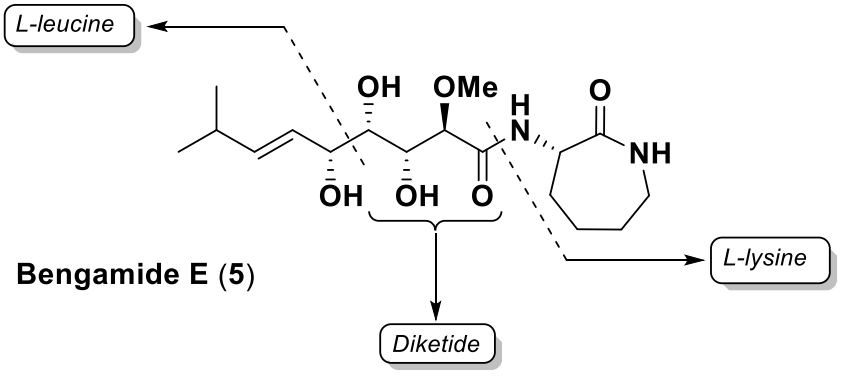

Figure 4. Proposal of the biosynthetic origin of the bengamides.

1.1.5. Biological properties of the bengamides

The bengamides display outstanding and prominent different biological properties, including antitumor, antibiotic, antifungal and antiviral activities.

Antitumor properties and mechanisms of action of the bengamides

Regarding to the antitumoral properties of these compounds, preliminary studies showed that they presented a cytotoxicity *in vitro* against larynx epithelial carcinoma at 1.0 μg/mL.[27] Later biological evaluations proved the potent antitumoral activity of different members of the bengamides family against different tumoral cells lines, with IC_{50} in a range between 10 to 100 mM.[13]

Further biological studies were accomplished and confirmed the interesting biological activities of the bengamides as new potent antitumoral drugs. Therefore, IC_{50} values of the natural bengamides A (**1**), B (**2**), E (**5**), F (**6**), M (**13**), O (**15**), P (**16**) and Z (**20**) related a high activity *in vivo* against MDA-MB-435 (human carcinoma). Furthermore, the highest activity was found in the bengamides which had a fatty acid linked to the caprolactam ring (bengamides A (**1**), B (**2**), M (**13**) and O (**15**)) (**Table 2**). Specifically, they were 100 times more potent than their analogues without esters (bengamides E (**5**), F (**6**), P (**16**) and Z (**20**)). Although these results indicated the importance of the lipophilic ester linked with the caprolactam ring for *in vitro* activity, *in vivo* studies showed minor differences regarding to the antitumoral activity due to possible water-solubility issues of these natural products.

Table 2. *In vitro* antitumoral activity of the bengamides against MDA-MB-435.

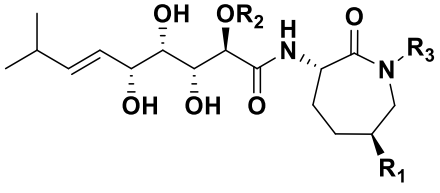

Bengamide	R_1	R_2	R_3	MDA-MB-435 IC_{50} [µM]
A (**1**)	$OCO(CH_2)_{12}CH_3$	H	H	0.001 ± 0.0006
B (**2**)	$OCO(CH_2)_{12}CH_3$	CH_3	H	0.012 ± 0.003
M (**13**)	$OCO(CH_2)_{11}CH(CH_3)_2$	CH_3	H	0.0101 ± 0.0021
O (**15**)	$OCO(CH_2)_{10}CH(CH_3)_2$	CH_3	H	0.00029 ± 0.0005
Z (**20**)	OH	CH_3	H	2.9 ± 1.5
E (**5**)	H	H	H	3.3 ± 1.2
F (**6**)	H	CH_3	H	2.9 ± 2.9
P (**16**)	H	H	$CO(CH_2)_{12}CH_3$	1.2 ± 7.9

In fact, it was demonstrated that bengamide B (**2**) was transformed intercellularly into bengamide Z (**20**), which suggested this last compound was the responsible of the antitumoral properties showed.[42] Thus, the different *in vivo* activities obtained for bengamide B (**2**) and Z (**20**) could be provided by the low absorption cellular of bengamide Z (**20**).

Among all the natural bengamides, bengamide B (**2**) showed the best NCI-60 profile, being comparable to traditional antitumoral agents. Furthermore, it was studied that bengamide B (**2**) was able to stop two phases of the cellular cycle, G1 phase and G2/M by FACS (Fluorescence-Activated Cell Sorting) analysis of normal and tumoral cells, respectively. Additionally, other biological experiments concluded that G1 phase stop was carried out through the blocking of G1/S which stopped in G2/M phase of the cellular cycle was not inhibited during the mitosis, it was during de cytokinesis.[13,43,44] All these biological studies suggested that the cytotoxicity exhibited by the bengamides was due to the inhibition of a new bilogical target.[45]

Towbin *et al.* in 2013 investigated the biological mechanism of these antitumoral compounds through extensive biological studies, which allowed to excluded biological target for the bengamides such as DNA, tubulins, actines, topoisomerases or proteases.[45]

On the other hand, proteomic studies in H1299 cells[45] detected an alteration in a subset of proteins (the isoforms 14-3-3) after a treatment *in vitro* with LAF389 **26**, which is a synthetic analogue of the bengamides more soluble in water than the natural congeners, showed potent inhibition of tumour growth *in vitro* as well as *in vivo.*[46] As a result, isoforms methionine aminopeptidases MetAP1 and MetAP2 were determined as the targets of the bengamides.

This last important finding promoted more research in the effect of analogue **26** in the proliferation of endothelia cells which was compared with the mechanism action of fumagillin (**28**) (**Figure 5**), a described

antitumoral agent which inhibit MetAP2.[47,48] These studies showed that **26** was less specific than fumagillin (**28**). Consequently, the toxicity of the bengamides was justified by the absence of selectivity for MetAPs isoforms.[45] However, biological studies with bengamides M (**13**) and O (**15**) exhibited a selectivity of 10 to 20 for the isoform MetAP1 against to MetAP2 (**Table 3**) giving rise to a favourable antitumoral profile for these compounds.[12,49]

Table 3. Enzymatic inhibition MetAPs of the bengamides.

Compound	MetAp1[IC_{50} (μM)]	MetAp2[IC_{50} (μM)]
Bengamide A (**1**)	1.9 ± 0.2	10.5 ± 3.8
Bengamide B (**2**)	29.3 ± 10.4	17.9 ± 7.9
Bengamide G (**7**)	26.8 ± 18.3	>50
Bengamide L (**12**)	37.1 ± 13.4	>50
Bengamide M (**13**)	5.4 ± 2.3	>50
Bengamide N (**14**)	40.2 ± 14.3	>50
Bengamide O (**15**)	2.7 ± 0.4	>50
Fumagillin (**28**)	NA	0.03
Ovalicin (**29**)	NA	0.0004

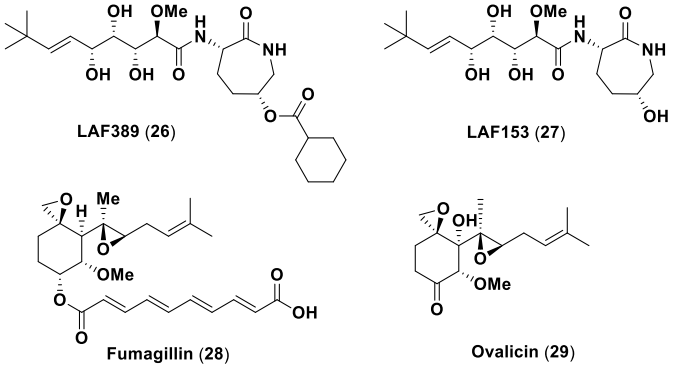

Figure 5. Inhibitors of MetAPs: bengamides analogues LAF389 and LAF153, fumagillin and ovalicin.

Once the enzyme MetAPs were identified as the targets of the bengamides, biological studies were focused on the mechanism of action of these natural products to understand the reason why this inhibition triggered into the blockage stopped of the antitumoral cells growth. It should be highlighted that due to the complexity of this mechanism of action, it is still being studied nowadays.

Firstly, it is important to know the bengamide's structure and the main function of methionine aminopeptidases enzymes to understand the Mechanism Of Action (MOA) of these natural products. Thus, these enzymes represent a kind of aminopeptidases which depend on a metal which can break the *N*-terminal methionine in peptides or proteins[50] both in a co-transitional and post-transitional way[51] playing an important role in the protein degradation process.[52]The removal of the terminal methionine by MetAPs is an important stage in maturation of proteins and it is essential to promote aminoterminal modifications.[52] In fact, this inhibition is relevant due to the involvement of MeAtP2 is involved in the tumoral growth.[53]

It is also important to have in mind that from a biomedical perspective, MetAP2 has been studied in more detailed than MetAP1 because of the discovery of MetAP2 as a biologic target of different antitumoral drugs, such as fumagillin (**28**) and ovalicin (**29**) together with their synthetic analogues and other synthetic molecules.[54] Despite of numerous studies about the role of MetAP2 in the develop of blood vessel, the exact role of this enzyme in the angiogenesis is not described yet.[55]

The identification of MetAPs as the molecular targets for the bengamides gave rise to an important research line in the synthesis of more selective analogues, which could help to understand the role of MetAPs in the cancer growth. As part of these studies, Torwin *et al.*[45] were able to describe the structure of MetAP2-bengamide complex by X-Ray analysis, revealing that **26** was not the real inhibitor, but the non-acylated derivate **27**. This enzyme-substrate structure contributed to understand the interaction

way of these antitumoral compounds in the active site of the methionine amino peptidases.[50]

Moreover, the analysis of the MetAP-bengamide complex allowed to obtain some important conclusions. Specifically, the hydrophobic pocket next to the active center, which contains the residues Phe-219, His-382 and Ala-414, interacted with the terminal alkyl group of *E*-olefin, which is present in the bengamides structure. On the other hand, the pocket 2 was constituted by the residues Leu-328, Phe-366 and His-231, which were exposed to the external medium and interacted with the caprolactam ring. Moreover, hydroxyl groups were coordinated with the cofactor metals resulting an octahedral geometric center (**Figure 6**)**.** The described inhibitors of MetAP2 fumagillin **28** and ovacilin **29** exhibited a different interaction in contrast to bengamides as they formed a covalent link by nucleophilic attack of the amine group of His-231 with an oxirane ring present in these molecules (**Figure 6**).[48]

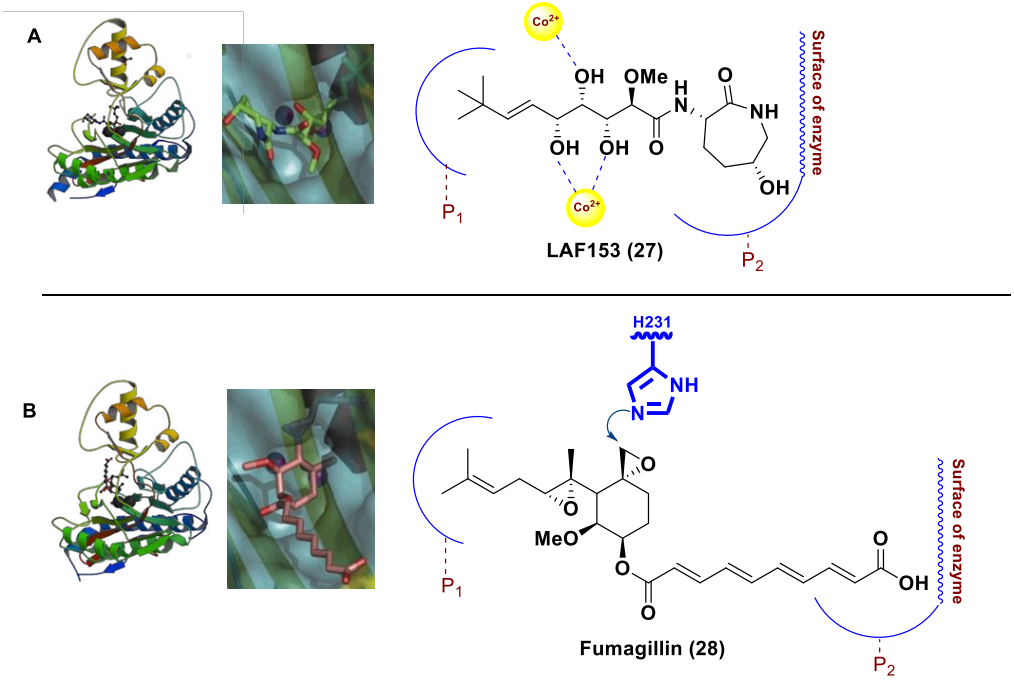

Figure 6. Crystal structures of the MetAp2-inhibitor complexes for LAF153 (PDB-YQYZ) and Fumagillin (PDB-1BOA) and interaction mode in the active site.[47]

Recently, in 2012, Ye *et al.* performed several studies about the role of the bengamides as inhibitors of MetAPs.[56] In particular, they described the X-Ray structures of four bengamide analogues (**30**-**33**) (**Figure 7**) in a complex with HsMetAP1 in the Mn (II) form, monitored in a similar way of link enzyme-substrate for these analogues regarding to the natural bengamides. The only difference respect to their natural congeners was the interaction with pocket 2, due to the structural differences at the caprolactam fragment. These four derivates exhibited IC_{50} values similar to the described inhibitors of HsMetAP1 in state Mn (II). Since all these products differ in the fragment of the caprolactam ring, this study suggested that the interaction between the active center and the alkyl terminal fragment and hydroxyl groups was more important than the interaction with the caprolactam ring. However, the activity *in vivo* changed when this caprolactam ring moiety was modified.

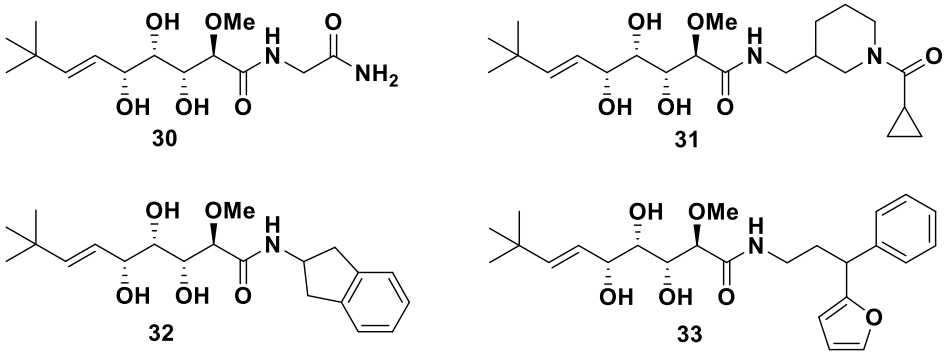

Figure 7. Molecular structures of **30-33** analogues.

In addition, enzymatic studies have showed that the inhibition of MetAP2 by siRNA did not disrupt the growth of endothelial cells.[57] In light of this study, the conclusion was that MetAP2 was not essential for the proliferation of endothelial cells and that this enzyme was not the target for the antiangiogenic effect exhibited by bengamides and fumagillins. However, co-crystalized with MetAP2 human could let to consider it as the target.[45,58] Thus, a possible reason which could explain these contradictory results could be that a new enzyme of the MetAPS family was present in

humans, which could be expressed in endothelial cells. Even so, the mayor part of experiments reinforces the idea of MetAP2 as an essential target.[58,59]

Recently, Crews *et al.* have discovered that the bengamides are able to inhibit nuclear factor Kapp B (NF-kB). [26] In this biologic study, it was demonstrated that the interaction between this enzyme and the necrosis factor Kappa B could explain the antitumoral activity of these natural products. In short, it is necessary more studies to get a conclusion.

Antibiotic properties of the bengamides

First studies about the antibiotic properties of these natural products were carried out by Crews *et al.*, who discovered that bengamides A (**1**) and B (**2**) exhibited antibiotic activity against *Streptococcus pyrogenes*.[60]

Interestingly, MetAps are present in eukaryotic as well as prokaryotic cells which indicates that they are essential for the bacteria.[61] Additionally, MetAps are homogeneous in the catalytic domain in the bacterias in contrast to mammalian cells which present an extension at the *N*-terminal extension. However, as this extension is not necessary for the enzyme activity in human, could be important for bacteria explaining the inhibition selectivity.[62]

Taking into consideration this, in 2011 Yet *et al.* confirmed that the bengamides could inhibit MetAps of *Mycobacterium tuberculosis*.[63] Additionally, they analysed the active site of mtMetAP1a and mtMetAp1b and it was described the active site of the enzyme as a pocket with hydrophobic environment where is located a divalent metal such as Mn (II), Fe (II), Co (II) or Ni (II). In this way, the difference between prokaryotic and eukaryotic cells is found outside of this pocket. So, the research of the reason why it was obtained more potent activities in bacteria than in mammalian become a new challenge.[64]

In this sense, Yet *et al.* designed seven different analogues of the bengamides with structural modifications at the caprolactam ring to increase the

antibiotic activity, which were evaluated as potent antibiotics agents (**50**-**56**) (**Figure 8**). [63]

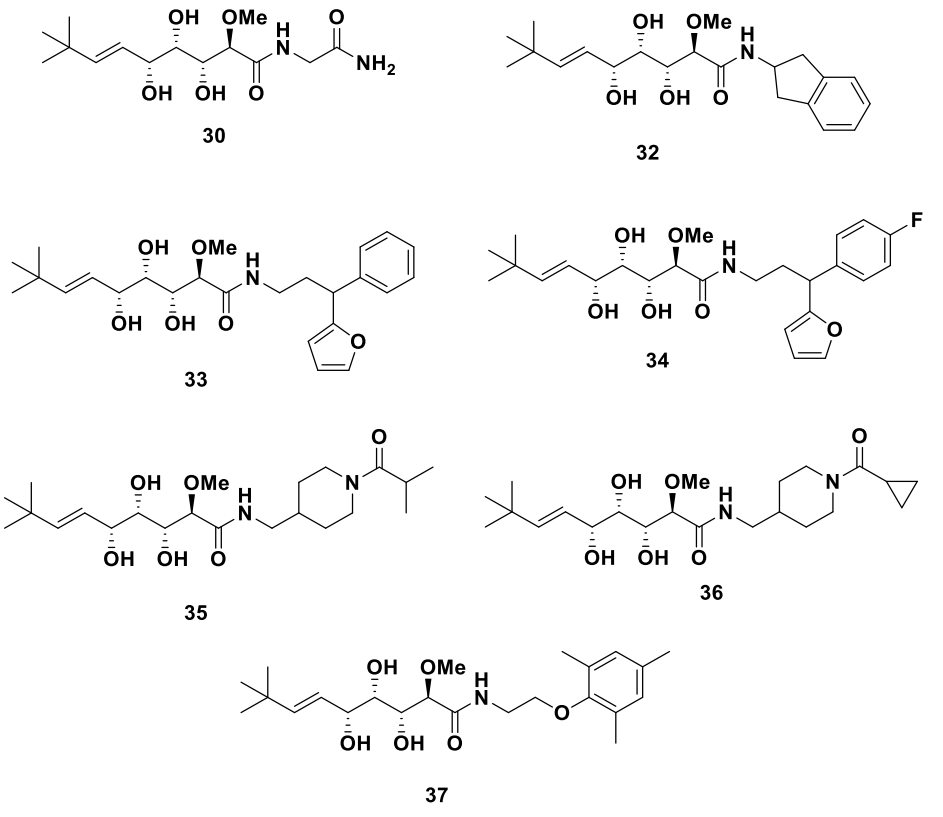

Figure 8. Molecular structures analogues of the bengamides **30** and **32-37** described by Yet *et al.*

Finally, this study showed that the interaction between the analogue inhibitor and the divalent metal ion was crucial for the antibiotic activity. **Table 4** shows that the most potent analogues were **30**, **32**, **35** and **36** due to the interaction of the aromatic rings present in these analogues and cofactors Co (II), Mn (II), Ni (II) and Fe (II).[63]

Table 4. Biological activities of the bengamide analogues **30–37** against *M. tuberculosis* and human K562 cells.

Bg	IC_{50} [μM] against MetAP1a[a]			M. tuberculosis MIC[μM][b]		K562 IC_{50} [μM][e]
	Co^{II}	Mn^{II}	Fe^{II}	MABA[c]	LORA[d]	
30	31	11	18	29%	28%	>333
32	6.0	11	5.5	15%	8%	79.6
33	8.1	12	6.7	48%	12%	96.5
34	45	68	67	0%	0%	>333
35	88	187	110	0%	0%	>333
36	21	49	14	122	0%	>333
37	7.9	6.9	4.5	50.6	107.4	37.8

[a]MtMetAP1a: MetAP of M. t*uberculosis* expressed in E. Coli and purified as apo-enzyme. [b]Minimum inhibitory concentration or percent inhibition at 128 μM (IC_{50}). [c]Microplate Alamar Blue assay against M. *Tuberculosis* strain $H_{37}Rv$ (replicating phenotype). [d] Low-oxygen recovery assay against M. *tuberculosis* strain $H_{37}Rv$-CA-lux AB (non- replicating persistent phenotype). [e] Human leukemia-derived cells.

In this study, the X-ray structures of the complexes of MtMetAP1 with **36** and **37** were described. Thus, the interaction between the triol system of these analogues with the metal ions by coordination was observed as well as the interaction between the *tert*-butyl alkene chain with the P1 pocket through a hydrophobic interaction.[56] Additionally, the antibiotic activity of **36** was associated with the interaction of the trimethylphenyl group with the shallow cavity opening in the enzyme, which resulted the most potent analogue against *M. tuberculosis*.

Besides, the effects of these new analogues in the growth of human K526 cells were evaluated to know if these antibiotic analogues were able to inhibit MetAPs in human enzyme resulting that **30**, **32**, **35** and **36** were cytotoxic. Through this study it was demonstrated the necessity of developing new analogues of the bengamides much more selective for the target.

In the search of more selective analogues, Yu *et al.* achieved an extensive screening to identify new leads against M. *tuberculosis*.[65] Thus, in this study, 11 extracts from the *Porifera phylum* and 5 from the *Chordata phylum* were evaluated, detecting MIC_{50} in a range of 50-0.39 μg/mL. Among all these extracts, it highlighted a MIC_{50} of 0.39 and 1.56 μg/mL. From this extract was isolated bengamide B (**2**), being this natural product the responsible of the antitubercular activity of the extract. The cytotoxicity of the bengamides against different human cells was studied resulting positive values. Moreover, bengamide B (**2**) was employed in a therapeutic treatment against *M. Tuberculosis* together with rifampicin which showed a strong synergy.

All these promising results gave rise to design new analogues which possess more antitubercular activity, and less cytotoxicity as will be explain in Chapter 3 (synthesis of new analogues of bengamides).

Antifungal properties of the bengamides

The antifungal activity of the bengamides was first studied against *Candida albicans* and *Saccharomyces braziliensis*m, but it resulted inactive.[60]

In 2015, Molinski *et al*.[66,67] carried out a research about the antifungal activity of bengazoles A-G (**1**-**7**) (**Figure 9**), natural compounds which are isolated from the marine sponge *Jaspis sp*. as well as the bengamides, against *Candida* spp. and how the presence of bengamide A (**1**) could influence this activity. To understand the Mechanism Of Action (MOA) of these antifungal compounds, the bengazoles were compared with already described antifungal azoles due to the similar structure of them. Furthermore, it was suggested that the MOA of the bengazoles could be similar of these azoles: the inhibition of 14 α-demethylase, which is an enzyme involved in the biosynthesis of Ergosterol. Thus, this study was set out with the isolation of bengazol A (**56**) from an extract of *Jaspis* sp. After obtaining a pure fraction of bengazol A (**56**) the MOA was compared with already described azoles to know if it could inhibit the biosynthesis

of Ergesterol. The result of this study revealed that there was an antifungal activity, however there was not change in the concentration of Ergosterol. Then, it was possible to concluded that the MOA of the bengazoles and the azoles was different. After this result, the influence of bengamide A (**1**) in the antifungal activity of bengazoles A-G (**38**-**44**) was studied keeping constant the amount of these bengazoles and changing the loading of bengamide A. They concluded that in a ratio of 1:400 (bengazoles A-G: bengamide A) the antifungal activity of bengazoles was no detected. Them, when the concentration of bengamide A (**1**) was lower, a dose-dependent behaviour was observed, finding in a ratio 2:1 (bengamide A:bengazoles) that the zone of inhibition increased a 50%, which confirmed a synergistic activity of the bengazoles and bengamide A (**1**) (**Figure 9**).

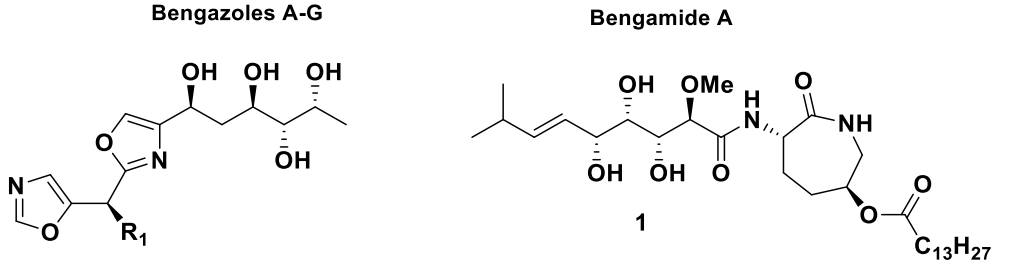

A (**38**): $R_1 = C(=O)(CH_2)_{12}CH_3$
B (**39**): $R_1 = C(=O)(CH_2)_{11}CH(CH_3)_2$ iso
$R_1 = C(=O)(CH_2)_{01}CH(CH_3)CH_2CH_3$ anteiso
C (**40**): $R_1 = C(=O)(CH_2)_{12}CH_3$
D (**41**): $R_1 = C(=O)(CH_2)_{10}CH(CH_3)_2$
E (**42**): $R_1 = C(=O)(CH_2)_{13}CH_3$
F (**43**): $R_1 = C(=O)(CH_2)_{11}CH(CH_3)CH_2CH_3$
G (**44**): $R_1 = C(=O)(CH_2)_{14}CH_3$

Figure 9. Molecular structures of bengazoles A-G (**38-44**) and bengamide A (**1**).

Antiviral properties of the bengamides

More recently, Brockman *et al.* demonstrated the role of bengamide A (**1**) as a new potent antiviral by the inhibition of the NF-kB-dependent HIV (Human Immunodeficiency Virus)-1 replication.[66,68] This study revealed that the antiviral activity was around EC_{50} 15 nm which was comparable to the activity of known antiviral agents such as indinavir, efavirenz and raltegravir. The study of the mechanism of action of bengamide A (**1**) as antiviral is still in progress.

1.2. Nanoparticles as a controlled drug delivery system

1.2.1. *Nanomedicine: the importance of the nanoparticles in the cancer treatment*

Nanotechnology is the science which is focused on the development and application of new devices or systems in the nanoscale, which includes a size between 1 to 1000 nm scale.[69] This science is multidisciplinary, including physics, chemistry, material science, manufacturing and engineering fields which give rise to interesting and valuable applications.[70] Among all these applications, nanomedicine has been focussing on the development of drug delivery systems for biomedical applications[71] as an excellent alternative to traditional cancer treatment.

Due to all the limitations that conventional anticancer therapies present, it is necessary to search for alternative cancer treatments more efficient and less toxic. In this search, nanomedicine plays an important role:

- Nanoparticles can encapsulate drugs with poor water solubility allowing longer presence of these drugs in the body, improving the bioavailability.[72]
- The accumulation of the drug inside of the tumour is higher than traditional therapies due to the enhanced permeability and retention effects (EPR).[73]
- The specific release of the drug in the tumoral cells depends on the type of nanoparticle. Different biological factors on the tumour area, such as pH, redox potential, or enzymes, can be used to control the delivery of the drug. Moreover, the use of external factors such as light, magnetism, ultrasound and X-rays allow a synergistic effect, more specificity, and less toxicity in the cancer treatment.[74]
- Nanocarriers allow the encapsulation of more than one drug at the same time, and the combination with other treatments such as

photothermal therapy (PTT), photodynamic therapy (PDT) or chemodynamic therapy (CDT).[74]

On the other hand, it is important to know the actual limitations of nanomedicine, to develop new nano-systems or strategies to overcome the following limitations:[75]

- The high cost of production due to the difficulty of scale up their synthesis.
- Toxicity of some types of nanoparticles, such as metals nanoparticles.
- Low drug-loading efficiency and drug expulsion during the storage.

1.2.2. *Different types of nanoparticles: organic, inorganic and carbon-based nanoparticles*

Nanoparticles can be classified according to different criteria but, based on the chemistry, they can be classified in three groups: organic, inorganic and carbon-based as illustrate in **Figure 10**.

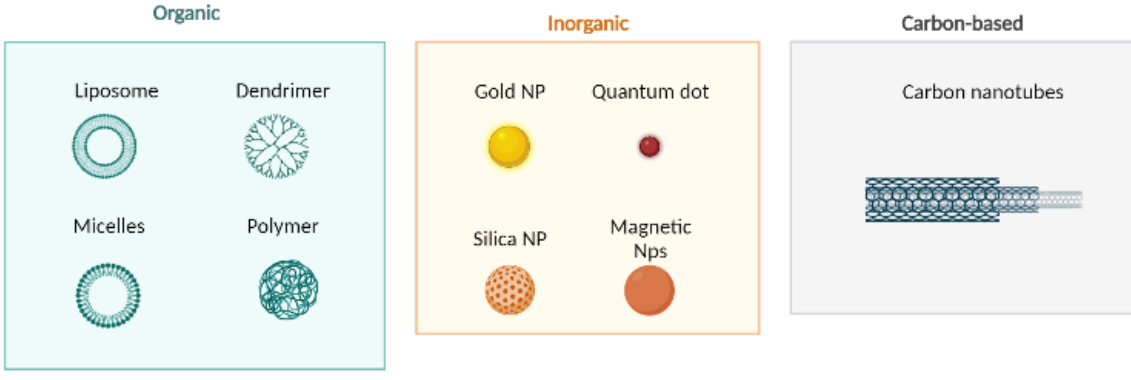

Figure 10. Different types of nanocarriers.

Among the **organic nanoparticles**, liposomes, solid lipid nanoparticles (SLN), nanostructured lipid carriers (NLC), cyclodextrins, micelles, polymeric systems and dendrimers have been strongly developed. This kind of nanoparticles have been explored due to their high biocompatibility and capacity to load different anticancer drugs.

Lipid nanoparticles: this type of nanoparticles is usually composed by a bilayer of phospholipids which have amphipathic characteristics resulting small vesicles, where can be encapsulated hydrophobic as well as hydrophilic drugs. [76] Although, they are biodegradable and can be functionalized with ligands such us antibodies or carbohydrates.[77]

The exhaustive study of these nanocarriers has resulted in the development of liposome nanoparticles to administrate anti-cancer drugs *in vivo* such us docetaxel[78] and nucleic acids.[79]

Solid lipid nanoparticles (SLN): SLN are composed of mono-, di- or triglycerides, fatty acid, and complex glyceride mixtures. They have a size range of 50-1000 nm. Moreover, these nanocarriers present several advantages, such as site-specific targeting, physical stability over long period of time, encapsulation of hydrophobic as well as hydrophobic drugs, low cost, and biocompatibility.[80] Due to all these reasons, different drugs have been encapsulated into these systems, such as paclitaxel (PTX), which was encapsulated into a hybrid of magnetic SLNs.[81]

Nanostructured lipid carriers (NLC): NLC are composed of solid and liquid liposomes.[80] The principal objective of those nanocarriers is to overcome the disadvantages of SLNs and they can have higher loading capacity. Thus, the size is 10-1000 nm and drugs such as thymoquinone or 6-gingerol have been encapsulated into these nanocarriers.[82,83]

Cyclodextrins (CDs): It is a type of cyclic oligosaccharides which are obtained from biodegradation of starch using a glucotransferase enzyme. This type of organic nanoparticles is used to encapsulate active drugs in their hydrophobic cavities. Due to their polysaccharide structure, they can

be easily functionalized by modification of hydroxy groups (-OH).[84] As result of their low toxicity, it has been developed different drug-CDs systems for the cancer treatment such us breast cancer (DOX into a CD nanocarrier modified with folic acid) or gastrointestinal cancers (oxaliplatin into a CD nanoparticle).[85]

Micelles: the principal characteristic of micelles is their spherical shape which is constituted by an amphiphilic polymeric block resulting a hydrophobic core and a hydrophilic shell.[80,86] Thus, oxaliplatin has been incorporated into micelles, in this case resulting metal complexes. The *in vivo* biological evaluation of them showed an increasing of the cytotoxicity but a promising inhibition value of the tumour.[87] In other cases, this type of nanoparticle has been used for the transport of two different drugs, which were encapsulated in different ways into the micelle, to obtain a synergistic antitumoral effect.[88] Moreover, genes and nutraceuticals have also been included into these systems showing several advantageous properties such as good solubility, permeability, bioavailability and achieving a decrease in the administered drug dose which means less side effects during the cancer treatment.[89]

Polymeric nanoparticles: these nanosystems are synthetized by the polymerisation of monomers, which are biodegradables and biocompatible.[90] Among others, it stands out polyethylene glycol (PEG), poly(4-vinylpyridine) (P4VP), poly-ε-caprolactone (PCL), poly(*N*-isopropylacrylamide) (NIPAM), polylactic acid (PLA), poly(lactic-co-glycolic) acid (PLGA) or polymethacrylate (WFP).[91] The antitumoral drugs can be encapsulated into the polymeric nanoparticle or adsorbed in their surface.[92]

It is important to highlight the excellent compatibility and stability of polymeric nanocarriers in biological fluids. Therefore, in 1976 was the first time that a polymer was studied as a drug delivery system.[93] Since this study, many polymers have been developed and functionalized with different ligands to become more specific.

Besides, US Food and Drug Administration (FDA) as well as the European Medicines Agency (EMA) approved next polymers as a safety method of cancer treatment: poly(*D,L*-lactide) (PLA), poly(*D,L*-glycolide) (PLG), co-polymer poly(lactide-co-glycolide) (PLGA), polyalkylcyanoacrylates or poly-Ɛ-caprolactone.[94]

Dendrimers: this kind of nanocarriers are composed by repetitive ramifications with a geometric pattern of arms which are extended from the nucleus. Nanoparticles constituted by these compounds have been designed to increase the efficacy of antitumor drugs.[95] By using these nanosystems, the drug is specifically target to the tumor tissue which is achieved due to the presence of the dendrimer arms since the terminal positions allow binding of active molecules or antibodies.[96]

In 2015, She *et al.* developed a doxorubicin (DOX)-dendrimer delivery system. Specifically, DOX was conjugated with "pegylated" dendrimers through hydrazone-type bonds, which exhibit a pH-dependent cleavage, releasing the drug upon reaching the medium a pH of 5.0.[97] Moreover, they have synthesized dendrimers of polyamidoamine for the transport of cisplatin, which presents a double functionalization: pH-dependent release and active targeting by the incorporation of herceptin.[98]

On the other hand, **inorganic nanoparticles** have been used as anticancer drug delivery systems due to their biocompatibility, low toxicity, high surface to volume ratio, and capacity to load anticancer drugs.[77] Among all these inorganic nanocarriers can stand out: gold, quantum dot, silica and magnetic nanoparticles.

Gold NPs: the size and the shape of gold nanoparticles can be easily modified by different methods of synthesis.[99,100] In the biomedical area Au-nanoparticles are useful due to their ability of converting light into heat and have been used as anticancer agents in photothermal therapy (PTT).[101] Furthermore, they can be modified with different ligands such as antibodies, which increase the specificity of these anticancer systems.[102]

Quantum dot: the size of quantum dot is commonly around 1-10 nm, which means that are the smallest nanocarriers.[103] Quantum dots are biocompatible, can modulate fluorescence and present a large surface area in relationship to their volume.[77] However, the trend to agglomerate and the hydrophobic behaviour, limit the use as an anticancer drug delivery system. Fortunately, these limitations have been partially surmounted by the modification with ionic species and different ligands.[104]

Silica NPs: the main characteristic of silica nanoparticles is the easy control during the synthesis of their size, porous structure, biocompatibility, and capacity of modifications structure with different ligands.[77]

Magnetic NPs: the interest of magnetic nanoparticles in biomedicine is based on their capacity of acting as heat regulators for hyperthermia treatments, but also in their ability to target the drug in the tumour with help of an external magnetic field.[105] They can be functionalized with ligands such as polyethylene glycol (PEG) to improve the half-time-life in the body.[106] Specifically, hybrid of magnetic nanoparticles and together with polymeric materials is studied in this PhD Thesis.

Finally, among all **carbon-based nanoparticles**, carbon nanotubes are nanometer-sized hollow cylinders that are synthesized from carbon in a hexagonal arrangement, which can present a single-layer or multi-layer structure.[107] They have been used in different cancer treatments encapsulating anticancer drugs such as: DOX[108], paclitaxel[109], docetaxel[110], oxaliplatin[111], methotrexate, or small interfering RNAs.[77] Moreover, different surface modifications have been carried out to overcome the hydrophobic character of these nanocarriers and to gain more biocompatibility.[112]

1.2.3. Mechanism of targeting drug into the tumour and surface modifications of nanoparticles

The mechanism of targeting in the tumour by the nanoparticles can be classified in active and passive (**Figure 11**).

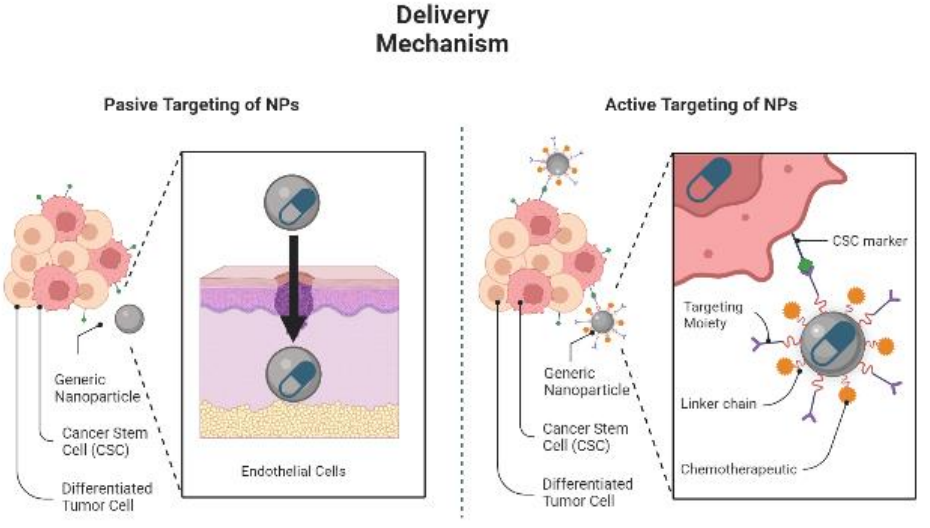

Figure 11. Delivery mechanism of nanocarriers.

- Passive targeting: the efficacy of this process depends on the size of the nanoparticles. Thus, nanoparticles are accumulated in the neoplastic tissues, which are characterized by the leaky vasculature and impaired lymphatic drainage.[113] However, during this process the Mononuclear Phagocyte System (MPS) recognises nanoparticles as a stranger body. To overcome this problem, coating of NPs with PEG has been designed.[72] Interestingly, in 2017 a nanoparticle system named genexol-PM, which delivery mechanism was passive targeting, was approved in Korea and marketed in Europe.[114]
- Active targeting: in this process the nanoparticle contains specific ligands, such as antibodies or folic acid, which interact with receptors present in the endothelial membrane.[115] To achieve the active targeting in nanoparticles, they can be surface-functionalized. The functionalization of nanoparticles increases the selectivity for the

tumour cells. The ligands that can be used in the design of specific nanocarriers are illustrated in **Figure 12**.

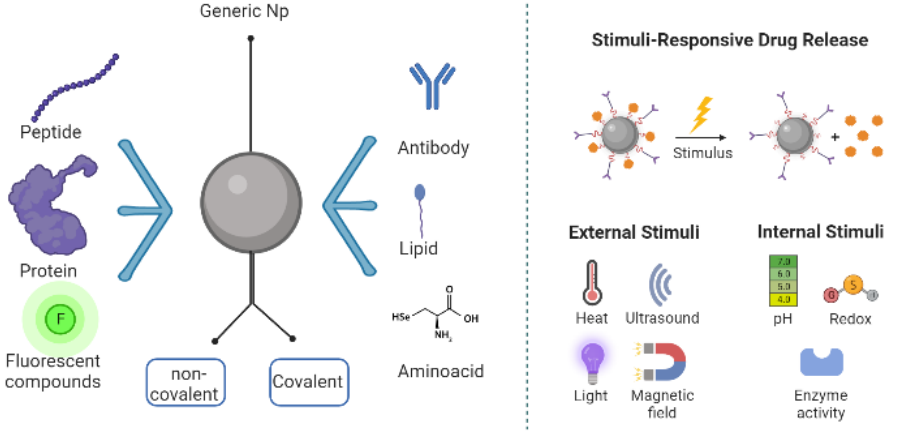

Figure 12. Functionalization of nanoparticles.

The principal methods of functionalization of nanoparticles with different ligands are[116]:

- Non - Covalent bond: this strategy is based on weak interactions between the nanoparticle and the ligand, such us electrostatic, ionic or Wan Der Walls. The advantage of this method is that it does not chemical change of the nanoparticle core.
- Covalent bond: this strategy is based on a strong chemical link between the nanoparticle and the ligand. Thus, this method introduces changes in the nanoparticle properties, i.e., magnetic, or fluorescent properties.

Once the nanoparticles have been functionalized, they will respond to stimuli, in order to release the drug in the specific tumor depending on the ligand characteristics of the nanoparticle. These stimuli can be internal (pH, enzyme, redox, temperature) or external (temperature, magnetic field, sound, light) (**Figure 12**). External stimuli are used to direct the nanoparticle towards the tumor, for example, when a magnetic field is applied to a magnetic nanoparticle. Recently, DOX has been encapsulated into magnetic micelles to control the release of this drug.[117] Also,

paclitaxel has been encapsulated into a Fe_3O_4-palmitoyl-chitosan matrix.[118] On the other hand, the internal stimuli allow to the nanoparticle to release the drug into the tumour through, for example, a change of the pH or the temperature in the endothelial cells.

1.2.4. Nanoparticles approved by Food and Drug Administration as antitumoral treatments

In **Table 5** it is shown, nanoparticles approved by Food and Drug Administration (FDA) for their use in cancer therapy. Thus, the first nanocarrier approved by the FDA for the clinical cancer treatment was a polymer protein conjugate in 1994. Since this year, 14 nanodrugs have been approved for the clinical practice.[119]

Table 5. Nanocarriers approved by FDA for cancer treatment.

Comercial name	Type of nanoparticle	Drug	Indications	Year
Zinostatin stimalamer	Polymer protein conjugate	Stryrene maleic anhydrude neocarzinostatin	Renal and hepatic cancer	1994
Feridex	Iron oxide nanoparticles	Ferumoxide	Magnetic resonance imaging contrast media (Cancer detection)	1996
Caelyx	PEG-Liposemes	Doxorubicin	HIV-associated Kapoi's sarcoma, ovarian cancer, metastatic breast cancer, multiple myeloma	1996
DaunoXome	Liposome	Daunorubicin	HIV-associated Kapoi's Sarcoma	1996

Comercial name	Type of nanoparticle	Drug	Indications	Year
Lipo-DOX	Liposome	Doxorubicin	Kapoi´s Sarcoma, breast and ovarian cancer	1998
DepoCyt	Liposome	Cytarabine	Neoplastic meningitis	1999
Myocet	Liposome	Doxorubicin	Breast cancer	2000
Eligard	Plymeric	Leuprolide acetate	Prostate cancer	2002
Abraxane	Albumin Bound	Paclitaxel	Advanced non-small-cell cancer, lung cancer, pancratic cancer, breast cancer	2005
Oncaspar	PEG-protein-conjugate	L-Asparaginase	Leukemia	2006
Genexol-PM	PEG-polymeric Micelle	Paclitaxel	Breast cancer, Lung cancer, Ovarian cancer	2007
MEPACT	Liposome	Mifamurtide	Osteosarcome	2009
NanoTherm	Iron oxide		Gliobastoma	2010
Marqibo	Liposome	Vincristine	Philadelphia chromosome negative acute lymphoblastic leukemia	2012
MM-398-Onivyde	PEG-Liposome	Irinotecan	Metastatic pancreatic cancer	2015

CHAPTER 2. OBJECTIVES

This PhD Thesis focuses on the design and synthesis of new analogues of bengamides and their inclusion into hybrid nanoparticles for biomedical use.

To achieve this challenge, the following specific objectives have been established:

Objective 1. Synthesis of new bengamide analogues and their corresponding biological evaluations.

Objective 2. Synthesis of thermosensitive polymeric nanoparticles with a magnetic core to employ as controlled drug delivery system.

Objective 3. Encapsulation of antitumoral drugs, including bengamide analogues, into these magnetic-polymeric nanosystems and their corresponding biological evaluations.

CHAPTER 3. SYNTHESIS OF NEW ANALOGUES OF BENGAMIDE

3.1. Background in the synthesis of the bengamides

3.1.1. Total synthesis of the natural congeners

Due to the interesting biological properties of the bengamides, described before, many total syntheses and new analogues of these natural products have been designed and efficiently achieved, giving rise to a novel research line. Thus, the first total synthesis of bengamide E (**5**) was described by Ogawa[38] using *L*-Quebrachitol (**45**) as suitable starting material. Moreover, different monosaccharides such as *D*-Glucolactone (**56**),[37,43,120] *L*- and *D*-Glucose (**55**,**54**),[37,121] *D*-Glyceraldehyde (**53**)[122] or *D*-Tartaric Acid (**50**)[8] were employed as starting materials which provided the right chirality to obtain the polyhydroxylated side chain of the bengamide's structure (**Figure 13**).

In contrast to these syntheses based on the chiral approach, the first synthesis carried out by Mukai *et al.* towards bengamide E (**5**) was based on a Mukaiyama-aldo reaction as synthetic strategy, starting from the achiral precursor **51** and the silylenol ether **52**.[123,124] Few years later, this synthesis was improved using *D*-Tartaric Acid (**50**) as starting material by the same authors.

At this point, to understand the complex of the challenge of preparing the others natural bengamides is necessary to be emphasized that the synthesis of bengamide E (**5**) did not require the caprolactam ring to be substituted, in contrast from other natural members, such as bengamide A (**1**) or B (**2**), which was required a total stereoselectivity in the construction of this system (**Figure 13**).

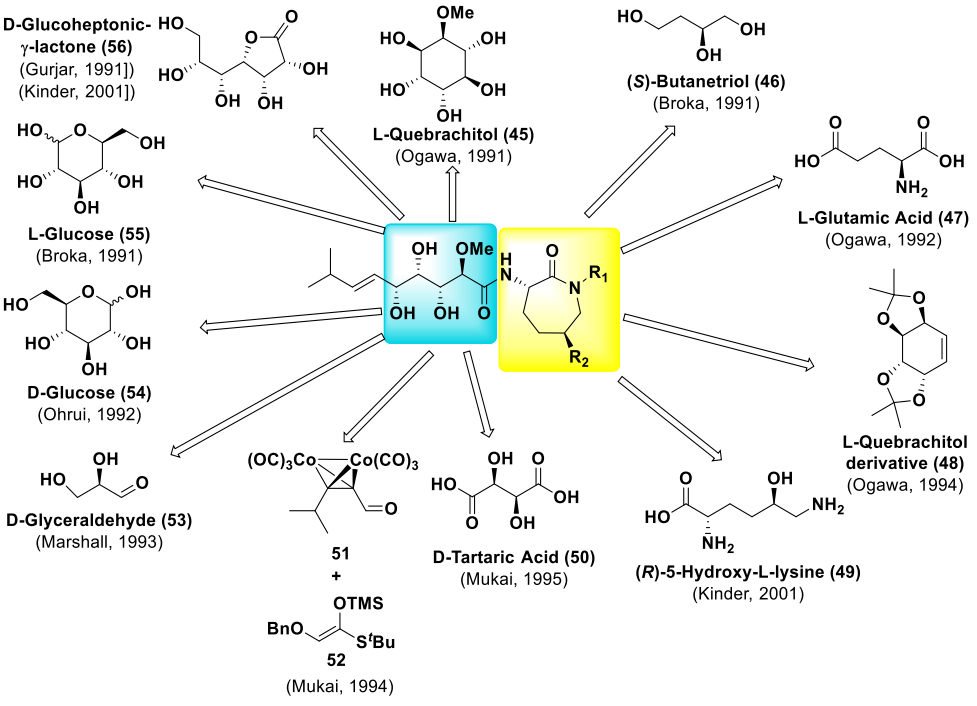

Figure 13. Total synthesis of the natural bengamides from 1991 to 2001.

In recent years, there has been a growing interest in the synthesis of these natural products. Specifically, in 2001 Banwell and McRae described a synthesis of the enantiomer of bengamide E starting from 1,2-dihydrocatechol (**57**), which was easily synthetized from the microbial oxidation of benzyl bromide.[125] Thus, **57** was subjected to different stages: formation of the epoxide intermediate, opening reaction of this epoxide and a protection step reaction of the hydroxyl groups to yield finally the trisilyl ether **59**. Then, the ozonolysis of this compound in DCM-MeOH yielded the corresponding aldehyde, which reacted with the sulfone **60** in basic medium to obtain only the alkene *E* **61**. Finally, the ester group of **61** was hydrolysed, and the resulting acid was coupled with cyclo-*L*-lysine to obtain, after a deprotection step of silyl ether groups, the enantiomer of bengamide E (***ent*-5**) (**Scheme 2**).

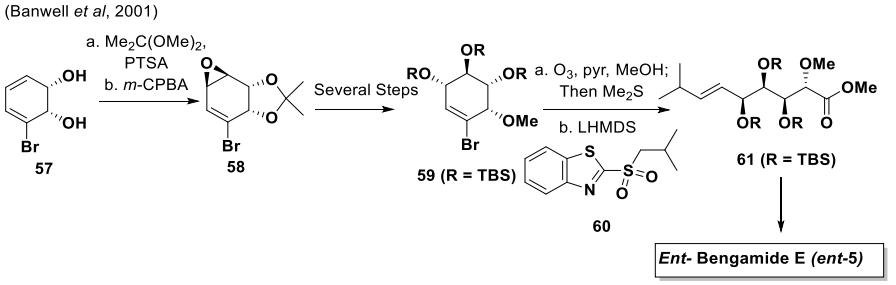

Scheme 2. Total synthesis of *Ent*-bengamide E by Banwell *et al.*

One year later, Liu *et al.* described the synthesis of bengamide E (**5**) starting from the alcohol **62**, which was obtained from diisopropyl *D*-tartrate. Therefore, they based on different aldol reactions as synthetic strategy for the construction of the side chain C-10.[126] After various stages, the introduction of the alkene *E* was carried out through a Julia-Kocienski reaction and the resulting aldehyde was subjected to an aldol reaction with the thioether **65**, under Annunziata condition,[127] to obtain a mixture 1:1 of diastereoisomers *anti.* Once these diastereoisomers were separated, the compound **66** was coupled with cyclo-*L*-lysine. After the last step, a reduction of the benzylether protecting group, bengamide E (**5**) was obtained (**Scheme 3**).

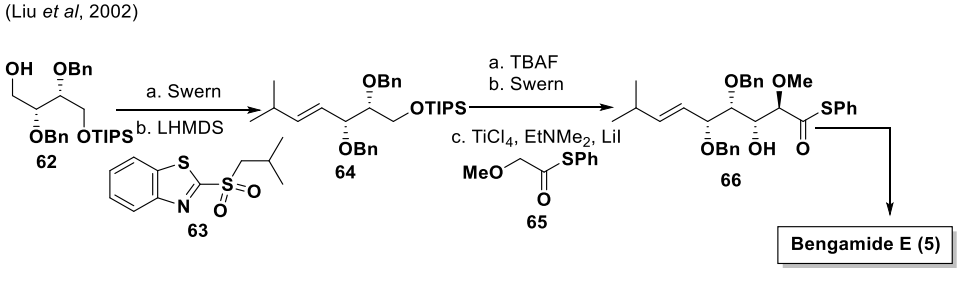

Scheme 3. Total synthesis of bengamide E by Liu *et al.*

A new approach to the synthesis of the bengamides based on a new kind of aldol reactions was carried out by the research group of Boeckman *et al.* who described a total synthesis of bengamides B (**2**), E (**5**) and Z (**20**).[128,129] To achive the synthesis of the side chain C-10, they proposed two consecutives asymmetric aldol reactions in *syn* and *anti* from the α,β-

unsaturated aldehyde **68**. Thus, the first aldol reaction was carried out with the chiral acetamide **67**, which under Et_2BOTf and DIPEA, reacted with **68** to afford the corresponding *syn* product with an excellent diastereoselectivity. The resulting amide **69** was prepared for the second aldol reaction, and then, the resulting aldehyde was reacted with the silylenol ether **70** in presence of $SnCl_4$ to obtain the compound **71**. This compound **71** represents the key intermediate in this synthesis which, by coupling with the corresponding 2-aminocaprolactam fragment, yielded bengamides B (**2**), E (**5**) and Z (**20**) (**Scheme 4**).

(Boeckman *et al*, 2002)

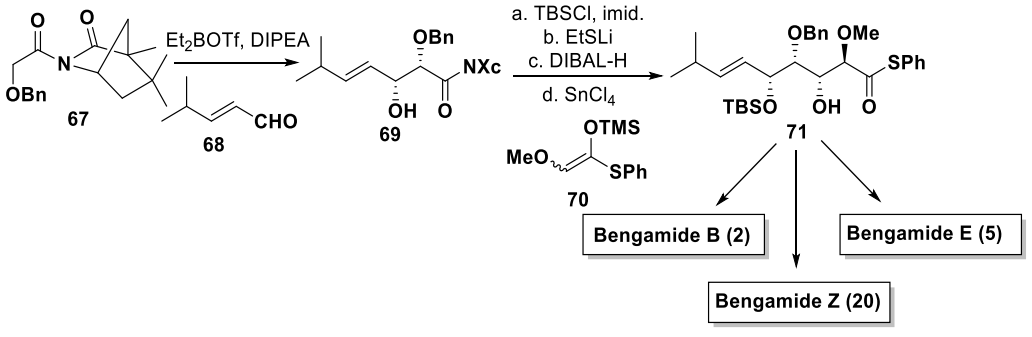

Scheme 4. Total synthesis of bengamide E, B and Z by Boeckman *et al.*

In 2005, our research group, described a total synthesis of bengamide E (**5**) based on three key steps: [130]

I. A cross metathesis reaction for the introduction of the alkene *E*.
II. Ring opening epoxide reaction for the introduction of the polyketide chain.
III. A coupling reaction to obtain the amide link to introduce the caprolactam moiety.

Therefore, the synthesis was initiated from the aldehyde **72** which was subjected to the following synthetic sequence: a Wittig reaction, a reduction step and a Sharpless Asymmetric Epoxidation (SAE) obtaining the epoxy alcohol **73** with a complete stereoselectivity. After a regioselective oxirane ring opening reaction of **73** with methanol, a chemoselective

oxidation of the resulting diol afforded the corresponding carboxylic acid, which subjected to a coupling with **74**, to successfully obtain the product **75**. Then, through an olefin cross metathesis reaction, disubstituted alkene *E* was introduced in a good yield and complete stereoselectivity. Finally, bengamide E (**5**) was synthetized after an acidic deprotection reaction of the acetal group (**Scheme 5**).

A second synthesis was developed by our research group in 2010,[33] by the application of the synthetic methodology based on stabilized sulfonium ylides derived from amides.[131] Thus, the aldehyde **77** reacted with a chiral sulfonium salt in basic medium to obtain in a good yield and excellent diastereoselectivity (>98%) the epoxy amide derived **78**, which was reduced to the corresponding epoxy alcohol after a treatment with $LiBHEt_3$. Then, this epoxy alcohol was employed using the previous methodology of bengamide E (**Scheme 5**). In this case the opening reaction and the formation of the *E*-alkene resulted in a better yield compared with the previous synthesis described by the group. Then, the opening of the oxirane ring was carried out by a treatment with MeOH in presence of $B(OMe)_3$, by application of the methodology developed by Miyashita.[132] After steps of oxidation and coupling of the corresponding acid with caprolactam **74**, the vinyl derivate **80** was obtained. This compound **80** was subjected to a Negishi coupling reaction in presence of diisopropylzinc and Pd(0) as catalyst, to afford the terminal olefin derivative. Finally, after a deprotection reaction, bengamide E (**5**) was synthetized in an alternative procedure, which resulted shorter and more efficient than the first synthesis described by our research group in 2005 (**Scheme 5**).

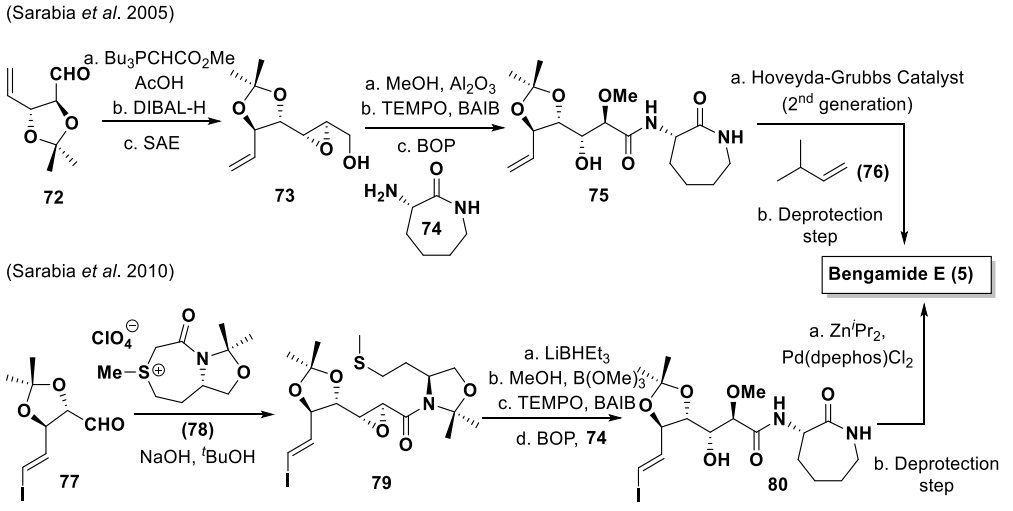

Scheme 5. Total synthesis of bengamide E (**5**) by Sarabia's groups.

Finally, in 2013 two new synthesis of bengamide E (**5**) were described. The first one by Li *et al.*,[133] who described a synthesis of this compound together with two new analogues which were obtained from the α-methyl-*D*-glucopyranose **81** through a synthetic sequence already described. Accordingly, employing Dondoni methodology,[134] the aldehyde **82** reacted with the thiazol derived **83**. Then, after TBAF (tetra-n-butylammonium fluoride) treatment and a methylation reaction of the resulting alcohol, a diastereoisomeric mixture 1:1 of compound **84** was obtained. After the transformation of the thiazol into the acid and the coupling with caprolactam **74**, an olefin cross metathesis reaction led to the precursor of bengamide E (**5**), which was converted into the final product after deprotection reaction steps (**Scheme 6**).

A second synthesis of bengamide E (**5**) was described by Prasad *et al.*[135] starting from bis-(dimethylamide) derived from the *D*-tartaric acid **85**, which through a reaction with the carbanion of 1,3-dithiane, yielded compound **86**, sequential steps of reduction and methylation.[136] Then, an olefination of Horner-Wadsworth-Emmons yielded a stereoselective introduction of *E*-terminal olefin. Therefore, the oxidation of the thiane group yielded the acid **87** which was coupled with caprolactam **74**. Finally, the

reduction of the ketone group through a treatment with $NaBH_4/CeCl_3$ and an acidic deprotection of the acetal group yielded bengamide E (**5**) (**Scheme 6**).

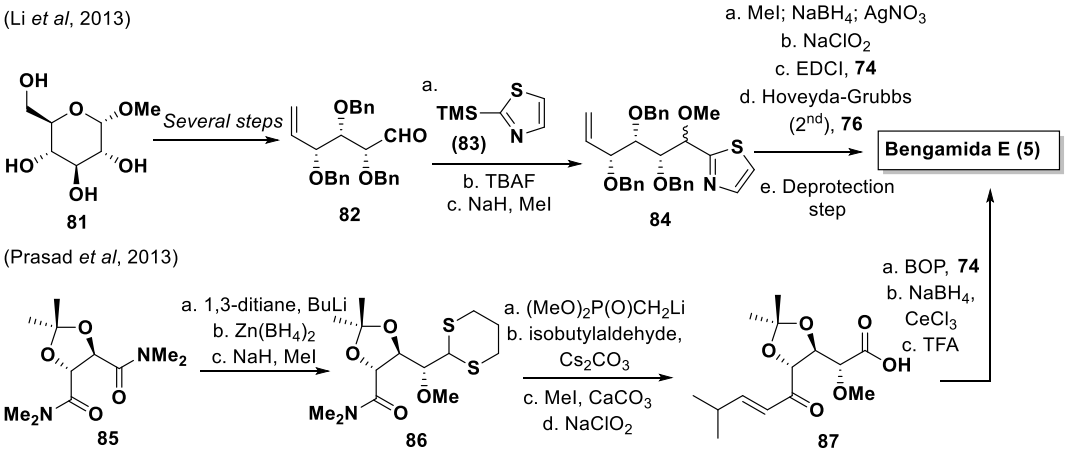

Scheme 6. Total synthesis of bengamide E by Li and Prasad.

In **Table 6** there is a summary of different described synthesis towards the bengamides family, with the number of steps and overall yields.

Table 6. Total synthesis of natural bengamides.

Bengamide	Author/Year	Starting material	Number of steps[a]	Yield[b] (%)
E (**5**)	Ogawa/1991[137]	*L*-Quebrachitol	15	0.40 %
E (**5**)	Broka/1991[138]	*L*-Glucose	16	11.20 %
B (**2**)	Broka/1991[138]	*L*-Glucose	16	5.90 %
E (**5**)	Ohrui/1992[121]	*D*-Glucose	17	0.80 %
A (**1**)	Ogawa/1992[36]	*L*-Quebrachitol	16	0.24 %
E (**5**)	Mars-hall/1993[122]	*D*-Manose	12	10.71 %
E (**5**)	Mukai/1994[123]	Isobutyraldehyde	18	3.06 %
B (**2**)	Ogawa/1994[124]	*L*-Quebrachitol	16	0.09 %
E (**5**)	Mukai/1995[139]	Isobutyraldehyde	18	4.70 %
E (**5**)	Mukai/1995[139]	DIDT[3]	16	5.00 %
B (**2**)	Kinder/2001[43]	*D*-Gluconolactone	7	7.21 %
E (**5**)	Kinder/2001[43]	*D*-Gluconolactonae	7	5.43 %
ent-E (***ent*- 5**)	Banwell/2001[125]	Bromobenzene	12	5.70 %
E (**5**)	Liu/2002[126]	DIDT[3]	10	9.74 %
B (**2**)	Boeck-man/2002[128,129]	Ethyl 2-hydroxyace-tate	12	10.86 %
E (**5**)	Boeck-man/2002[128]	Isobutyraldehiyde	10	23.56 %
Z (**20**)	Boeck-man/2002[128]	Isobutyraldehyde	10	17.86 %
E (**5**)	Sarabia/2005[140]	Diethyl *D*-tartrate	18	2.85 %
E (**5**)	Sarabia/2010[33]	Diethyl *D*-tartrate	14	4.15 %
E (**5**)	Li/2013[133]	*D*-Glucose	16	4.00 %
E (**5**)	Prasad/2013[136]	Diethyl *D*-tartrate	12	7.05

[a] The number of the steps for the longest sequence.

[b] The yield for the longest lineal sequence, without consider caprolactams synthesis for bengamides A, B and Z.[3] DIDT = Diisopropyl D-tartrate

3.1.2. Synthesis of new antitumoral analogues of bengamide

The structure of the bengamides can be modified to improve the interaction with their biological targets, the MetAPs enzymes, which results an increase of the antitumoral activity of these products. Therefore, a map could be developed through studies of Structure-Activity Relationship (SAR). The principal structural points subjected to modification are represented in the **Figure 14**.

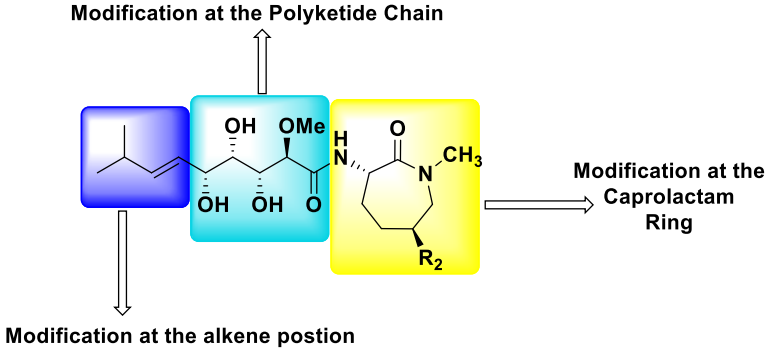

Figure 14. Design of the bengamides: possible modification in their structure.

First analogues of the bengamides were synthetized by the research group of Kinder in 2001,[141] who designed a library of various analogues derived from bengamide B (**2**). In particular, these analogues had a caprolactam ring substituted with an ester group, resulting in significant *in vitro* and *in vivo* activities. However, poor water solubility could hamper clinical studies of these antitumor drugs. To solve this solubility issue, were considered different modifications at the caprolactam ring moiety and at the alkyl terminal group position were considered. The synthesis of these modified analogues was based on the previously synthetic strategies stablished to prepare the natural bengamides by Kinder *et al.*, starting from *D*-glucolactone **56**. More specifically, the terminal isopropyl group of bengamide E (**5**) was substituted for a *tert*-butyl group.[43] Therefore, starting from the aldehyde **88** through Takai-Utimoto reaction using 1,1-diiodopentane the *E*-olefin was introduced (**90**) to obtain the intermediate lactone **90**, a key compound in this synthesis.[142]

The coupling of this lactone with the caprolactam **91**, which was obtained from the commercially available compound *(5R)*-5-hydroxi-*L*-lysine, yielded the precursor of bengamide **92**. Then, after an esterification reaction and a deprotection step of acetal groups, gave rise to different synthetic analogues of bengamide A (**93-106**), including the previously mentioned LAF389 (**26**). It is worth to note the opposite configuration of position C-5' in the caprolactam ring with respect to the natural bengamides. Moreover, these authors synthetized the *tert*-butyl analogue of bengamide B (**108**) by reaction of the lactone **90** with the caprolactam ring **107**, which was prepared from **91** (**Scheme 7**).

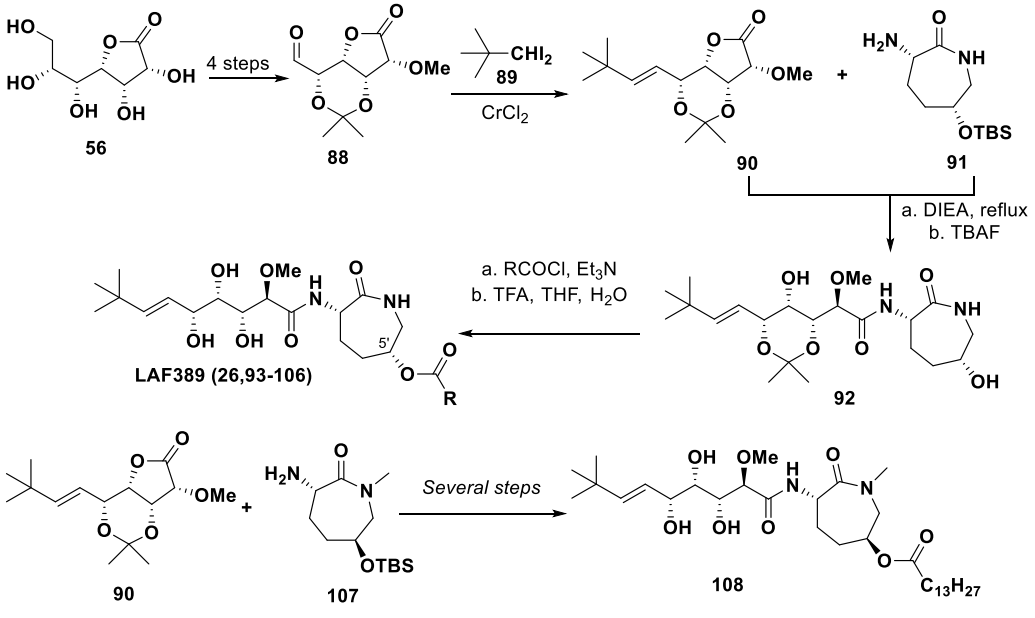

Scheme 7. Synthesis of bengamides analogues by Kinder *et al.*

The cytotoxicity of these new analogues was evaluated by measure of their antiproliferative activity against breast human carcinoma cells (MDEA-MB-435) *in vitro* as well as *in vivo* (**Table 7**) to conclude the relationship between antitumoral activity and modifications of the structure of the bengamides. It was concluded that the modification in the analogue **26,** which consisted in the replacement of the myristate ester, characteristic of the natural bengamides A (**1**) and B (**2**), by the

cyclohexanecarboxilate ester with an inversion at the configuration at the C-5' position, led to a significant increase of the antitumoral activity. These results showed that the inversion of the stereochemistry at C-5' centre and the increased water solubility resulted in a higher antitumoral activity of bengamide. Additionally, the activity was improved by the introduction of the *tert*-butyl group at the alkene moiety.

Table 7. Antitumoral activity of bengamides analogues synthetized by kinder *et al.* IC_{50} [µM].

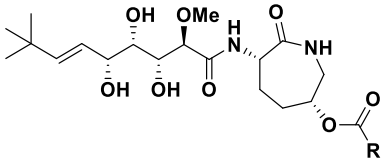

Bengamide	R-	MDA-MB-435	Bengamide	R-	MDA-MB-435
93	$CH_3(CH_2)_{12}$-	< 0.01	**99**	$PhCH_2CH_2$-	0.01 ± 0.01
94	Ciclopentil	0.13 ± 0.01	**100**	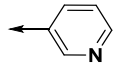	5.85 ± 0.01
26	Ciclohexil	0.04 ± 0.00	**101**	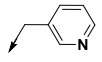	0.46 ± 0.04
95	Cicloheptil	0.02 ± 0.01	**102**	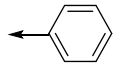	0.37 ± 0.01
96	$ChxCH_2$-	0.06 ± 0.00	**103**	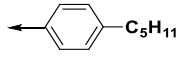	0.02 ± 0.01
97	$PhCH_2$-	0.26 ± 0.04	**104**	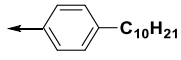	0.03 ± 0.04
98	*E*-PhCH=CH-	0.02 ± 0.00	**105**	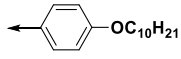	0.01 ± 0.00
106	-	0.01 ± 0.00	**B (2)**		0.012 ± 0.003

According to these results, Novartis developed an optimized synthesis towards the analogue **26** in a scale of 100 g in 2003 to carry out pre- and

clinical studies.[46] Therefore, LAF389 (**26**), was prepared and clinically studied. Unfortunately, the absence of activity and the unpredictable cardiotoxicity gave rise to the interruption of these clinic studies.[143] The cardiotoxicity exhibited by these bengamide analogues was ascribed to the lack of selectivity against isoforms MetAP1 and MetAP2 and to the low bioavailability. Despite of that results, these studies elicited an intense synthetic towards the development of new analogues with better activity, selectivity, and solubility properties.

MIn 2008, Nan *et al.* employed the Ring Cross metathesis methodology (RCM) which was previously described by their synthesis of functionalized amino caprolactams,[144] to perform a modification at the caprolactam moiety. Consequently, 5', 6' and 7' positions were modified through the reaction between the lactone **90** and different amino caprolactams, which was obtained from diene precursor **109** (**Scheme 8**).[145] The cytotoxicity of these new analogues (**111-126**) was evaluated by the measure of their antiproliferative activity against MDA-MB-435 showing that the modified 5' position did not increase the antitumoral activity, while the modification at 6' position showed better results. However, *N*-substituted analogues exhibited the best biological activity in all the analogues prepared by these authors (**Table 7**). Moreover, this activity increased when the R_1 chain was longer, but this trend was not showed in *N*-aryl substituted analogues, whose biological activities were lower.

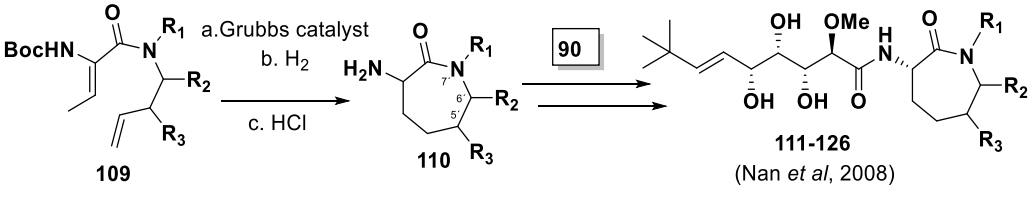

Scheme 8. Synthesis of new bengamides analogues by Nan *et al.*

Table 8. Antitumoral activity (IC_{50}, μM) of bengamides analogues by Nan *et al*. (2008).

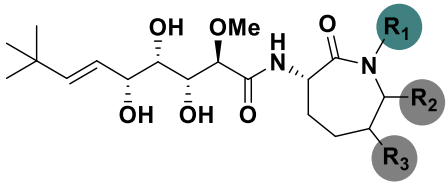

Bengamide	R_1 (R_2, R_3 = H)	MDA-MB-435	Bengamide	R_1 (R_2, R_3 = H)	MDA-MB-435
111	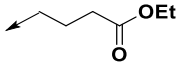	1.120 ± 0.240	**119**		0.396 ± 0.046
112	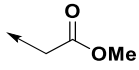	0.25 ± 0.021	**120**	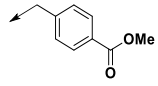	0.236 ± 0.064
113	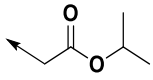	0.424 ± 0.017	**121**	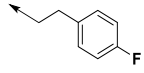	0.557 ± 0.129
114	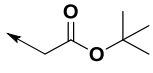	0.275 ± 0.005	**122**	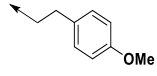	0.269 ± 0.041
115	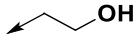	0.202 ± 0.005	**123**	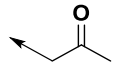	0.276 ± 0.029
116	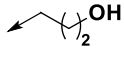	0.424 ± 0.068	**124**	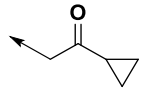	1.286 ± 0.226
117	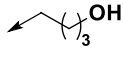	0.358 ± 0.071	**125**	**Me**	0.626 ± 0.234
118	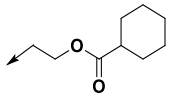	0.017 ± 0.008	**126**	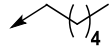	0.781 ± 0.160

A deeper modification at the caprolactam moiety was carried out by Nan *et al.* in 2011, according to which a new library of bengamide analogues was generated characterized by an open chain in substitution of the caprolactam ring.[146] Specifically, this caprolactam ring, which was characteristic of the natural congeners, was substituted by different open peptidic chains (**Scheme 9**).

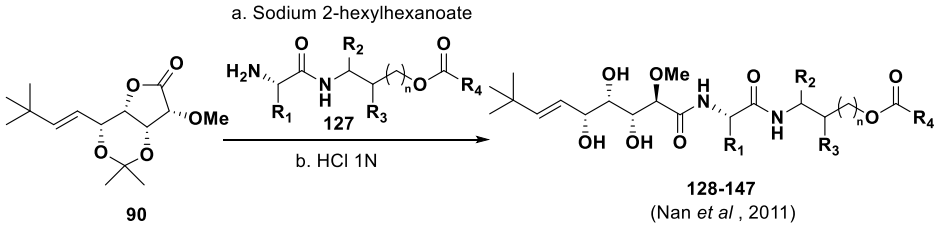

Scheme 9. Synthesis of new ring-opened bengamides analogues by Nan *et al.*

The biological studies (**Table 9**) of these 20 bengamide analogues against MDA-MB-435 showed that compound **145** (**Figure 15**) was one of the most powerful analogues thus far, with an IC_{50} value of 4 nM, in conjunction with an excellent solubility in water, resulting a very promising potent analogue.

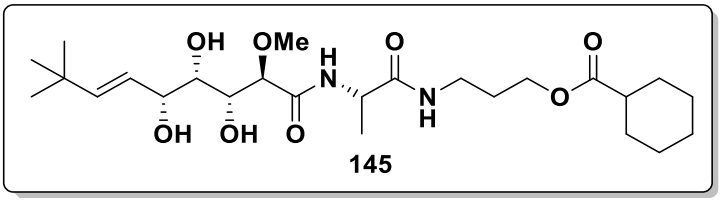

Figure 15. Molecular structure of new potent bengamide analogue by Ye *et al.*

Table 9. Antitumoral activity (IC_{50}, nM) of bengamides analogues by Nan *et al.* (2011)

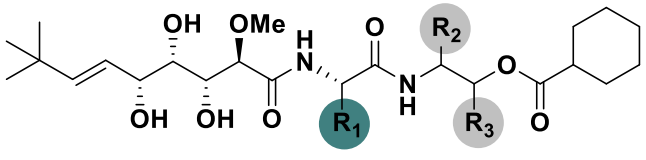

Bengamide	R_1 (R_2, R_3 = H)	MDA-MB-435	Bengamide	R_1 (R_2, R_3 = H)	MDA-MB-435
128	**Me**	31 ± 14	**131**	***i*Propyl**	195 ± 10
129	***i*Butyl**	125 ± 9	**132**	**BocNH$(CH_2)_4$-**	141 ± 22
130	***n*Butyl**	157 ± 8	**133**	***Sec*-Butyl**	208 ±76

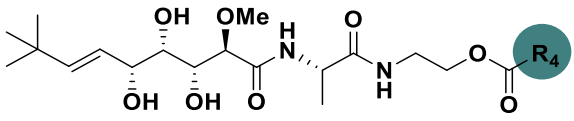

Bengamide	R_4	MDA-MB-435	Bengamide	R_4	MDA-MB-435
134		19 ± 4	**140**	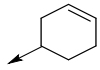	16 ± 37
135		10 ± 1	**141**	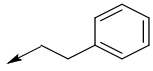	12 ± 2
136		293 ± 80	**142**		9 ± 7
137	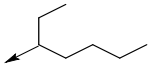	125 ± 35	**143**		675 ± 15
138		154 ± 37	**144**		20 ± 13
139	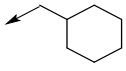	31 ± 14			

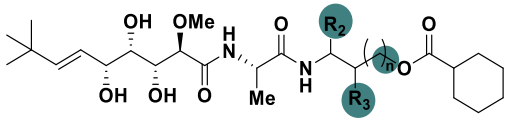

Bengamide	R_2	R_3	n	MDA-MB-435
145	H	H	1	4 ± 11
146	COOEt	H	0	65 ± 6
147	*H*	Me	0	17 ± 11

In 2011, Ye *et al.* designed a new class of bengamide analogues which were able to inhibit in an effective way the methionine aminopeptidase of *Mycobacterium Tuberculosis*.[63] However, this inhibition was lower in human cells. After obtaining these results, it was decided to do not modify the triol and the alkene fragment to keep the interactions between the two

metal ions in the pocket 1 and the side chain C-10, while the caprolactam moiety was modified to study the interaction in the pocket 2. The synthesis of these new analogues was carried out by the coupling between the lactone **90** with different amines to obtain, after deprotection steps, analogues **30** and **32-37** (**Scheme 10**).

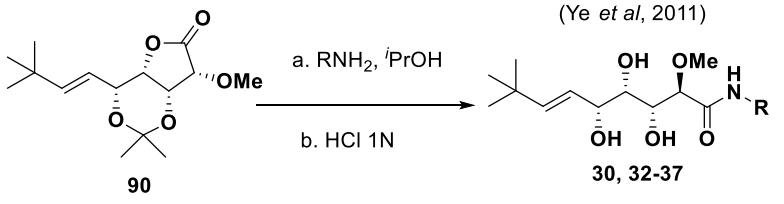

Scheme 10. Synthesis of new bengamides analogues by Ye *et al.*

Their inhibition activities were studied in *Mt*MeraP1 and *Mt*MeTAP1c which were activated by metal ions Co^{2+}, Mn^{2+}, Ni^{2+} and Fe^{2+}. All these compounds were partially inactive against Co^{2+} or Fe^{2+} of *Mt*MetAP1c, and completely inactive in Ni^{2+} form, showing selectivity for Mn^{2+} form in a low range of μM. Additionally, these compounds showed a better antitubercular activity against *Mycobacterium tuberculosis,* although their activities against methionine amino peptidase in human (K562) was interesting (**Figure 16**).[63]

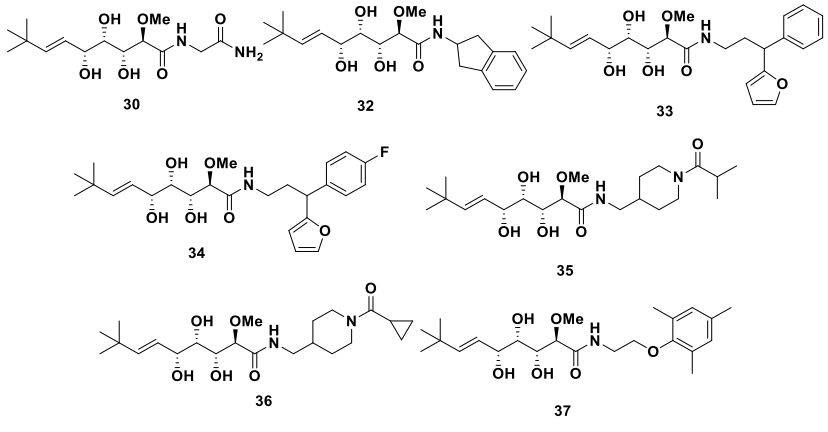

Figure 16. Molecular structure of new potent bengamide analogues by Ye *et al.*

All these modifications in the structure of the bengamides allowed to understand the importance of the role of polyhydroxy chain in the interaction of these antitumoral compounds with the methionine aminopeptidases active site. This point was demonstrated by the synthesis of different polyketides modified analogues and their corresponding biological evaluation. The effect of the stereochemistry of this chain was studied through the preparation of three new analogues: 3,4-epi, 2-epi and 2,3-epi bengamides E (**148**-**150**).[133,147,148] Moreover, together with all these analogues of bengamide E (**5**), enantiomer of the natural product was prepared (***ent*-5**) and biologically evaluated.[125] Additionally, it was possible to demonstrate the importance of the methoxy group in the position 2 through analogues **151**-**157** and epoxy derivates numbers **161**-**163**, which were designed and considered as formal hybrids of the bengamides and the fumagillin families (**Figure 17**).[148] The biological studies of these products against different tumoral cell lines showed that the polyhydroxyl chain and the stereochemistries of these chiral centres were essential to retain the biological activity and that any configurational or constitutional change of this chain could be translated into a completely loss of the antitumoral activity. In conclusion, it was demonstrated that the polyol system could not be subjected to structural changes, due to the interaction between hydroxyl groups with the metal ion in a strong octahedral coordination at the active site of the MetAPs.

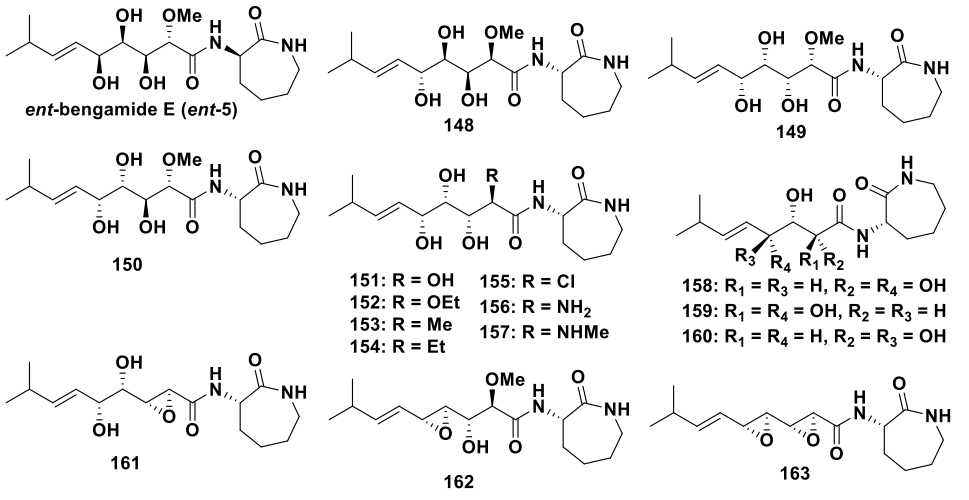

Figure 17. Molecular structure of bengamide analogues modified in the polyhydroxy chain.

After all these studies, our research group developed a synthesis towards modified bengamides at the alkene position.[149] Until that moment, the only modification at the bengamide's structure in this position was the introduction of the *tert*-butyl group instead of the isopropyl group. It is important to have in mind that this terminal alkene group interacted via a hydrophobic interaction in pocket 1 of MetAP's active site, so it was designed a modification to improve this interaction. In this research, different analogues were synthetized using the chiral sulfur ylides methodology, previously described.[131] Thus, the chiral epoxy amides **164**-**167**, were prepared for the introduction of new alkyl groups at the alkene position. These epoxy amides were transformed into **22** and **171**-**184**, which, through a cross metathesis or Pd couplings (Suzuki[150], Sonogashira[151] and Negishi[152]), yielded bengamides **19**-**210**, including, LBM648 **187** (**Scheme 11**).

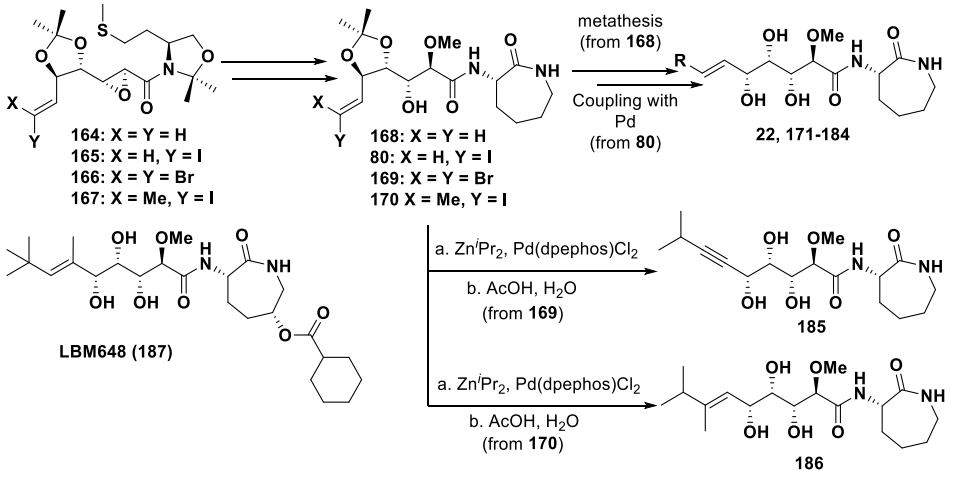

Scheme 11. Modification of the bengamides at the alkene position by Sarabia *et al.*

The cytotoxicity of these new analogues was studied against human colon adenocarcinoma cell line (HT29), human breast carcinoma (MDA-MB-231), human fibrosarcoma (HT1080) and human promyelocytic leukemia (HL60) and endothelial cells (BAE). The results obtained from this evaluation showed that the ramification of the lateral polyketide chain at the alkene position gave rise to a completely lost of the cytotoxicity. On the other hand, the analogue which had a cycle at the olefin position, such as the cyclopentyl analogue **171**, showed the best values of cytotoxicity among all the synthetized analogues. Particularly, analogue **171** was much more active than the natural bengamide E (**5**). Additionally, the biological evaluation of the analogue containing a *tert*-butyl group (**172**) in the olefinic position instead of the characteristic isopropyl group of natural bengamides also yielded positive results. In conclusion, the importance of the interaction of the substituents at the alkene position and pocket 1 was fully demonstrated (**Figure 18**).

Sarabia *et al.* 2013

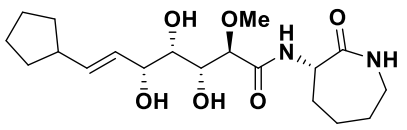

171

IC_{50} (μM) = 0.44 ± 0.06 (MDA-MB435)
IC_{50} (μM) = 0.12 ± 0.05 (HT1080)
IC_{50} (μM) = 0.19 ± 0.01 (HL60)
IC_{50} (μM) = 0.10 ± 0.02 (BAEC)

Sarabia *et al.* 2013

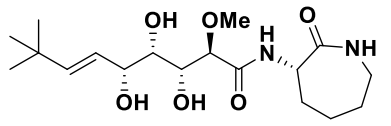

172

IC_{50} (μM) = 2.2 ± 0.1 (MDA-MB435)
C_{50} (μM) = 0.25 ± 0.05 (HT1080)
IC_{50} (μM) = 1.1 ± 0.2 (HL60)
IC_{50} (μM) = 0.17 ± 0.01 (BAEC)

Bengamida E

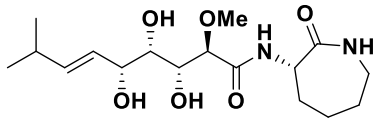

5

IC_{50} (μM) = 1.64 ± 0.54 (MDA-MB435)
C_{50} (μM) = 0.29 ± 0.03 (HT1080)
IC_{50} (μM) = 0.68 ± 0.10 (HL60)
IC_{50} (μM) = 0.28 ± 0.03 (BAEC)

Figure 18. Molecular structure of the potent analogue **171**, **172** and bengamide E (**5**).

Last modifications in the structure of bengamides have been focused on the caprolactam ring. Thus, in 2017, Pham *et al.* changed the configuration at the caprolactam ring.[153] The general synthetic methodology was based on the coupling between the lactone **90** and different enantiomeric amino-caprolactam under microwave irradiation at 100 W (**Scheme 12**).

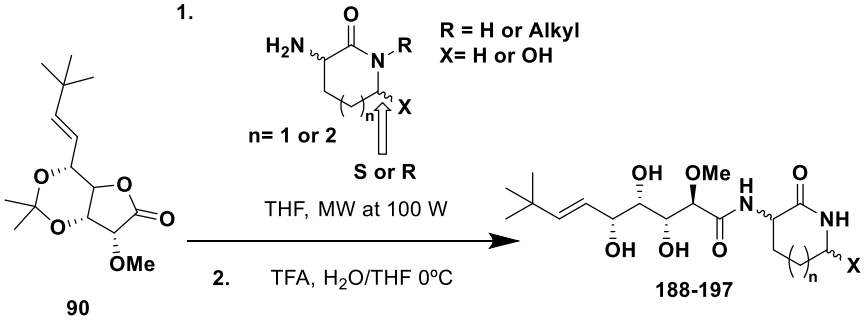

Scheme 12. Synthetic strategy to prepare new bengamides analogues by Pharm *et al.*

Interestingly, the biological evaluation of these new analogues was hopeful. Thus, the 2'-epimer (**188**) analogue of bengamide E (**5**) was more potent than the natural congener, showing better values of cytotoxicity against six cancer lines (**Figure 19**). Similar results were obtained for the 2-*R* analogues. Moreover, the caprolactam ring was also substituted by three different alkyl groups (**192-197**) giving rise to an interesting selectivity against some cancer cell lines with some of them with IC_{50} values less than 1 μM.[154]

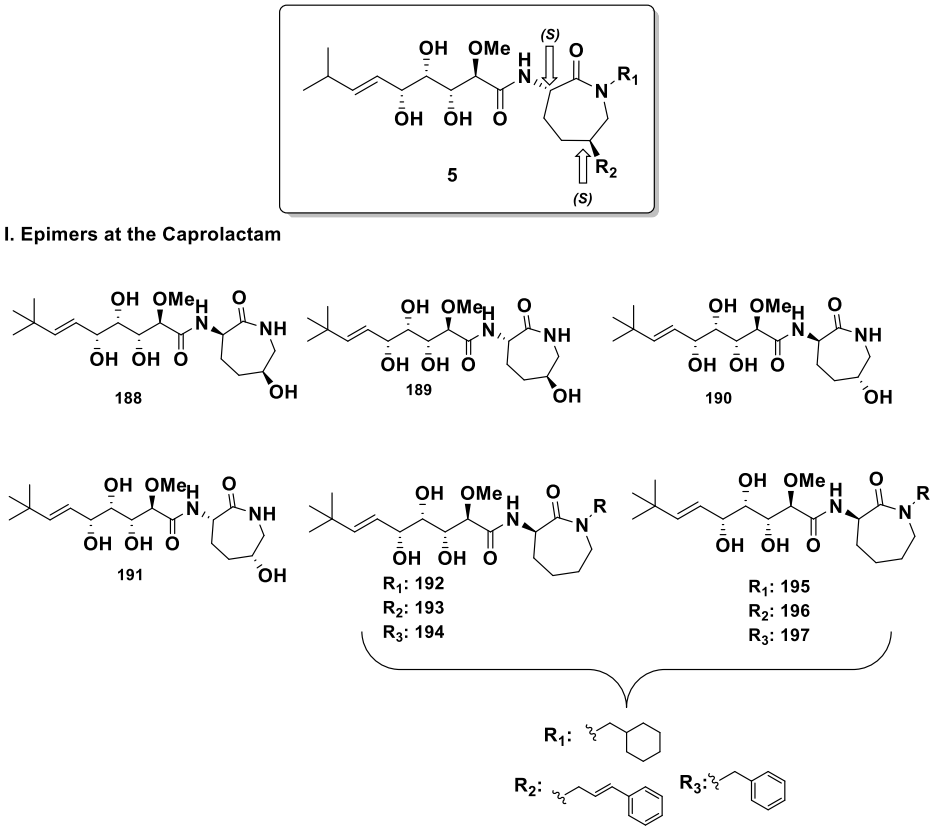

Figure 19. Epimers analogues of bengamide E prepared by Pham *et al.*

On the other hand, 6-membered caprolactam analogues were also prepared and biologically studied (**Figure 20**). Unfortunately, the antitumoral activities were lower than the obtained for the 7-membered analogues.[154]

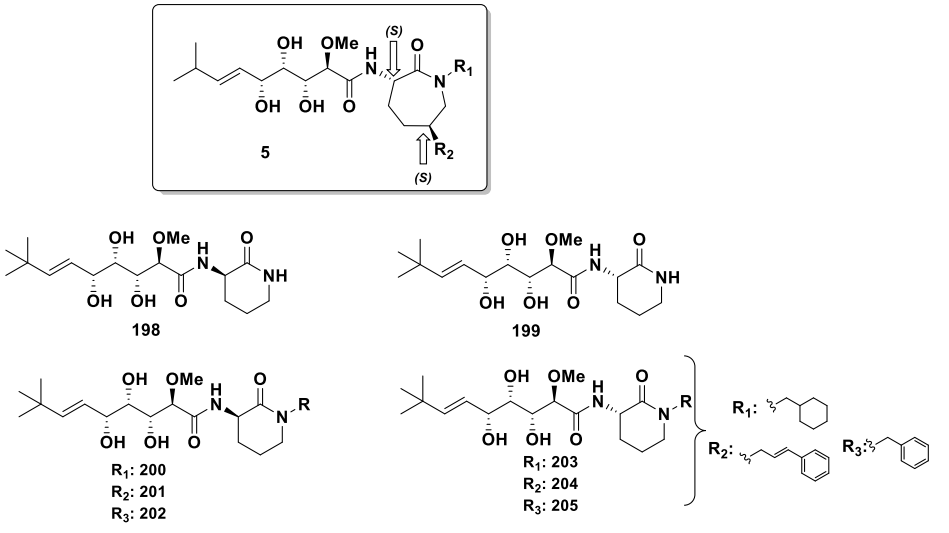

Figure 20. Epimers 6-membered analogues of bengamide E.

In brief, an extensive study of relationship structure-activity (SAR) and synthesis of new analogues of bengamides have been carried out by different research groups with the best biological values summarized in **Figure 21.**

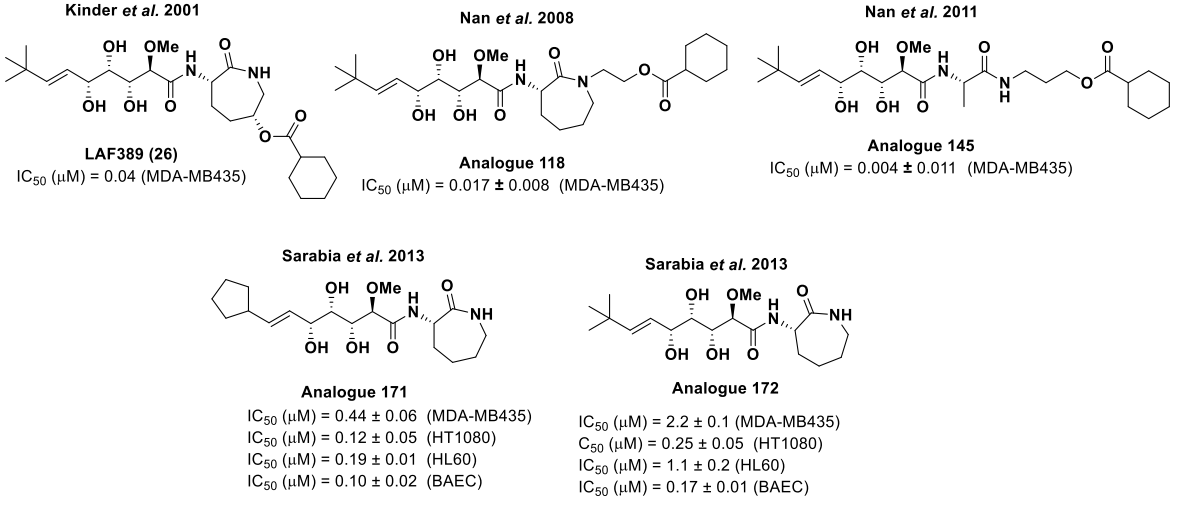

Figure 21. Summary of active bengamide analogues.

3.1.2. Synthesis of new antibiotic bengamide analogues

As mentioned before, during last year the research line of the bengamides has been focused on their antibiotic activity. Thus, trying to increase this interesting activity exhausted research was required.

Firstly, Nan *et al.,* as described in the previous section, designed and synthesized a library of ring-opened bengamide analogues.[146] Thus, from this synthetic study and after evaluating the antibiotic activity of all these new analogues, analogue **206** was identified as a hit due to their biological interest. Starting from this hit, they designed a second generation of ring-opened bengamide library.[155] Therefore, by the coupling between lactone **90** and different dipeptides, a total of six new analogues were prepared (**Scheme 13**) which displayed potent activities against *Staphylococcus Aureus.*

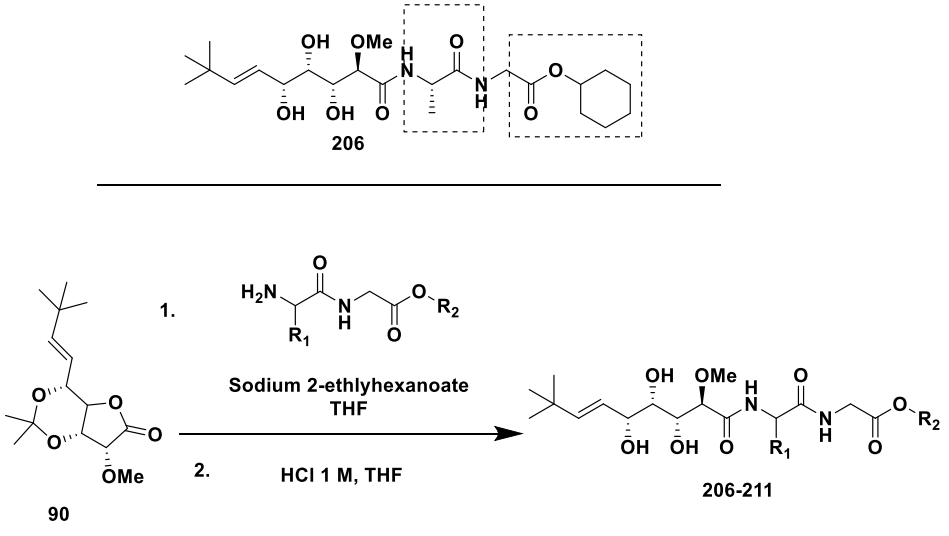

Scheme 13. General procedure to obtain second generation of ring-opened bengamides by Nan *et al.*

Then, in light of these interesting results, they decided to modify the ester group to increase the stability of these new analogues. As it is showed in **Table 10**, different alkyl and aryl groups were used to modify this moiety. Unfortunately, all these compounds were not active enough against S.

aurues strains. Therefore, they thought that the ester of the analogue **206** was essential to maintain the antibacterial activity (**Table 10**).

Table 10. Antibacterial activity (MIC) of analogues **206-211** modified at the ester position.

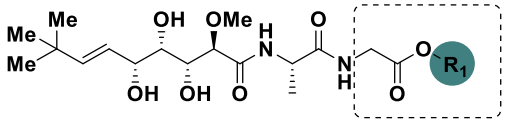

Bengamide	R_1	MIC [µg/mL]	Bengamide	R_1	MIC [µg/mL]
206	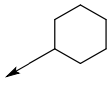	[0.78 - 1.56]	**209**	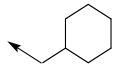	[0.39 - 0.78]
207	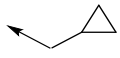	[1.56 - 3.13]	**210**	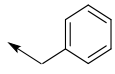	[0.39 - 0.78]
208	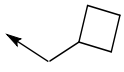	[0.78 - 1.56]	**211**	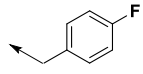	[0.78 - 1.56]

After obtaining these results, they attempted to increase the antibiotic activity of **206,** considering that **211** showed the same MIC and that esters are unstable at the metabolisms, they prepared a flexible ester with a linear alkynyl group **212**, which could increase the antibacterial activity. Thus, they decided to keep this alkyne group to explore in more detailed the relationship between R_2 and the antibiotic activity (**Figure 22**).

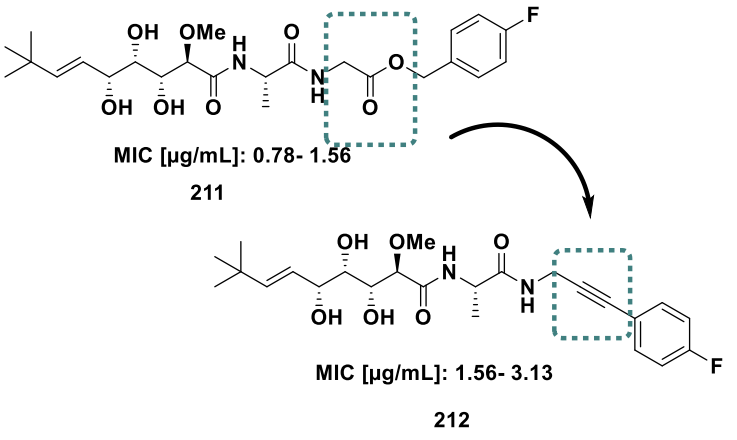

Figure 22. Structural modification of ester **227** to alkylnyl **228.**

Then, over this analogue **212**, it was decided to replace the methyl group (R_2) by alkyl and aryl groups (

Table 11). The biological evaluation of these new analogues revealed that **214** and **216** were able to active ClP (ciproflaxin) to degradate α-casein of different strains of *S. aureus* with values of MIC between 1.56-3.13 and 6.25-12.5 µg / mL, being **214** the most active.[156]

Table 11. Antibacterial activity of new analogues of bengamide.

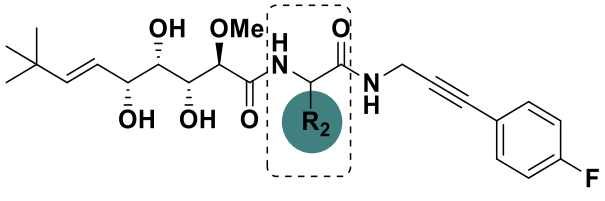

Bengamide	R_1	MIC [µg/mL]	Bengamide	R_1	MIC [µg/mL]
212	Me	[1.56 - 3.13]	**215**	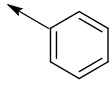	[3.13 - 6.25]
213	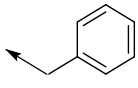	[6.25 - 12.5]	**216**	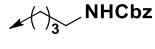	[0.78 - 1.56]
214	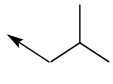	[0.78 - 1.56]	**217**	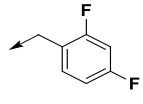	[6.25 - 12.5]

After these results, Nan and co-workers decided to maintain the benzyl group as R_2 substituent and change the *para*-fluoride group. Therefore, they synthetized a total of 12 analogues (**213**, **218**-**229**) with different substituents at the aromatic fragment. Finally, they concluded that the antibacterial activity in this position depended on the presence of a halogen atom and the position of this substituent, being analogue **227** (MIC= 6.25-12.5 μg / mL) used in the next experiments (**Table 12**).[155]

Table 12. Antibacterial activity of new analogues of bengamide.

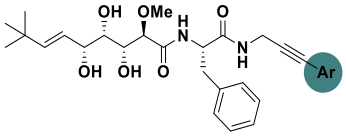

Bengamide	R_1	MIC [μg/mL]	Bengamide	R_1	MIC [μg/mL]
213	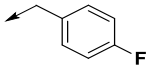	[1.56 - 3.13]	**224**	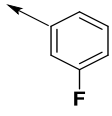	[25.0 - 50.0]
218	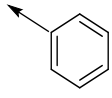	[12.5 - 25.0]	**225**	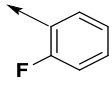	>50
219	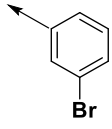	[12.5 - 25.0]	**226**	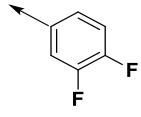	[12.5 - 25.0]
220	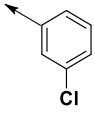	[6.25 - 12.5]	**227**	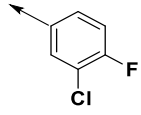	[6.25 - 12.5]
221	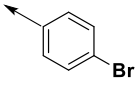	[6.25 - 12.5]	**228**	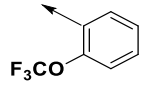	[25.0 - 50.0]
222	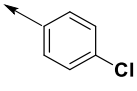	[6.25 - 12.5]	**229**	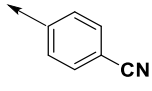	[12.5 - 25.0]
223	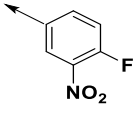	[12.5 - 25.0]			

Therefore, considering the best biological results were for analogues **217** and **227**, a new analogue **230** was synthesized to develop a potent antibiotic compound (**Figure 23**). Even though this analogue displayed activation on the degradation of protein substrate by SaClP with EC_{50} of 3.13-6.25 μM, it was still active against *S.aureus* in a ClpP-dependent role. Finally, the conclusion of this study let to know that this new library of bengamides could be a new class of potent antibiotics by targeting the *S. aureus* ClpP protease.[155]

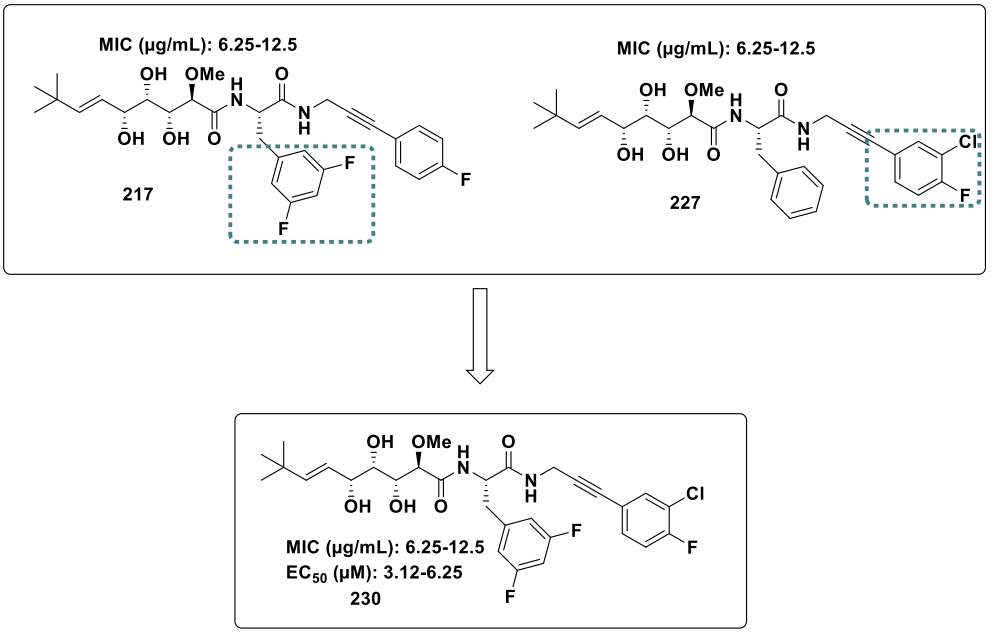

Figure 23. Design of new potent antibacterial analogue **230** by Nan *et al.*

Recently, in 2021, in the search of new analogues of bengamide with a potent antibacterial activity against methicillin-resistant *Staphylococcus aureus* (MRSA), Nan *et al.* synthetized a new third library of ring-opened bengamide analogues.[157] Then, taking again **206** analogue as the lead compound, they generated 24 new analogues by employing the previously methodology indicated (**Scheme 9**). Firstly, they decided to modify the methyl group of the *L*-alanine residue. On one side, they changed the stereochemistry of the alanine group (**232**) and the methyl group by

different alky groups (**235**-**237**) but maintaining the stereochemistry (**Figure 24**).

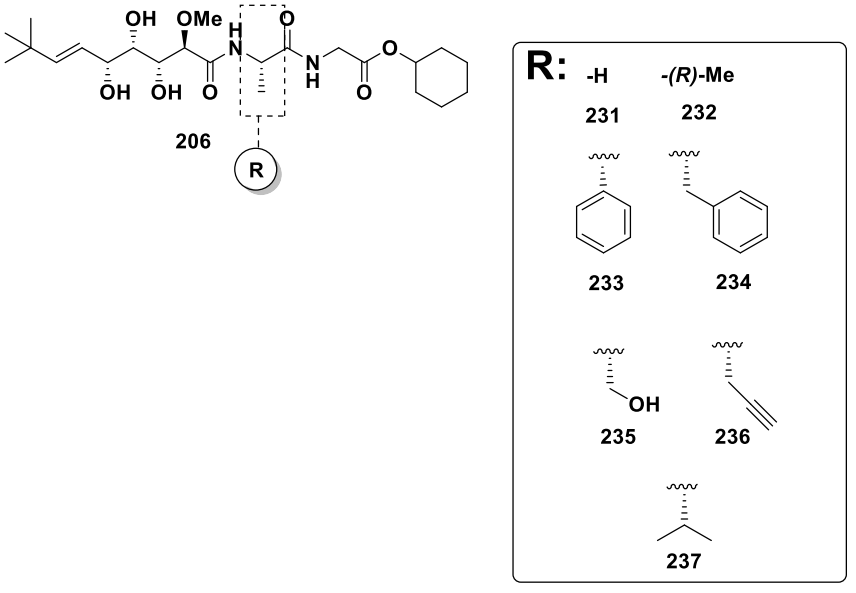

Figure 24. Modification of the hit at the *L*-alanine moiety by Nan *et al.*

Unfortunately, these new analogues did not show antibacterial activity against MRSA. Then, it was concluded from these studies that the methyl group of the *L*-alanine and the configuration of this chiral centre were essential to keep the antibiotic activity.

Having in mind this conclusion, they decided to modify the ester group trying to improve the antibiotic activity. Therefore, new analogues **238**-**245** were prepared and after biological evaluation, it was demonstrated that a bulky aliphatic group was necessary to maintain the antibiotic activity (**Figure 25**). In this sense, they prepared analogues with bigger cycles at the ester position **246**-**250**, giving rise to really encouraging results. From this study, it highlights the analogue **247,** which was identified as the most potent analogue.

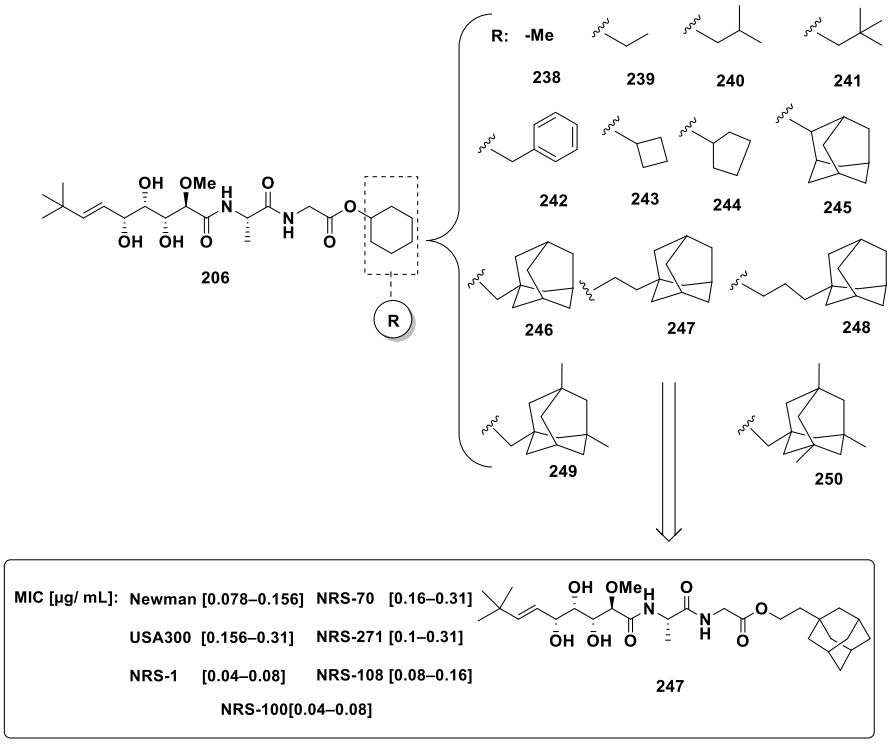

Figure 25. Modification of analogue **206** at the ester substituent by Nan *et al.*

Moreover, they decided to modify the alkene position preparing analogues **251** and **252**. Unfortunately, these analogues did not show the antibacterial activity which give rise to conclude thar this position was essential to maintain the activity (**Figure 26**).

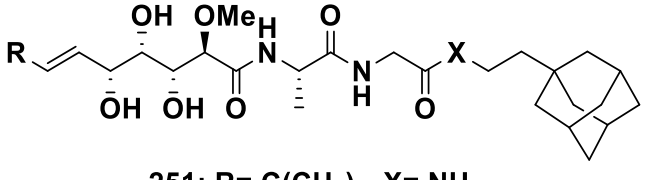

251: R= $C(CH_3)_3$, X= NH
252: R=H, X= O

Figure 26. Molecular structure of analogues **251** and **252**.

On the other hand, considering the low metabolic stability of ester they decided to prepare the amide **251**. However, the biological activity of this compound was lower than its ester analogue (**Figure 27**).

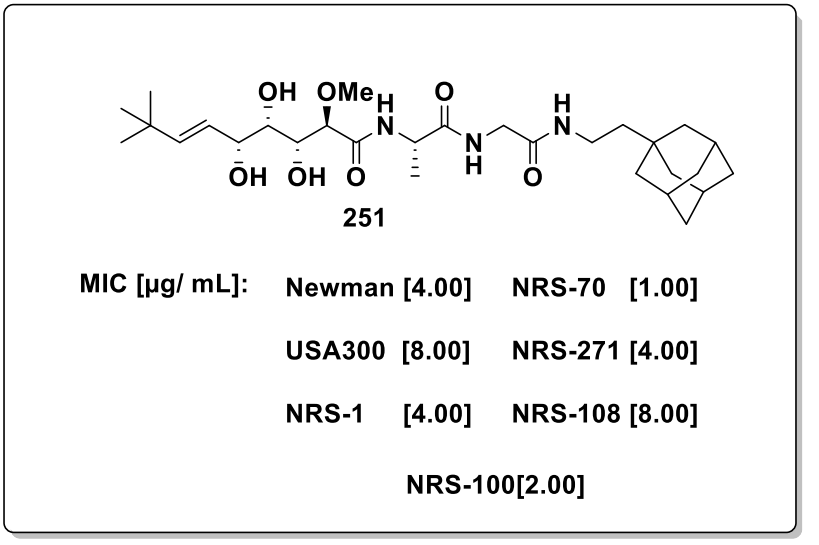

Figure 27. Biological values of analogue **251.**

3.2. A synthetic approach towards new bengamide analogues

Considering all the biological and chemical studies that have been carried out around the bengamides family, the main objective of this PhD Thesis is the development of a straightforwad and efficient synthesis towards new analogues of bengamides which could become new antitumoral drugs, more potent and more selective for the MetAPs. This aim, the moiety subjected to structural modifications that led to increase the antitumoral activity is the caprolactam fragment (**Scheme 14**).

Based on the general structure of the natural bengamides, two fragments of the structure will be modified:

- Firstly, the isopropyl group will be replaced by a *tert*-butyl group, increasing the hydrophobic interactions between bengamide and pocket 1 of the MetAps.[149]
- Secondly, considering the results obtained by Nan *et al.*,[146] the caprolactam fragment will be substituted by different peptidyl derivative chains, which are more polar and can increase the interaction of the bengamide with the pocket 2 of the enzyme.
- Finally, the polyketide fragment will not be subjected to any modification, keeping the constitution and absolute configuration of the chiral natural counterparts.

In **Scheme 14** is summarized the synthetic strategy for the preparation of new analogues of bengamide which will be followed in this PhD Thesis. Thus, the compound described by Nan *et al.*[146] **145** will be used as a hit molecule. Therefore, the synthesis of bengamide analogues is proposed following **Scheme 14**, in which the caprolactam fragment would be substituted by *L*-alanine derivative. On the other hand, the side chain C-10, characteristic of the studied compound, could be provided by lactone **90**, key compound in this synthesis. This lactone could be obtained by means of an olefin cross-metathesis reaction between the alkene **254** and the

between the 3,3-dimethyl-1-butene alkene. Finally, lactone **254** in turn could be obtained from the commercial *D*-glucoheptanoate-1,4- lactone **56.**

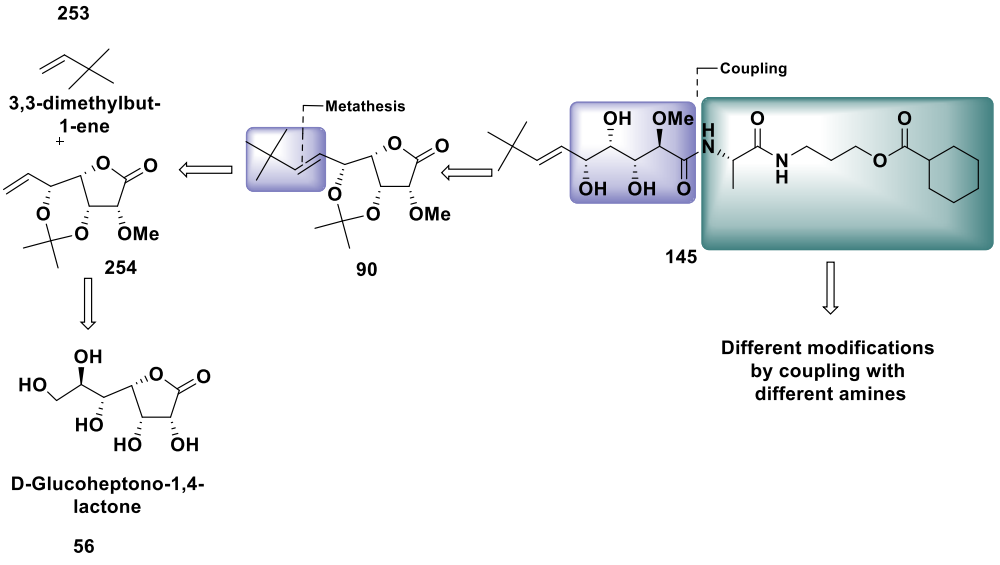

Scheme 14. Retrosynthetic analysis towards new analogues of bengamide.

3.3. Synthesis of bengamide analogues 145 and 172

Prior to the generation of a new library of caprolactam-modified bengamide analogues, we decided to synthetize the already described compounds **172** and **145** to compare biological activities with the reported data and trying to increase the antitumoral activity by encapsulating into different nanoparticles (**Figure 28**).

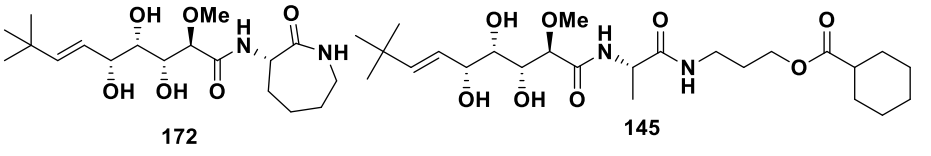

Figure 28. Molecular structure of bengamide analogues: analogue of bengamide E (172) by Sarabia et al. and analogue 145 by Nan *et al.*

*3.3.1. Synthesis key alkene intermediate **90***

With the aim of validating the retrosynthetic analysis proposed (**Scheme 14)** the main side chain C-10 of the bengamides was prepared through the synthesis of the key **intermediate 254** which was prepared following the **Scheme 15**.

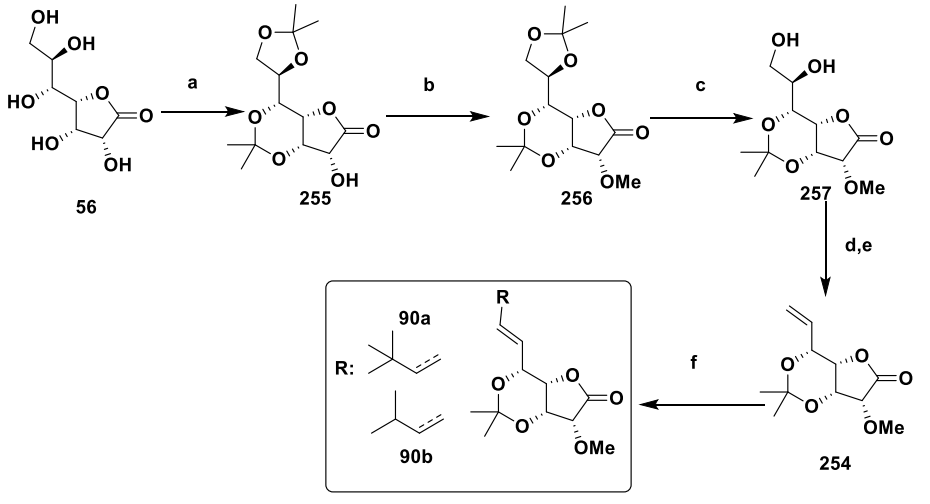

Scheme 15. Synthetic strategy towards the key intermediates **254** and **90.**

***Reagents and conditions*.** (a) **56**, Acetone, 25 ºC, 48 h. (b) **255**, K_3PO_4, Me_2SO_4, Toluene, 25 ºC, 24 h. (c) **256**, H_2O:AcOH 1:1, 25 ºC, 72 h. (d) Olefin Cross Metathesis.

With this purpose, the synthesis of the required disubstituted alkene **90** was started from the commercial lactone **56** (*D*-glucoheptono-1,4-lactone) which was protected in the form of acetal. Thus, two different conditions were tested to obtain this intermediate (**Scheme 16**). The first method employed was the treatment of **56** with 2,2-dimethoxypropate, anhydrous acetone and sulfuric acid as catalyst.[46] However, under these conditions the ester **258** was obtained, consequently the opening reaction of the lactone was occurred. On the other hand, the second method was the treatment of **56** with anhydrous acetone and iodine in catalytic amounts to obtain the desired acetal **255** in 93 % yield.[46]

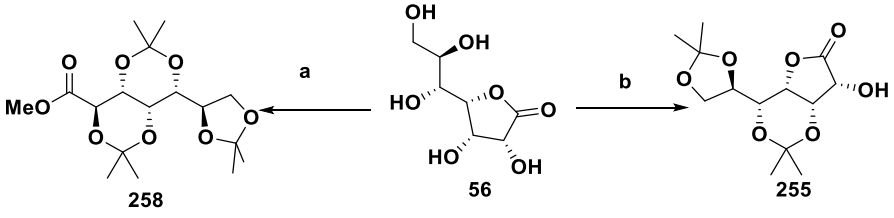

Scheme 16. Acetal protection of lactone **56.**

***Reagents and conditions*.** (a) **56**, Acetone, 2,2-Dimethoxypropane, 25 ºC, 48 h. (b) **56**, Acetone, I_2, 25 ºC, 48h, 93 %.

Once the protection reaction of commercial lactone **56** was achieved, the methylation of the free alcohol was carried out using dimethyl sulfate in presence of potassium phosphate, which provided the basic medium necessary alcohol methylation.[46] Thus, this reaction provided the derived **256** in 69 % (**Scheme 17**).

The next step was a deprotection reaction, which selectively hydrolysed the primary acetal versus the secondary due to the steric hindrance.[46] Thus, by a treatment of a H_2O:AcOH (1:1) mixture the diol **257** was obtained in 54 % (**Scheme 17**).

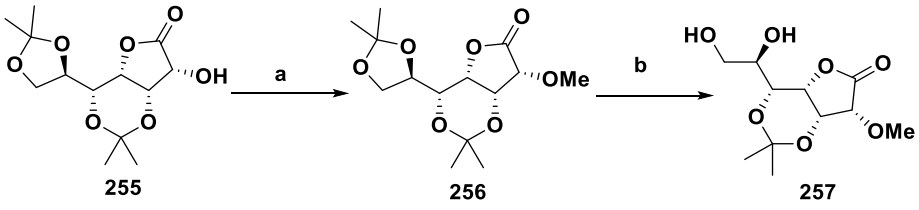

Scheme 17. Synthesis to diol lactone **257.**

***Reagents and conditions*.** (a) **255**, Me_2SO_4, K_3PO_4, Toluene, 24 ºC, 16 h, 69 %. (b) **256**, H_2O:AcOH (1:1), 25 ºC, 16 h, 54 %.

With compound **257** in hand, next challenge would be the elimination through an orto ester intermediate to obtain the monosubstituted alkene **254**. Thus, a Grank and Estwood[46,158] reaction was performed with the diol **257** subjected to a treatment with trimethyl orthoformate in toluene with catalytic amounts of acid to obtain **259** in 99 % yield. Then, this orto ester intermediate **259** was then subjected to a heating treatment in presence of acetic anhydride, to obtain the terminal alkene **254** in 98 %. At this point of the synthesis, this alkene could be subjected to an Olefin Cross Metathesis to obtain different disubstituted alkenes which are keys in the synthesis of bengamides (**Scheme 18**).

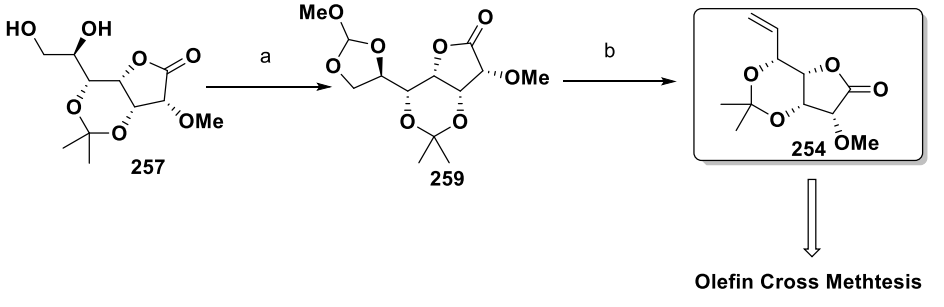

Scheme 18. Synthesis to obtain the terminal alkene **254.**

***Reagents and conditions*.** (a)**257**, TMOF, PPTs, Toluene, 25 ºC, 12 h, 99 %. (b) **259**, Acetic anhydride, 150 ºC, 3 h, 98 %.

At this point of the synthesis, purifications by flash-column chromatography were not necessary to obtain the alkene **254** with the required purity, being all the compounds purified by a recrystallization process obtaining them in high purities.

Once the terminal alkene **254**, it was obtained was proceeded to perform olefin cross metathesis[159] with two different alkenes: 3-methyl-1-butene **260a** and 3,3-dimethyl-1-butene **260b**, in the presence of Hoveyda-Grubbs Catalyst 2nd Generation to yield the coveted cross metathesis products: *E*-isomers alkenes **90** (37 %) and **261** (15 %) (**Scheme 19**).

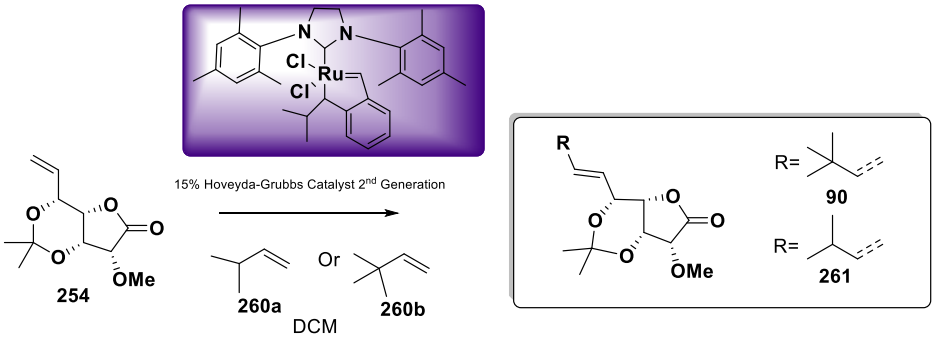

Scheme 19. Olefin cross metathesis reaction.

Reagents and conditions. (a) **254**,**260a**, Grubbs catalyst, CH_2Cl_2, 40 ºC, 12 h, 37 %. (b)**254**, **260b**, Grubbs catalyst, CH_2Cl_2, 40 ºC, 12 h, 15 %.

*3.3.2. Opening-lactone reaction of compound **90** to obtain bengamide analogue **172.***

Once the synthesis of the key product **90** was achieved, an opening lactone reaction was proposed as the synthetic strategy enabling to access to different bengamides. Thus, with this purpose, the *E*-alkene **90** was opened with caprolactam hydrochloride **79** by use of the basic salt sodium 2-ethylhexanoate (**Scheme 20**) to afford precursor **262** in 27 %.[46] To complete the synthesis, a final deprotection step of the acetal group was performed using aqueous acetic acid (AcOH) to obtain the analogue of bengamide E **172** in 70 %, which was prepared with the proposal of

include this active compound into different nanoparticle systems, as will be explained in **chapter 5.**

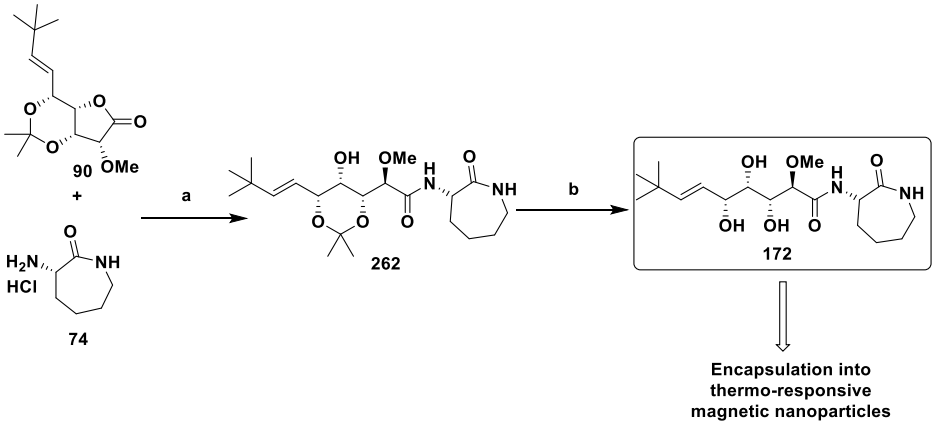

Scheme 20. Synthesis analogue of bengamide E **172.**

***Reagents and conditions*.** (a) **90**,**74**, sodium 2-ethylhexanoate, dry THF, 25 ºC, 48 h, 27 %. (b) **262**, 70 % aq AcOH, MeOH, 70 ºC, 2 h, 70 %.

*3.3.3. Opening-lactone reaction of compound **90** to obtain bengamide analogue **145***

As it was mentioned in the introduction section, in 2012 Nan *et al*. designed a new analogue of bengamide which proved to be a potent antitumoral derivative with high values of IC_{50} (4 nM), becoming in a promising antitumoral agent.[146] This analogue of bengamide was characterized by the presence of containing *L*-alanine peptide derivative fragment instead of the caprolactam ring, which is present in the natural congeners (**Figure 29**). Thus, we decided to synthetize this promising molecule and carry on a deeper biological study.

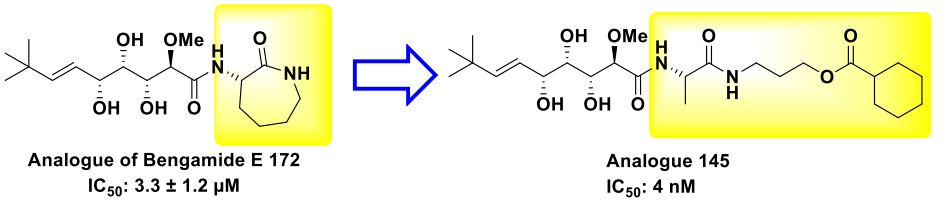

Figure 29. Molecular structure of potent analogue **145.**

In order to obtain the desired analogue **145**, the *L*-alanine derivative was synthetized which would be used as the nucleophilic agent in a ring-opening lactone reaction.[146] Thus, Boc-*L*-alanine **263** was coupled with amino-alcohol **264** by the use of the coupling agent 1-Ethyl-3-(3-dimethylaminopropyl)carbodiimide (EDC). Once the alcohol **265** was obtained, an esterification with cyclohexane carboxylic acid was carried out to obtain the desired *L*-alanine derivative **267** (**Scheme 21**).

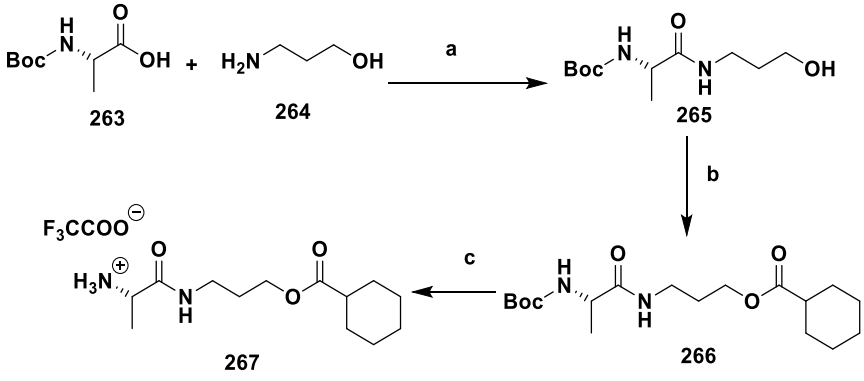

Scheme 21. Synthesis of amino acid derivative **267.**

Reagents and conditions. (a) **263, 264,** EDC, CH_2Cl_2, 25 ºC, 12 h, 52 %. (b) **265**, cyclohexane carboxylic acid, EDC, DMAP, CH_2Cl_2, 25 ºC, 12 h, 63 %. (c) **266**, TFA, CH_2Cl_2, 25 ºC, 12 h.

Then, after a Boc-deprotection of the amino group present on the *L*-alanine amino acid derivative, an opening reaction of lactone **90** was performed under basic conditions, by treatment with sodium 2-ethylhexanoate, to provide precursor **268** in 20 %. To complete the synthesis, an

acidic treatment afforded the bengamide analogue **145** in 89 % (**Scheme 22**).

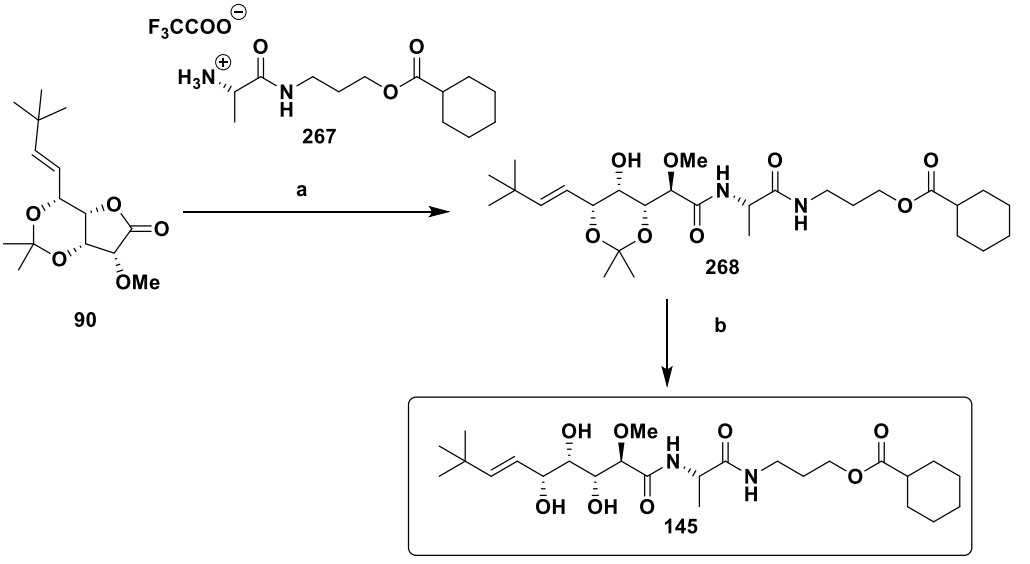

Scheme 22. Synthesis analogue of bengamide **145.**

Reagents and conditions. (a) **90, 267**, sodium 2-ethylhexanoate, dry THF**,** 48 h, 25 ºC, 20%. (b) **268**, HCl (1N), THF, 3 h, 89 %.

*3.3.4. Biological evaluation of analogues **145** and **172***

Cytotoxicity studies against different cell lines

At this stage of the work, having been prepared two analogues of bengamides (**145** and **172**), we proceeded with the biological studies. In collaboration with the group of Prof. José Prados and Prof. Consolación Melguizo from the Department of Anatomy and Embryology of Granada University, preliminary biological evaluations were performed based on the two bengamides analogues previously prepared against a panel of various tumor cell lines.[160] Thus, the cytotoxicity activities of bengamides analogues **145** and **172** were determined using seven different colorectal cancer cell lines, namely CCD18, T84, SW480, HCT15, HT29, MC38 and MCF7 (**Table 13**). From these results it is important to highlight that for

both bengamides the values were encouraging, showing high antitumoral activity in all cell lines comparing with reference compound (oxaliplatin or 5-fluorouracil) except for the MCF7 and MC38 lines. On the other hand, although bengamides **145** and **172** showed good values for all studied cell lines, obtaining the best results for MCF7, T84 and SW840, some differences were found between both analogues (**Figure 30**):

- Analogue **145** was much more effective against MCF7, T84 and SW840 than the analogue of bengamide E **172**.
- The difference in IC_{50} values between analogue of the bengamide E and control drugs was not relevant while this bengamide analogue **145** showed better values than these reference compounds.
- The only cell line in which **172** showed better IC_{50} values than the analogue **145** was in HTC15 cell line.

Table 13. Determination of IC_{50} (mM) [a] of Bengamide analogues **145** and **172** in tumor and non-tumor cell lines.

Cell Line	Bengamide 172	Bengamide 145	Reference Compound [b]
CCD18	4.70 ± 0.28	5.08 ± 0.39	7.35 ± 0.41
T84	0.36 ± 0.03	0.07 ± 0.02	2.68 ± 0.16
SW480	0.59 ± 0.07	0.08 ± 0.00	6.35 ± 0.54
HCT15	1.90 ± 0.15	2.44 ± 0.25	6.58 ± 0.35
HT29	1.02 ± 0.19	0.66 ± 0.18	6.14 ± 0.94
MC38	1.60 ± 0.13	6.51 ± 1.12	0.33 ± 0.01
MCF7	0.49 ± 0.05	0.13 ± 0.01	0.04 ± 0.01

[**a**] Half-maximal inhibitory concentration (IC_{50}) values calculated from dose-response curves as the concentration of compound that inhibits cell survival by 50% compared to control. They are expressed as means ± SD of triplicate samples-each;
[**b**] The reference compounds were doxorubicin for MCF7 and 5-fluorouracil for the rest of the cell lines (colon cell lines).

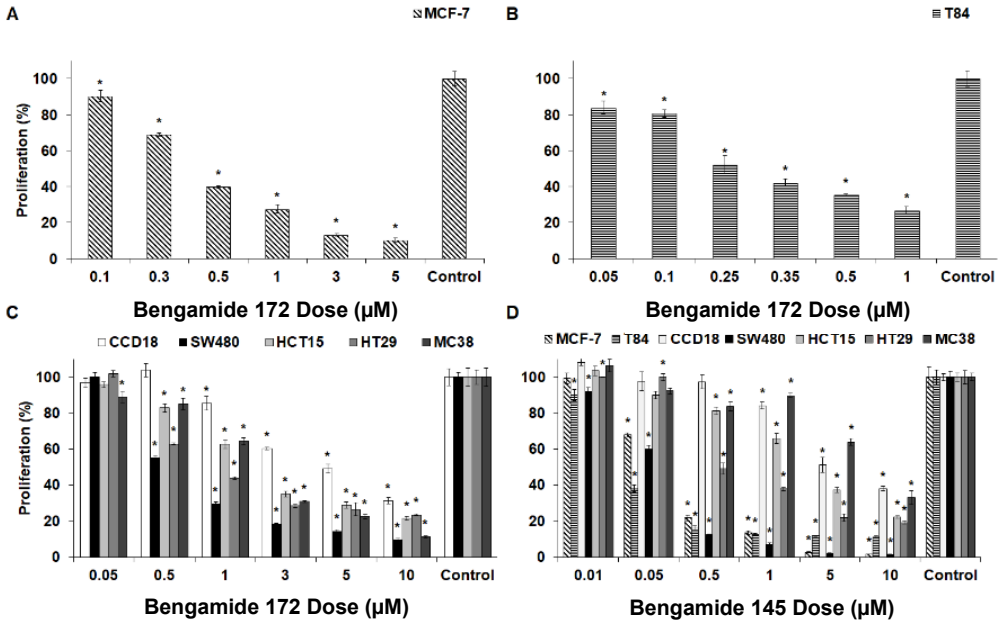

Figure 30. Antiproliferative assays of **172** and **145** compounds. Bengmide **172** effect after 72h of treatment in (**A**) MCF7; (**B**) T84 and (**C**) rest of the cell lines. Bengamide **145** effect after 72h of treatment in all cell lines (**D**). Data represent the mean values ± SD of triplicate cultures. * Statistically significant differences ($p < 0.05$) with the untreated control.

Biological evaluation: cell cycle analysis

To complete all these biological studies, cell cycle analysis was carried out in both analogues of bengamide (**Figure 31**).[160]

Cell cycle analysis showed differential behavior when cells were treated with **145** (named Ben V in **Figure 31**) and **172** (named Ben I in **Figure 31**). Indeed, in T84 cells, a statistically significant ($p < 0.05$) increase of the G2/M phase was observed with both treatments. However, this increase was much greater after exposure to **145** (or Ben V), including a slight reduction ($p < 0.05$) in the G0/G1 and S phases. No differences with the control were observed in the SubG1 phase for **172** (or Ben I) and **145** (or Ben V) ($p > 0.05$). In contrast, normal colon CCD18 cells showed a marked increase ($p < 0.05$) in the SubG1 and S phases with compounds **172** (or Ben I) and **145** (or Ben V) (at IC_{50} doses), while a slight increase

(p < 0.05) was observed in the G2/M phase, especially for **145** (or Ben V).

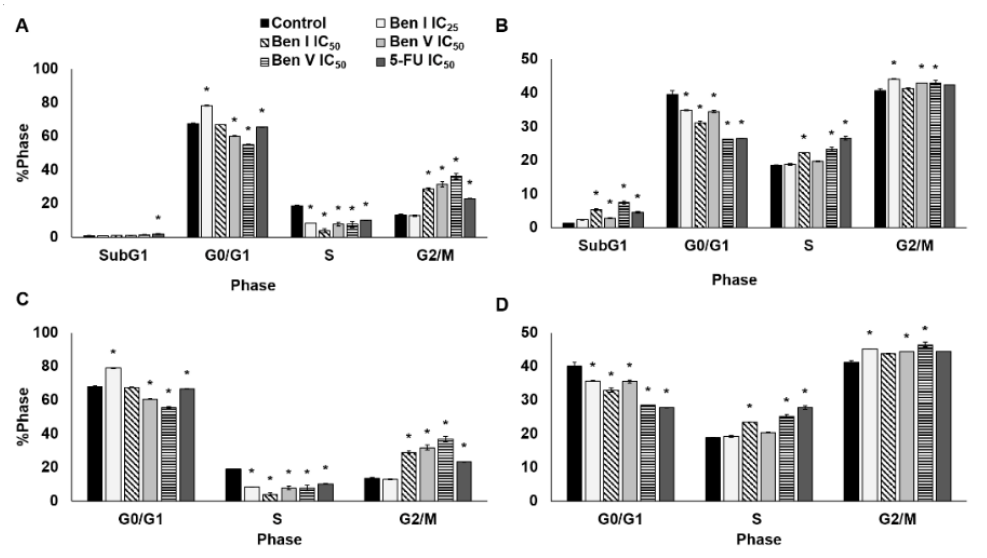

Figure 31. Cell cycle analysis after Ben I (**172**) and Ben V (**145**) exposure. Effect of Ben I (**172**), Ben V (**145**) and 5-FU (positive control) in cell cycle of lines T84 (A) and CCD18 (B). Cell cycle analysis without consider SubG1 phase in T84 (C) and CCD18 (D). * Statistically significant differences (p < 0.05) with the untreated control.

The results of all these biological studies clearly revealed that analogue **145** displayed the best biological values against all the tumoral lines that together with the biocompatibility in blood cells, became this compound a promising treatment against colorectal cancer (CRC). To research the role of this compound as a therapeutic strategy against CRC, biological studies *in vivo* were performed for which was necessary to obtain an amount of at least 150 mg of analogue **145**.

*3.3.5. Synthesis of analogue **145** to carry out in vivo studies*

After obtaining biological results that revealed the analogue**145** as a promising antitumor agent, a major amount of this analogue was required to perform *in vivo* essays.

To address this challenge, it was necessary to optimize to the maximum the total synthesis of this bengamide analogue. Therefore, different reaction conditions (**Table 14**) were used trying to optimize the opening lactone reaction whose yield was very modest, limiting the access to multi-mg amounts of the analogue **145**.

Table 14. Optimization of the opening lactone reaction.

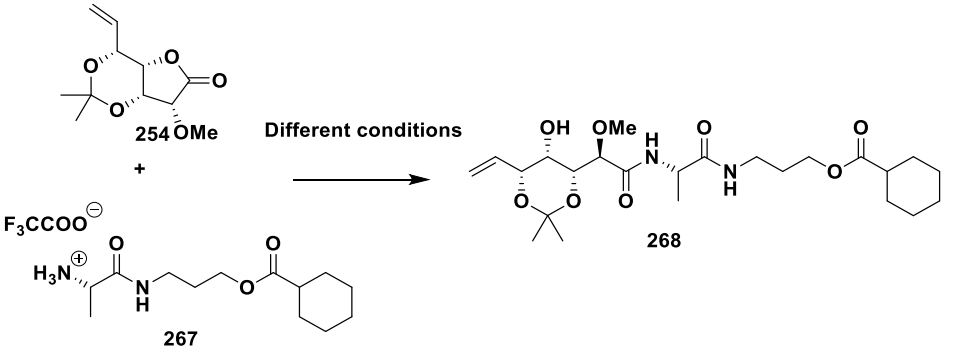

Entry	Base (eqv.)	Dry solvent (T)	Yield
1	Sodium 2-ethylhexanoate	THF (50 ºC)	29 %
2	Sodium 2-ethylhexanoate	THF (60 ºC)	27 %
3	Sodium 2-ethylhexanoate	Dioxane (80 ºC)	22 %
4	TEA	*i*-PrOH (40 ºC)	25 %
5	TEA	THF (25 ºC)	5 %
6	DIPEA	i-PrOH (40 ºC)	28 %
7	DIPEA	THF (60 ºC)	30 %

As showed **Table 14**, different bases and solvents were employed but, in all cases, the yields of this reaction were not above 30%, which limited this synthetic strategy to obtain a large amount of bengamide analogues. Considering these discouraging results, the synthetic strategy to obtain bengamide analogue **145** was changed to get the necessary amount of this potent antitumoral compound. Thus, a coupling between the acid **269** and the *L*-alanine derivative **267** was proposed to afford precursor **270** in the required quantity (**Scheme 23**).

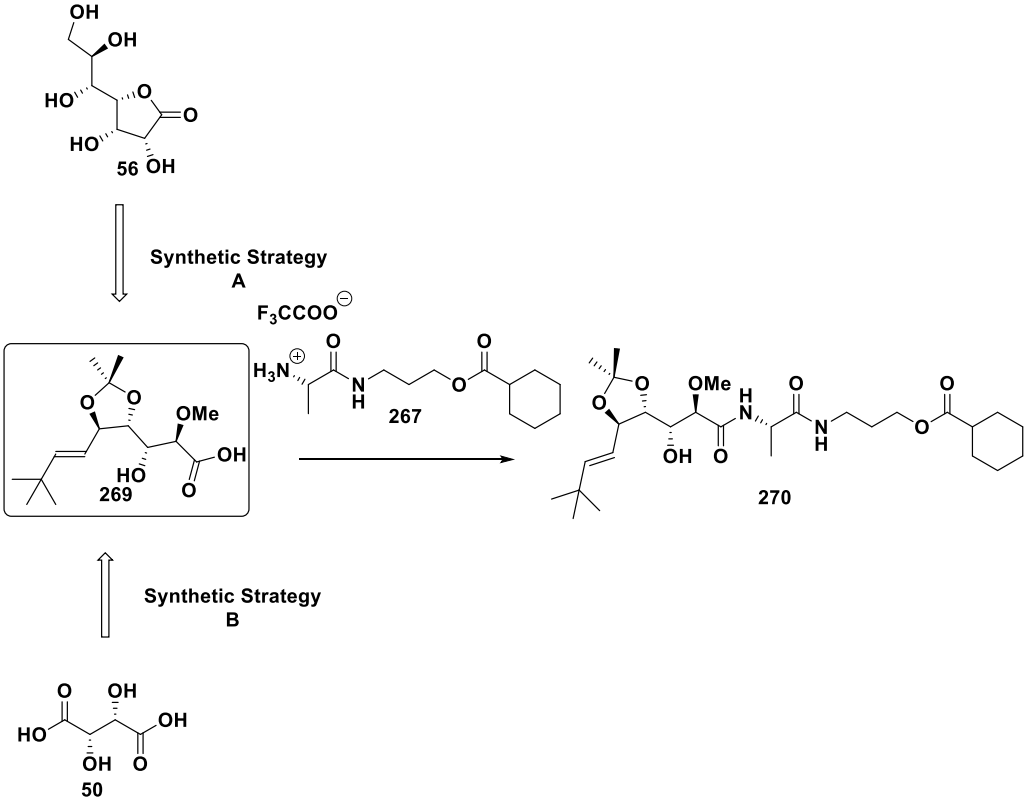

Scheme 23. Synthetic strategies towards precursor **270** in the required quantity.

The synthetic efforts towards analogue **145**, were focus on obtaining the acid **269**. To obtain the desired key acid two strategies were proposed:

- Synthesis A: from the *D*-Glucoheptono-1,4-lactone **56**.[46]
- Synthesis B: from the *D*-tartaric acid **50**.[161]

Synthesis A. Synthesis starting from *D*-Glucoheptono-1,4-lactone **56**

At this stage of the work, to take advantage of the intermediate **254**, a reduction of this lactone was proposed to obtain the diol **271** and selective oxidation to the desired acid **272**, which would be used in a coupling with the *L*-alanine derivative **267**. Thus, $LiBH_4$ was employed to obtain the diol **271** in a 40 % and the primary alcohol was chemoselectively oxidized using TEMPO/BAIB (bisacetoxyiodobenzene) system to obtain the acid **272.** With this acid **272** in hand, a coupling reaction was performed with *L*-alanine aminoacid derivative by a treatment with benzotriazole-1-yl-oxy-tris-(dimethylamino)-phosphonium hexafluorophosphate (BOP). Unfortunately, under this coupling conditions the acid lactonized recovering lactone **254** (**Scheme 24**).

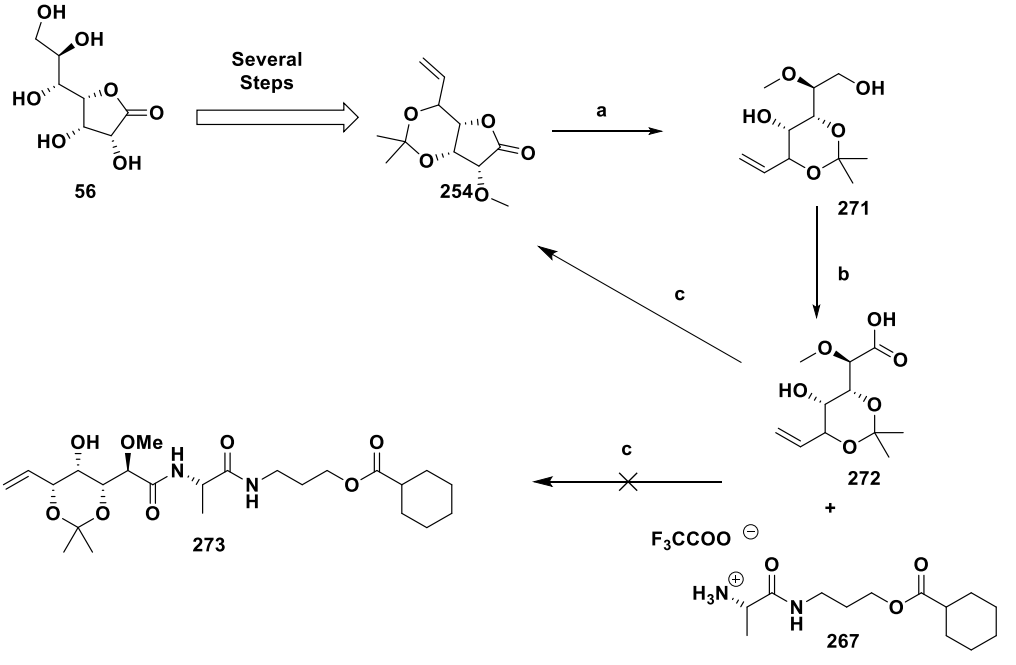

Scheme 24. Synthetic strategy A to obtain precursor **273.**

Reagents and conditions. (a) **254,** $LiBH_4$, THF, 25 ºC, 12 h, 40%. (b) **271,** TEMPO, BAIB, CH_3CN:H_2O (1:1), 25 ºC, 3 h. (c) **272, 167**, BOP, DIPEA, DMF, 25 ºC, 12 h.

Synthesis B. Synthesis from the *D*-tartaric acid **50**[139]

After obtaining these discouraging results through the synthesis A, the synthesis B was carried out in accordance with the synthesis described by Mukai *et al*.[161] Thus, this synthesis was started from *D*-tartaric acid **50** which was treated with methanol in presence of amberlyst-15 to obtain the methyl diester **274**. Then, next step was a protecting reaction of hydroxyl groups in positions C-3 and C-4, to obtain acetal **275**, which 2-methoxypropene was used under acidic conditions.

After the protection reaction, a reduction of this compound **275** with sodium borohydride yielded the diol **276**, which was subjected to a selective monoprotection reaction with *tert*-butyldimethylsilyl chloride (TBSCl) with sodium hydride (NaH), obtaining the mono-silyl ether **277** in 80 % (**Scheme 25**).

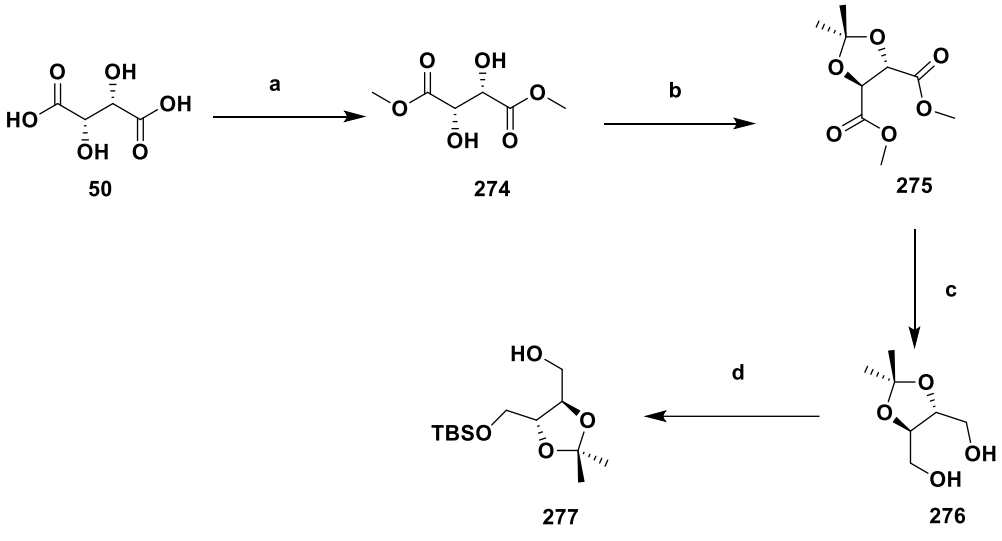

Scheme 25. Synthetic strategy to obtain the silyl ether **277.**

Reagents and conditions. (a) **50**, Amberlist-15, MeOH, Reflux, 12 h. (b) **274**, 2-Methoxipropeno, CSA, CH_2Cl_2, reflux, 12 h. (c) **275**, $NaBH_4$, MeOH, 25 ºC, 12 h, 40 % over 3 steps. (d) **276**, TBSCl, NaH, CH_2Cl_2, 25 ºC, 2 h, 80 %.

Once the alcohol **277** was obtained, a Swern oxidation reaction of this alcohol was performed to yield aldehyde **278**.[162] With this aldehyde in

hand, a Wittig reaction[163] in presence of the ylide derived from Methyltriphenylphosphonium bromide was carried out to obtain the terminal alkene **279** in 63 % over 2 steps.[164] Then, a deprotection reaction of the silyl ether group using TBAF was performed to yield the alcohol **280** in 80 %, which was subjected to a Swern oxidation reaction again to obtain the desired aldehyde **72**. This aldehyde **72** was used in a modified Wittig reaction by Martin,[165] employing tributyl phosphonium to obtain alkene *trans* **281** (**Scheme 26**).

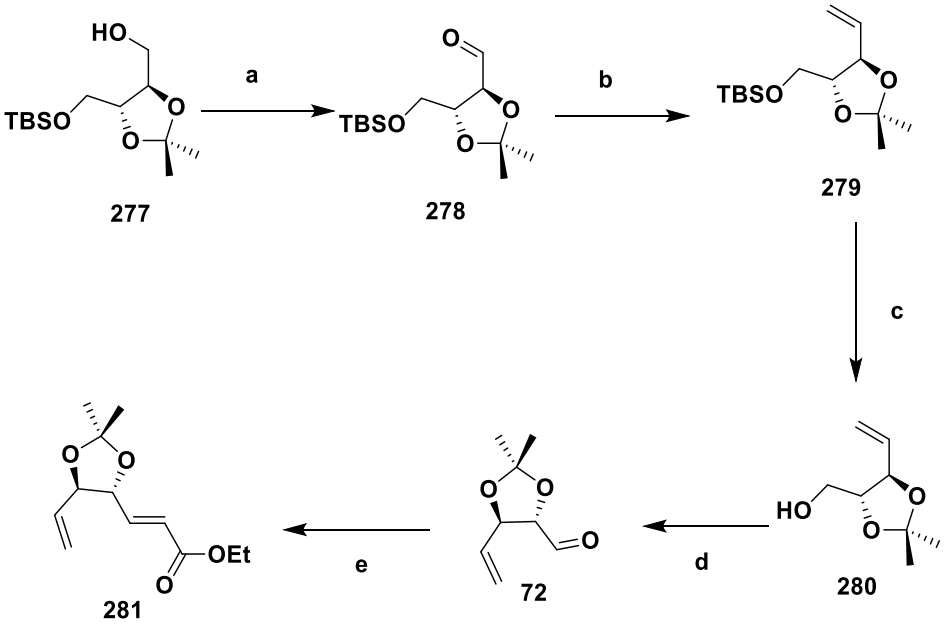

Scheme 26. Synthetic strategy towards ester **281.**

Reagents and conditions. (a) **277**, $(COCl)_2$, DMSO, TEA, CH_2Cl_2, -75 ºC, 1h. (b) **278**, Methyltriphenylphosphonium bromide, NaHMDS, THF, 25 ºC, 3h, 63% over 2 steps. (c) **279**, TBAF, 25 ºC, 1h, 80 %. (d) **280**, $(COCl)_2$, DMSO, TEA, CH_2Cl_2, -75 ºC, 1 h. (d) **72**, $Bu_3PCH_2CO_2EtBr$, NaOH, Benzoic Acid, Toluene, 90 ºC, 1 h, 70 % over 2 steps.

After a reduction reaction of the ester **281** with DIBAL-H, the resulting allylic alcohol **282**, obtained in 75 %, was subjected to a Sharpless Asymmetric Epoxidation (SAE) reaction[166] by treatment with $Ti(OiPr)_4$, *D*-(-)-DET (*D*-(-)-diethyltartrate) as chiral inductor and TBHP (*tert*-butyl hydroperoxide) obtain the key epoxy alcohol **73** in 60 %. To achieve the oxirane-

ring opening reaction, the Miyashita conditions were employed, providing in an effective way the opening product with an excellent regio- and- stereoselectivity.[132] In the event, oxirane **73** was treated with MeOH in the presence of trimethyl borate and DBU (1,8-Diazabycyclo[5.4.0]undec-7-ene) to increase the nucleophilic character of methanol. Finally, the targeted diol **283** was obtained in 83 % (**Scheme 27**).

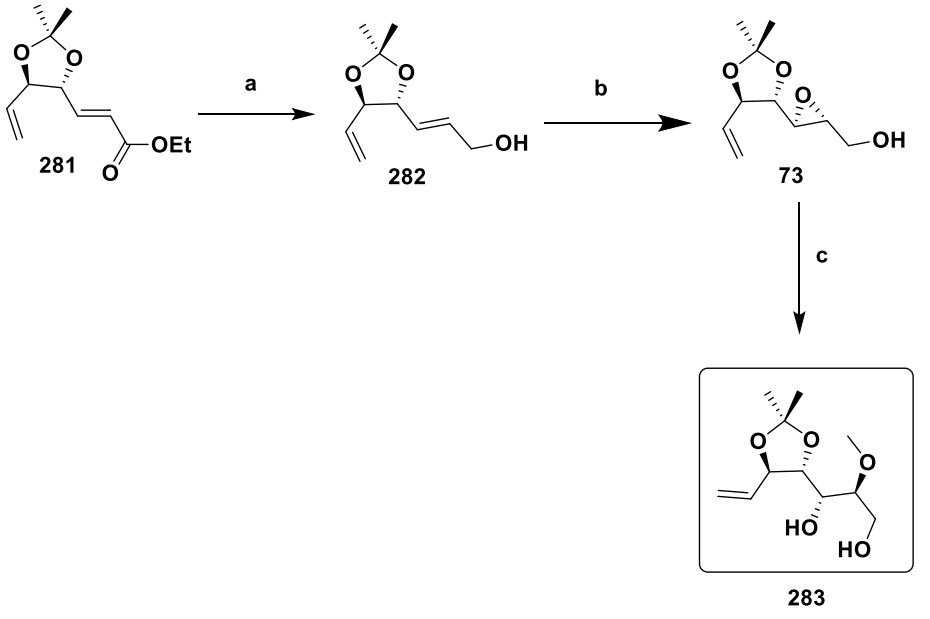

Scheme 27. Synthetic strategy to obtain key alkene intermediate **283.**

Reagents and conditions. (a) **281**, DIBAL-H, CH_2Cl_2, -78 ºC, 45 min, 75 %. (b) **282,** $Ti(OiPr)_4$, *D*-(-)-DET, TBHP, CH_2Cl_2, -20 ºC, 48 h, 60 %. (c) **73**, DBU, $B(OMe)_3$/MeOH, 70 ºC, 12 h, 83 %.

Once the product **283** was obtained, an Olefin Cross Metathesis was undertaken to obtain the disubstituted alkene **283** by using Hoveyda-Grubbs 2nd generation as a catalyst.[167,168] However, the high sensitivity of this reaction required a strict inert atmosphere and anhydrous solvent to obtain the desired *trans* alkene. Finally, the reaction worked obtaining the alkene **284** in a yield of 40 % and recovering starting material which could be employed for to an Olefin Cross Metathesis again (**Scheme 28**).

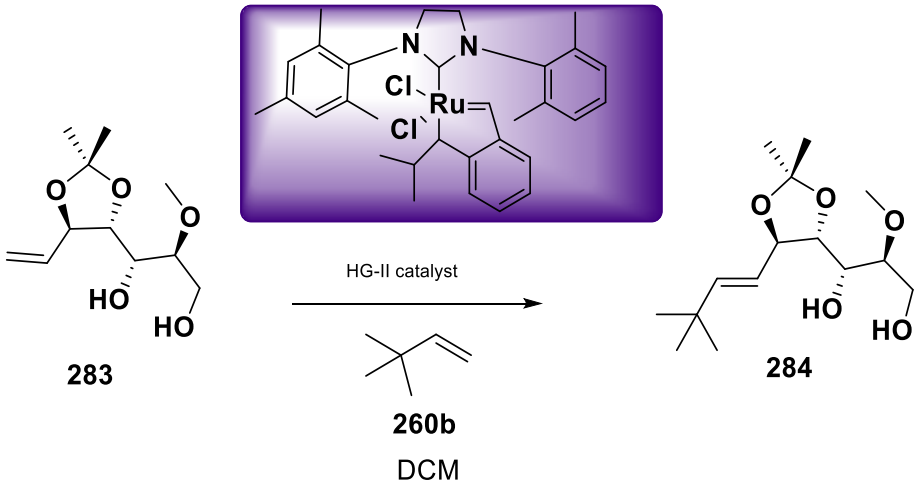

Scheme 28. Olefin Cross Metathesis.

Reagents and conditions. **283**, **260b**, Grubbs catalyst, CH_2Cl_2, 40 ºC, 12 h, 40 %.

At this point of the synthesis, the next step would consist in an oxidation and subsequent coupling with the *L*-alanine derivative amino acid **267**. Thus, the system TEMPO/BAIB (bisacetoxyiodobenzene) was employed to achieve the chemoselective oxidation of alcohol primary versus the secondary, yielding the acid **287**.[169] Then, this acid was coupled with **267** using the coupling agent benzotriazole-1-yl-oxy-tris-(dimethylamino)-phosphonium hexafluorophosphate BOP and the base diisopropylethylamine (DIPEA).[149] Unexpectedly, the reaction did not work, obtaining degradation products instead. The most likely reason of this result is the presence of Grubbs catalyst in the product **284** which could affect the oxidation reaction. It was decided then that the best method to avoid this problem was a change on the steps order of the synthesis. Then, the oxidation reaction was performed over alcohol **283** and coupled with **267** under the same conditions which were mentioned before. Fortunately, there was a significant positive result by using this strategy obtaining the coupled product without any problem (**Scheme 29**).

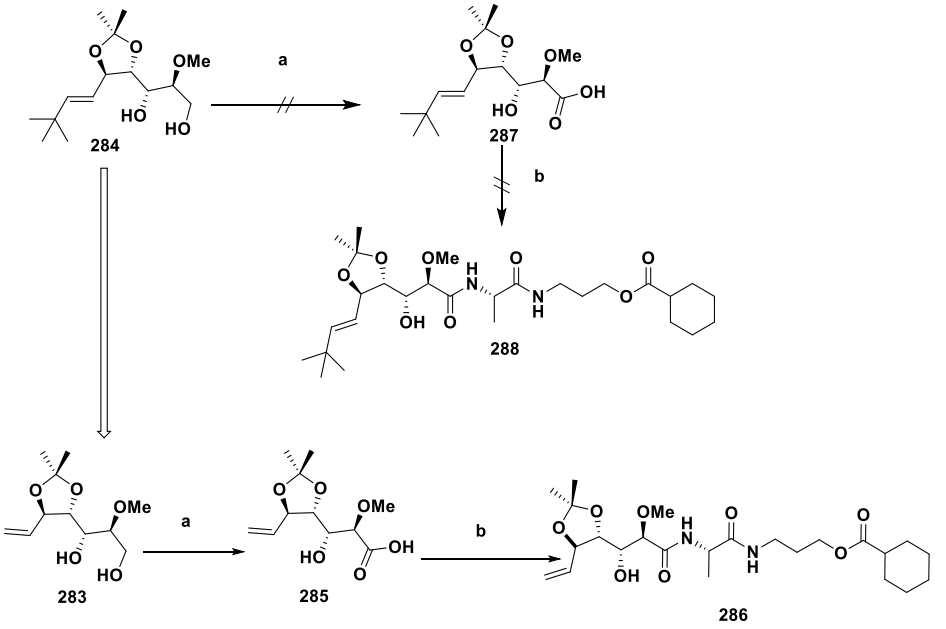

Scheme 29. Synthetic strategy towards alkene precursor **288.**

Reagents and conditions. (a) **283**, TEMPO, BAIB, CH_3CN:H_2O (1:1), 25 ºC, 3h. (b) **285, 267**, BOP, DIPEA, DMF, 25 ºC, 12h, 40 % over 2 steps.

Once the coupled product was obtained, an olefin cross metathesis was tested using the same conditions which were employed before to incorporate the *E*-alkene. However, the reaction failed, and the only product obtained was the staring material, **284**. Then, different conditions of this reaction were tested (**Table 15**) concluding that the best condition was the use of toluene as solvent to increase the temperature reaction and using the alkene 3,3-dimethylbut-1-ene (**260b**) as co-solvent.

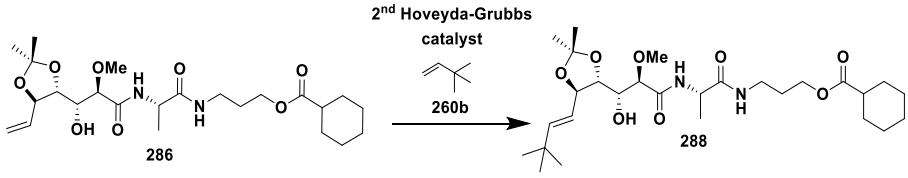

Table 15. Optimization of Olefin Cross Metathesis reaction.

Entry	Alkene	Grubbs catalyst	Solvent	Temperature	Yield
1	1.00 equiv.	0.15 equiv.	DCM	40 ºC	-
2	1.00 equiv.	0.25 equiv.	DCM	40 ºC	5 %
3	1.00 equiv.	0.25 equiv.	Toluene	80 ºC	20 %
4	Co-solvent	0.25 equiv.	Toluene	80 ºC	50 %

As **Table 15** shows, the best value of the yield of the Cross Olefin Metathesis was observed when the alkene was used in a considerable excess and the temperature was increased to 80 ºC by change the solvent with toluene.

Finally, the last step to obtain the analogue **145** in a large amount (150 mg) was the acidic hydrolysis of the acetal group, obtaining finally **145** which was employed for the *in vivo* studies (**Scheme 30**).

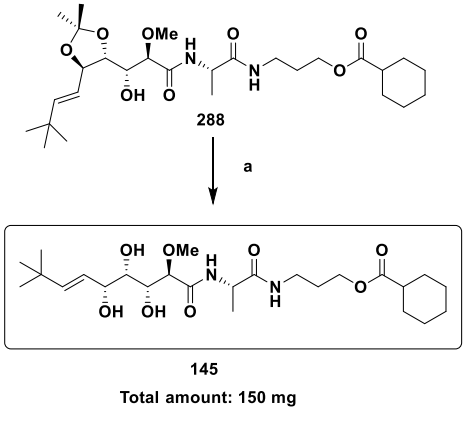

Scheme 30. Hydrolysis of precursor **288.**

***Reagents and conditions*.** (a) **288**, AcOH/H_2O, MeOH, 80 ºC, 2 h, 89 %.

*3.3.6. Advanced biological essays for bengamide analogue **145***

At this stage of the work, the analogue **145** was available in sufficient amount and ready for *in vivo* biological studies. These studies were conducted in collaboration with the group of Prof. José Prados and Prof. Consolación Melguizo from the Department of Anatomy and Embryology of Granada University.[170]

In vitro biological evaluation against different tumoral cell lines

The cytotoxic effects of bengamide **145** were assessed in a range of 21 cell lines, both tumoral and non-tumoral, with diverse origins including breast, pancreas, lung, brain, colon, and liver. This evaluation was conducted after 72 hours of drug exposure, and the IC_{50} (half-maximal inhibitory concentration) for each cell line was computed (as shown in **Table 16**)

Table 16. Determination of IC_{50} (μM)[c] of **145** in different cell lines.

Organ	Cell line	Bengamide 145
Breast	MCF7	0.50 ± 0.15
	MDA-MB-231	5.00 ± 0.07
	SKBR3	25.92 ± 8
	MCF10A	1.82 ± 0.31
	E0771	19.54 ± 1.27
Pancreas	Panc1	4.04 ± 0.61
	Panc2	1.09 ± 0.19
Lung	A549	0.41 ± 0.2
	NCI-H460	0.16 ± 0.02
	NCI-H520	> 75
	H69	4.80 ± 1.52
	Ñ132	1.04 ± 0.17
	LL2	4.02 ± 0.72
Brain	SK-N-SH	8.97 ± 1.02
	A172	1.11 ± 0.23
	SF468	29.52 ± 1.93
	LN229	1.35 ± 0.46
Colon	T84	1.35 ± 0.28
	CCD18Co	> 75
	Mc38	28.88 ± 4.14
Liver	HepG2	14.98 ± 0.58

[c] Half-maximal inhibitory concentration (IC_{50}) values calculated from dose-response curves as the concentration of compound that inhibits cell survival by 50% compared to control. They are expressed as means ±SD of triplicate samples each.

As can be observed in **Table 16**, the IC_{50} values displayed a wide range, spanning from 0.16 to greater than 75 μM. The most significant impact on cell viability was observed in the lung cancer cell lines NCI-H460 and A549, with IC_{50} values of 0.16 ± 0.02 and 0.41 ± 0.2 μM, respectively.

Among the three non-tumour cell lines which were included in the *in vitro* assay, two exhibited IC_{50} values similar to those of the tumour cell lines: 1.82 ± 0.31 and 1.04 ± 0.17 μM for MCF10A and L132, respectively. However, the colon non-tumour cell line, CCD18Co, had an IC_{50} value exceeding 75 μM.

In the case of murine tumour cell lines, the one from the pancreas (PANC2) and the one of pulmonary origin (LL2) showed a substantial reduction in viability with IC_{50} values of 1.09 ± 0.19 μM and 4.02 ± 0.72 μM, respectively. In contrast to the cell lines from breast, E0771 (IC50 = 19.54 ± 1.27 μM), and colon, MC38 (IC50 = 28.88 ± 4.14 μM).

In conclusion, the low IC_{50} of bengamide **145** in PANC2 and LL2 cell lines made them particularly interesting candidates for *in vivo* assays in immunocompetent mice.

Bengamide **145** reduces the colony-forming capacity of lung tumour cell lines

In the colony formation assay, all four lung cell lines treated with IC_{10} and IC_{25} concentrations of bengamide **145** exhibited a decreased ability to form colonies when seeded at low cell density (**Figure 32**). At the IC_{25} dose of bengamide **145** (0.1 μM for A549 and NCIH460, 3 μM for LL2, and 0.4 μM for L132), all cell lines displayed nearly complete suppression of colony formation, with statistically significant differences observed in all cases.

Furthermore, the fraction of cells resistant to treatment with an IC_{50} concentration of bengamide **145** for 72 hours showed a minor reduction in colony-forming ability compared to the control. However, this reduction was not statistically significant in any of the cell lines.

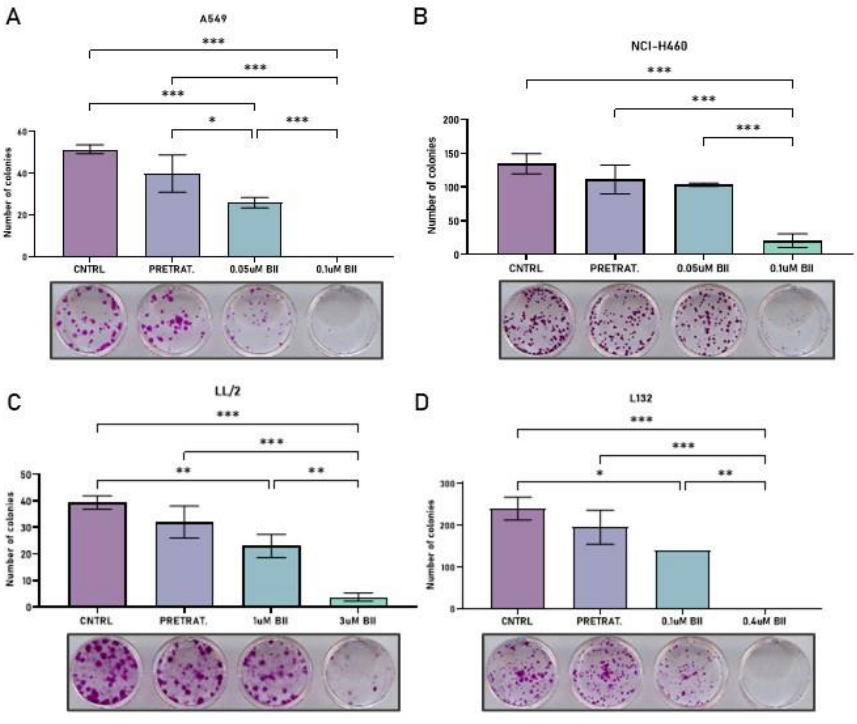

Figure 32. Effect of bengamide **145** on colony formation capacity. Colony growth analysis of A549 (A), NCIH460 (B), LL2 (C) and (D) L132 after IC_{50} bengamide **145** pretreatment (72 h) and after IC_{10} and IC_{25} bengamide **145** treatment. Data are presented as mean ±SD of three replicates. * $p < 0.05$, ** $p < 0.01$ and *** $p < 0.001$.

Bengamide **145** inhibits the growth of multicellular tumor spheroid (MTS) of lung tumor cell lines.

Multicellular Tumour Spheroids (MTS) were employed to investigate the effects and penetration of bengamide **145** in a three-dimensional system that mimics 3D tumours *in vivo*. As can be observed in **Figure 33**, cell viability at the end of the experiment (after 9 days), exhibited a significant reduction in all the cell lines studied, even when no differences in MTS volume were observed, as evidenced in the case of the A549 cell line.

In addition to a decrease in viability, the other cell lines also showed a reduction in MTS size for the different treatments (IC_{50}, $2IC_{50}$, and $4IC_{50}$) compared to the control. Furthermore, there were variations in MTS size between different treatment doses, indicating a dose-dependent

response. Specifically, NCIH460 MTS treated with bengamide **145** (0.15, 0.3, and 0.6 μM, corresponding to IC_{50}, $2IC_{50}$, and $4IC_{50}$) displayed reductions in size of 15.7%, 26%, and 36.6%, respectively, by day 9 (**see Figure 33B**).

The murine lung cancer cell line LL2 exhibited the most noticeable size differences, with reductions of 49.2%, 65.6%, and 80.2% (at concentrations of 4, 8, and 16 μM, corresponding to IC_{50}, $2IC_{50}$, and $4IC_{50}$) compared to the control at the end of the experiment (**Figure 33C**).

Finally, the L132 cell line also showed size differences at the end of the experiment, but it was the cell line in which the effects of the drug on MTS size took the longest time to appear (**Figure 33D**).

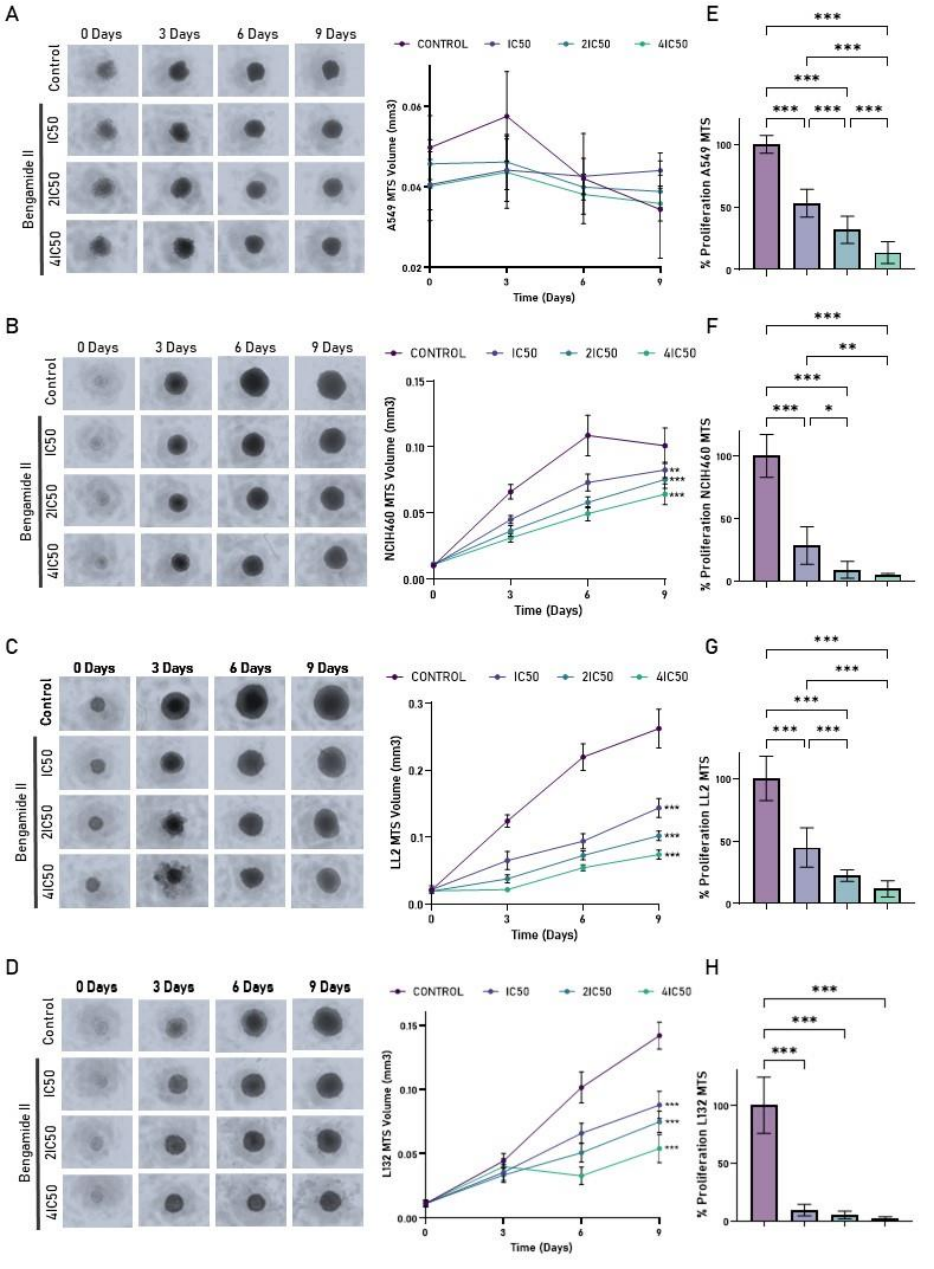

Figure 33. Analysis of Multicellular Tumour Spheroid (MTS) growth modulation by bengamide **145**. Representative images and Graphic representation of A549 (A), NCIH460 (B), LL2 (C) and L132 (D) volume (mm^3) monitorization at different times after exposure to different doses of bengamide **145** (IC_{50}, $2IC_{50}$ and $4IC_{50}$). Untreated MTS were used as control. Data represent the mean value ± SD of 10 replicates. ** $p < 0.01$ and *** $p < 0.001$ vs. control group. CCK8 analysis of A549 (E), NCIH460 (F), LL2 (G) and L132 (H) MTS at day 9. Data represent the mean value ± SD of 10 replicates. * $p < 0.05$, ** $p < 0.01$ and *** $p < 0.001$.

Modulation of Cell Cycle by bengamide **145**

The A549 and LL2 (lung cancer) cell lines treated with bengamide **145** exhibited statistically significant changes in cell cycle analysis. Specifically:

- In the A549 cell line, there was a statistically significant ($p < 0.001$) increase in the G2/M phase with bengamide **145** treatment at all evaluated time points. Additionally, at longer treatment times (24 and 48 hours), an arrest in the G0/1 phase was observed (**see Figure 34A**).
- Similar results to A549 were observed in the LL2 cell line, with an arrest in the G2/M phase seen at 12 and 48 hours of treatment (**see Figure 34B**).
- In the LL2 cell line, there was also a progressive increase in subG1-phase cells observed with longer treatment times compared to the baseline condition, as depicted in **Figure 34D**. These differences were less pronounced in the A549 cell line, as shown in **Figure 34C.**

The induction of cell cycle arrest in the G2/M phase by **145** was similarly observed in a study conducted by Garcia Pinel *et al*. using the colon cancer cell line T84.[160] Furthermore, Philips *et al.* revealed arrest in G1 and G2/M phases of cell cycle, data supported by western blot analysis of key cell cycle regulators.[44]

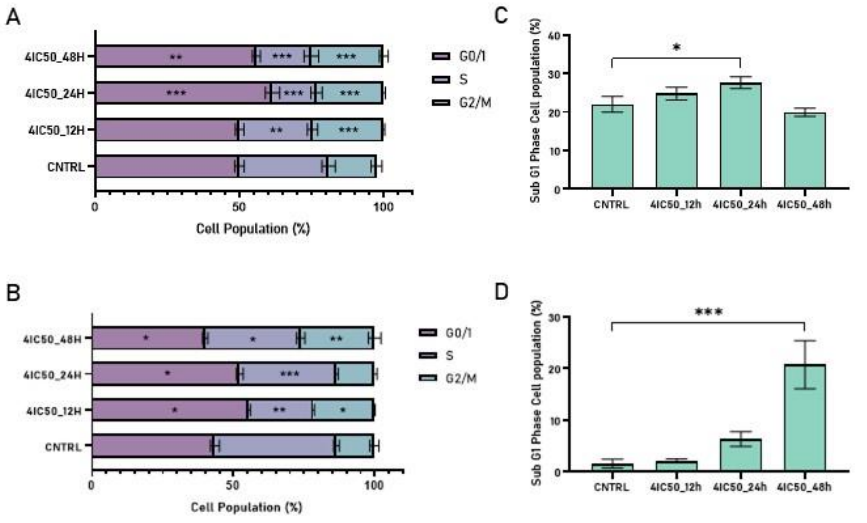

Figure 34. Cell cycle modifications in lung cancer cell lines treated with bengamide **145**. Graphical representation of $G_{0/1}$, S and G_2/M phases of cell cycle analysis after treatment with 4IC50 of bengamide **145** at different time points (12, 24 and 48 h) in A549 (A) and LL2 (B) cell lines. Modulation Sub G_1 cell cycle phase by bengamide **x** in A549 (C) and LL2 (D). Data represent the mean value ± SD of 3 replicates. * $p < 0.05$, ** $p < 0.01$ and *** $p < 0.001$ vs. control group.

Molecular mechanisms of bengamide **145** treatment

To investigate the molecular mechanism of cell death induced by bengamide **145**, various proteins associated with apoptosis mechanisms, including caspases 3, 8, and 9, as well as PARP1 and VEGFA, were examined in both the human non-small lung cancer cell line A549 and the murine lung cancer cell line LL2. Here are the key findings:

- Caspase 3: bengamide **145** induced the activation of caspase 3 in the A549 cell line. Furthermore, an increase in caspase-3 cleavage was observed at longer treatment times (48 hours) compared to shorter durations and the control (**Figure 35A**).
- Caspase 8: there was increased activation of caspase 8 in both cell lines treated with bengamide **145**, indicating it is involvement in the apoptosis process (**Figure 35A**).

- Caspase 9: in contrast, bengamide **145** treatment did not appear to significantly increase caspase 9 activation, suggesting a potential differential role in the apoptosis pathway (**Figure 35A**).
- PARP1: the expression of PARP1 in the A549 cell line seemed to be largely unaffected by bengamide **145** treatment. However, in the murine LL2 cell line, a decrease in PARP1 protein was observed at longer treatment times (**Figure 35B**).
- VEGFA: The expression of VEGFA displayed a progressive decrease that was inversely correlated with the duration of treatment with bengamide **145** in both cell lines (**Figure 35B**). Therefore, this suggests a potential role of bengamide **145** in regulating VEGFA expression.

These findings shed light on the molecular mechanisms underlying the effects of bengamide **145** on these cell lines, particularly in relation to apoptosis and the regulation of specific proteins involved in cell survival and angiogenesis.

Moreover, a RT-qPCR (quantitative reverse transcription polymerase chain reaction) analysis was conducted to assess the modulation of genes associated with various aspects, including stemness (SOX2, NANOG, OCT4, CD133, CD44), DNA methylation (DNMT1), DNA repair (PARP1), epithelial phenotype (EPCAM), malignancy and proliferation (STAT3, EGFR, Ki67), and cell resistance to treatment (MDR1) following exposure to bengamide **145** treatment for 72 hours. The results revealed the following effects of bengamide **145** on gene expression in different cell lines:

- In the A549 cell line, treatment with bengamide **145** at IC_{50} doses significantly decreased the expression of CD133 and NANOG while increasing the expression of SOX2 and EPCAM (**Figure 35C**).
- Similar outcomes were observed in the NCIH460 cell line, with the downregulation of CD133 and NANOG following bengamide **145**

treatment. Additionally, there was a reduced expression of OCT4, CD44, and EPCAM in response to bengamide **145** treatment (**Figure 35D**).

- In the L132 cell line, only a slight, yet statistically significant, increase in NANOG expression was observed when treated with bengamide **145** (**Figure 35E**).
- The murine LL2 cell line showed an increase in the expression of STAT3 and Ki67, and a more modest increase in PARP1 and EGFR in response to bengamide **145** treatment (**Figure 35F**).

In conclusion, these findings indicate that bengamide **145** treatment has varying effects on the expression of genes related to different biological processes, depending on the specific cell line being studied. It suggests that bengamide **145** may influence various cellular pathways and processes associated with cancer cell behaviour and response to treatment.

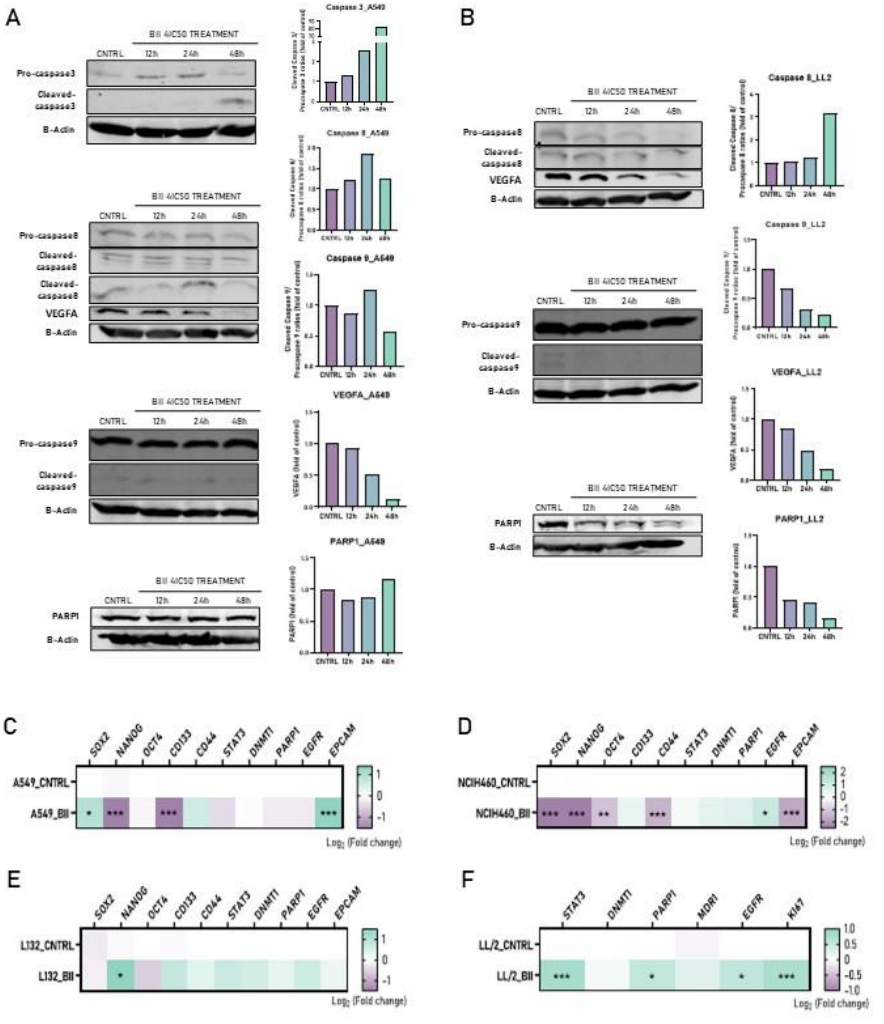

Figure 35. Western Blot and RT-qPCR analysis. Representative Western Blot and densitometric analysis of Caspase 3, 8 and 9, PARP1 and VEGFA protein expression in A549 (A) and LL2 (B) lung cancer cell lines untreated (CNTRL) and treated with 4IC50 of bengamide **145** at different time points (12. 24 and 48 h). β-actin was used as an internal control. RT-qPCR analysis of SOX2, NANOG, OCT4 CD133, CD44, STAT3, DNMT1, PARP1, EGFR and EPCAM gene expression after bengamide **145** treatment in A549 (C), NCIH460 (D), L132 (E) cell lines and STAT3, DNMT1, PARP1, MDR1, EGFR and Ki67 gene expression after bengamide **145** treatment in LL2 (E) cell line. Data are represented as mean value of Log2 (fold change) ± SD compared to each control. * $p < 0.05$, ** $p < 0.01$ and *** $p < 0.001$.

In vivo toxicity assay

In a toxicity assay conducted to determine the highest dose of bengamide **145** that could be administered to mice without toxic effects, three doses were tested: 10, 20, and 30 mg bengamide **145** per kilogram of mouse (n=5 per group). The results are as follows:

- The group treated with the highest dose (30 mg/kg) displayed toxicity after four days of treatment, which occurred during the second treatment cycle. One mouse exhibited a decrease in body weight and subsequently died. This event was repeated in the third treatment cycle with another individual (**Figure 36 A**). As a result, treatment with this dose was discontinued and eliminated from further experiments. However, the remaining mice were kept alive for continued monitoring.
- On the other hand, the treatment groups administered with 10 and 20 mg bengamide **145** per kilogram of mouse retained all individuals alive at the end of the experiment. No noticeable alterations in health status or body weight were observed in these groups (**Figure 36 B**).

As a result of this biological study, it indicates that the 30 mg/kg dose of bengamide **145** had toxic effects in mice, while the 10 mg/kg and 20 mg/kg doses were well-tolerated and did not result in significant adverse effects on the mice's health or body weight.

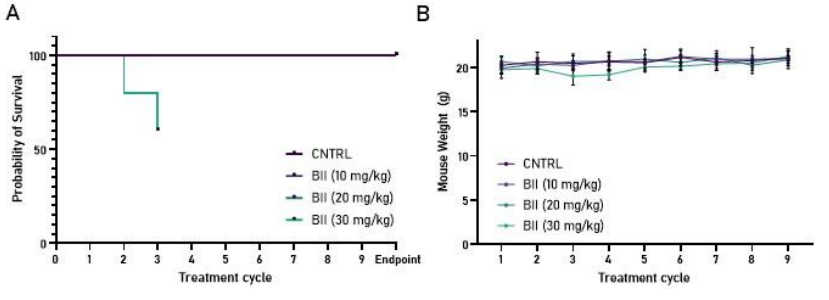

Figure 36. *In vivo* toxicity assay. (A) Survival plot of different mice treated group. (B) Mouse weight monitorization among treatment cycles.

Subsequent analysis of mice blood to evaluate the potential impact of different treatment doses on hematological parameters revealed no significant abnormalities. This suggests that there was no observed toxicity in any of the treatment groups, indicating that the hematological parameters remained within normal ranges (**Table 17**).

Table 17. Hemogram of control and bengamide **145** treatment groups at the end point of in vivo toxicity test.

Parameters	CNTRL	Bg (10 mg/kg)	Bg(20 mg/kg)	Bg (30 mg/kg)
WBC (10^3/µl)	2.12 ± 0.97	3.15 ± 0.45	3.06 ± 1.38	6.72 ± 1.14
RBC (10^6/µl)	8.72 ± 0.54	8.96 ± 0.31	9.11 ± 0.29	9.35 ± 0.22
HGB (g/dL)	14.11 ± 0.59	20.15 ± 1.38	-	18.7 ± 1.24
HCT	40.33 ± 2.59	41.17 ± 1.77	42.31 ± 1.28	43.65 ± 1.26
PLT (10^3/µl)	246 ± 69.05	664.63 ± 61.37	687.9 ± 39.98	716 ± 94.34
LYM (%)	91.91 ± 5.17	96.51 ± 1.46	95.58 ± 1.23	96.23 ± 0.58
MON (%)	0.47 ± 0.33	0.29 ± 0.12	0.15 ± 0.12	0.38 ± 0.15
NEU (%)	3.88 ± 1.95	1.85 ± 0.64	3.29 ± 0.98	2.7 ± 0.36
EOS (%)	1.07 ± 0.62	0.41 ± 0.41	0.18 ± 0.15	0.07 ± 0.05
BAS (%)	0.7 ± 0.46	0.4 ± 0.24	0.8 ± 0.32	0.62 ± 0.24
RDW	14.85 ± 0.52	14.72 ± 0.52	14.77 ± 0.29	15.15 ± 0.41
MPV (fL)	6.47 ± 0.52	5.92 ± 0.43	5.63 ± 0.08	5.73 ± 0.2
PCT	0.22 ± 0.12	0.33 ± 0.12	0.39 ± 0.02	0.33 ± 0.13
PDW	30.82 ± 8.37	23.52 ± 7.43	18.55 ± 1.27	22.28 ± 7.95

WBC = Total number of white blood cells; RBC = Total number of red blood cells; HGB = Hemoglobin; HCT = % Volume of blood occupied by red blood cells (hematocrit); PLT = Total number of platelets; LYM% = % of Lymphocytes; MON% = % of Monocytes/Macrophages; NEU% = % of Neutrophils/Polymorphonuclear leukocytes; EOS% = % of Eosinophils; BAS% = % of Basophils; RDW = Red blood cell distribution width; MPV = Mean platelet volume; PCT = % Volume of blood occupied by platelets (thrombocrit); PDW = Platelet size distribution. Data are presented as mean ± standard deviation.

Bengamide **145** treatment significantly reduces subcutaneous tumour growth

Bengamide **145** treatment demonstrated a significant reduction in subcutaneous tumour growth in a study involving the subcutaneous induction of lung tumours in C57BL/6 mice using the LL2 cell line. Here are the key findings:

- Survival and Mouse Weight: there were no discernible differences in terms of survival and mouse weight between the control group and the treatment group administered with 20 mg/kg of bengamide **145** (**Figure 37 A** and **Figure 37 B**).
- Tumour Size: significant differences in tumour size became evident starting from the third treatment cycle. After nine treatment cycles, the group treated with bengamide **145** exhibited a substantial decrease in tumour volume, amounting to 43 % when compared to the control group (**Figure 37 C**).
- Tumour Weight: The data on tumour volume was corroborated by weighing the excised tumours at the end of the experiment. The treated group displayed a 33.6 % reduction in tumours weight (**Figure 37 D**).
- Gene Expression Analysis: RT-qPCR gene expression analysis was performed on tumours tissue from all surviving mice at the end of the experiment. Among all the cancer-related genes studied, only EPCAM showed a significant decrease in the group treated with bengamide **145** compared to the control group (**Figure 37 E**).

These results conclude that bengamide **145** treatment effectively reduced subcutaneous tumours growth in the experimental model, with minimal impact on mouse health and weight. Furthermore, changes in the expression of certain genes, such as EPCAM, were observed in the tumours tissue, suggesting potential alterations in cancer-related processes.

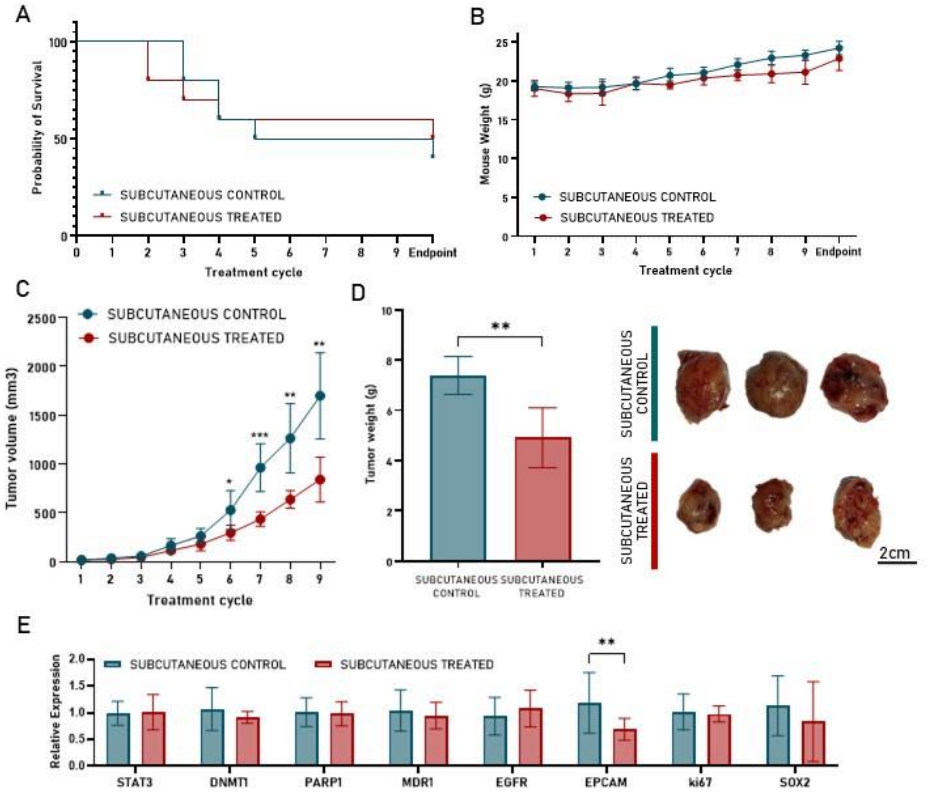

Figure 37. *In vivo* subcutaneous tumour induction and follow up after treatment with bengamide **145**. (A) Survival plot of mice after 9 bengamide **145** treatment cycles. (B) Graphical representation of mice weights measured in each treatment cycle. Measurements were taken every 3 days and monitored for 21 days. (C) Graphical representation of subcutaneous tumour volume growth in C57BL/6 mice generated from the LL2 cell line. Untreated mice were used as controls. (D) Illustrative images subcutaneous tumour size and representation of subcutaneous tumour weight in C57BL/6 mice at the experiment end point. (E) RT-qPCR analysis of *STAT3*, *DNMT1*, *PARP1*, *MDR1*, *EGFR*, *EPCAM*, *KI67* and *SOX2* gene expression in tumours from subcutaneous control and treated mice groups. Data represent the mean value ± SD. * $p < 0.05$, ** $p < 0.01$ and *** $p < 0.001$ vs. control group.

Treatment with bengamide **145** significantly inhibited the formation of metastases from LL2

In an experiment involving the injection of LL2 cells through the tail vein, which results in pulmonary metastasis in C57BL/6 mice, the potential

impact of bengamide **145** treatment on the development of metastatic nodules in the lungs was assessed. The following observations were made:

- Survival: intriguingly, the bengamide **145**-treated metastatic group exhibited significantly prolonged survival compared to the metastatic control group (**Figure 38 A**), with a *p*-value of 0.019. This suggests a potential beneficial effect of bengamide **145** in this metastatic model.
- Mouse Weight: there were no significant differences in the weight of mice between the metastatic control group and the metastatic treated group (**Figure 38 B**). This indicates that bengamide **145** treatment did not adversely affect the weight of the mice.
- Metastatic Evaluation: Metastases were evaluated by examining the gross morphology of the thoracic cavity (**Figure 38 C**) and the weight of the lungs (**Figure 38 D**) at the end of the experiment. The metastatic control group showed more pronounced pathology compared to the bengamide **145**-treated mice.

Overall, these findings suggest that bengamide **145** treatment had a positive impact on survival and reduced the pathology associated with pulmonary metastases in this experimental model.

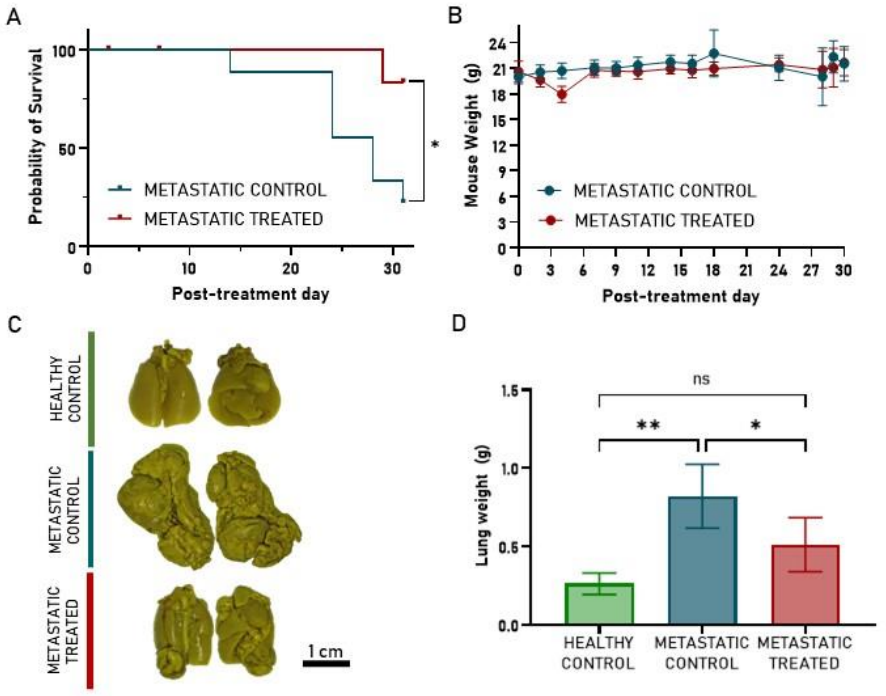

Figure 38. *In vivo* metastatic model induction and follow up after treatment with bengamide **145**. (A) Survival plot of mice after 9 bengamide **145** treatment cycles. (B) Graphical representation of mice weights measured in each treatment cycle. Measurements were monitored for 30 days. (C) Illustrative images of thoracic cavity of C57BL/6 metastatic model mice generated from the LL2 cell line. Untreated mice were used as controls. (D) Graphical representation of lung weight in C57BL/6 mice at the experiment end point.

3.4. Synthesis of new analogues of bengamide

*3.4.1. Structural modification of analogue **145***

Considering the promising results of analogue **145**, it was decided to modify the structure of this potent product. Specifically, the *L*-alanine residue would be replaced by the introduction of new amino acids. Hence, a *L*-azetidine residue was introduced instead of *L*-alanine analogue with the aim of providing rigidity to this compound which could be positive to enhance the interaction with the target MetAPs as shown in **Scheme 31**.

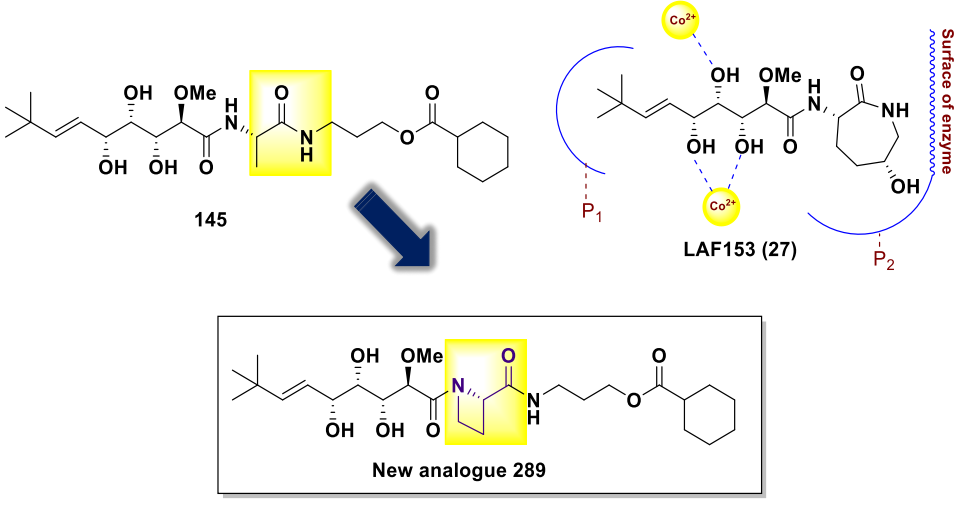

Scheme 31. Structural modification to new potent analogue of bengamide.

First, the *L*-azetidine derivative was prepared following the synthesis which is showed in **Scheme 32**. Thus, the synthesis of this amino acid derivative started from the acid of *L*-azetidine which was protected as the *N*-Boc to yield 47. Then, this compound **291** was coupled with **293** by treatment with 1-ethyl-3-(3-dimethylaminopropyl)carbodiimide hydrochloride (EDC), hydroxybenzotriazole (HOBt) and diisopropylethylamine (DIPEA) in DCM to yield the desired peptide **294** residue in 72 %.

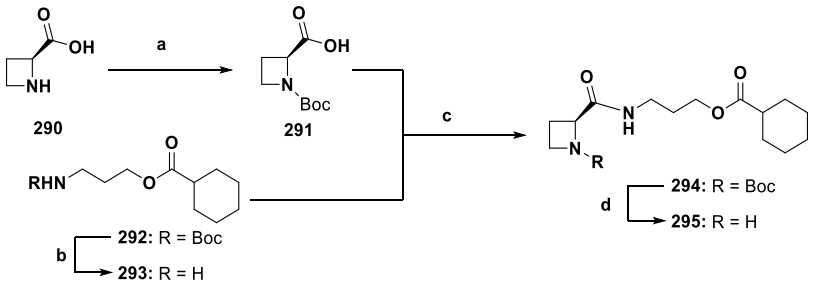

Scheme 32. Synthesis towards *L*-azetidine derivative **294.**

***Reagents and conditions*.** (a) **290**, Boc_2O, NaOH, EtOH:H_2O (1:1), 25 ºC, 12 h. (b) **292**, TFA, CH_2Cl_2, 25 ºC, 1 h. (c) **291**, **293**, EDC, HOBt, DIPEA, CH_2Cl_2, 25 ºC, 12 h, 72 % over 2 steps. (d) **294**, TFA, CH_2Cl_2, 25 ºC, 1 h.

Once the protecting group of **294** was removed using trifluoroacetic acid, the compound **295** was coupled with the acid **285** employing benzotriazol-1-yloxytris(dimethylamino)phosphonium hexafluorophosphate (BOP) and diisopropylethylamine (DIPEA), as previously employed to obtain the analogue **145,** obtaining **296** in 70 %. The coupled product **296** was then subjected to the formation of the disubstituted alkene through an olefin cross metathesis by the action of the 2nd generation Hoveyda-Grubbs as catalyst to obtain precursor **297** in 27 %. Finally, after an acidic hydrolysis of acetal group the coveted analogue **289** was obtained with success in 70 % (**Scheme 33**).

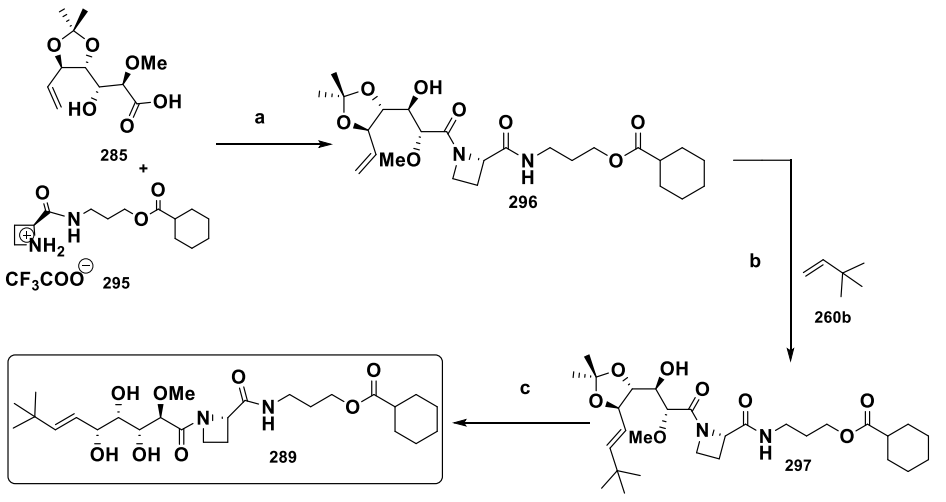

Scheme 33. Synthesis towards new bengamide analogue **289.**

***Reagents and conditions*.** (a) **286**,**295**, BOP, DIPEA, DMF, 25 ºC, 12 h, 70 % over 2 steps. (b) **296**, **260b**, 2nd Hoveyda-Grubbs catalyst, toluene, 80 ºC, 27 %. (c) **297**, AcOH aq, MeOH, 70 ºC, 70 %.

3.5. New synthetic methodology to peptidyl bengamides: Solid Phase Synthesis

3.5.1. Synthetic strategy towards new peptidyl bengamide analogues

To understand how the modification of the caprolactam ring of the natural bengamides affects to their antitumoral activity, we decided to explore the replacement of the caprolactam ring for ta collection of dipeptidyl derivatives, for which a new methodology required to be designed. Thus, this new methodology was based on the solid phase synthetic strategy, which could be a fast and efficient synthesis for these new analogues as shows **Scheme 34**. The interest of these new peptidyl analogues is based on two reasons:

1. The study of the structural behaviour of open-chain analogues that showed high activity according to the analogues developed by Nan *et al*.[146]

2. Better solubility in water compared to their natural congeners.

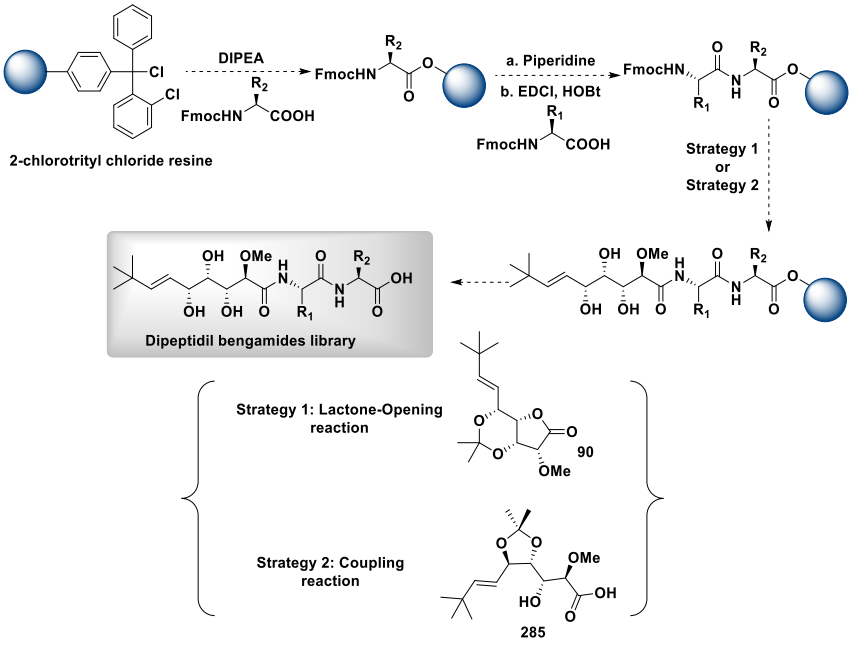

Scheme 34. Design of new peptidyl analogues of bengamides.

With the aim of developing this new synthetic methodology, two strategies were proposed:

1. Opening reaction of lactone **90** with dipeptides loaded on a solid support.
2. Coupling reaction between the acid **285** with dipeptides in solid-phase dipeptides.

3.5.2. Peptide synthesis

Initially, to complete the synthetic proposal (**Scheme 34**) different amino acids or dipeptides were prepared following the methodology which is showed in the **Scheme 35.**[171] Thus, amino acid and dipeptide were synthetized on a 2-chlorotrityl chloride (CTC) resin using the Fmoc strategy.[172,173] In this way, Fmoc-*L*-alanine was linked on to the CTC resin by esterification with *N,N*-diisopropylethylamine (DIPEA) to obtain resin **291**.

After removing the Fmoc (9-fluorenylmethoxycarbonyl) group by treatment with 20% of piperidine in *N,N*-dimethylformamide (DMF), this amino acid resin **299** was used in different test reactions to validate strategy synthetic 1 as well as synthetic strategy 2 (**Scheme 35**) as described later.

On the other hand, to obtain two new analogues of dipeptidyl bengamides the Fmoc amino acid derivative, Fmoc-*L*-alaline-OH, was loaded on to the resulting resin **299** by the action of the coupling agent *N,N*-diisopropylcarbodiimide (DIC) in the presence of 1-hydroxybenzotriazole (HOBt) in DMF obtaining the desired dipeptide **301**. Furthermore, following the same methodology the dipeptide resin **304** was prepared.

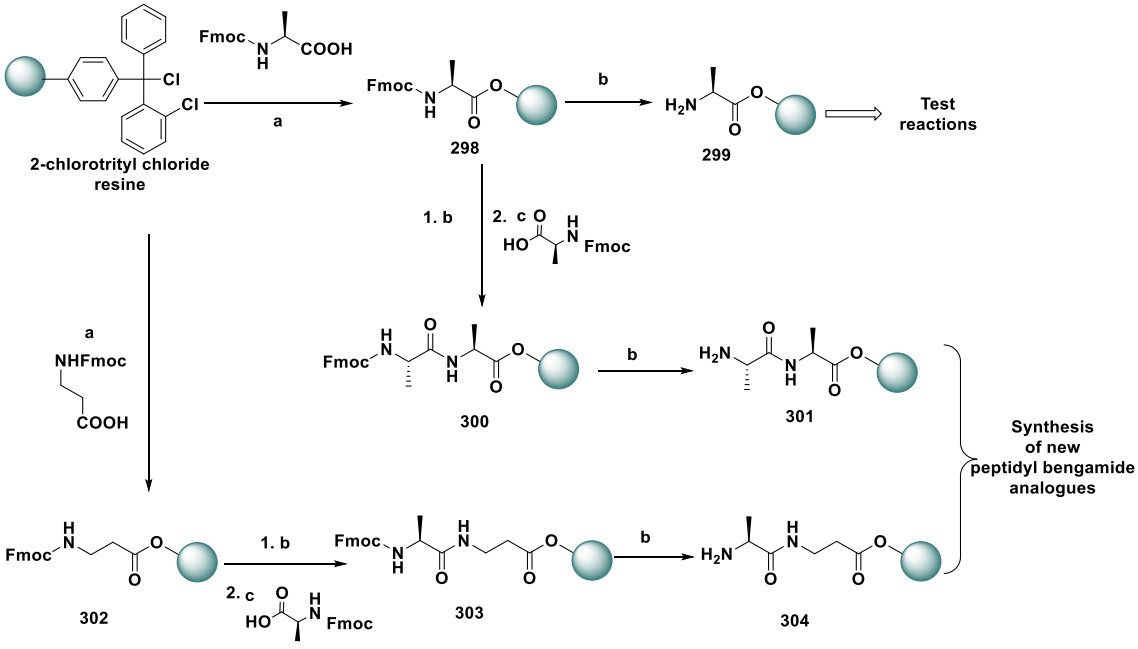

Scheme 35. Solid phase synthesis of dipeptides.

Reagents and conditions. (a) Resin CTC, DIPEA, DMF, 25 ºC, 24 h. (b) Resin, 20 % Piperidine in DMF, 25 ºC, 30 min. (c) Resin, amino acid, DIPEA, HOBt, DMF, 25 ºC, 16 h.

3.5.3. Strategy 1: Synthesis of new peptidyl analogues through opening lactone reaction

Firstly, the opening reaction of the lactone **254** with the amino acid **305** was tested in solution employing triethylamine (TEA) as base to activate the amino acid and isopropanol as solvent. Fortunately, the opening product **306** was obtained in 59 %. Finally, the acetal group was removed by the treatment with trifluoroacetic acid (TFA) to afford **307** in 69 %(**Scheme 36**).

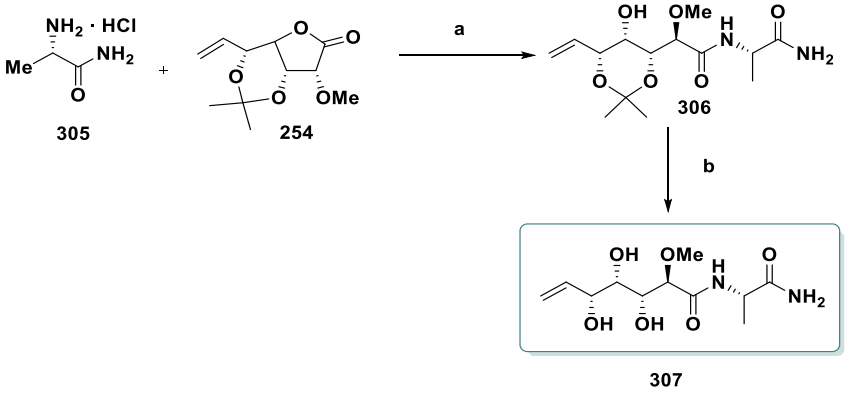

Scheme 36. Opening ring reaction of lactone **254** with amino acid **305.**

***Reagents and conditions*.** (a) **305**, **254**, TEA, *i*-PrOH, 80 ºC, 48 h, 59 %. (b) **306**, TFA, CH_3CN, 25 ºC, 3 h, H_2O, 69 %.

Considering these positive results, it was decided to extend these reaction conditions in solid phase methodology. Thus, once the resin **308** was prepared, it was used to open lactone **254** using the same conditions as mentioned before (**Scheme 37**).

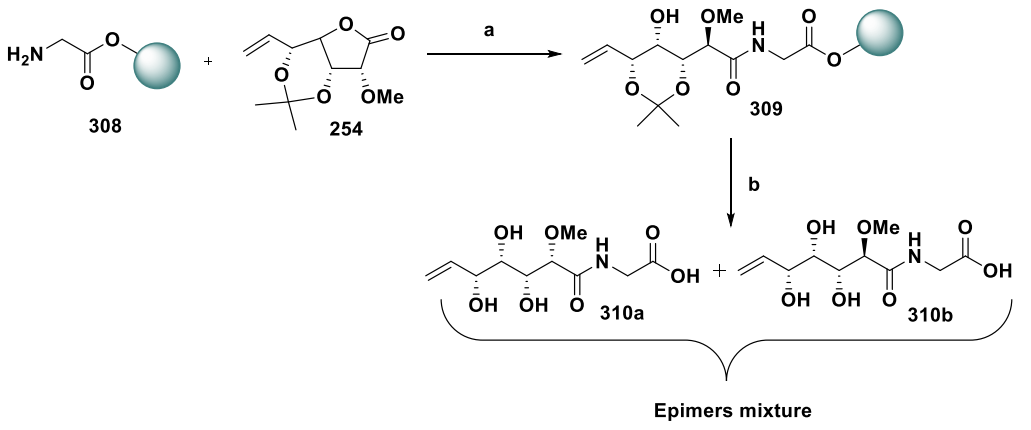

Scheme 37. Opening lactone reaction in solid phase.

Reagents and conditions. (a) **308**, **254**, TEA, *i*-PrOH, 80 ºC, 48 h. (b) **309**, TFA, CH_3CN, 25 ºC, 3 h, H_2O.

However, after cleaving the dipeptide by treatment of **309** with TFA, a mixture of different epimers was observed according to ^1H nuclear magnetic resonance spectra (NMR) (**Figure 5**).

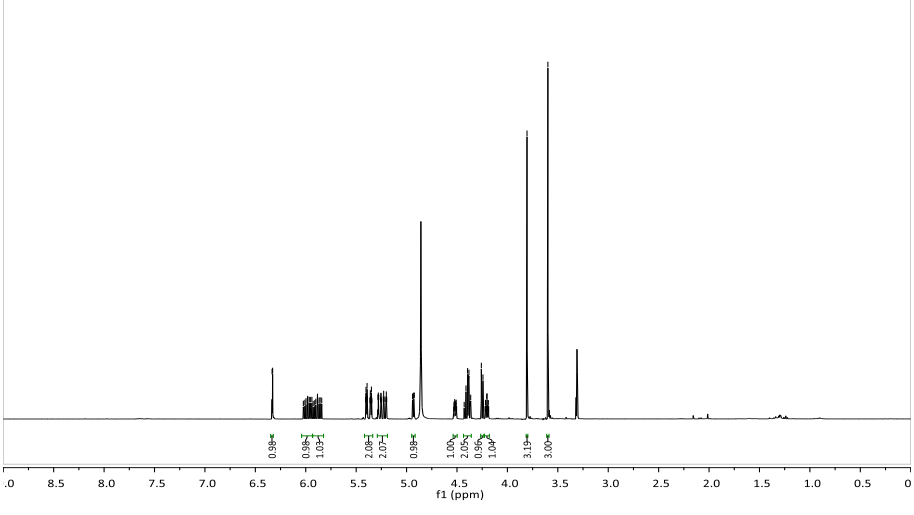

Figure 39. ^1H-NMR spectra of **310a** and **310b.**

The synthetic efforts to develop this new methodology towards bengamide analogues, different conditions were tested to obtain the

corresponding of bengamides with no epimerization which are represented in **Table 18**.

Table 18. Optimization lactone opening reaction in solid phase.

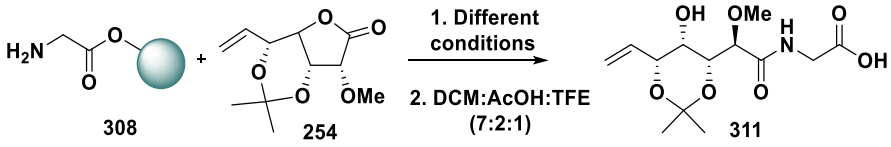

Entry	Base	Solvent	Time	Temperature	Yield
1	Sodium 2-ethylhexanoate	THF	24 h	r.t.	40 %
2	Sodium 2-ethylhexanoate	THF	24 h	60 ºC	37 %
3	DIPEA	DMF	24 h	80 ºC	20 %
4	TEA	*i*-PrOH	48 h	r.t.	25 %

Thus, using entry 1, 2 and 3 conditions the product was obtained, not detecting epimerization (**Figure 40**). However, the yield was very modest and attempts to increased it by using higher temperatures or different bases, resulted fruitless in all cases. Given these results it was decided to check the strategy 2.

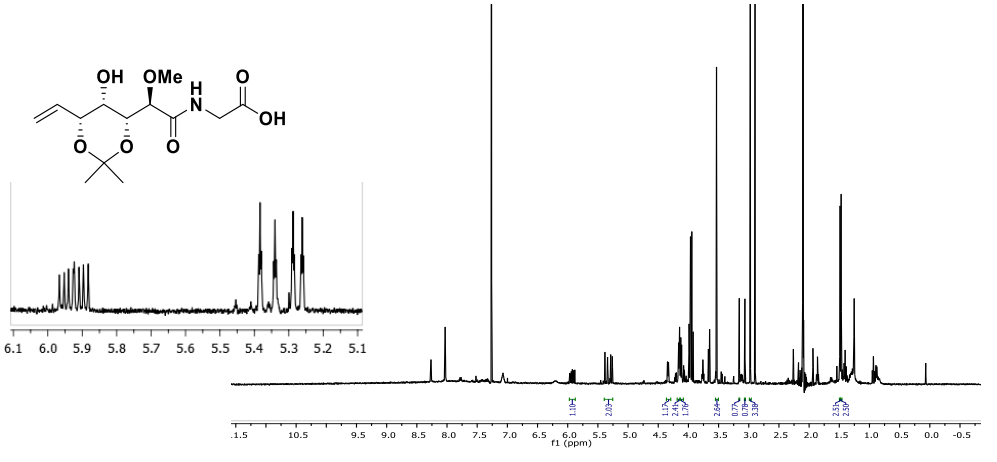

Figure 40. ^{1}H-NMR spectra of **311.**

*3.5.4. Strategy 2: Synthesis of new peptidyl analogues through coupling reaction of acid **285** with resin loaded with dipeptides*

In this strategy, the acid **285** was coupled with **298** under the same conditions which were employed to obtain the analogues **145** and **172** in solution (**Scheme 38**). After releasing the resin, the coupled product **312** was obtained in 70 %. In this way, the synthetic strategy 2 in solid phase was successfully validated.

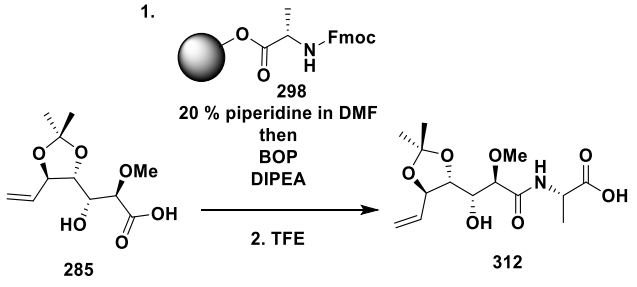

Scheme 38. Synthetic strategy 2 to obtain peptidyl bengamide analogues.

Thus, it was proceeded with the coupling of two-dipeptides (**301** and **304**) which were coupled with the acid **285.** Firstly, this acid was coupled with **301** to obtain the coupled product in the resin. Then, the *E*-alkene was introduced through an Olefin Cross Metathesis performed in the solid phase which was catalysed by 2nd generation Hoveyda-Grubbs catalyst under the optimized conditions employed the previous analogues. At this point of the synthesis, it was decided to release the compound **314** from the resin using a mixture of DCM:AcOH:TFE (7:2:1) to afford this precursor in 25 %. Finally, it was employed an acidic hydrolysis step to remove the acetal group to afford the desired analogue **315** in a 70 %.

Secondly, the acid **285** was coupled with the dipeptide **304** to obtain the coupled product which was suggested to an Olefin Cross Metathesis. In this case, to carry out the release and deprotection step in one pot, the analogue **317** was obtained by a release from the resin by using in 25 % (**Scheme 39**).

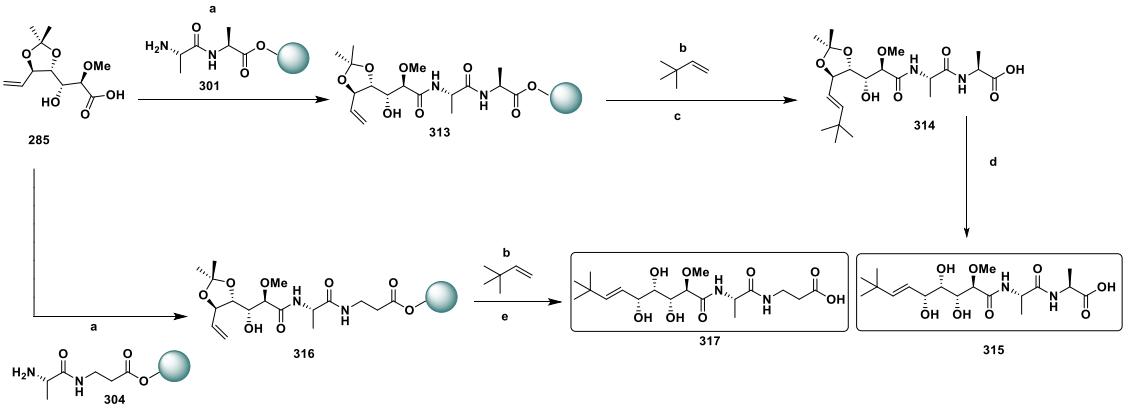

Scheme 39. Synthesis towards new peptidyl bengamide analogues **315** and **317.**

Reagents and conditions. (a) **285, 301** or **304**, BOP, DIPEA, DMF, 25 ºC, 24h. (b) **313** or **316,** 3,3-dimethylbut-1-ene, Grubbs catalyst, Toluene, 80 ºC. (c) DCM:AcOH:TFE (7:2:1), 25 ºC , 30 min (d) AcOH aq, 80 ºC, 2h.

3.6. Summary

In conclusion, bengamide analogues **145** and **172** have been biologically evaluated. Furthermore, analogue **145** have been prepared in sufficient amounts to carry out *in vivo* assays and analogue **172** was prepared with the aim of being encapsulated in nanoparticles as will be explained in the chapter 5.

Moreover, three new bengamide analogues have been prepared trying to increase the antitumoral activity of these natural compounds. Finally, a new synthesis strategy was delineated and employed through solid phase methodology to prepare the bengamide analogues **315** and **317 (Figure 41)**.

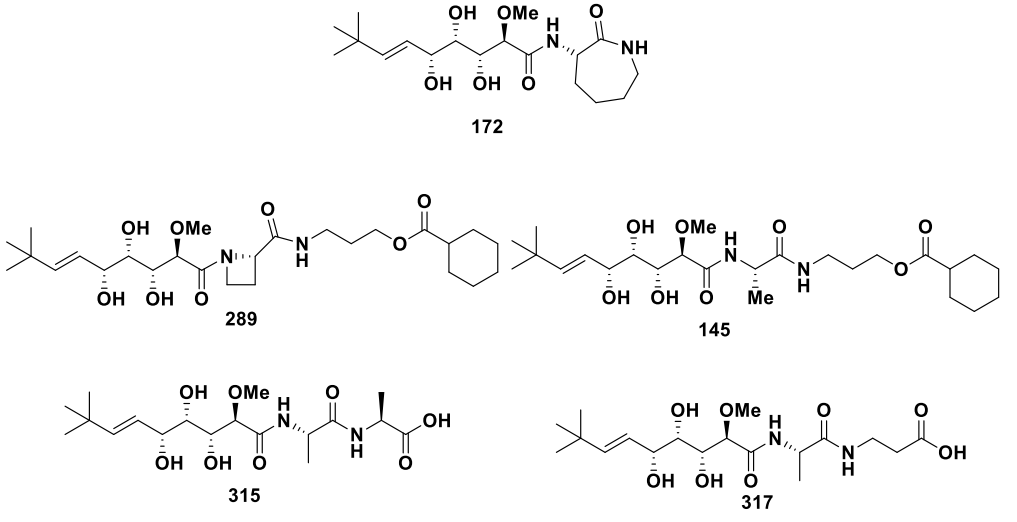

Figure 41. Summary of bengamide analogues synthetized.

CHAPTER 4. THERMOSENSITIVE POLYMERIC NANOPARTICLES WITH MAGNETIC CORE

4.1. Background in nanoparticles as drug delivery system

In this research, the design of nanoparticles will be focus on the polymeric *p*NIPAM nanoparticles due to the bioavailability and biocompatibility of this polymer. Specifically, *p*NIPAM is a thermosensitive microgel and has been used to cover the magnetics centres.[174]

The *p*NIPAM has been described as a polymer which is able to form colloidal microgels systems composed of amide groups, which are hydrophilic, and lateral chains of an isopropyl group, which are hydrophobic. The synthesis to obtain this type of *p*NIPAM nanogel was first described by Pelton and Chibante[175] and it is carried out by radical polymerization in the presence of a crosslinking agent (*N,N'*-methylenebisacrylamide) and a radical initiator (2,2'-azobis(2-methylpropionamide)) (V50) (**Scheme 40**).

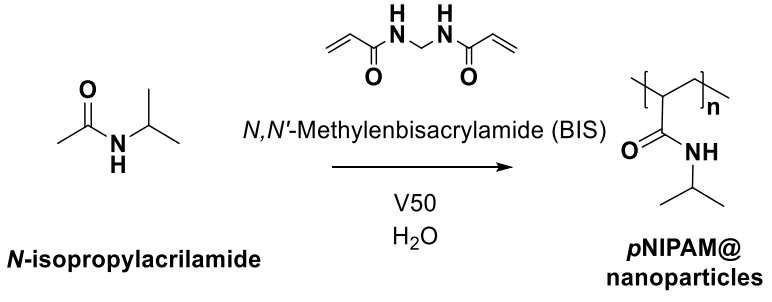

Scheme 40. Polymerisation reaction to obtain *p*NIPAM nanoparticles.

One of the most significant properties of these nanogels is the thermosensitivity. Therefore, this polymer responds to temperature variations. This is explained by the intermolecular interactions between the molecules of the solvent and the polymer itself. At low temperatures the *p*NIPAM is soluble in water, since the polymeric network forms hydrogen bonds with water molecules, being the solvent-polymer interaction greater than polymer-polymer interactions, and consequently the polymer is in a **swollen state**. In contrast, at higher temperatures hydrogen bonds are broken, so polymer-polymer interaction is greater, causing the

contraction of the polymer and a decrease of the size and consequently the polymer is **collapsed**. The lower critical solubility temperature (LCST) at which this process occurs is 32 ºC for *p*NIPAM in water.[176] It is important to highlight the reversible character of this temperature-dependent process.

The LCST of *p*NIPAM is an important factor in the use of these nanoparticles as a controlled-drug delivery system. Thus, LCST (32 ºC) almost coincides with the body temperature, which means that the nanoparticle releases the drug when it is found in the human body (**Figure 42**).

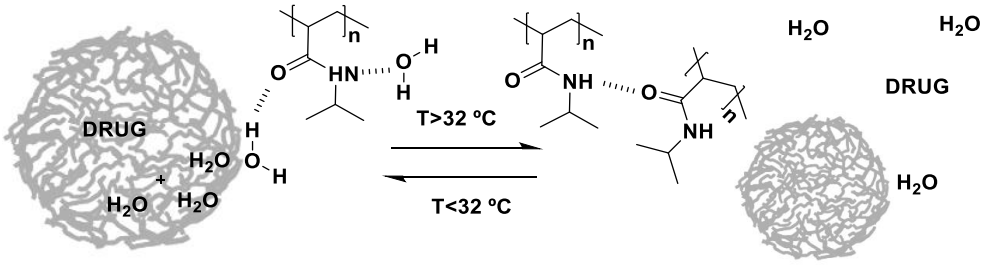

Swollen state: below LCST (32 ºC) the residues of *N*-isopropylacrylamide interact via hydrogen bonds with water and the drug.

Collapsed state: above LCST (32 ºC) the NPs form intramolecular hydrogen bonds between residues of *N*-isopropylacrylamide, in such way it collapses and releases the drug.

Figure 42. States of *p*NIPAM NPs in function of LCTS.

The interest of this polymer in our research group gave rise to the development of a novel hybrid of a bimetallic core of AuAg with a shell of *p*NIPAM microgel, which presents as highly efficient thermoresponsive catalysts toward the reduction of 4-nitrophenol to 4-aminophenol.[177] In this sense, we also studied the effect of the crosslinker concentration in the structure of hybrid core@shell nanoparticles (Au@*p*NIPAM).[178]

Last years, the interest of this polymer for the controlled drug release has increased. For example, different active anticancer drugs have been encapsulated into *p*NIPAM NPs such as 5-fluorouracil (5-FU) and oxaliplatin (OXA). Specifically, Rejinold *et al*. encapsulated 5-FU into *p*NIPAM nanogels which, in presence of fibrinogen, increased breast cancer cells apoptosis.[179] Besides, 5-FU was also incorporated into poly(*p*-nitrophenol

acrylate)-co-(*N*-isopropylacrylamide) to obtain nanohydrogels with different drug loading.[180] Another drug which has been encapsulated into *p*NIPAM nanosystem is OXA. Thus, Patil *et al.* prepared chitosan-graft-poly-*N*-isopropylacrylamide were loaded different amounts of OXA and Peng *et a*l. developed a dual responsive microgel for OXA encapsulation which was loaded via conjugation.[181,182] Additionally, chistosan-g-poly(*N*-isopropylacrylamide) (Cs-g-*p*NIPAM) co-polymer was prepared to develop pH- and thermo-responsive nanoparticles for tumour-specific OXA delivery.[183]

With this background, was decided to design a hybrid system of *p*NIPAM that includes a magnetic core (Fe_3O_4, magnetite) to use as controlled delivery system, due to all the high performance in biomedicine proposed this system, from magnetic resonance diagnostic.[184] All these interesting applications are a consequence of their super magnetic character and their nanometric size. This behaviour is defined by having a high magnetic susceptibility typical of materials ferromagnetic and ferrimagnetic, but with the characteristic of varying the direction of the magnetic spins under the influence of temperature.[185]

During last years, the development of hybrid nanosystems which includes a magnetic core, and a polymeric shell has been deeply studied. The interest of these hybrids is based on the capacity of respond to an external magnetic field, which can improve the transport activity and the application of an alternating magnetic field reducing the tumour through hyperthermia.[186] In 2017, Kim *et al.* described a magnetic-polymeric nanosystems whose core was magnetite, and the shell was *p*NIPAM-co-AL (using allylamine as comonomer) which was functionalized with folic acid as targeting ligand for cervical cancer cell lines.[187] Shen *et al.* encapsulated 5-FU into a *p*NIPAM@Fe_3O_4 systems, where mesoporous SiO_2 was used as the channel for drug release.[188] More recently, a nanoparticle with two different compartments was developed by Liu *et al.* the nanoparticle was

formulated as *p*NIPAM@PEDOT/Fe_3O_4@PTMPTA which respond to an electric and a magnetic field.[189]

Absolutely, nanoparticle size plays a crucial role in shaping their therapeutic and diagnostic applications. The size of nanoparticles has a substantial impact on various aspects of therapeutic delivery:

- **Blood Circulation Half-Life**: the size of nanoparticles influences how long they can circulate in the bloodstream. Smaller nanoparticles might have an extended circulation half-life, allowing them more time to reach their target sites.[190,191]
- **Targeting**: nanoparticle size is a critical factor in achieving targeted delivery to specific tissues or cells. Designing nanoparticles with a size that facilitates interaction with targeted receptors or cellular structures enhances their precision in therapeutic applications.[192,193]
- **Cellular Uptake**: the ability of nanoparticles to be taken up by cells is influenced by their size. Smaller nanoparticles may have advantages in cellular uptake due to their size and surface properties.[194]
- **Tumour Penetration**: in cancer therapy, the size of nanoparticles is crucial for effective tumour penetration. Nanoparticles need to navigate through the tumour microenvironment, and their size can impact their ability to penetrate deep into tumour tissues.[195]

Understanding and controlling the size of nanoparticles is therefore essential for optimizing their performance in various biomedical applications, ensuring they can effectively reach and interact with their intended targets.

Moreover, the optimal size of nanoparticle for a biomedical application is between 10 nm and 250 nm of diameter due to the following reasons:

- Certain classes of nanoparticles with a diameter less than approximately 10 nm face rapid elimination by the kidneys. The renal

filtration barrier, crucial for the efficient clearance of small molecule drugs, has an effective size cutoff of around ≈10 nm. This means that nanoparticles larger than this cutoff may have different fate and interactions within the biological system, influencing their pharmacokinetics and biological responses.[196]

- The colloidal properties of nanoparticles impose a size limitation. Certainly, the upper size limit of nanoparticles can be influenced by the targeted cellular receptors. However, in general, nanoparticles with a diameter exceeding 250 nm tend to activate the complement system and undergo rapid removal from the bloodstream. According to Moghimi *et al.,* there is a suggestion of a maximum size limit of 150 nm for spherical nanoparticles to prevent filtration in the spleen.[197]

These considerations highlight the importance of customizing the size of nanoparticles based on the intended application and the specific biological interactions they are expected to encounter within the body.

Due to all this background, in this research work will be study the synthesis of hybrid systems of polymeric nanoparticles to encapsulate different active drugs.

4.2. Preparation of pNIPAM nanoparticles

4.2.1. *Preparation of pNIPAM@*

First, the preparation of solid polymeric *p*NIPAM nanoparticles was optimized with the objective of control the size of these drug delivery systems. Therefore, the preparation of *p*NIPAM@ nanoparticles, which were obtained following the detailed procedure in *section 7.3.2.1*., was carried out under radical polymerization conditions of the monomer *N*-isopropylacrylamide in aqueous solution, using 2-methylpropionamidine (V50) as radical initiator and *N,N'*-methylenebisacrylamide (BIS) as crosslinker.

The synthesis was performed at 70 ºC under an Ar atmosphere. **Figure 43** shows a Transmission Electron Microscopy (TEM) imagen of a nanoparticle (*p*NIPAM@) obtaining through this synthesis, where there is a good monodispersity and nanoparticles have a size of diameter 490 ± 3.0 nm.

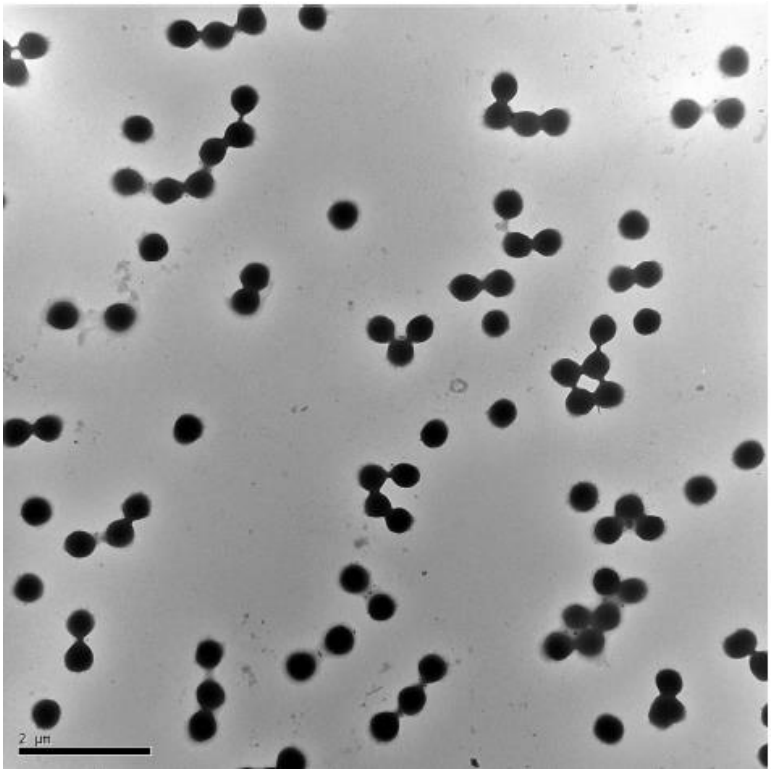

Figure 43. TEM micrographs of *p*NIPAM@ nanoparticles.

With the aim of achieve a controlled size, a monodispersing, and an aggregation of particle optime for the biomedical application due to the needed size of the nanoparticles in a range of 10 nm - 250 nm to use they as drug delivery system as was explained in the previous section, here we synthetized these polymeric nanoparticles using different concentrations of monomers and different percentages of crosslinker. Moreover, the importance of controlling the nanoparticle size lies in the influence of this parameter in the cellular interaction and biodistribution of the polymer *in vivo* and *in vitro* biological studies.

As is shown in **Table 19**, the polymerization reaction was carried out using different concentrations of comonomer, from 50 nM to 250 nM, while the percentage of crosslinker was modified in a range of 0 to 10 %. Finally, the radical initiator was used in a constant concentration of 100 mM in all cases.

Table 19. *p*NIPAM radical polymerization conditions.

	***p*NIPAM**	***N*-isopropylacrylamide**		***N,N´*-methylenbisacrylamide**		
Entry	**nM**	**mmol**	**g**	**mmol**	**g**	**% mol**
1	50	1.0	0.113	0.1	0.015	10
2	75	1.5	0.170	0.15	0.023	10
3	100	2.0	0.226	0.2	0.031	10
4	150	3.0	0.339	0	0	0
5	150	3.0	0.339	0.075	0.015	2.5
6	150	3.0	0.339	0.15	0.023	5
7	150	3.0	0.339	0.21	0.032	7.5
8	150	3.0	0.339	0.3	0.046	10
9	200	4.0	0.453	0.4	0.062	10
10	250	5.0	0.566	0.5	0.077	10

After preparation of the different nanoparticles (**Table 19,** entries 1-10) Transmission Electron Microscopy (TEM) analysis was employed to determine the morphology and the size of these systems. Specifically, the size of all these nanoparticles was in a range between 490 ± 3.0 nm and 530 ± 5.5 nm. Despite of the size of the nanoparticles is not optimal for a biomedical use, as well as they will use in hybrids nanoparticles, we posited that the incorporation of the magnetic core into the polymeric network could result in a reduction in size, as elucidated subsequently.However, the level of aggregation changed in fact of the concentration of monomers:

- At high concentrations of monomer (**Table 19,** entries 9 and 10) was observed a higher aggregation of the shells (**Figure 44**).

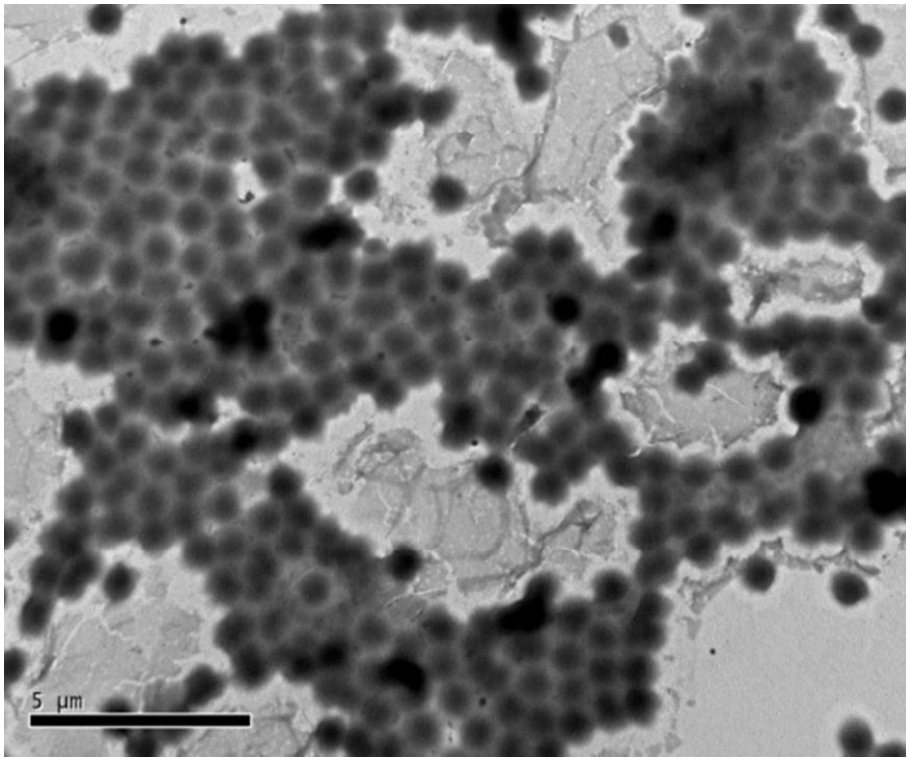

Figure 44. TEM micrographs of pNIPAM@ nanoparticles at high concentrations of monomer (200 nM).

- At low concentrations of monomer and keeping constant (10%) the BIS concentration (**Table 19,** entries 1-3) less nanoparticles were observed which means low yield; indeed, any attempt to improve the sample monodispersity by adding lower cross-linker concentrations was unsuccessful (**Table 19,** entries 4 and 5)**,** (**Figure 45**).

-

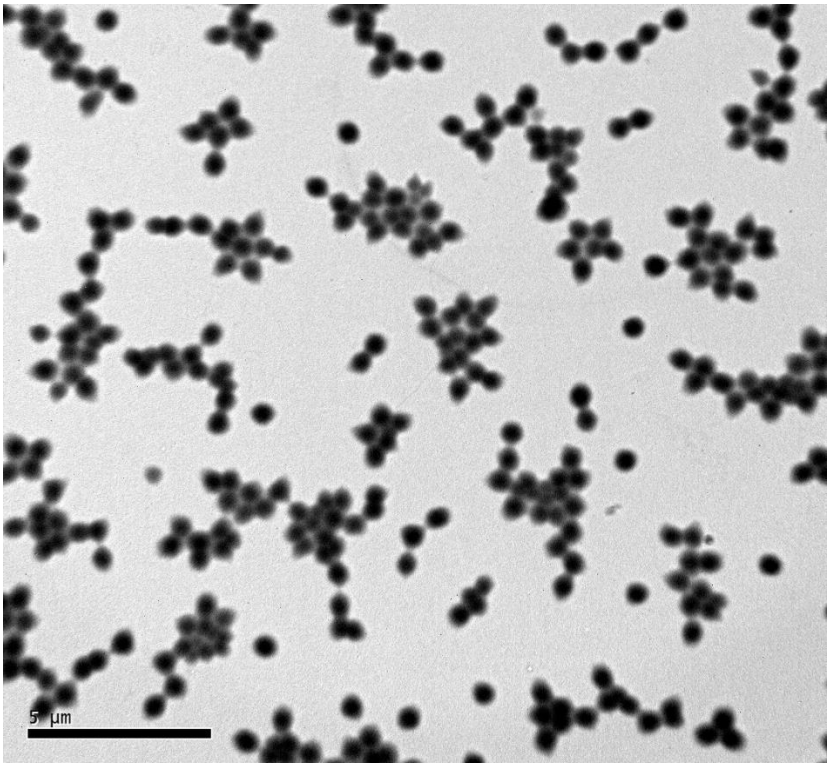

Figure 45. TEM micrographs of pNIPAM@ nanoparticles at low concentrations of monomer (150 nM).

The conclusion drawn from these experiments is that the best conditions for the preparation of solid *p*NIPAM@, with a high monodispersity and low aggregation, are the used for a concentration of 150 nM of the monomer *N-i*sopropylacrylamide, 5 % of crosslinker *N,N'*-methylbisacrylamide respect to the monomer and 100 mM of the radical initiator V50 (**Table 19,** entry 6) (**Figure 46**).

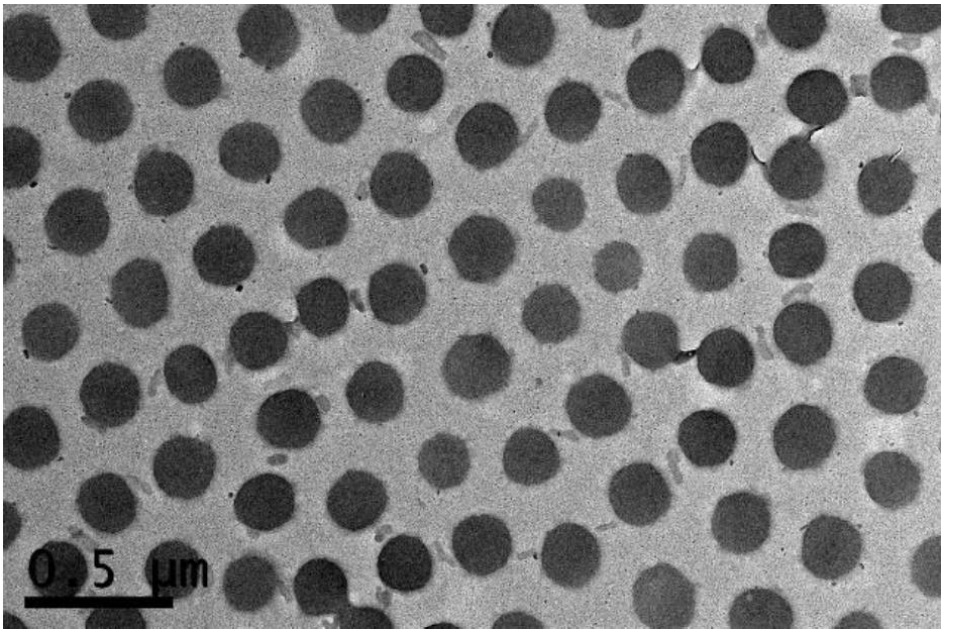

Figure 46. TEM micrographs of *p*NIPAM@ nanoparticles in a concentration 150 nM.

4.2.2. *Synthesis of pNIPAM polymeric nanoparticles with different co-monomers (pNIPAM-co-3BA@, pNIPAM-co-AA@ and pNIPAM-co-AL@)*

Once the synthesis of *p*NIPAM@ was optimized, different co-monomers were used to obtain co-polymeric (*p*NIPAM-co-@) nanoparticles. Specifically, the co-monomers 3-butenoic acid (3-BA), acrylic acid (AA) and allylamine (AL) were employed to obtain the desired nanoparticles: *p*NIPAM-co-3-BA@, *p*NIPAM-co-AA@ and *p*NIPAM-co-AL@ (**Figure 47**).

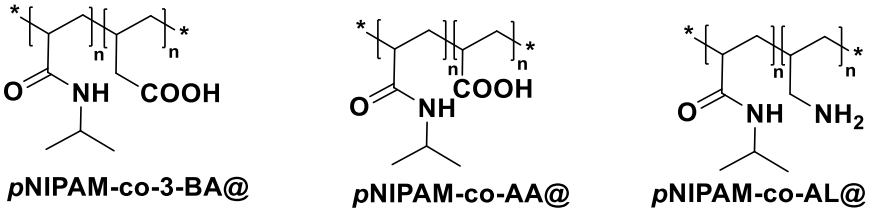

Figure 47. Molecular structure of *p*NIPAM NPs with different co-monomers.

After following the procedure described in the experimental *section 7.3.2.2.,* the presence of the comonomers in the polymeric network was confirmed by ZP analysis, showing values at pH = 8 of -16 ± 0.305 mV and -14 ± 0.244 mV for the *p*NIPAM-co-3BA@ and *p*NIPAM-co-AA@ nanosystems, respectively, which means that a partial deprotonation of the carboxylic acid groups (-COOH) into microgel network is occurring.

On the other hand, ZP value for *p*NIPAM-co-AL@ NPs was around 7.08 ± 0.63 mV at pH=2 which means the protonation of the amines group (-NH_2) present in the polymeric network. Finally, ZP values for these systems in neutral or acidic condition was 0 mV.

After TEM analysis of all these NPs, was concluded that the morphology of them was not affected by the addition of the comonomers into the polymer network, resulting a similar morphology with respect to the obtained for *p*NIPAM@. As is illustrated in **Figure 48**, the TEM images of the *p*NIPAM-co-comonomers@, show low polydispersity and a size in a range between 519 ± 3.0 nm and 540 ± 5.5 nm of diameters, which means a similar value of *p*NIPAM@ NPs. In conclusion, the particle morphology and size were not affected by the chemical composition.

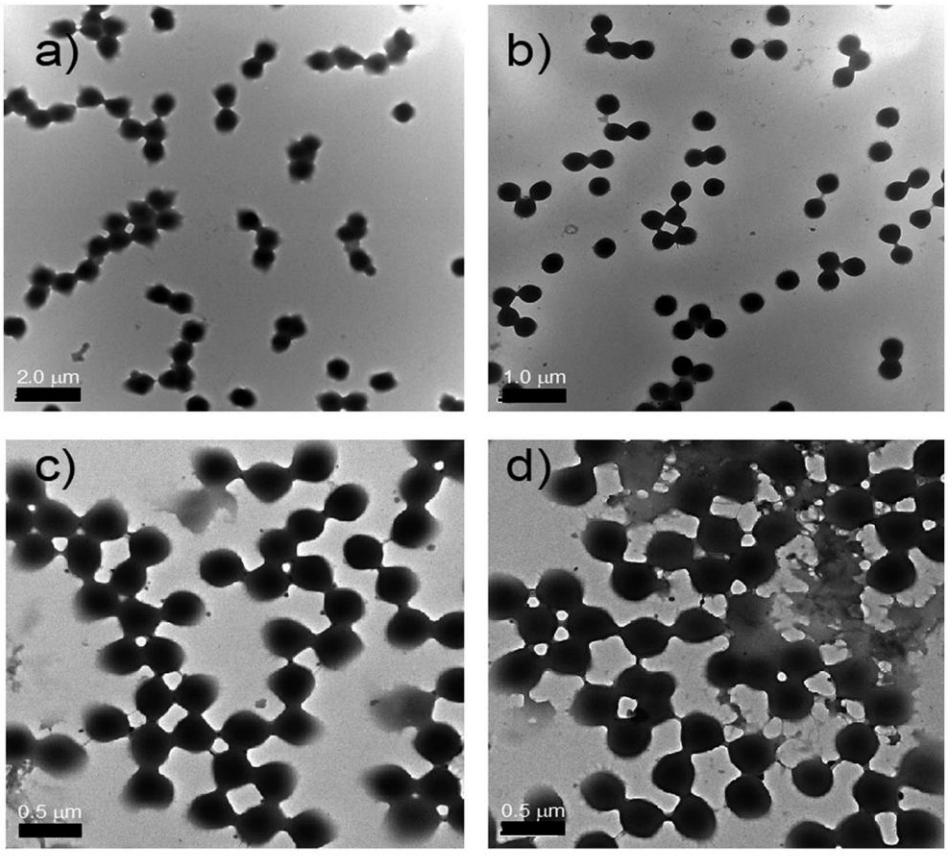

Figure 48. TEM micrographs of (a) *p*NIPAM@ NPs (monomer concentration 150mM and 5% BIS) and the co-polymeric systems: (b) pNIPAM-co-3BA@ (c) *p*NIPAM-co-AA@, and (d) *p*NIPAM-co-AL@).

4.3. Preparation of magnetic *p*NIPAM nanoparticles

4.3.1. Synthetic strategy towards hybrids nanoparticles

Scheme 41 shows the general strategy employed for the preparation of hybrid *p*NIPAM@Fe_3O_4 NPs. Thus, magnetic cores were prepared by co-precipitation of $FeCl_6$-H_2O and $FeCl_2$.Then, they were covered with *p*NIPAM by a radical polymerisation around and different drugs were able to be encapsulated into these novel hybrid systems. To complete the study of this nanosystems, the delivery time of the different drugs should be studied in a dialysis membrane (**Scheme 41**).

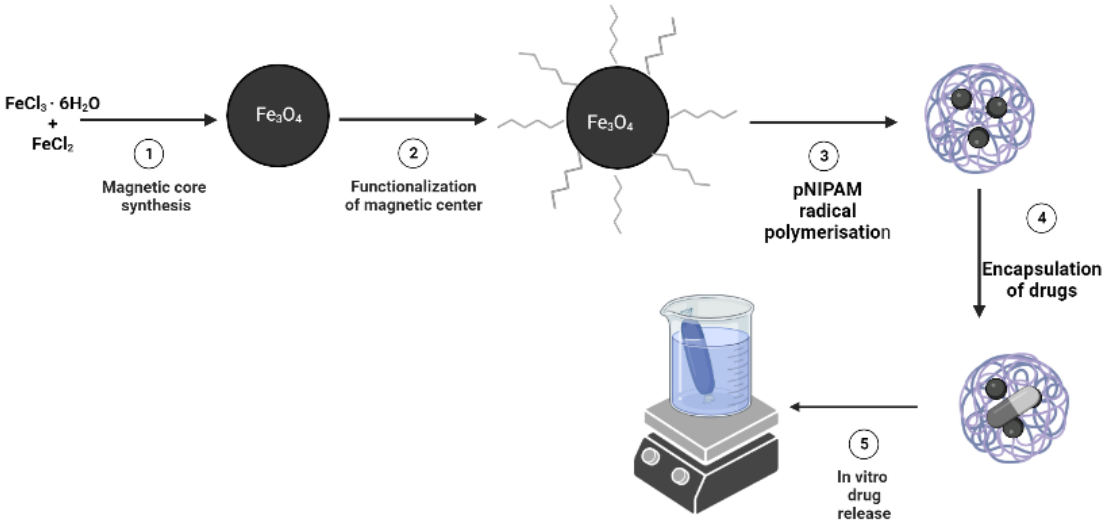

Scheme 41. Methodology employed to develop a hybrid drug delivery system and encapsulation of drug into these nanosystems.

4.3.2. Synthesis of the magnetic core (@Fe_3O_4)

The method employed for the synthesis of the magnetic nanoparticles (@Fe_3O_4) was the coprecipitation in water which was described by Massart *et al.* in 1981, following the procedure in *section 7.3.3.* using as bases tetramethylammonium hydroxide (TMAOH) 25% (in methanol or water) and NaOH.[175] This method is based on the mixture of ferric and ferrous ions in a molar proportion 2:1 (Fe(III):Fe(II)) in basic medium.

$$\mathbf{Fe^{2+} + 2Fe^{3+} + 8OH^{-} \leftrightarrow Fe(OH)_2 + Fe(OH)_3 \rightarrow Fe_3O_4\downarrow + 4H_2O}$$

The size and the morphology of the magnetic nanoparticles (MNPs) obtaining through this method depends on different parameters such as: which salts are employed, the molar proportion of ferric and ferrous ions, pH values, temperature reaction or other parameters as the way of the addition of the base. Moreover, the absence of oxygen is favourable to avoid the oxidation of MNPs. So, the Ar atmosphere is necessary during the synthesis.[175]

The principal advantage of this method is that the MNPs obtained are hydrophilic and stables in aqueous medium. It is a fast and reproducible method which present a high yield.

For all the magnetic nanoparticles prepared was determined the dry residue, taking an aliquot of 1 mL and drying it at 80 ºC. The results showed a concentration of 7.2 mg/mL of Fe_3O_4 for the synthesis which employed TMAOH 25% in methanol and 8.66 mg/mL of Fe_3O_4 when TMAOH 25% was employed. Finally, when the base was changed by NaOH for the preparation of the particles, the dry residue was lower with a value of 4 mg/mL.

In conclusion, these results confirm that the synthesis process was more effective when the coprecipitation method was carried out using as base medium TMAOH in water. Thus, **Figure 49** shows TEM micrographs for NMPs obtained by the coprecipitation method with TMAOH 25 % in water.

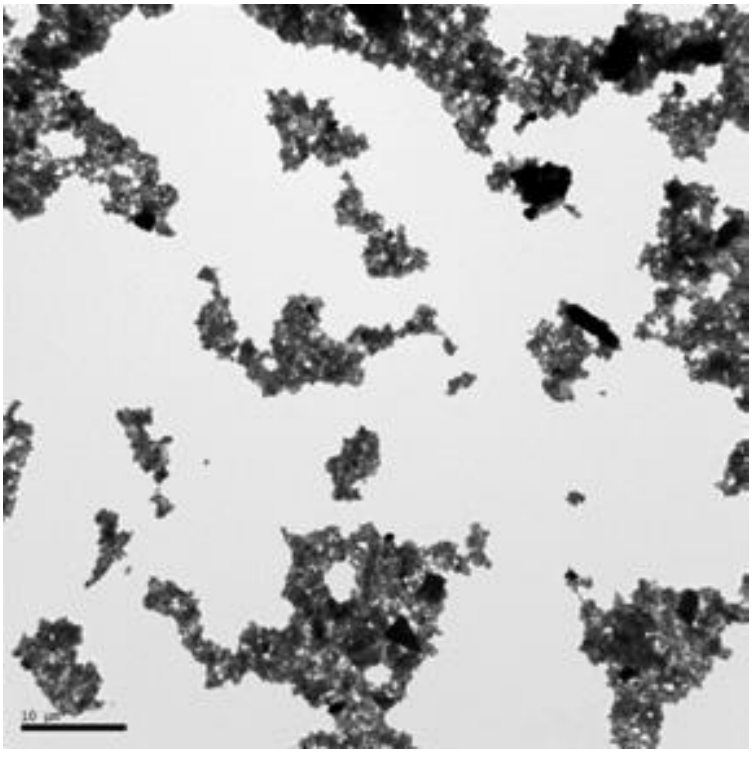

Figure 49. TEM micrographs of magnetics nanoparticles synthetized by coprecipitation method using TMAOH in water.

4.3.3. *Functionalization of the magnetic core: @Fe_3O_4-3-BA and @Fe_3O_4-AA*

The next step was the functionalization of the magnetic core with two different alkenes following the detailed procedure in *section 7.3.4.,* as is showed in **Scheme 42**: 3-butenoic acid (3-BA) and acrylic acid (AA), were employed to increase the affinity between the polymer and the MNPs. Moreover, the magnetic core is not compatible with the organic polymer and a superficial functionalization was needed which means a chemical modification of the surface, inducing changes in the physicals, chemical and biological properties. Thus, to achieve the polymer coating around these magnetic nanoparticles was incorporated a terminal alkene.[175,198,199] This functionalization process serves to safeguard the

magnetic nanoparticles (MNPs) from oxidation, enabling the subsequent polymer growth to encapsulate the magnetic core.[200]

To avoid the aggregation of these particles by a combination of Van der Walls and magnetic interactions, which could affect to efficacy of these NPs, sonication and cetyltrimethylammonium bromide (CTAB) as surfactant were used during the functionalization process.[201]

Strong evidences of that the functionalization was successful were found when DLS measured changed: in case of core functionalized with 3-BA 144.3 nm ± 7.9 and in the case of AA 140.3 nm ± 8.0, this size is consisted with the described by Laurenti *et al.* where the size of the clusters of magnetite in the MNPs of Fe_3O_4 decreased with the amount of 3-butenoic acid added during the functionalization process.[198]

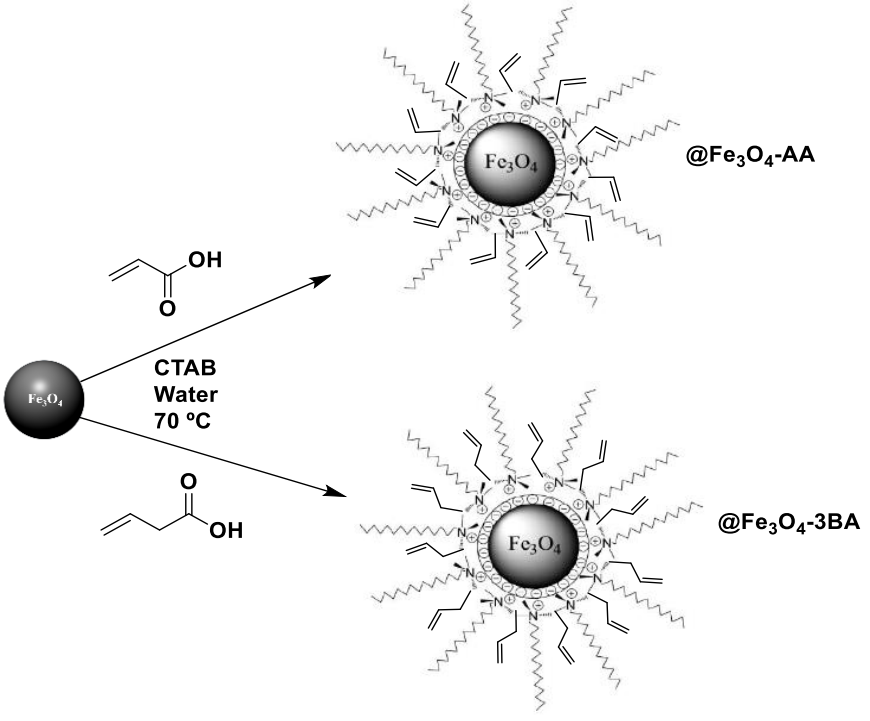

Scheme 42. Surface modification of MNPs with acrylic acid and butanoic acid.

Reagents and conditions. (a) Fe_3O_4 nanoparticles, AA, CTAB, water, 70 ºC (b) Fe_3O_4 particles, 3-BA, CTAB, water, 70 ºC.

4.3.4. Growth of the polymer pNIPAM around the magnetic core: pNIPAM@Fe_3O_4-3BA and pNIPAM@Fe_3O_4-AA

Once magnetic nanoparticles were functionalized with terminal alkenes, polymerization was carried out around the magnetic cores (@Fe_3O_4-3BA or @Fe_3O_4-AA) following the procedure explained in the experimental *section 7.3.5.* (**Scheme 43**).

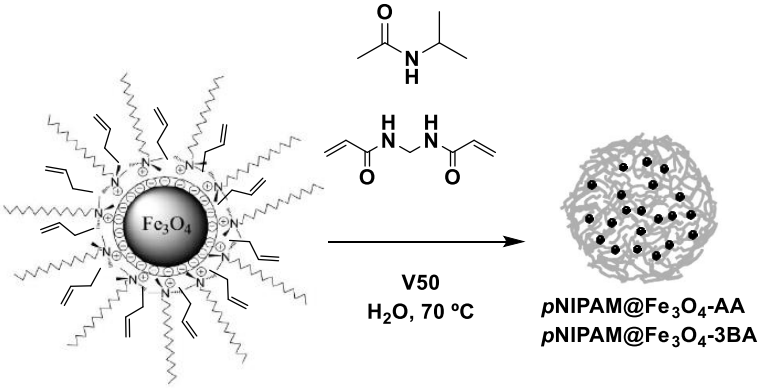

Scheme 43. Growth of *p*NIPAM around MNPs.

Thus, Z-Potential was measured to these hybrid systems: values obtained were in an order of -14 ± 0.3 mV at pH = 8 which confirms the presence of carboxylic acids (-COOH) deprotonated in the polymeric network at this pH value. These results are consistent with the chemical composition of the particles, as with the previous results obtained for *p*NIPAM@. Moreover, **Figure 50** shows TEM micrographs for these hybrid systems observing the magnetic core and the polymeric shell. In contrast, some of these polymeric shells are free, which means that there are not magnetic cores inside them and the size of them is around 300 ± nm of diameter, despite of that the size of the *p*NIPAM@Fe_3O_4 was smaller than the obtained for the *p*NIPAM@ NPs it is required a smaller NPs for a biomedical use (10 nm- 250 nm), so an optimization of the synthesis process was required.

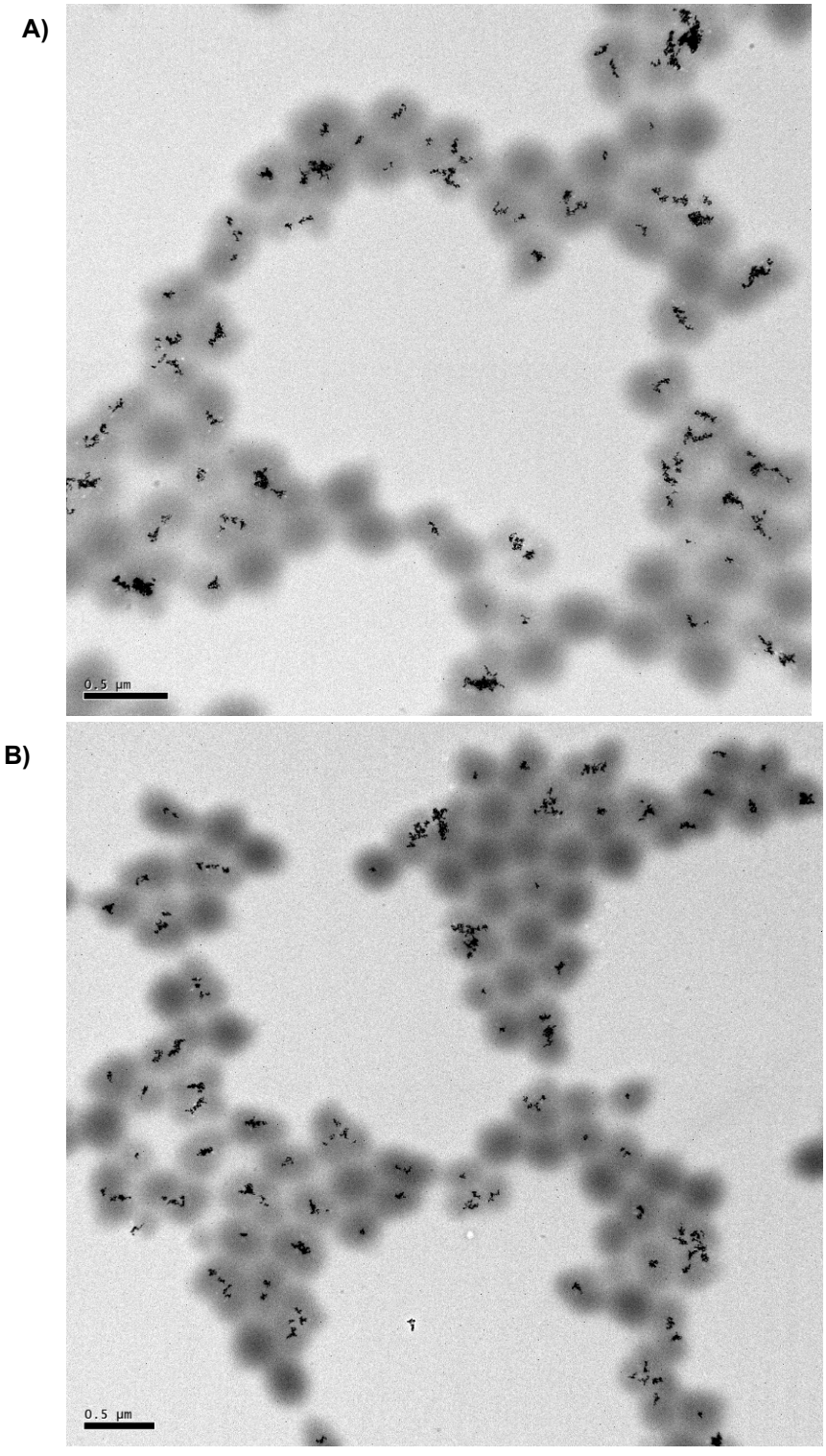

Figure 50. TEM micrographs for A) *p*NIPAM@Fe_3O_4-3BA and B) *p*NIPAM@Fe_3O_4-AA.

4.3.5. Optimization of the preparation of pNIPAM @Fe_3O_4-AA @Fe_3O_4-3BA systems

Study of the concentration of monomer

Several concentrations of monomers (NIPAM) were tested with the aim of study the control of the size of *p*NIPAM@Fe_3O_4-AA and @Fe_3O_4-3BA in fact of this parameter. Specifically, concentrations 50, 75, 150 and 200 mM of *N*-isopropylacrylamide (NIPAM) were studied, maintaining in a 10 % the crosslinker BIS with respect to the monomer. Thus, **Figure 51** illustrates the different morphology of hybrid nanosystems (*p*NIPAM@Fe_3O_4-3BA) prepared in fact of concentration of monomer employed.

In **Figure 51 A** it can be observed the TEM image obtained for *p*NIPAM@Fe_3O_4-3BA system. In this case the radical polymerization reaction was carried out by using a 50 mM concentration of *N*-isopropylacrylamide. When 50 mM concentration was employed, the smallest NPs were found. Moreover, the image confirms the formation of the hybrid system, due to the high contrast cluster of oxide metal spheres coated by a low contrast mono-dispersed polymer shell. In most of the cases, magnetic clusters are coated by a spherical polymer, however, there is an important presence of non-coated free magnetite aggregates, and some magnetic clusters are coated by a non-defined or irregular polymer shell.

By using a concentration of 75 mM of NIPAM (**Figure 51B**) the number of free magnetic cluster decreases with respect to the previous concentration (50 mM). However, the number of polymeric shells without magnetic core increased.

Finally, **Figure 51, C** and **D** show TEM imagines obtained by using a concentration of 150 mM and 200 mM of the monomer, respectively. It is important to note that there was not detected free polymer shell, probably due to the high concentration of monomer. However, magnetite clusters

are covered by irregularly shaped microgels. Moreover, some of the hybrid nanoparticles appear to be fused together with the magnetic core in the center, which is explained by the large amount of monomer used in the preparation process which could lead to an instability of NPs.

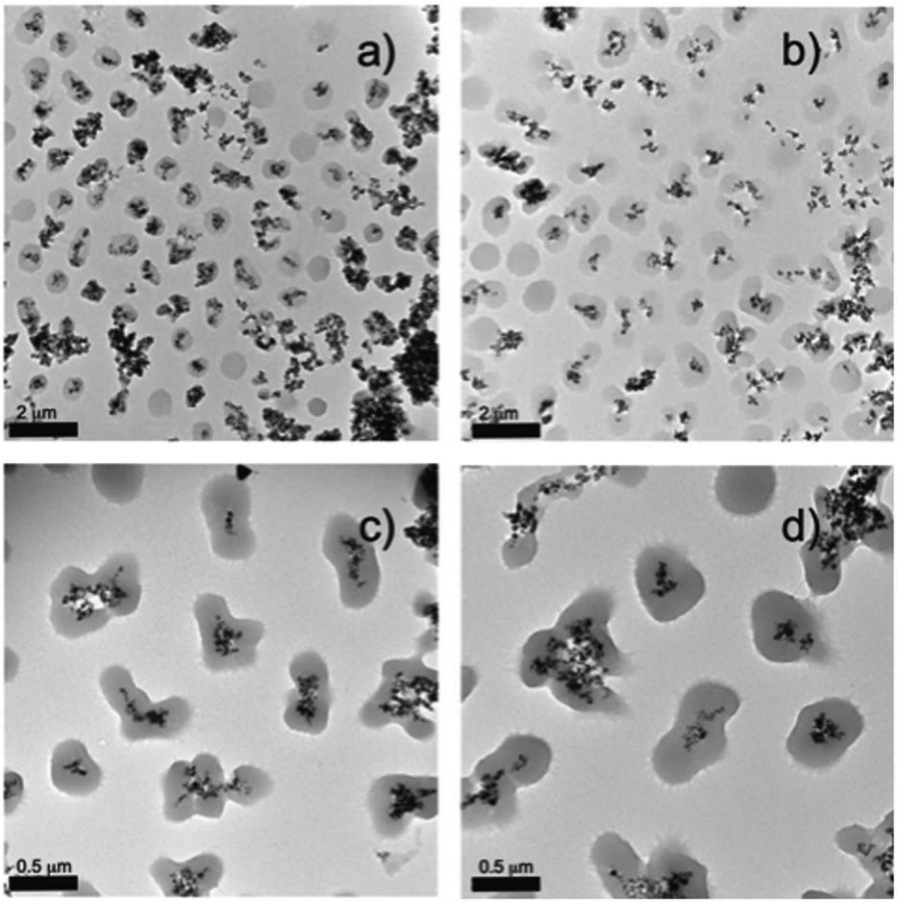

Figure 51. TEM micrographs of *p*NIPAM@Fe_3O_4-3BA samples prepared with different monomer concentrations (a) 50, (b) 75, (c) 150 and (d) 200 mM.

Comparing all these results, concentration of 50 mM was optimal to generate a good spherical nanoparticle and smaller size. From the analysis dimensional, a mean size distribution of 250 ± 1.0 nm is deduced from diameter, which could be ideal for the encapsulation and release of active drugs.

Study of the concentration of crosslinker

Once was stablished the monomer concentration, was proceeded to study the effect of employ different concentrations of crosslinker (BIS, *N,N´*-methylenbisacrylamide), used during the synthesis process at this concentration (50 mM). By the way, different percentages of crosslinker were tested 0 %, 2 %, 5 % and 7 % with respect to the monomer concentration. Therefore, **Figure 52** illustrates the different morphology of hybrid nanosystems (*p*NIPAM@Fe_3O_4-3BA) prepared in fact of percentage of crosslinker employed.

In **Figure 52A**, it can be observed the TEM image obtained for *p*NIPAM@Fe_3O_4-3BA system obtaining by using a 0 % of crosslinker. In this case, microgels of *p*NIPAM were not detected and a homogeneous network of magnetic nanoparticles is observed. Thus, in a total absence of crosslinker (ultra-low cross linked) the radical polymerization process does not occur.

TEM micrograph obtaining by using a percentage of crosslinker of 2 % is illustrated in **Figure 52B**. Once the crosslinker was employed, hybrid systems core@shell were detected. However, the number of magnetics nanoparticles including into the microgel was low and free *p*NIPAM nanoparticles were found, which means a reduction in the magnetic properties of these hybrid nanosystems.

The nanoparticles prepared by using a percentage of 7 % of BIS (**Figure 52D**) showed hybrid systems with magnetic clusters observing a variable number of magnetic cores. Successfully, employing a 5 % of crosslinker (**Figure 52C**) homogeneous spherical hybrid core@shell were found.

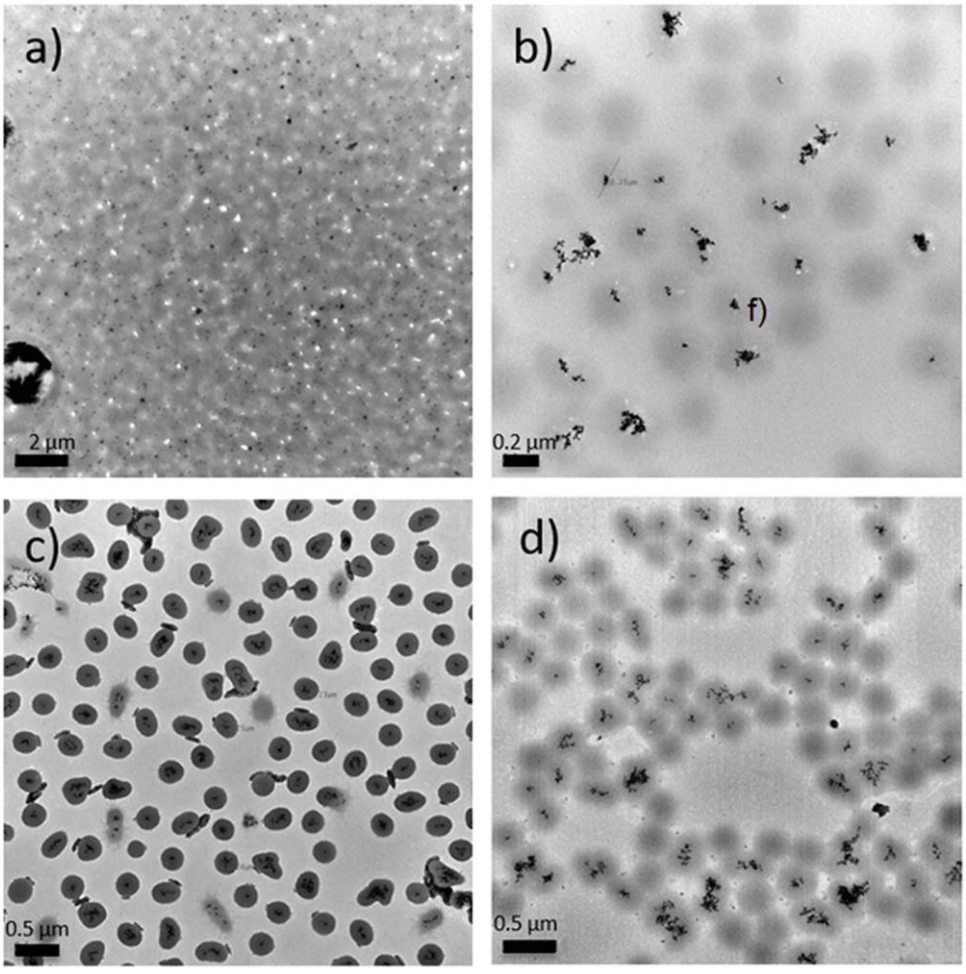

Figure 52. TEM micrographs of *p*NIPAM@Fe_3O_4-AA prepared at different cross-linker percentages: (a) 0, (b) 2.5, (c) 5 and (d) 7%.

In conclusion, the optimal conditions for the preparation of hybrid particles (core@shell) with a good defined morphology are: 50 mM of the monomer *N*-isopropylacrylamide, 5 % of the crosslinker *N,N'*-Bismethylenacrylamide with respect to the monomer, and 100 nM of the radical initiator 2,2'-Azobis(2-methylpropioanmide). Under these conditions, the average particle sizes are 240 ± nm of diameter, which means an ideal size to use these hybrid systems as drug delivery system. In **Scheme 44** is summarized the optimal conditions of synthesis.

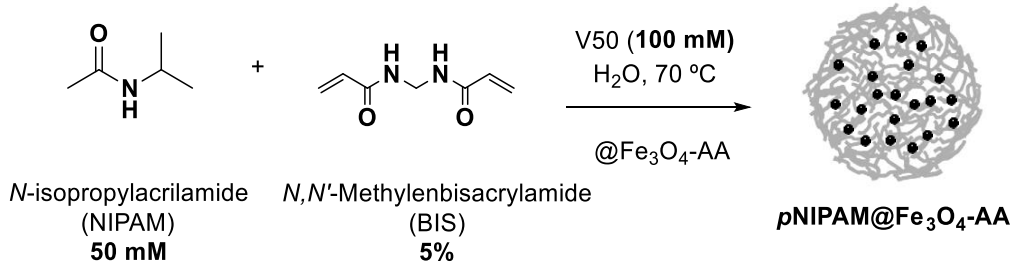

Scheme 44. Optimal conditions for the synthesis of hybrid magnetic nanoparticles of *p*NIPAM (255 nm of diameters).

In addition, figure x shows an enlargement of a *p*NIPAM@Fe_3O_4-AA NPs obtained in the optimal synthesis conditions. **Figure 53 A** shows an enlarged image of a nanoparticle in which the magnetic cluster in the centre of the polymer is clearly visible. Also, the size of the nanoparticles was determined on the TEM images obtained using *ImageJ* and *Origin* image analysis software. The values of the obtained sizes are reflected in **Figure 53 B** in a histogram of size and frequency distribution, observing the minimum particle size of 212 nm and the maximum of 308 nm, confirming the average size of the nanoparticle of 255 nm.

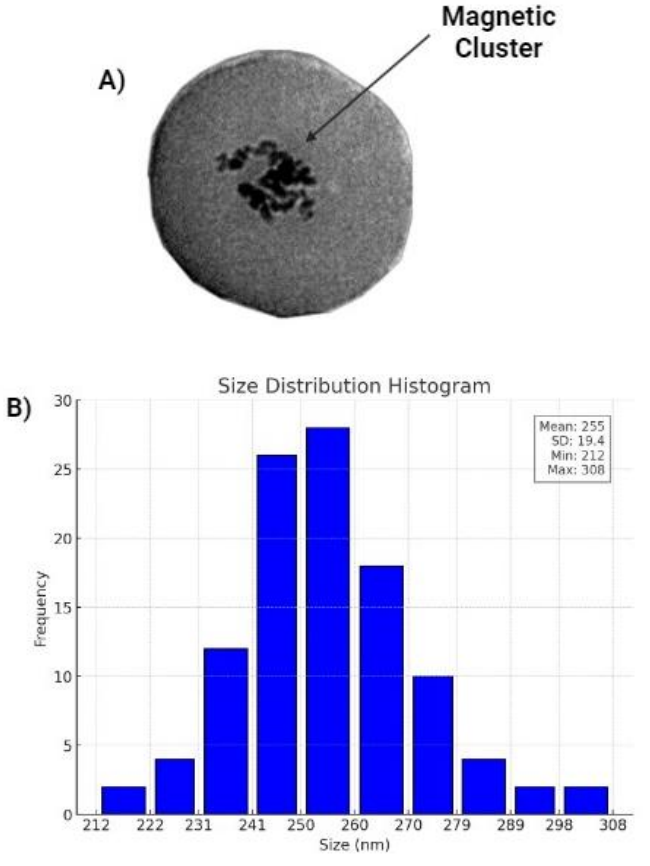

Figure 53. pNIPAM@Fe_3O_4-AA NPs A) TEM micrograph B) Size distribution histogram.

4.3.6. *Preparation of pNIPAM-co-Al@Fe_3O_4-AA*

Once the optimal conditions for the preparation of hybrid nanosystems were stablished, they were extended to prepare *p*NIPAM-co-Al@Fe_3O_4 as is detailed in *the section 7.3.5*. (**Scheme 45**).

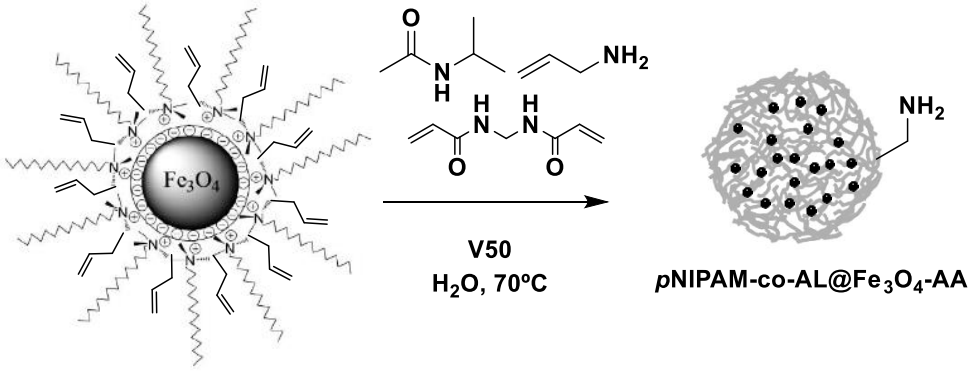

Scheme 45. Polymerisation process using allylamine as comonomer around the ferrite magnetic cores.

Figure 54 shows the resulting hybrid nanosystems when allylamine is used as comonomer, obtaining the desired structure core@shell with an average particle size are 267 ± nm. On the other hand, ZP was studied for these *p*NIPAM-co-AL@Fe_3O_4-AA, at pH= 8 a value of -11 ± 0.3 mV was obtained and, at pH= 2 it was 2.03 ± 0.6 mV, which confirms the presence of amine (-NH_2) groups due to the protonation of them at acid pH.

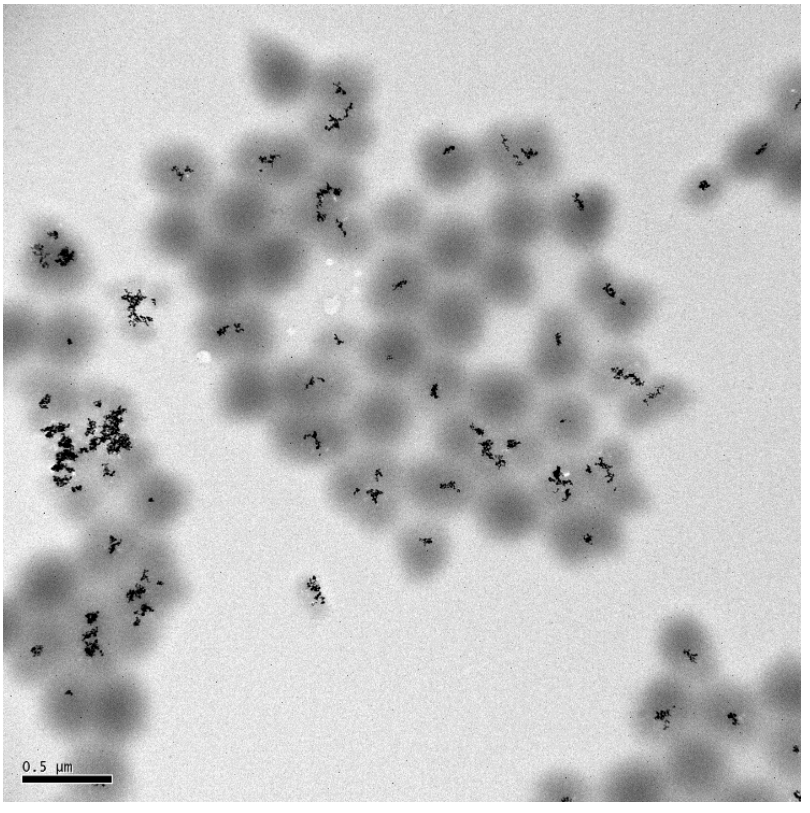

Figure 54. TEM image of *p*NIPAM-co-AL@Fe_3O_4-AA.

4.3.7. Hydrodynamic diameter (DH) and LCST

The hybrid nanosystems *p*NIPAM@Fe_3O_4-AA, which were previously prepared using the ideal conditions of **Scheme 44**, were deeper studied. Specifically, the LCST was determined for which the hydrodynamic diameter has been measured through DLS.

Figure 55 A shows the measure of the D_H for solid *p*NIPAM@ nanoparticles (red line) and for the *p*NIPAM@Fe_3O_4-AA system (black line). Therefore, size measurements were analysed over a temperature range between 24 ºC (size of 590 nm) to 46 ºC (size of 252 nm), with samples taken at intervals of 2 ºC. In this range of temperature, we can observe the two microgel states: **collapsed state** (at high temperatures) and **swollen state** (at low temperatures).

On the other hand, **Figure 55 B** represents the change of size of both particles in nanometres in fact of the temperature. As this Figure illustrates, the maximum value is at 34 ºC which means that it is the LCST, i.e., the temperature at which the nanosystems change of state. Moreover, this temperature is the same for both type of NPs, which means that the presence of a magnetic core does not affect to the final size of nanoparticles.

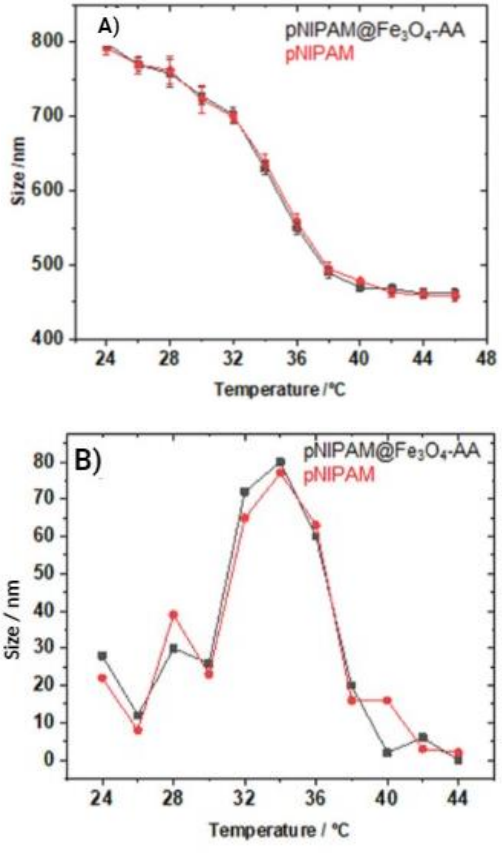

Figure 55. (a) hydrodynamic diameter of the *p*NIPAM@Fe_3O_4-AA (black line) and pure *p*NIPAM (red line) microgels in function of temperature; (b) change of particle size in function of temperature for *p*NIPAM@Fe_3O_4-AA (black line) and pure *p*NIPAM (red line) microgels.

Finally, **Figure 56** shows a representation of polymeric chains (*p*NIPAM@) with the magnetic core inside and the states that this

nanoparticle can presente in fuction of the temperature: **swollen** and **collapsed**.

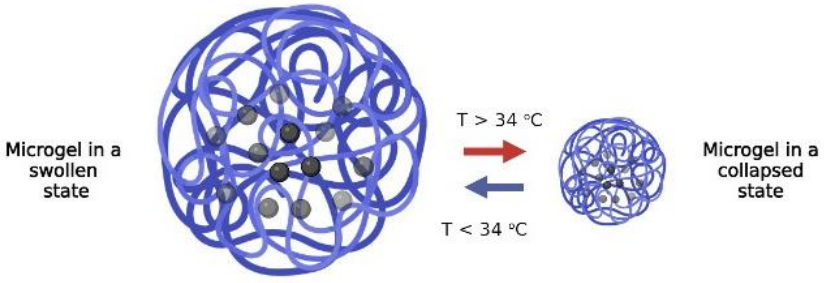

Figure 56. Particle size change in fact of the temperature.

4.3.8. Iron content analysis

The iron content of the *p*NIPAM@Fe_3O_4-3BA and *p*NIPAM@Fe_3O_4-AA systems with 150 mM NIPAM and 5 % BIS was analysed using the atomic absorption technique. 205 mg/g and 198 mg/g of iron (RSD 3.8%), respectively, were found in the systems according to this technique.

4.4. Functionalization of *p*NIPAM-co-AL @Fe_3O_4-AA with FITC (fluoresceinisothiocyanate)

*p*NIPAM-co-AL@Fe_3O_4-AA NPs were prepared with the objective of functionalization with fluorescent molecules to visualize hybrid systems using a confocal microscope, and to follow the internalization in biological environments. Thus, *p*NIPAM-co-AL@Fe_3O_4-AA, through the detailed procedure in the experimental *section 7.3.6.*, was functionalized with fluorescein isothiocyanate to obtain fluorescently labelled nanoparticles. Functionalization was achieved by using the free amine group in the polymeric nanoparticles, which reacted with the thioisocyanate group of the FITC, giving rise to a thiourea group, to obtain FITC-*p*NIPAM-co-AL@Fe_3O_4-AA (**Scheme 46**).

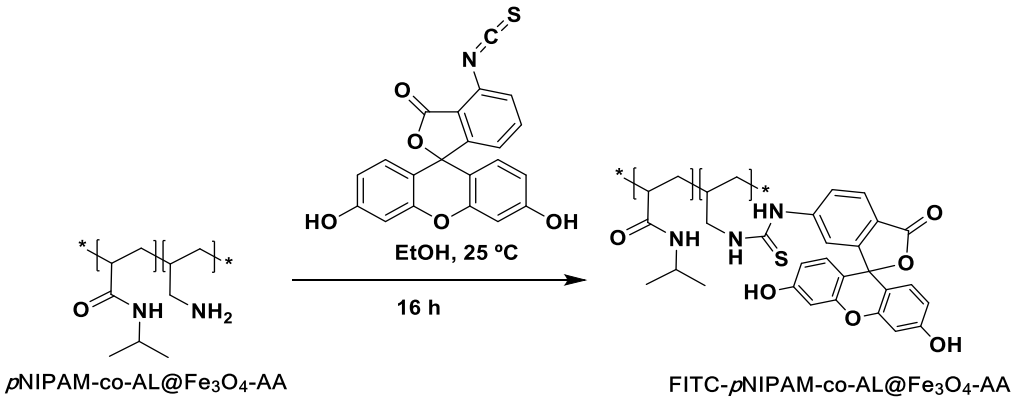

Scheme 46. Fluorescent labelling with FITC of *p*NIPAM-co-Al@Fe_3O_4-AA.

The incorporation of the chromophore FITC was confirmed through confocal fluorescence microscopy, exciting the sample at a wavelength of 429 nm and emitting in 518 nm. **Figure 57** shows the imagens obtaining through the confocal fluorescence microscope.

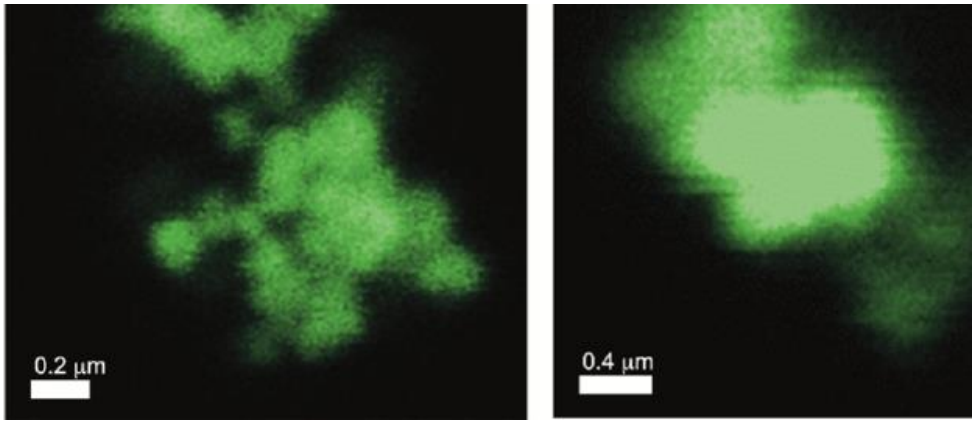

Figure 57. Confocal images of FITC- *p*NIPAM-co-AL- @Fe_3O_4-AA.

Finally, in **Figure 58** there are illustrated the TEM imagens for hybrids NPs FITC-*p*NIPAM-co-AL @Fe_3O_4-AA. The diameter size of this NPs is 255 nm of diameter, which is included in the ideal size for the application of this nanoparticles as drug delivery systems. As show these imagens spherical microgels are dispersed and there is not cluster of Fe_3O_4.

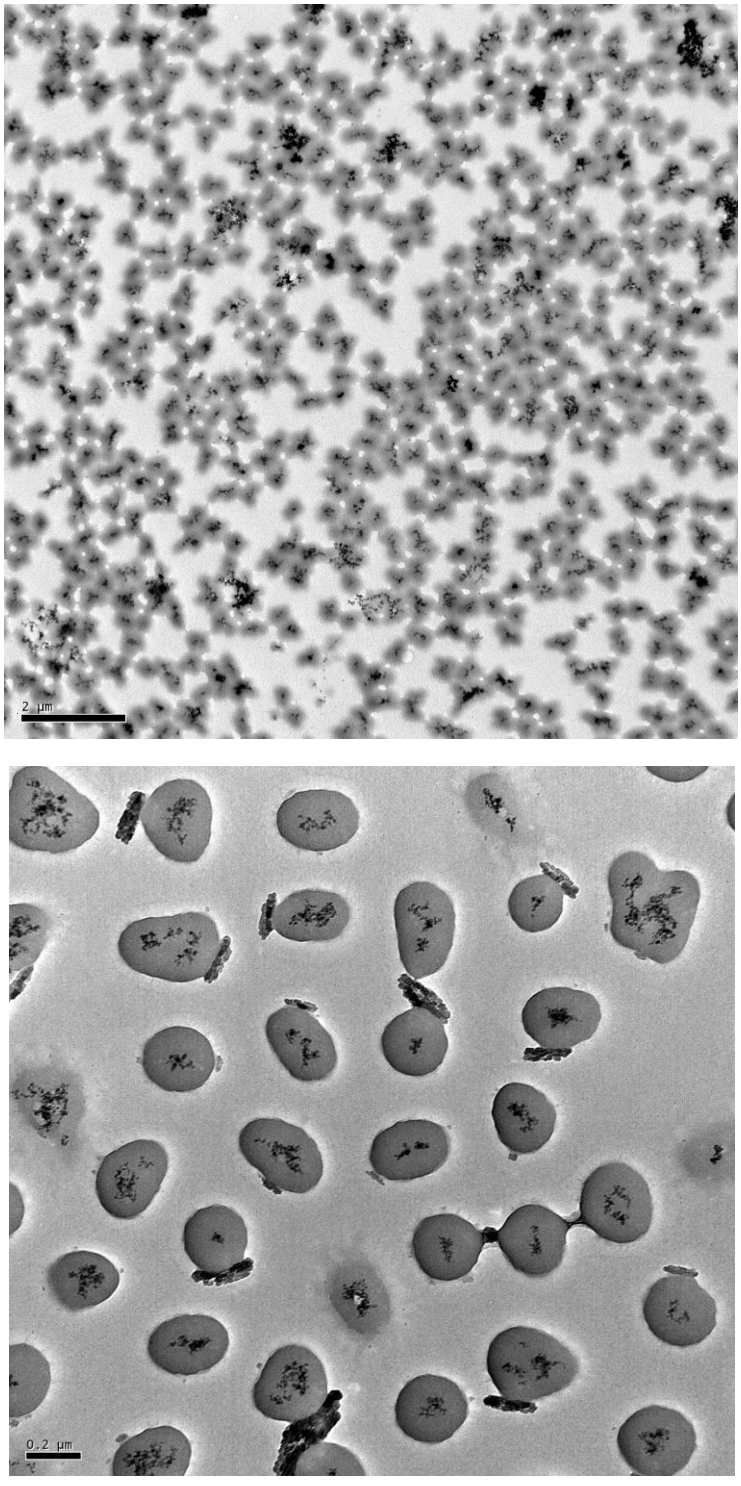

Figure 58. TEM micrographs of FITC-*p*NIPAM-co-AL@Fe_3O_4-AA NPs.

4.5. Summary

In conclusion, it has been stablished a synthesis towards different nanoparticles:

- Solid-polymeric nanoparticles (*p*NIPAM@, *p*NIPAM-co-3-BA@, *p*NIPAM-co-AA@ and *p*NIPAM-co-AL@).

- *p*NIPAM@Fe_3O_4 hybrid nanoparticles (*p*NIPAM@Fe_3O_4-AA, *p*NIPAM@Fe_3O_4-3BA and *p*NIPAM-co-AL@Fe_3O_4-AA).

- Fluorescent functionalized FITC-*p*NIPAM-co-AA@Fe_3O_4-AA nanoparticles.

CHAPTER 5. ENCAPSULATION OF ACTIVE DRUGS INTO POLYMERIC-MAGNETIC NANOPARTICLES

5.1. Encapsulation and release of 5-fluorouracil and oxaliplatin. Cytotoxicity of systems

The encapsulation of different drugs has been carried out using different models of the nanoparticles that were described in the previous chapter. The drug loading was carried out at 20 ºC because at this temperature the *p*NIPAM remains in a swollen state and the drug can be included inside the system in an easier way. Drug encapsulation efficiency (EE%) has been calculated using UV spectroscopy of the supernatant after centrifugation.

$$EE\ \% = \frac{D_T - D_F}{D_T} \cdot 100$$

where D_T is the initial added concentration of drug and D_F is the concentration of the free drug after centrifugation.

5.1.1. *Encapsulation of 5-fluorouracil and* oxaliplatin

The traditional treatment of colorectal cancer is chemotherapy, administered in stage II or III or higher.[186] Among all these treatments, 5-fluorouracil (5-FU) is commonly used together with other antitumor drug such as oxaliplatin (OXA) (**Figure 59**).[5] Specifically, 5-FU is an analogue of pyrimidine that inhibits the enzyme thymidylate synthase[202,203] and OXA is an antitumor drug belongs to the platinum family which has synergistic effect with fluoropyrimidines.[181,183] However, the low selectivity and specificity of these drugs give rise to side effects during the cancer treatment that together with the rapid metabolization and excretion of 5-FU and the introduction of peripheral neuropathy by OXA, means a limitation to use these drugs as cancer treatment.[204,205] Considering all these limitations and the interest of these anticancer drugs, here we decided to encapsulate 5-FU and OXA into the *p*NIPAM@Fe_3O_4 nanosystems.

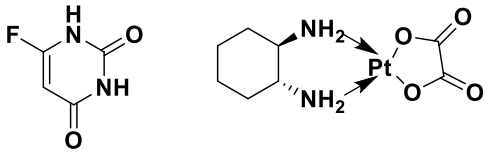

5-FU OXA

Figure 59. Chemical structure of 5-FU and OXA.

Therefore, the encapsulation of 5-FU was carried out into the next nanosystems: *p*NIPAM@, *p*NIPAM@Fe_3O_4-3BA and *p*NIPAM-co-AL@Fe_3O_4-AA, while OXA was included into *p*NIPAM@ and *p*NIPAM@Fe_3O_4-3BA. Both anticancer drugs were incorporated into the different nanosystems at 20 ºC to ensure the swollen state of the *p*NIPAM and the time of encapsulation was of 48 h.

To carry out the encapsulation process, amounts between 3 and 20 mg of the active compound were added to a suspension of the corresponding nanoparticle in MiliQ water. **Table 20** collects the amount of nanoparticles employed and the corresponding active drug. Besides, the EE % of these polymeric systems was established using UV spectroscopy. Therefore, the absorbance was measured in a UV-vis spectrophotometer at 257 and 248 nm, respectively for 5-FU and OXA, since these drugs absorb at this wavelength, in the samples previously centrifuged to remove the excess of non-encapsulated drug (**Table 20**).[186]

Table 20. Encapsulation efficiency (EE%) of 5-FU and OXA into *p*NIPAM nanosystems

Entry	Drug (mg)	*p*NIPAM NPs (mg)	EE (%)
1	5-FU (20)	*p*NIPAM@ (10)	36.3
2	5-FU (20)	*p*NIPAM@Fe_3O_4-3BA (10)	60.7
3	5-FU (3)	FITC-*p*NIPAM-co-AL-@Fe_3O_4-AA (6)	60
4	5-FU (6)	*p*NIPAM-co-AL@Fe_3O_4-AA (17)	65
5	OXA (10)	*p*NIPAM@(10)	38.5
6	OXA (10)	*p*NIPAM@Fe_3O_4-3BA (10)	77.5
7	OXA (10)	*p*NIPAM-co-AL@Fe_3O_4-AA (10)	73.5

As can be observed in **Table 20** good encapsulation is achieved in most of the cases (entries 2-4, 6 and 7). However, EE % was lower for pure *p*NIPAM@ nanosystems (entries 5 and 1). On the other hand, best values were showed by systems which contains a magnetic core (entries 2, 3, 4, 6 and 7). This fact can be explained by the higher size of the swollen state of hybrids systems *p*NIPAM@Fe_3O_4(-3BA/-AA) which is up to 800 nm as was, facilitating drug loading.

If the results obtained for 5-fluorouracil and oxaliplatin are compared, we can appreciate that values of encapsulation efficiency for OXA are higher than the obtained for 5-FU. This is explained by the solubility of 5-FU in water which is better, and it remains in aqueous solution during the encapsulation process.

Moreover, the presence of encapsulated 5-FU was confirmed by ^{1}H-NMR. **Figure 60 A** shows the ^{1}H-spectra of the polymer (*p*NIPAM@), where the proton signals of the polymer can be assigned. Thus, at 1 ppm

it is observed the typical signal belongs to the isopropyl group of the *p*NIPAM@. On the other hand, **Figure 60 B** shows the ^{1}H-spectra of the polymer after include 5-FU into the polymeric network, where can be observed the proton signals of the polymer together with a singlet at 9 ppm which belongs to the 5-FU structure.

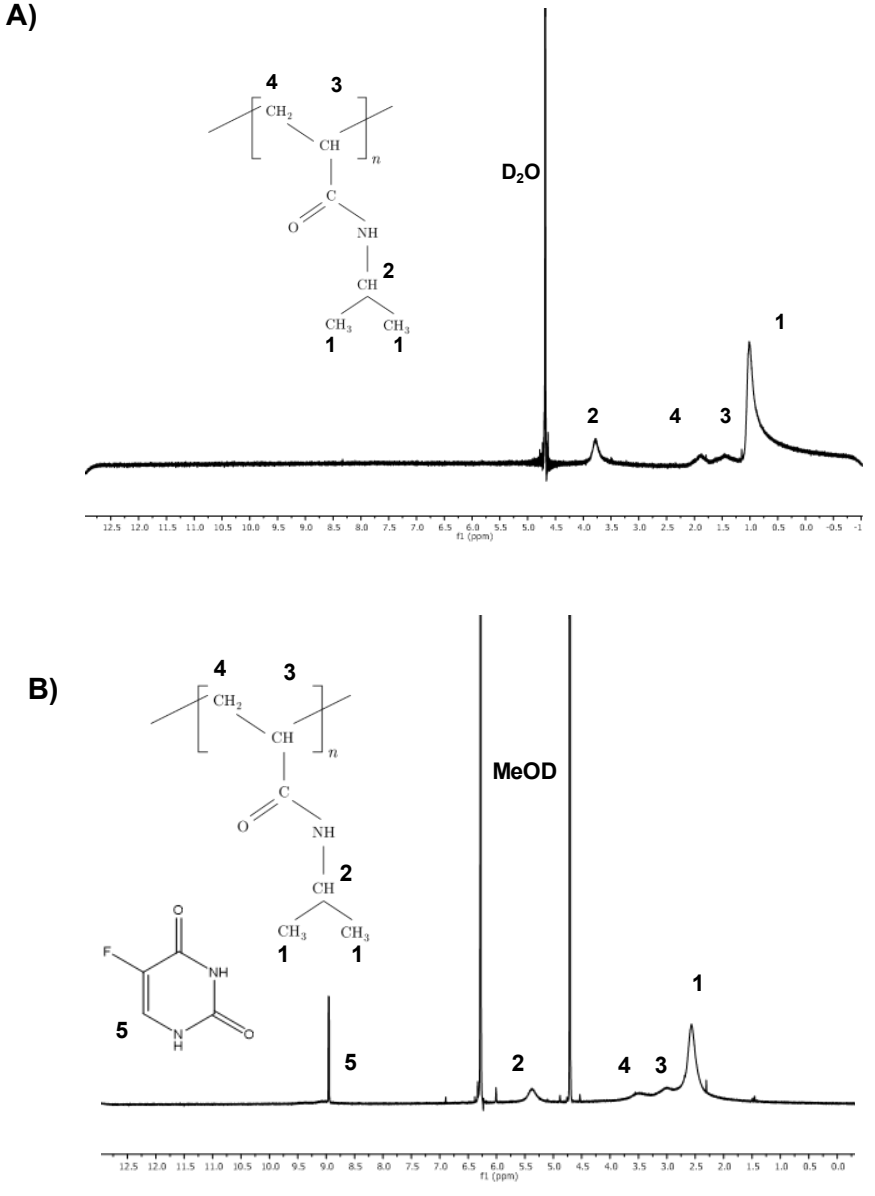

Figure 60. A) ^{1}H-NMRspectra of *p*NIPAM@ B) ^{1}H- NMRspectra of *p*NIPAM@+ 5-FU.

5.1.2. In vitro release essays of 5-fluorouracil and oxaliplatin

The *in vitro* drug release study was carried out using a cellulose dialysis bag. PBS buffer was employed as solvent in this experiment to maintain the pH of the solution in 7.4 (stationary phase) and a constant stirring of 100 rpm was maintained.

After obtaining the encapsulated drug into the nanoparticles systems was studied their *in vitro* release. This release study was carried out at several temperatures: 4, 20 and 40 ºC using PBS medium. Thus, aliquots of 3 mL were withdrawn of the solution at intervals of 10 min during the first hour and every 12 h in a 40 h period. The release medium was replaced with the same volume with PBS buffer. The results are collected in **Figure 61** and **Figure 62**.

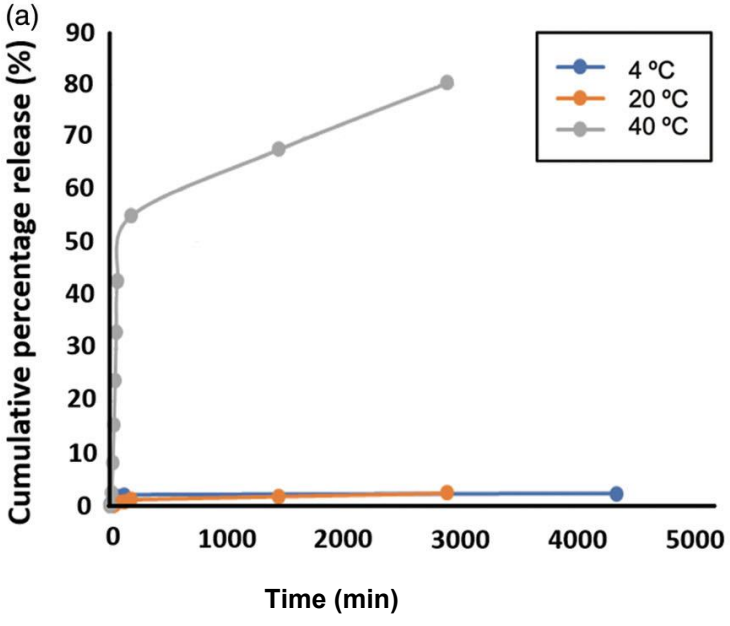

Figure 61. Drug release. *p*NIPAM@+5FU at 5, 25 and 4 ºC.

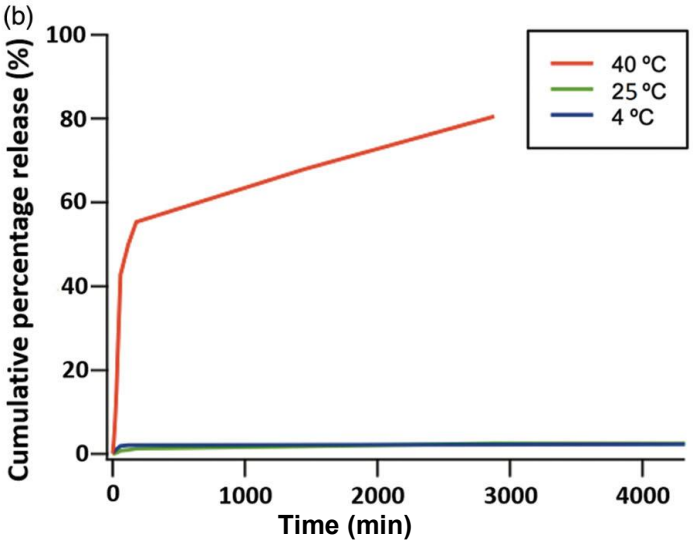

Figure 62. Drug release. *p*NIPAM@Fe_3O_4-AA+OXA at 5, 25 and 40 ºC.

As can be seen in **Figure 61** and **Figure 62**, at temperatures of 4 ºC and 20 ºC, only a cumulative release of 2.5 % was observed for both drugs which means that the swollen polymeric network state remains the drug at temperatures below LCTS (32 ºC). Predictably, at 40 ºC the drug was released in a 42 % along the first 60 minutes, reaching 81 % after 48h because the temperature of the study was above LCTS and the microgels is in a collapsed state. (**Figure 61** and **Figure 62**).

5.1.3. *Cytotoxicity and biocompatibility of pNIPAM@, pNIPAM @Fe_3O_4-3BA, FITC-pNIPAM-co-AL@Fe_3O_4-AA and pNIPAM-co-AL@Fe_3O_4-AA nanoparticles*

Activity studies of *p*NIPAM@, *p*NIPAM@Fe_3O_4-3BA, FITC-*pNIPAM*-co-AL@Fe_3O_4-AA and *p*NIPAM-co-AL@Fe_3O_4-AA nanoparticles were carried out in collaboration with Prof. José Prados and Prof. Consolación Melguizo from the Department of Anatomy and Embryology of Granada University. In **Figure 63** are collected the results obtained from the cytotoxicity assay of the different *p*NIPAM@ nanoformulation in T84 colon cancer cell line. Therefore, from this study can be concluded that *p*NIPAM@ nanoformulations did not show cytotoxicity in the T84 human

colon cancer cell line, while *p*NIPAM@Fe_3O_4-3BA was slight cytotoxic in the concentration of 10 µg/ mL of *p*NIPAM doses showing a small viability decrease.[186]

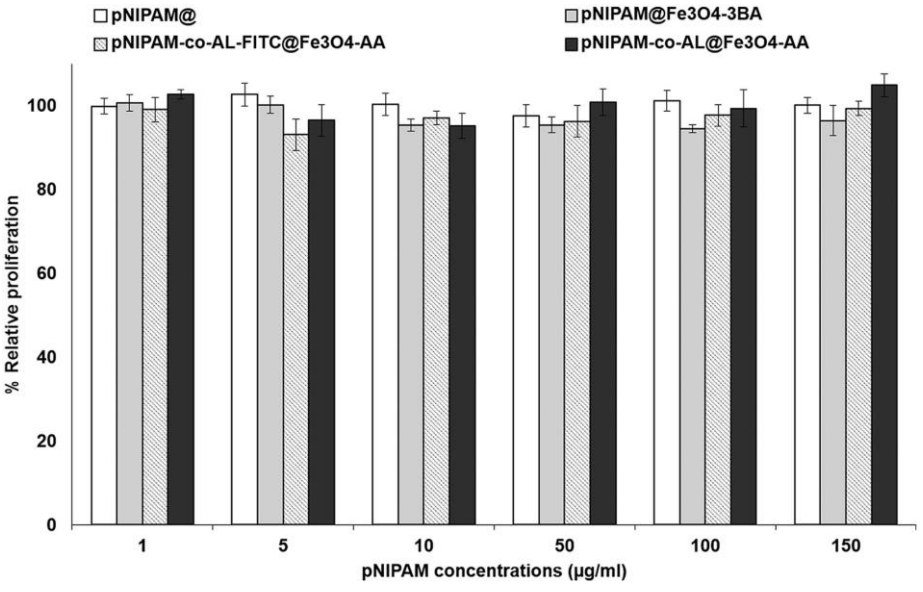

Figure 63. Cytotoxicity assay of blank *p*NIPAM@nanoformulations in T84 colon cancer cell line. Results are expressed as the mean ± SD and the experiment was made in triplicate cultures.

In addition, to ensure the biocompatibility of the nanosystems synthesized, a study in blood cells was carried out with *p*NIPAM@ and *p*NIPAM@Fe_3O_4-3BA. As it is observed in **Figure 64**, in general the nanoformulations did not produce any erythrocyte lysis even at the highest concentrations tested (150 µg/mL of *p*NIPAM@) (**Figure 64 A**) and only *p*NIPAM-co-AL@Fe_3O_4 showed a low haemolysis. Moreover, no agglutination of erythrocytes was observed in any of the nanoformulations tested after 1 h (**Figure 64 D**). Finally, *p*NIPAM nanoformulations neither produced toxicity in white blood cells any of tested doses after 1 h (**Figure 64 B**) or 12 h (**Figure 64 C**).

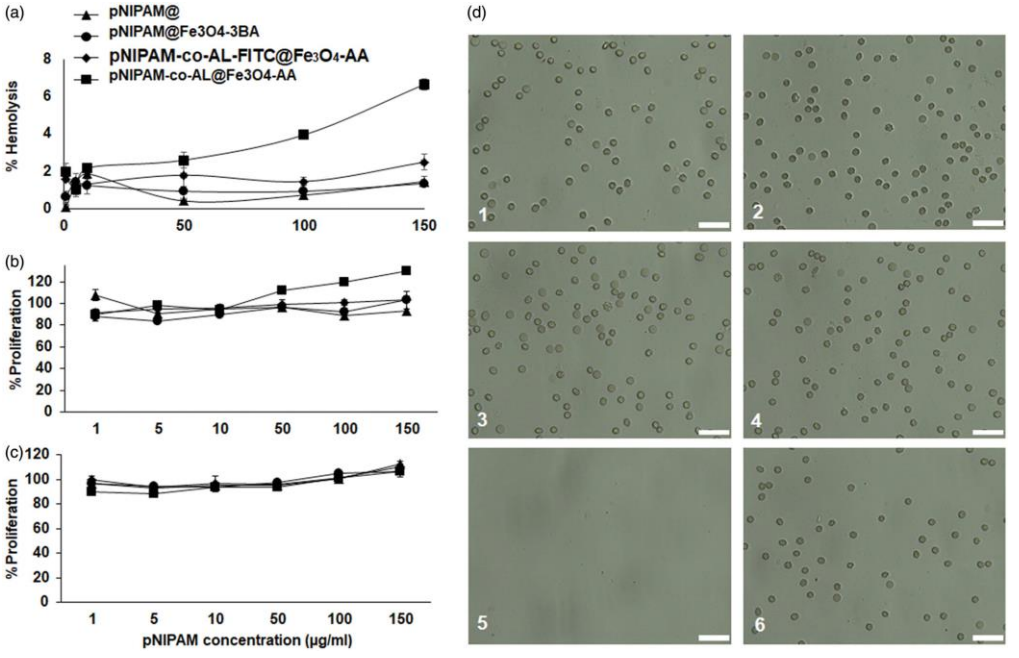

Figure 64. Blood biocompatibility assays. Haemolysis assay with red blood cells (a). CCK-8 test on peripheral blood lymphocytes at 1 h (b) and 12 h of exposition (c). Light microscopy images of human erythrocytes after 1 h of treatment with a *p*NIPAM@ (d1), *p*NIPAM@Fe_3O_4-3BA (d2), *p*NIPAM-co-AL-FITC@Fe_3O_4-AA (d3) *p*NIPAM-co-AL@Fe_3O_4-AA (d4), at a dose of 150 µg/mL. The images (d5) and (d6) are positive and negative control respectively. Scale bar 25 µm.

All these cytotoxicity studies concluded that *p*NIPAM@, *p*NIPAM@Fe_3O_4-3BA and *p*NIPAM-co-AL-FITC@Fe_3O_4-AA have excellent biocompatibility with human blood cells which is an essential characteristic for *in vivo* use.

5.1.4. *Proliferation studies of the drugs-loaded pNIPAM@ nanosystems*

Additionally, these biological studies were carried out in the nanoparticles systems loaded with drugs (5-FU and OXA) against colon cancer line, the results of these studies are showed in **Figure 65**. Among all these nanoformulations, *p*NIPAM@Fe_3O_4-3BA + 5-FU showed the best effect against T-84 cancer cells (inhibition proliferation of 57 %, close to the observed for free 5-FU). These results suggest the possible application of combined therapy (5-FU and OXA) using a single nanoformulation that

could be directed to the tumour through an external magnetic field. Thus, the presented hybrid systems possess potential applications in localised drug delivery making it a very promising tool for colon cancer therapy.

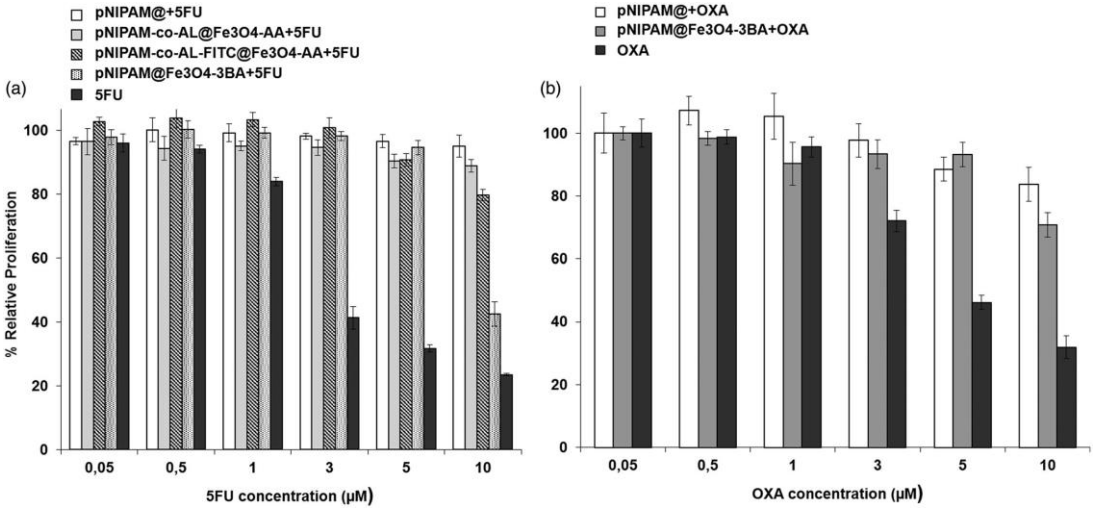

Figure 65. Cytotoxicity of different *p*NIPAM-loading drug nanoformulations. T84 tumour cell line was exposed to different treatment of *p*NIPAM nanoformulations loaded with 5-FU (a) and OXA (b) compared to their respective free drugs.

5.2. Encapsulation of bengamide analogue 172 into polymeric magnetic nanoparticles

Analogue of bengamide **172** was encapsulated into *p*NIPAM@ nanosystems following the procedure detailed in *section 7.4.1*. It is important to note, the method to calculate the encapsulation efficiency (EE%) was different from the used in 5-fluorouracil and oxaliplatin encapsulation, mainly due the low absorption of bengamide prevented the calculate the drug encapsulation efficiency (EE%) using UV spectroscopy, since no absorption was observed in UV-Vis.

Therefore, the method employed to calculate the EE% consisted in lyophilization the supernatant and weighting bengamide after centrifugation which was not encapsulated into the nanoparticle (**Figure 66**).

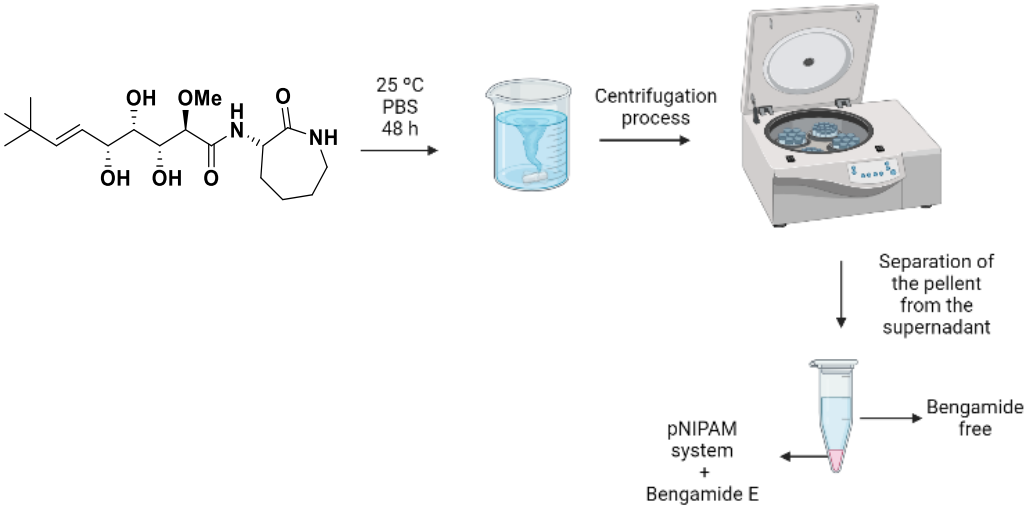

Figure 66. General procedure for encapsulation of bengamide **172 i**nto *p*NIPAM@ nanoparticles.

After following this procedure, bengamide **172** was encapsulated into *p*NIPAM@, *p*NIPAM@Fe_3O_4-3BA and FITC-*p*NIPAM-co-AL@Fe_3O_4-AA. The encapsulation efficiencies (EE%) obtained are showed in **Table 21**.

Table 21. Encapsulation efficiency (EE %) of bengamide **172** into *p*NIPAM nanosystems at 20 ºC

Entry	bengamide 172 (mg)	*p*NIPAM NPs (mg)	Encapsulation efficiency (%)
1	5	*p*NIPAM@ (10)	21
2	5	*p*NIPAM@Fe_3O_4-3BA (10)	28.3
3	5	FITC-*p*NIPAM-co-AL-@Fe_3O_4-AA (6)	32.1
4	5	*p*NIPAM-co-AL@Fe_3O_4-AA (17)	22

Unfortunately, obtained values were lower than the calculated for 5-FU and OXA. Highlight, the best value was obtained from the FITC-*p*NIPAM-co-AL@Fe_3O_4-AA (**Table 21,** entry 3). Therefore, it is remarkable that the molecular size of the bengamide is larger than the commercial drugs previously employed (5-FU and OXA) in the encapsulation into *p*NIPAM@ NPs, so could hinder the encapsulation process. Moreover, in **Figure 67** can be compared the 3D structure of 5-FU with the 3D structure of bengamide analogue **172**. Thus, the molecular size was calculated for 5-FU (3.88 Å) and bengamide **172** (8.97 Å) using Chem3D programme, through these calculations can be concluded that the incursion of bengamide could be much more difficult than 5-FU into *p*NIPAM@ nanoparticles due to the molecular size.

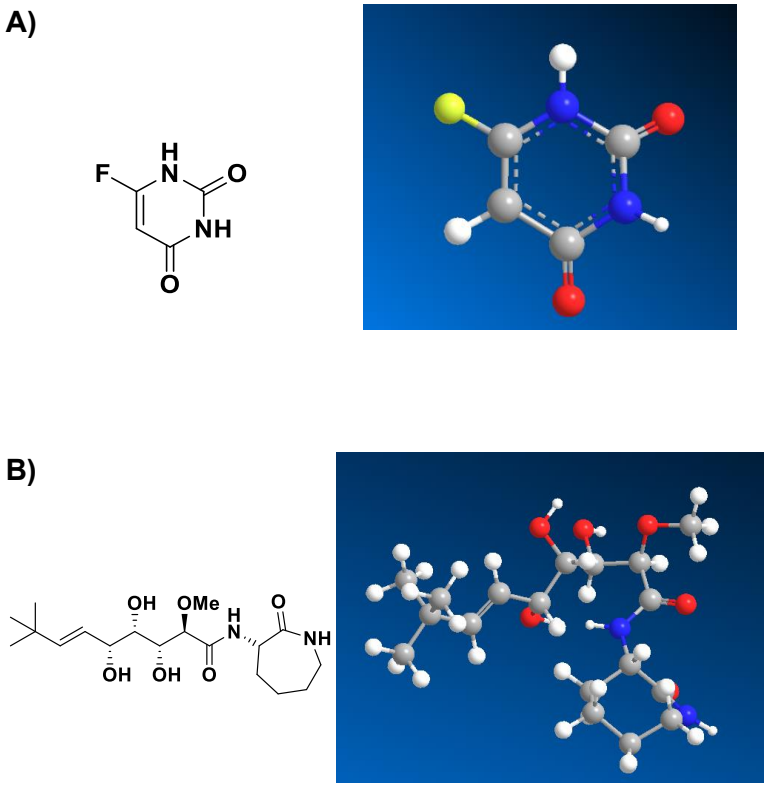

Figure 67. 3D structure of (a) 5-FU and (b) bengamide **172** simulated using chem 3D.

To improve these results, encapsulation was carried out at lower temperatures (5 ºC) to ensure the swollen state of the nanoparticles (**Figure 68**), which means a larger size of these nanosystems and could increases the encapsulation efficiency of bengamide **172** (**Table 22**).

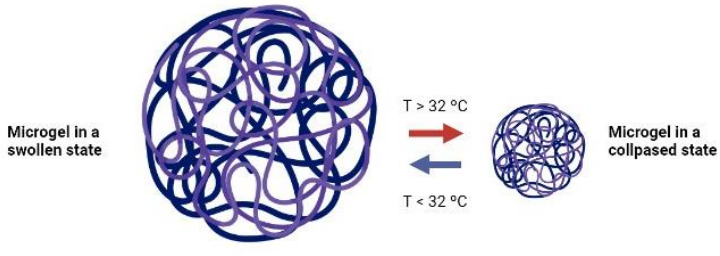

Figure 68. Schematic of the phase transition between the microgel in the sllowen state (left), and the microgel in the collapsed state (right) as a function of temperature.

Table 22. Encapsulation efficiency (EE %) of bengamide **172** into *p*NIPAM nanosystems at 5 ºC.

Entry	Bengamide 172 (mg)	*p*NIPAM NPs (mg)	Encapsulation Efficiency (%)
1	5	*p*NIPAM@(10)	15
2	5	*p*NIPAM@Fe_3O_4-3BA (10)	32.2
3	5	FITC-*p*NIPAM-co-AL @Fe_3O_4-AA(6)	44
4	5	*p*NIPAM-co-AL@Fe_3O_4-AA (17)	26

Table 22 shows the EE % obtained after carrying out the encapsulation process at 5 ºC. All the encapsulation efficiency values increased (**Table 22**, entries 1-4) with respect to the previously obtained carrying out the experiment at 20 ºC (**Table 22**, entries 1-4).Moreover, it is remarkable that best values of EE % were obtained when *p*NIPAM@Fe_3O_4 nanosystems compare to solid *p*NIPAM@, due to the bigger size of these magnetic NPs which means that bengamide **172** could be included into them in an easy way. It should be note that the best value is obtained for the FITC-*p*NIPAM-co-AL@Fe_3O_4-AA nanosystem, as well as happened when the encapsulation process was performed at 20 ºC, which could suggest an especial affinity of the bengamide for the nanoparticle which is fluorescent labelled. In conclusion, the molecular size of bengamide **172** influences the encapsulation process.

5.3. Encapsulation of others active drugs: analogues of tyrosol

5.3.1. Background in the synthesis of tyrosol analogues

In 2017, Prof. Miguel Ángel Medina from Department of Molecular Biology and Biochemistry of the Málaga University studied the bioactivity of two phenolic compounds from Virgin Olive Oil (VOO), tyrosol (**318**) and hydroxytyrosol (**319**) (**Figure 69**), in the context of cancer and angiogenesis (the process by which new blood vessels are formed from pre-existent ones).[206]

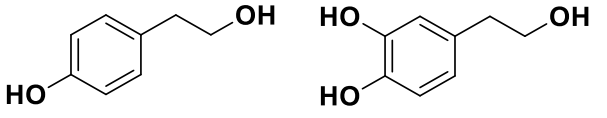

Tyrosol (318) **Hydroxytyrosol (319)**

Figure 69. Structure of tyrosol and hydroxytirsol.

Despite of the similarity in their structures, the effects of **318** were ahead of **319** itself, what promoted a second study in which a few synthetic derivatives were characterized, namely hydroxytyrosyl acetate (**320**), ethyl hydroxytyrosyl ether (**321**), nitrohydroxytyrosol (**322**), nitrohydroxytyrosyl acetate (**323**), and ethyl nitrohydroxytyrosyl ether (**324**) (**Figure 70**).[207] From this comparative study, both hydroxytyrosyl acetate **320** and ethyl hydroxytyrosyl **321** ether showed more potent effetcs than **319**.

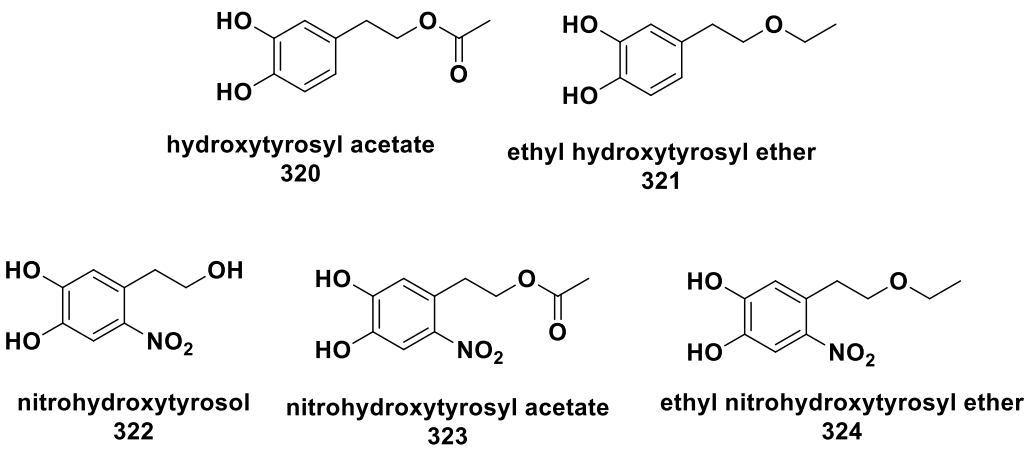

Figure 70. Molecular structure of hydroxytyrosol analogues.

Provided these results, was explored the antiangiogenic potential of six synthetic hydroxytyrosyl alkyl ethers,[208] among which **325** (C6) proved to be the most effective as an anti-angiogenic and pro-apoptotic agent. Therefore, **326** (C8) and **327** (C12) exerted high cytotoxic effects on cells at very low doses (low micromolar range), but due to solubility issues, was not able to properly determine this (**Figure 71**).

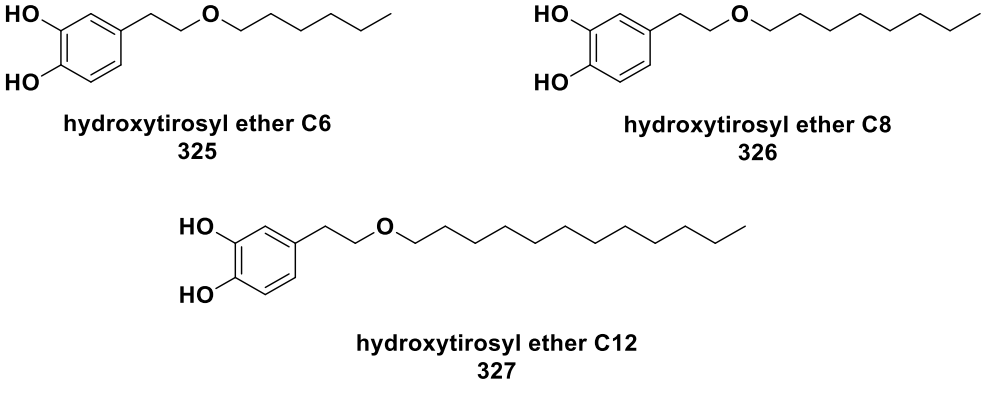

Figure 71. Structure of hydroxytyrosol alkyl ether analogues.

5.3.2. Synthesis of hydroxytyrosol ether analogues

The synthesis towards the hydroxytyrosol ether analogues began from **319**, which aromatics alcohols were protected using benzyl chloride and base yielding **328**. The next step was a substation reaction with three different alkane iodides to obtain **329**, **330** and **331** precursors. Finally, after removing benzyl protecting groups by hydrogenation using Pd/C the desired analogues **325**, **326** and **327** were obtained (**Scheme 47**).

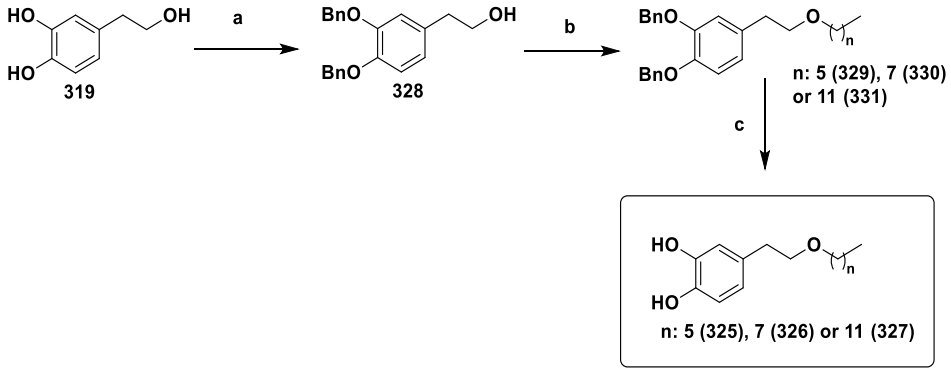

Scheme 47. Synthesis towards Hydroxytyrosol analogues,

Reagents and conditions. (a) **319,** BnBr, K_2CO_3, Acetone, 24 h, 25 ºC. (b) **328**, RI, NaOH, DMSO, 12 h, 25 ºC(c) H_2, Pd/C, EtOH, 12 h, 25 ºC (yield from 60 to 70%).

5.3.3. Biological evaluations of hydroxytyrosol ether analogues

At this point of the work, biological evaluations were carried out with collaboration with Prof. Miguel Ángel Medina from Department of Molecular Biology and Biochemistry of the Málaga University. Thus, proliferation assays (MTT assays) were carried out to evaluate cellular metabolic activity as an indicator of cell viability, proliferation, and cytotoxicity. Moreover, with this assay allows to obtain the proliferation curve of certain cell type exposed to the analogues synthesized, being able to calculate IC_{50} value (**Figure 72**).[209]

A)

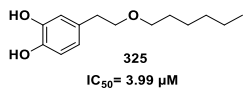

IC_{50}= 3.99 µM

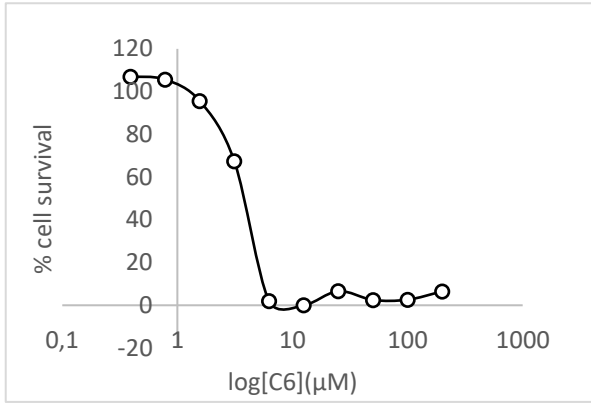

B)

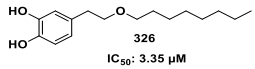

IC_{50}: 3.35 µM

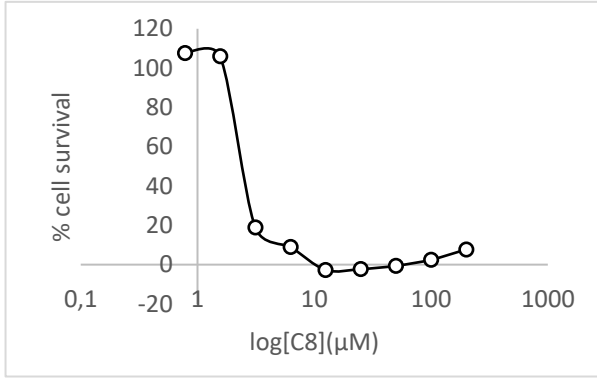

C)

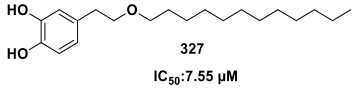

IC_{50}:7.55 µM

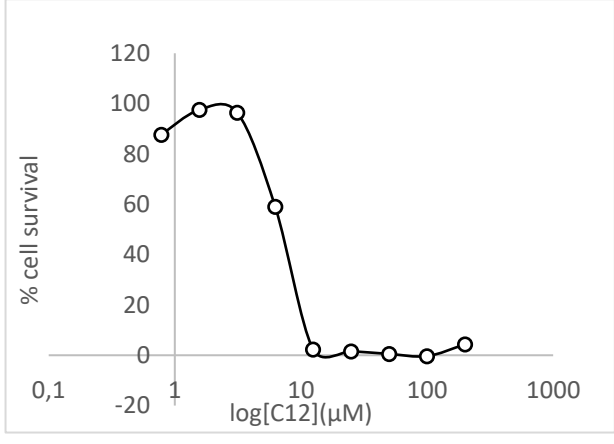

Figure 72. MTT essays for **325** (a), **326** (b) and **327** (c).

From these results can be observed that values of IC_{50} of **325** (**Figure 72,A**) are similar to the obtained for **326** (**Figure 72 B**), even though the value that was expected would be lower. Regarding to **327** (**Figure 72 C**), the value of IC_{50} is higher than expected value and solubility problems were observed during the experiment cause the lower solubility in water of this analogue.

To solve this problem, was decided to encapsulate the C12 analogue **327** in *p*NIPAM@ nanoparticles, as well as will be explain in the next section.

*5.3.4. Encapsulation of hydroxytyrosol ether C12 **327** into pNIPAM nanoparticles*

With the objective of avoiding the solubility problems of C12 analogue **327**, encapsulation into *p*NIPAM@ nanoparticles systems was proposed to avoid the precipitation of this product during the biological essays (**Figure 73**).

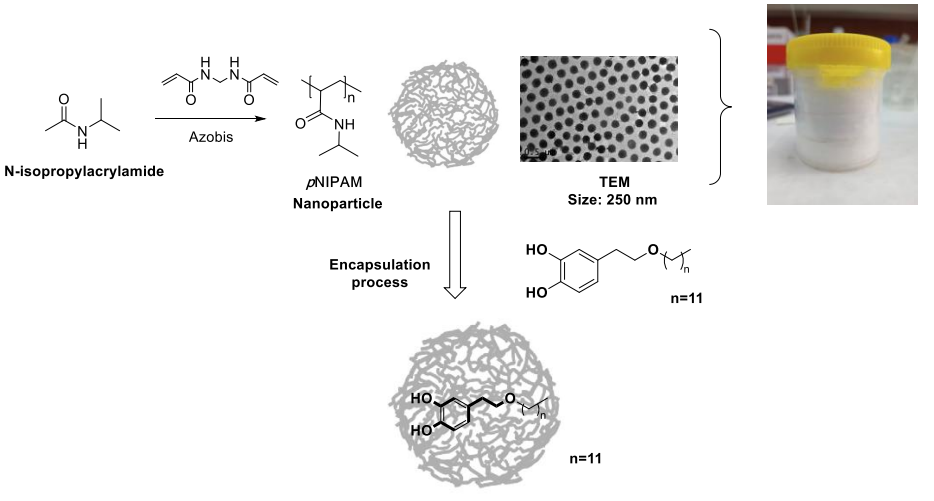

Figure 73. Encapsulation of analogue **327** into *p*NIPAM@ nanoparticles systems.

Thus, following the strategy of **Figure 73** the Efficience of Encapsularion (EE %) was of 63 % with an encapsulation of 0.45 mg of analogue in 1 mg of nanoparticle. With this nanoparticle in hand, the MTTs essays were carried out again with collaboration with Prof. Miguel Ángel Medina from Department of Molecular Biology and Biochemistry of the Málaga University. **Figure 74** shows the values for the encapsulated analogue and the free analogue. Unfortunately, values obtained for C12 analogue **327** and *p*NIPAM@+ C12 (**327**) analogue were similar, and it was not detected an increase in IC_{50} after encapsulating this compound into nanoparticles.

A)

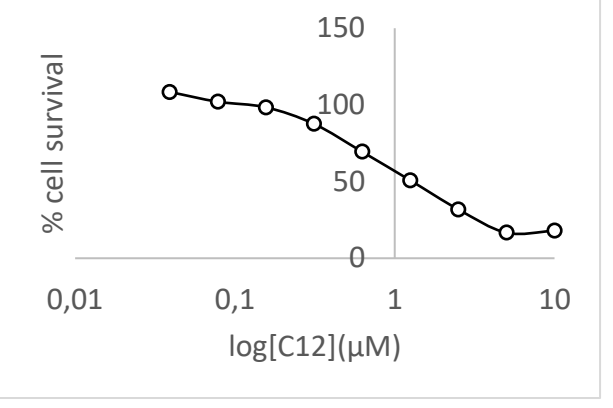

B)

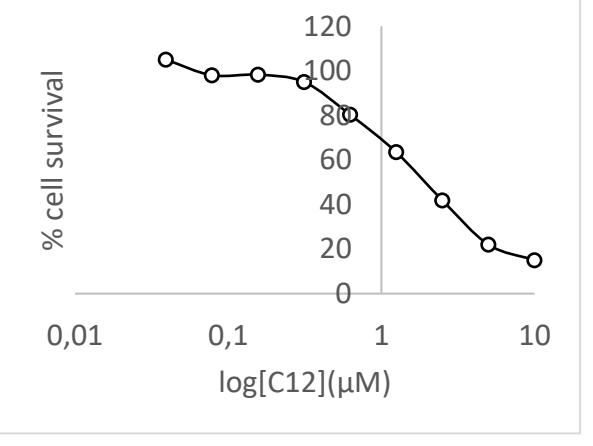

Figure 74. MMTs essays of (A) Free Hydroxytyrosol ether **327** (B) *p*NIPAM@+**327.**

After obtaining these results was concluded that biological essays were not carried out in a correct temperature to ensure the delivery of the drug from the nanoparticle. Moreover, this temperature was higher than the lower critical temperature solution (32 ºC), which is the temperature at which the microgel is in a collapsed state. Thus, at the beginning of the experiment drug is completely delivered and the data obtained is the same when free hydroxytyrosol ether **327** is evaluated (**Figure 75**).

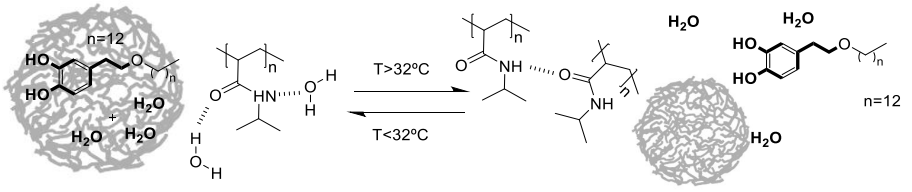

Figure 75. Lower Critical Temperatures of *p*NIPAM nanoparticles.

5.4. Summary

In conclusion, different drugs have been included into different nanosysten:

- 5-fluorouracil has been encapsulated into *p*NIPAM@, *p*NIPAM@Fe_3O_4-3BA and *p*NIPAM-co-AL@Fe_3O_4-AA and Oxaliplatin was included into *p*NIPAM@ and *p*NIPAM@Fe_3O_4-3BA.
- Bengamide **172** was encapsulated into *p*NIPAM@, *p*NIPAM@Fe_3O_4-3BA, FITC-*p*NIPAM-co-AL@Fe_3O_4-AA.
- Hydroxytirosyl ether C12 analogue **327** was included into *p*NIPAM@.

CHAPTER 6. CONCLUSIONS

After the development of this PhD Thesis in the field of total synthesis of natural products and biomedicine, the following conclusions can be drawn from each chapter:

Chapter 3: synthesis of new analogues of bengamides.

- The bengamide analogue **145** (7 steps, 2 % overall yield) and **172** (7 steps, 2 % overall yield) have been synthesized starting from *D*-glucoheptono-1,4-lactone.
- Preliminary biological evaluation of the bengamides analogues **145** and **172** showed that are biocompatible and more pronounced antiproliferative effect on tumour cell lines compare to normal cell which suggests these analogues as potent antitumoral treatment.
- The bengamide analogue **145** has been prepared in the necessary multi-milligrams amount to carry out *in vivo* essays.
- *In vivo* studies demonstrated that bengamide **145** significantly reduced tumour volume and metastases, consequently increasing overall survival and shows promise as a lung cancer treatment with substantial antitumor activity and notable safety.
- A new analogue of bengamide, **289**, was obtained starting from *D*-tartaric acid (15 steps, 0.6 % overall yield).
- A new methodology towards analogues of peptidyl bengamides has been developed based on the solid phase strategy which provided a fast and effective methods towards a new library of bengamides.
- Two new dipeptidyl analogues of bengamide, **315** and **317**, were prepared in a 0.6 % and 1 % overall yield (15 steps), respectively.

Chapter 4: thermosensitive polymeric nanoparticles with magnetic core.

- *p*NIPAM@ nanoparticle systems have been prepared, these nanogels were highly monodispersed and stables, optimizing the

process through the monomer concentration and the crosslinking percentage.

- These *p*NIPAM@ systems have been functionalized with different comonomers: 3 -butenoic acid, acrylic acid and allylamine (3-BA, AA and AL).
- Magnetic nanoparticles (@Fe_3O_4) were obtained through the co-precipitation method using TMAOH and NaOH as bases.
- The surface of the magnetic nanoparticles was modified using 3-butenoic acid and acrylic acid, in this way a double bond was obtained in the surface, which was essential for the polymerization process.
- Using the magnetic nanoparticles (@Fe_3O_4) as a magnetic core and polymerizing *p*NIPAM by free radicals, it was synthetized a hybrid system which was able to response to the temperature and magnetic changes.
- Different concentrations of monomer and crosslinker were employed to optimize the size and the aggregation of magnetic nanoparticles.
- *p*NIPAM-co-Al@Fe_3O_4 nanoparticles have been fluorescently labelled with Fluorescein isothiocyanate (FITC).

Chapter 5: encapsulation of active drugs into polymeric magnetic nanoparticles.

- Commercial drugs (5- fluorouracil and oxaliplatin) have been encapsulated into different *p*NIPAM@/*p*NIPAM@Fe_3O_4 systems.
- From a biological view, these nanoformulations showed great biocompatibility which suggest these systems for the cancer treatment. Moreover, the magnetic-polymeric nanoparticles (*p*NIPAM@Fe_3O_4) could be directly target to the tumour through an external magnetic field avoiding the secondary effects of chemotherapy.

- Bengamide **172** has been encapsulated into different *p*NIPAM nanosystems.
- Different analogues of hydroxytyrosol were synthesized and encapsuled into *p*NIPAM nanoparticles.

CHAPTER 7. EXPERIMENTAL SECTION

7.1. General Techniques

Chemical Techniques

All reactions were performed using oven-dried glassware (200 ºC) under an atmosphere of dry argon unless using aqueous reagents or otherwise stated. All solvents used in reactions were dried and distilled using standard procedures. DMF and DMSO were purchased from Sigma-Aldrich. THF and toluene were distilled from sodium and CH_2Cl_2 and MeOH from calcium hydride prior to use. All other solvents were used as supplied unless otherwise stated. All reagents were purchased from Aldrich, Across Chimica, Merk or Alfa Aesar and were used as supplied or purified using standard procedures as necessary. All solutions used in workup procedures were saturated unless otherwise noted.

Flash column chromatography (FCC) was performed using E.Merk silica gel 60 Å, particle size 230-400 mesh under air pressure. All solvents used for chromatographic purification were distilled prior to use. Analytical TLC was performed using silica gel 60 F_{254} ALUGRAM® SII G/UV254 plates and visualized by ultraviolet radiation (254 nm), potassium permanganate or acidic ceric ammonium molybdate as appropriate.

Quantities are reported to 3 significant figures and are rounded accordingly. Isolated yields are reported to 0 decimal places and “quant.” signifies a yield of 99.5% or higher. NMR spectra were recorded on Bruker Avance III plus Brucker (400 MHz) or on Avanceneo Bruker (500 MHz). Chemical shifts are reported in ppm with the resonance resulting from incomplete deuteration of the solvent as the internal standard ($CDCl_3$: 7.26 ppm, DMSO-d_6, 2.49 ppm, D_2O, 4.80 ppm and MeOD, 3.35 and 4.78 ppm). Chemical shifts are reported in ppm with the solvent resonance as the internal standard ($^{13}CDCl_3$: 77.0 ppm, t,). Data are reported as follows: chemical shift **δ**/ppm (integration (^1H only), multiplicity (s = singlet, d = doublet, t = triplet, q = quartet, br = broad, app = apparent, m = multiplet

or combinations thereof). ^{13}C signals are singles (unless otherwise stated), coupling constants *J* (Hz, assignment).

High resolution mass spectrometry (HRMS) was performed on a Bruker HCT-ULTRA mass spectrometer under Fast Atom Bombardment (FAB) conditions and on an ESI-TOF and APCI mass spectrometer in positive mode. HRMS signals are reported to 4 decimal places and are within 5 ±ppm of theoretical values.

7.2. Experimental Procedures and Characterization Related to Bengamides

*7.2.1. Synthesis of compound **255**. Protection reaction of D-Gluco-heptono-1,4-lactone lactone **56***

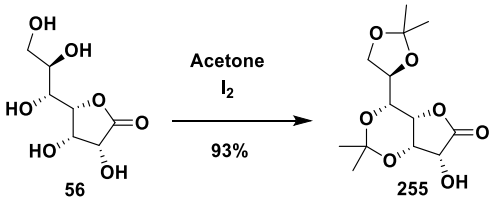

I_2 (190 mg, 0.75 mmol, 0.01 equiv.) was added to a stirred solution of *D*-Glucoheptono-1,4-lactone (15 g, 72.56 mmol, 1.00 equiv.) in anhydrous acetone (270 mL). The mixture was stirred at room temperature for 48 h. After this time, the reaction was quenched by addition of a saturated aqueous $Na_2S_2O_3$ solution, after separation of both layers, the aqueous phase was then extracted with EtOAc. The organic layer was washed again with a saturated aqueous $Na_2S_2O_3$ solution. Then, the organic layer was dried over anhydrous $MgSO_4$, filtered and solvents were concentrated under reduced pressure. The crude was purified by crystallization in a CH_2Cl_2 and Hexanes mixture. The resulting solid was filtered to obtain the desired lactone **255** (20.41 g, 93 %) as a white foam.

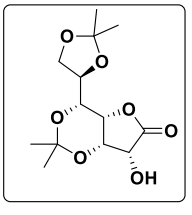

Physical aspect: white foam.

Rf: 0.20 (silica gel, 50 % EtOAc in Hexanes).

^{1}H NMR (400 MHz, $CDCl_3$) δ (ppm): 4.61 (dd, J = 4.1, 2.2 Hz, 1H), 4.49 (d, J = 4.0 Hz, 1H), 4.37 – 4.29 (m, 2H), 4.23 – 4.04 (m, 2H), 3.93 (dd, J = 8.9, 4.0 Hz, 1H), 3.83 (dd, J = 8.6, 2.0 Hz, 1H), 1.50 (s, 3H), 1.44 (s, 3H), 1.41 (s, 3H), 1.35 (s, 3H).

^{13}C (100 MHz, $CDCl_3$) δ (ppm): 174.7, 109.8, 99.0, 73.2, 71.8, 69.8, 68.8, 68.2, 67.1, 29.0, 27.1, 25.0, 19.7.

7.2.2. Synthesis of compound 256**. Methylation of the free hydroxyl group of **255

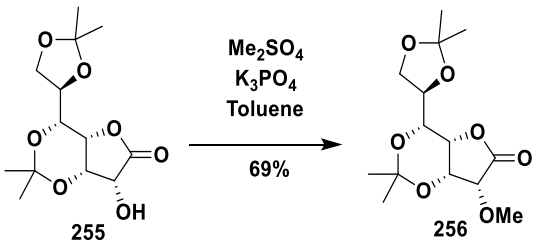

K_3PO_4 (26.50 g, 124.90 mmol, 3.00 equiv.) was added to a stirred solution of **255** (12 g, 41.60 mmol, 1.00 equiv.) in anhydrous toluene (120 mL). Then, Me_2SO_4 (11.80 mL, 124.90 mmol, 3.00 equiv.) was added and the mixture was stirred at room temperature for 24 h. After this time, solvent was removed in vacuo. The crude was diluted in EtOAc and brine. After separation of both layers, the aqueous phase extracted twice with EtOAc, dried over anhydrous $MgSO_4$, filtered and solvents were removed under reduced pressure. The crude was purified by crystallization in an EtOAc and Hexanes mixture. The resulting solid was filtered and to obtain the desired **256** (8.70 g, 69 %) as a white foam.

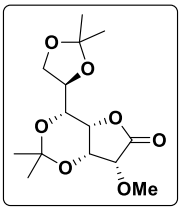

Physical aspect: white foam.

Rf: 0.29 (silica gel, 50 % EtOAc in Hexanes).

^{1}H NMR (400 MHz, $CDCl_3$) δ (ppm): 4.71 (dd, J = 3.9, 2.1 Hz, 1H), 4.34 (ddd, J = 8.5, 6.2, 4.0 Hz, 1H), 4.27 (t, J = 2.1 Hz, 1H), 4.15 – 4.07 (m, 2H), 3.93 (dd, J = 8.9, 4.1 Hz, 1H), 3.82 (dd, J = 8.6, 2.0 Hz, 1H), 3.66 (s, 3H), 1.49 (s, 3H), 1.43 (s, 6H), 1.35 (s, 3H).

^{13}C (100 MHz, $CDCl_3$) δ (ppm): 174.7, 109.8, 99.0, 79.9, 73.2, 71.8, 69.8, 68.8, 68.2, 67.1, 29.0, 27.1, 25.0, 19.7.

*7.2.3. **Synthesis of compound 257.** Selective hydrolysis of the primary acetal **256***

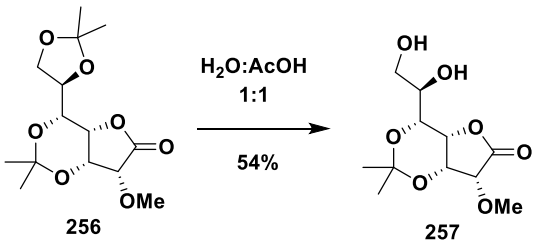

Lactone **256** (3.10 g, 10.30 mmol, 1.00 equiv.) was treated with a water: acetic acid mixture (1:1, 50 mL). The mixture was stirred at room temperature for 12 h. After this time, solvents were removed in vacuo. The crude was purified by crystallization in a MeOH and Et_2O mixture. The resulting solid was filtered to obtain the desired diol **257** (1.50 g, 54 %) as a white solid.

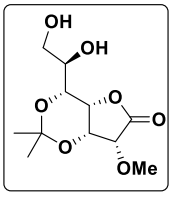

Physical aspect: white solid.

Rf: 0.50 (silica gel, 90 % EtOAc in Hexanes).

^{1}H NMR (400 MHz, MeOD) δ (ppm): 4.85 – 4.84 (m, 1H), 4.44 (t, J = 2.0 Hz, 1H), 4.42 (d, J = 3.9 Hz, 1H), 4.07 (dd, J = 9.1, 1.9 Hz, 1H), 3.78 (ddd, J = 9.1, 4.9, 2.5 Hz, 1H), 3.72 (dd, J = 11.5, 2.5 Hz, 1H), 3.59 (dd, J = 11.5, 4.9 Hz, 1H), 3.55 (s, 3H), 1.51 (s, 3H), 1.35 (s, 3H).

^{13}C (100 MHz, MeOD) δ (ppm): 175.7, 99.7, 80.3, 70.7, 69.1, 68.9, 63.8, 60.3, 58.8, 29.4, 19.6.

7.2.4. Synthesis of compound 259. *Reaction of Grank and Estwood to obtain intermediate ortho ester*

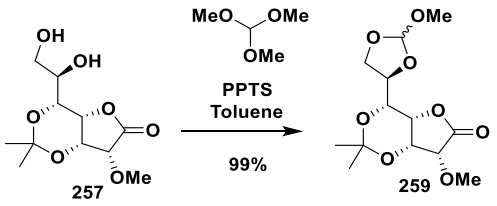

Trimethylorthoformate (6.30 mL, 57.20 mmol, 5.00 equiv.) was added to a stirred solution of diol **257** (3 g, 11.40 mmol, 1.00 equiv.) in anhydrous THF (30 mL). Then, PPTS (0.58 g, 2.30 mmol, 0.20 equiv.) was added and the mixture was stirred at room temperature for 12 h. After this time, the reaction mixture was filtered through a silica gel pad and the resulting clear solution was concentrated under reduced pressure to obtain the desired ortho ester **259** (3.48 g, 99 %) as a white foam which was used in the next step without any further purification.

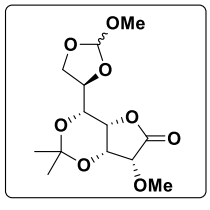

Physical aspect: white foam.

Rf: 0.50 (silica gel, 10% EtOAc in Hexanes).

^{1}H NMR (400 MHz, $CDCl_3$) δ (ppm): 5.75 (s, 1H), 5.72 (s, 1H), 4.72 (dd, J = 3.9, 2.1 Hz, 1H), 4.70 (dd, J = 3.9, 2.1 Hz, 1H), 4.52 (ddd, J = 8.2, 6.6, 4.0 Hz, 1H), 4.40 (ddd, J = 8.8, 6.4, 5.8 Hz, 1H), 4.27 (t, J = 2.1 Hz, 1H), 4.24 (t, J = 2.1 Hz, 1H), 4.20 – 4.15 (m, 1H), 4.16 – 4.11 (m, 2H), 4.03 (dd, J = 8.9, 2.0 Hz, 1H), 4.00 – 3.93 (m, 1H), 3.86 (dd, J = 8.2, 2.0 Hz, 1H), 3.65 (s, 6H), 3.34 (s, 3H), 3.31 (s, 3H), 1.49 (s, 3H), 1.48 (s, 3H), 1.43 (s, 3H), 1.42 (s, 3H).

^{13}C (100 MHz, $CDCl_3$) δ (ppm): 172.59, 116.99, 115.90, 98.86, 98.77, 79.13, 73.16, 73.07, 70.10, 68.78, 68.69, 68.42, 67.64, 67.48, 66.12, 59.29, 52.78, 51.82, 29.05, 19.58, 19.47.

7.2.5. Synthesis of compound 254. *Heat treatment of ortho ester* ***259***

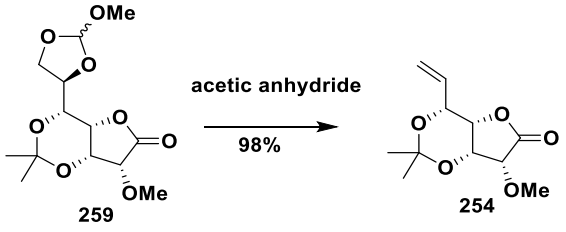

Ortho ester **259** (6.36 g, 20.90 mmol, 1.00 equiv.) was dissolved in acetic anhydride (250 mL). The mixture was stirred at 150 ºC for 3 h. After this time, the solvent was concentrated in vacuo. The resulting crude product was purified by flash-column chromatography (Silica gel, 60 % EtOAc in Hexanes) to obtain the desired terminal alkene **254** (4.68 g, 98 %) as a brown solid.

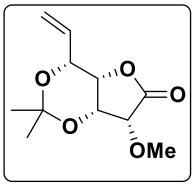

Physical aspect: brown solid.

Rf: 0.45 (silica gel, 80 % EtOAc in Hexanes).

^{1}H NMR (400 MHz, $CDCl_3$) δ (ppm): 5.98 (ddd, *J* = 17.1, 10.5, 6.4 Hz, 1H), 5.38 (ddt, *J* = 33.0, 10.4, 1.2 Hz, 2H), 4.74 (dd, *J* = 3.9, 2.1 Hz, 1H), 4.52 (ddt, *J* = 6.5, 2.2, 1.1 Hz, 1H), 4.20 – 4.06 (m, 1H), 4.05 (t, *J* = 2.1 Hz, 1H), 3.66 (s, 3H), 1.54 (s, 3H), 1.49 (s, 3H).

^{13}C (100 MHz, $CDCl_3$) δ (ppm): 172.86, 133.10, 119.03, 98.84, 79.12, 71.17, 69.86, 67.65, 59.24, 29.31, 19.38.

***7.2.6. Synthesis of compound 90**. Reaction of Olefin Cross Metathesis.*

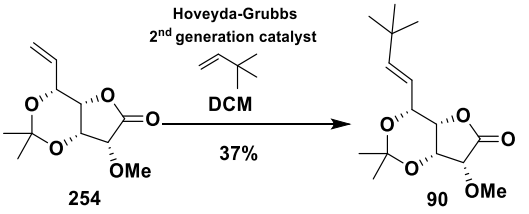

Olefin **254** (220 mg, 1.00 mmol, 1.00 equiv.) and Hoveyda-Grubbs 2nd generation catalyst (940 mg, 0.15 mmol, 1.00 equiv.) were dissolved in degassed CH_2Cl_2 (10 mL). Then, 3,3-dimethylbut-1-ene (420 mg, 5 mmol, 0.64 mL, 5.00 equiv.) was added dropwise at room temperature. The resulting mixture reaction was heated at 40 ºC in a sealed tube for 12 h. After this time, the crude mixture was concentrated in vacuo. The resulting crude was purified by flash-column chromatography (Silica gel, 40 % EtOAc in Hexanes) to obtain the desired *E*-alkene **90** (160 mg, 37 %) as a brown solid.

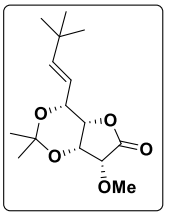

Physical aspect: brown solid.

Rf: 0.59 (silica gel, 80 % EtOAc in Hexanes).

^{1}H NMR (400 MHz, $CDCl_3$) δ (ppm): 5.84 (d, *J* = 15.8 Hz, 1H), 5.58 (dd, *J* = 15.8, 7.6 Hz, 1H), 4.71 (dd, *J* = 3.8, 2.1 Hz, 1H), 4.45 (d, *J* = 8.9 Hz, 1H), 4.09 (d, *J* = 3.8 Hz, 1H), 3.99 (t, *J* = 2.0 Hz, 1H), 3.66 (s, 3H), 1.53 (s, 3H), 1.49 (s, 3H), 1.03 (s, 9H).

^{13}C (100 MHz, $CDCl_3$) δ (ppm) : 172.99, 143.35, 122.20, 98.84, 79.20, 71.87, 70.18, 67.72, 59.30, 30.86, 29.41, 22.02, 21.98, 19.41.

*7.2.7. Synthesis of compound **261**. Reaction of Olefin Cross Metathesis*

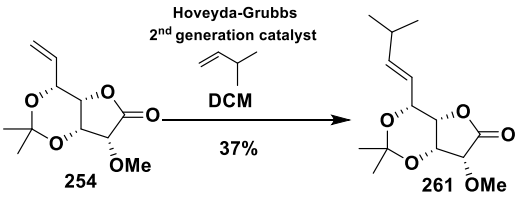

Hoveyda−Grubbs 2nd generation catalyst (16 mg, 0.02 mmol, 0.20 equiv.), olefin **254** (23 mg, 0.09 mmol, 1.00 equiv.) and 3-Methylbut-1-ene (60 mg, 0.27 mmol, 3.00 equiv.) were dissolved in degassed CH_2Cl_2 (8 mL), and the reaction mixture was heated at 40 °C for 24 h. After this time, the solvent was removed under reduced pressure. The resulting crude was purified by flash-column chromatography (Silica gel, 40 % EtOAc in hexanes) to obtain the desired product **261** (6 mg, 15 %) as a colourless oil.

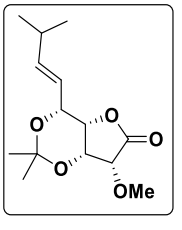

Physical aspect: colourless oil.

Rf: 0.55 (silica gel, 80 % EtOAc in Hexanes).

^{1}H NMR (400 MHz, $CDCl_3$) δ (ppm): 5.82 (ddd, J = 15.6, 6.2, 0.7 Hz, 1H), 5.62 (ddd, J = 15.6, 7.5, 1.4 Hz, 1H), 4.71 (dd, J = 3.9, 2.1 Hz, 1H), 4.45 (dd, J = 7.5, 1.8 Hz, 1H), 4.10 (d, J = 3.9 Hz, 1H), 3.99 (t, J = 2.1 Hz, 1H), 3.66 (s, 3H), 2.34 (dqd, J = 13.4, 6.7, 1.3 Hz, 1H), 1.53 (s, 3H), 1.48 (s, 3H), 1.01 (dd, J = 6.8, 1.5 Hz, 6H).

7.2.8. Synthesis of precursor 262**. Coupling reaction between caprolactam **74** and alkene **90

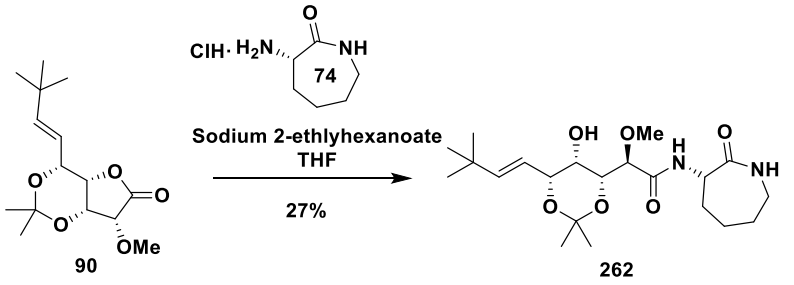

Alkene **90** (81 mg, 0.29 mmol, 1.00 equiv.) and Ɛ-aminocaprolactam **74** (70.3 mg, 0.43 mmol, 1.50 equiv.) were dissolved in anhydrous THF (15 mL). Then, sodium 2-ethylhexanoate (282 mg, 3.36 mmol, 6.00 equiv.) was added and the resulting mixture was stirred at room temperature for 48 h. After this time, cyclohexane and water were added and the mixture was stirred for 30 min at room temperature. The reaction mixture was diluted with CH_2Cl_2. After separation of both layers, the aqueous phase was extracted twice with CH_2Cl_2. The organic layer was washed with brine, dried over anhydrous $MgSO_4$, filtered and solvents were removed under reduced pressure. The resulting crude reaction was purified by flash-column chromatography (Silica gel, 5 % MeOH in CH_2Cl_2) to obtain the desired precursor **262** (32.5 mg, 27 %) as a brown solid.

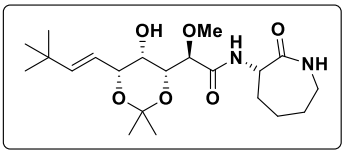

Physical aspect: brown solid.

Rf: 0.50 (silica gel, 10 % MeOH in CH_2Cl_2),

^{1}H NMR (400 MHz, $CDCl_3$) δ (ppm): 7.56 (d, J = 6.6 Hz, 1H), 6.29 (t, J = 6.5 Hz, 1H), 5.77 (dd, J = 15.8, 1.0 Hz, 1H), 5.52 (dd, J = 15.8, 6.7 Hz, 1H), 4.59 (ddd, J = 11.1, 6.5, 1.9 Hz, 1H), 4.27 (dt, J = 6.9, 1.2 Hz, 1H), 4.06 (dd, J = 7.3, 1.3 Hz, 1H), 3.87 (d, J = 7.3 Hz, 1H), 3.47 (s, 3H), 3.32 – 3.22 (m, 2H), 2.17 – 1.96 (m, 3H), 1.92 – 1.73 (m, 3H), 1.59 – 1.51 (m, 2H), 1.46 (s, 3H), 1.44 (s, 3H), 1.02 (s, 9H).

HRMS (H-ESI) m/z: $[M+H]^+$ calculated for $C_{21}H_{37}N_2O_6$ 413.2652; found 413.2675.

7.2.9. Synthesis of bengamide 172. Acidic hydrolysis of precursor 262

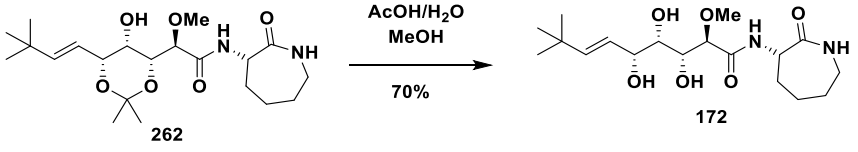

A 70 % aqueous AcOH solution (5.85 mL) was added dropwise to a stirred solution of precursor **262** (32.5 mg, 0.078 mmol, 1.00 equiv.) in MeOH (2.50 mL). The resulting reaction mixture was heated at 70 ^oC for 2 h. After this time, the crude reaction was diluted with EtOAc and the excess of AcOH was quenched by a saturated aqueous $NaHCO_3$ solution. The aqueous phase was extracted with EtOAc and the combined organic layers were washed with brine, dried over anhydrous $MgSO_4$, filtered and solvents were concentrates under reduced pressure. The resulting crude reaction was purified by flash-column chromatography (Silica gel, 10 % MeOH in CH_2Cl_2) to obtain the desired bengamide analogue **172** (20.54 mg, 43 %) as a colourless oil.

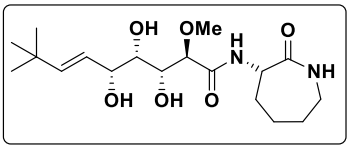

Physical aspect: colourless oil.

Rf: 0.10 (silica gel, 10 % MeOH in CH_2Cl_2).

^{1}H NMR (400 MHz, $CDCl_3$) δ (ppm): 7.98 (d, J = 6.4 Hz, 1H), 6.29 (t, J = 5.6 Hz, 1H), 5.82 (dd, J = 15.7, 0.9 Hz, 1H), 5.41 (dd, J = 15.7, 7.3 Hz, 1H), 4.54 (ddd, J = 11.3, 6.3, 1.2 Hz, 1H), 4.23 (dd, J = 6.6, 5.7 Hz, 1H), 3.84–3.76 (m, 2H), 3.60 (d, J = 4.8 Hz, 1H), 3.53 (s, 3H), 3.32–3.25 (m, 2H), 2.10–2.03 (m, 3H), 1.91–1.80 (m, 2H), 1.64–1.54 (m, 1H), 1.49–1.37 (m, 1H), 1.28–1.23 (m, 2H), 1.02 (s, 9H).

^{13}C NMR (100 MHz, MeOD) δ (ppm): 175.51, 171.47, 144.57, 124.00, 82.19, 73.81, 72.96, 71.20, 57.32, 51.85, 41.08, 32.36, 30.80, 29.26, 28.52, 28.47, 27.70.

HRMS (H-ESI) m/z: $[M+H]^+$ calculated for $C_{18}H_{33}N_2O_6$: 373.2339; found 373.2341

7.2.10. Synthesis of compound 266.

Coupling reaction between Boc-*L*-alanine and 3-aminopropan-1-ol

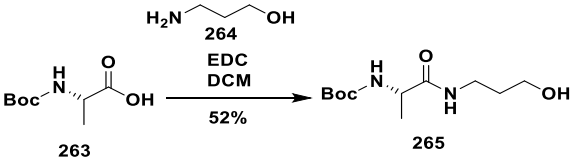

3-aminopropan-1-ol **264** (0.63 mL, 8.21 mmol, 3.10 equiv.) was added dropwise to a stirred solution of Boc-*L*-alanine **263** (0.50 g, 2.64 mmol, 1.00 equiv.) and EDC (1.25 g, 6.50 mmol, 2.50 equiv.) in CH_2Cl_2 (13 mL) at 0ºC. Then, the mixture was stirred at room temperature for 12 h. After this time, the solvent was concentrated in vacuo. The resulting crude reaction was purified by flash-column chromatography (Silica gel, 100 % EtOAc) to obtain the desired amino acid derivative **265** (314 mg, 52 %) as a colourless oil.

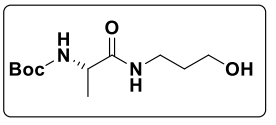

Physical aspect: colourless oil.

Rf: 0.43 (silica gel,100 % EtOAc),

^{1}H NMR (400 MHz, $CDCl_3$) δ (ppm): 6.63 (s, 1H), 5.09 – 4.90 (m, 1H), 4.12 (q, *J* = 7.1 Hz, 1H), 3.79 – 3.51 (m, 2H), 3.50 – 3.35 (m, 2H), 2.32 – 2.17 (m, 1H), 2.04 (s, 1H), 1.72 – 1.62 (m, 2H), 1.44 (s, 9H), 1.36 (d, *J* = 7.1 Hz, 3H).

Esterification of cyclohexane carboxylic acid and alcohol **265**

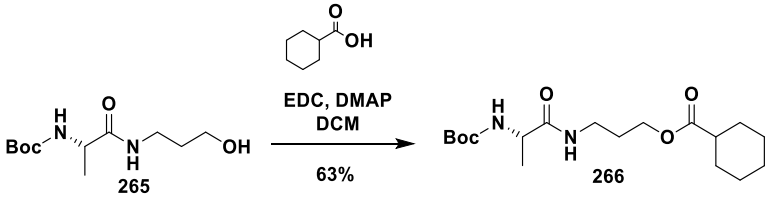

Cyclohexanecarboxylic acid (0.22 mL, 1.80 mmol, 1.30 equiv.) was added dropwise to a stirred solution of amino acid derivative **266** (314

mg, 1.34 mmol, 1.00 equiv.), EDC (518 mg, 2.7 mmol, 2.00 equiv.) and DMAP(1 7 mg, 2.70 mmol, 0.10 equiv.) in CH_2Cl_2 (20 mL). Then, the mixture was stirred at room temperature for 12 h. After this time, the solvent was concentrated in vacuo. The resulting crude reaction was purified by flash-column chromatography (Silica gel, 100 % EtOAc) to obtain amino acid derivative **266** (302 mg, 63 %) as a colourless oil.

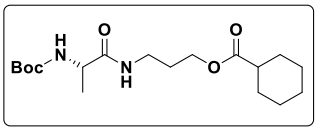

Physical aspect: colourless oil.

Rf: 0.56 (silica gel,10% MeOH in CH_2Cl_2).

^{1}H NMR (400 MHz, $CDCl_3$) δ (ppm): 6.66 (s, 1H), 5.26 (s, 1H), 4.21 – 4.02 (m, 2H), 3.36 – 3.20 (m, 1H), 2.38 – 2.21 (m, 3H), 1.98 – 1.68 (m, 12H), 1.42 (s, 9H), 1.33 (d, J = 7.1 Hz, 3H).

^{13}C NMR (100 MHz, $CDCl_3$) δ (ppm): 176.34, 172.70, 61.30, 51.46, 43.20, 36.12, 29.06, 29.03, 28.79, 28.32, 25.72, 25.45, 25.42.

7.2.11. Synthesis of precursor 268

Boc deprotection of amino acid derivative **266**

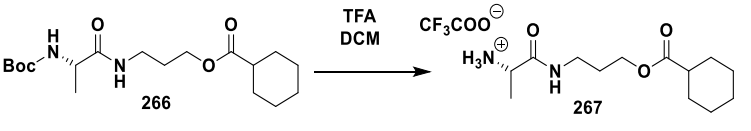

Trifluoracetic acid (2.62 mL, 34.32 mmol, 65.00 equiv.) was added dropwise to a stirred mixture of intermediate **266** (190 mg, 0. 528 mmol, 1.00 equiv.) in CH_2Cl_2 (13 mL) at 0 ºC. The resulting reaction mixture was stirred at room temperature for 3 h. After this time, solvents were concentrated in vacuo to obtain the desired amino acid derivative **267** as a light-yellow oil which was used in the next step without any further purification.

Opening reaction of lactone **90** with *L*-alanine derivative **267**

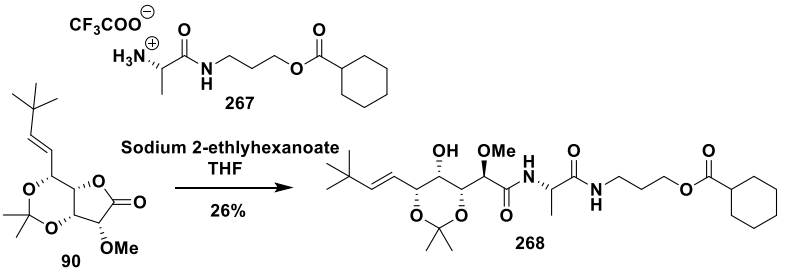

A mixture of alkene **90** (100 mg, 0.351 mmol, 1.00 equiv.) and amino acid derivative **267** (195 mg, 0.53 mmol, 1.50 equiv.) and sodium 2-ethylhexanoate (232 mg, 1.14 mmol, 4.00 equiv.) in anhydrous THF (12 mL) was stirred at room temperature for 4 days. After this time, cyclohexane and water were added and the mixture was stirred for 30 min at room temperature. The reaction mixture was diluted with CH_2Cl_2. After separation of both layers, the aqueous phase was extracted twice with CH_2Cl_2. The organic layer was washed with brine, dried over anhydrous $MgSO_4$, filtered and solvents were removed under reduced pressure. The resulting crude reaction was purified by flash-column chromatography (Silica gel, 5 % MeOH in CH_2Cl_2) to obtain the desired precursor **268** (53 mg, 26 %) as a light-yellow oil.

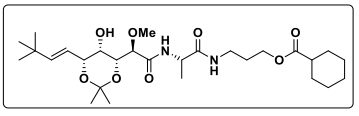

Physical aspect: light-yellow oil.

Rf: 0.20 (silica gel,10 % MeOH in CH_2Cl_2).

^{1}H NMR (400 MHz, $CDCl_3$) δ (ppm): 6.90 (d, J = 8.3 Hz, 1H), 6.73 (t, J = 6.3 Hz, 1H), 5.77 (d, J = 15.8 Hz, 1H), 5.50 (dd, J = 15.8, 6.9 Hz, 1H), 4.52 (dd, J = 8.3, 7.1 Hz, 1H), 4.26 (d, J = 7.1 Hz, 1H), 4.17 (dd, J = 6.0, 1.4 Hz, 1H), 4.14 – 4.05 (m, 3H), 3.92 (d, J = 6.1 Hz, 1H), 3.51 (s, 3H), 3.28 (qq, J = 13.3, 6.6 Hz, 4H), 2.29 (tt, J = 11.3, 3.7 Hz, 2H), 1.93 – 1.80 (m, 7H), 1.78 – 1.71 (m, 4H), 1.47 (s, 3H), 1.47 (s, 3H), 1.41 (d, J = 7.2 Hz, 3H), 1.01 (s, 9H).

^{13}C (100 MHz, $CDCl_3$) δ (ppm) : 176.40, 171.70, 170.67, 148.44, 121.64, 108.97, 81.78, 79.34, 79.09, 71.09, 61.36, 59.10, 48.56, 43.20, 36.20, 29.26, 29.03, 28.61, 27.26, 26.91, 25.71, 25.40, 18.00.

HRMS (H-ESI) m/z: $[M + H]^+$ calculated for $C_{25}H_{44}N_2O_8$ 541.3489; found 541.3504.

*7.2.12. Synthesis of bengamide analogue 145. Acidic hydrolysis of precursor **268***

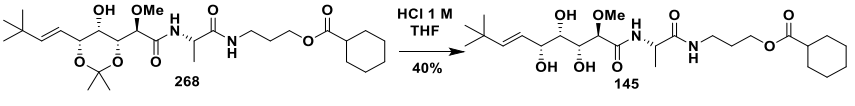

HCl (1 M, 17 mL) was added to a stirred solution of precursor **268** (54.3 mg, 0.098 mmol, 1.00 equiv.) in THF (17 mL). The resulting reaction mixture was stirred for 4 h at room temperature. After this time, the crude reaction was diluted with EtOAc and the excess of HCl was quenched by a saturated aqueous $NaHCO_3$ solution. After separation of both layers, the aqueous layer was extracted with EtOAc. The organic layer was washed with brine, dried over anhydrous $MgSO_4$, filtered and solvents were concentrated under reduced pressure. The resulting crude reaction

was purified by flash-column chromatography (Silica gel, 20 % MeOH in CH_2Cl_2) to obtain the desired **bengamide analogue 145** (19.6 mg, 40 %) as a colourless oil.

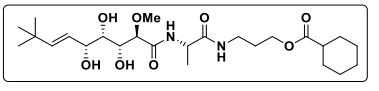

Physical aspect: colourless oil.

Rf: 0.10 (silica gel,10 % MeOH in CH_2Cl_2).

^{1}H NMR (400 MHz, $CDCl_3$) δ (ppm): 7.13 (s, 1H), 6.79 (s, 1H), 5.84 (d, *J* = 15.7 Hz, 1H), 5.49 (dd, *J* = 15.6, 6.4 Hz, 1H), 4.55 – 4.40 (m, 2H), 4.27 – 4.18 (m, 1H), 4.10 (t, *J* = 6.5 Hz, 2H), 4.00 (s, 1H), 3.83 (d, *J* = 4.2 Hz, 1H), 3.69 (s, 1H), 3.50 (s, 3 H), 3.40 – 3.26 (m, 2H), 3.18 (dt, *J* = 13.5, 6.2 Hz, 1H), 2.35 – 2.24 (m, 2H), 1.95 – 1.70 (m, 8H), 1.45 (d, *J* = 7.2 Hz, 3H), 1.25 (s, 4H), 1.03 (s, 9H).

^{13}C (100 MHz, $CDCl_3$) δ (ppm) : 176.90, 171.95, 171.37, 145.50, 141.01, 134.97, 130.20, 123.39, 82.53, 74.80, 73.29, 72.92, 61.69, 59.13, 48.82, 43.21, 36.19, 33.04, 29.44, 29.03, 28.46, 25.70, 25.40, 21.08, 17.85, 17.66.

HRMS (H-ESI) m/z: $[M + H]^+$ calculated for $C_{25}H_{44}N_2O_8$ 501.3176; found 501.3158.

*7.2.13. **Synthesis of compound 271.** Reduction reaction of lactone **254***

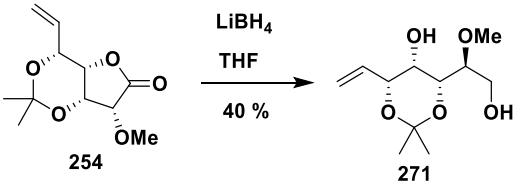

A solution of $LiBH_4$ 2 M in THF (0.22 mL, 0.44 mmol, 2.00 equiv.) was added dropwise to a stirred mixture of lactone **254** (50 mg, 0.22 mmol, 1.00 equiv.) in anhydrous THF (2 mL). The reaction mixture was stirred for 2 hours at 0 ºC. After this time, the reaction was quenched by the addition of an aqueous saturated $NaHCO_3$ solution. The crude was diluted with CH_2Cl_2. After separation of both layers, the aqueous phase was extracted, dried over anhydrous $MgSO_4$, filtered and solvents were removed under reduced pressure to obtain the desired diol **271** (20 mg, 40 %) as a colourless oil which was used in the next step without any further purification.

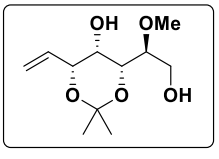

Physical aspect: colourless oil.

Rf: 0.50 (silica gel, 100 % EtOAc).

^{1}H NMR (400 MHz, $CDCl_3$) δ (ppm): 5.95 (ddd, J = 17.0, 10.5, 6.4 Hz, 1H), 5.45 – 5.28 (m, 2H), 4.75 (dd, J = 3.9, 2.1 Hz, 1H), 4.53 (ddt, J = 6.4, 2.3, 1.2 Hz, 1H), 4.14 (d, J = 3.9 Hz, 1H), 4.07 (t, J = 2.1 Hz, 1H), 3.63 (s, 3H), 1.53 (s, 3H), 1.47 (s, 3H).

^{13}C (126 MHz, $CDCl_3$) δ (ppm): 135.15, 117.63, 100.01, 79.99, 74.95, 72.03, 60.15, 58.52, 30.00, 19.89.

7.2.14. Synthesis of compound 274. *Acidic esterification reaction of D-tartaric acid*

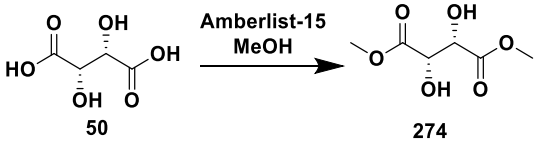

Amberlyst-15 (8g) was added to a stirred solution of *D*-tartaric acid **50** (50 g, 333.3 mmol, 1.00 equiv.) in MeOH (500 mL). Then, the mixture was heated at reflux for 12 hours. After this time, the crude was filtered. Then, solvents were removed under reduced pressure to obtain the desired ester **274** as a colourless oil which was used in the next step without any further purification.

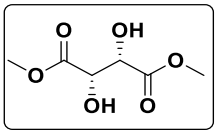

Physical aspect: colourless oil.

Rf: 0.6 (silica gel, 60 % EtOAc in Hexanes)

^{1}H NMR (500 MHz, $CDCl_3$) δ (ppm): 4.56 (s, 2H), 3.85 (s, 6H).

7.2.15. Synthesis of compound 275. *Acetal protection reaction of ester **274***

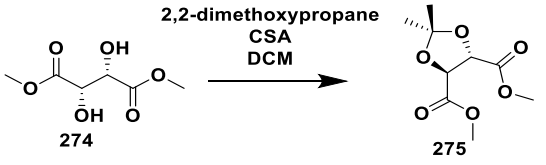

2,2-Dimethoxypropane (265 mL, 2183.31 mmol, 6.55 equiv.) was added to a stirred solution of ester **274** (59.4 g, 333.3 mmol, 1.00 equiv.) in CH_2Cl_2 (500 mL). Then, CSA (15.47 g, 66.6 mmol, 0.20 equiv.) was added portionwise at 0 ºC. The resulting mixture reaction was heated at reflux for 12 hours. After this time, solvents were removed under reduced pressure to obtain the desired acetal **275** as light-yellow oil which was used in the next reaction without any further purification.

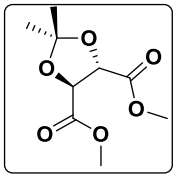

Physical aspect: light yellow oil.

Rf: 0.60 (silica gel, 20 % EtOAc in Hexanes).

^{1}H NMR (500 MHz, $CDCl_3$) δ (ppm): 4.82 – 4.78 (m, 2H), 3.82–3.81 (m, 6H), 1.49 – 1.48 (m, 6H).

*7.2.16. Synthesis of compound 276. Reduction of ester **275** with $NaBH_4$*

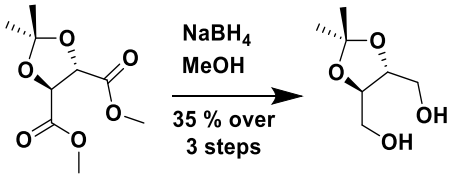

275 276

Sodium borohydride (64 g, 17 mmol, 5.00 equiv.) was added portionwise to a stirred solution of ester **275** (72.73 g, 333.3 mmol, 1.00 equiv.) in MeOH (800 mL) at 0 ºC. Then, the reaction mixture was stirred for 12 hours at room temperature. After this time, the reaction mixture was diluted with EtOAc and brine. After separation of both layers, the aqueous phase was extracted twice with EtOAc, dried over anhydrous $MgSO_4$, filtered and solvents were concentrated under reduced pressure. The resulting crude reaction was purified by flash-column chromatography (Silica gel, 80 % EtOAc in Hexanes) to obtain the desired diol **276** (19 g, 35 % over 3 steps) as a colourless oil.

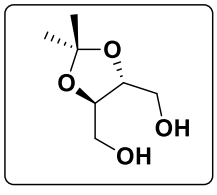

Physical aspect: Colourless oil.

Rf: 0.17 (silica gel, 20 % EtOAc in Hexanes).

^{1}H NMR (500 MHz, $CDCl_3$) δ (ppm): 4.02 – 3.98 (m, 2H), 3.83 – 3.78 (m, 2H), 3.73 – 3.68 (m, 2H), 1.43 (s, 6H).

***7.2.17. Synthesis of compound 277**. Monoprotection of the diol **276** as silylether*

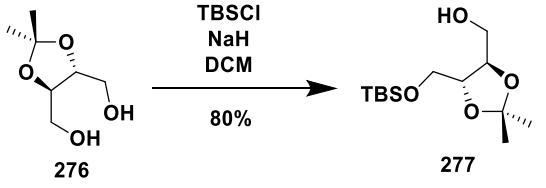

A solution of **276** (19 g, 117.15 mmol, 1.00 equiv.) in anhydrous THF (80 mL) was added dropwise to a stirred suspension sodium hydride (3.60 g, 117.5 mmol, 1.00 equiv.) in anhydrous THF (40 mL) at 0 ºC. The mixture reaction was stirred for 1 hour at this temperature. Then, a solution of TBSCl (17.60 g, 117.15 mmol, 1.00 equiv.) in anhydrous THF (40 mL) was added to the reaction mixture dropwise at 0 ºC. The resulting mixture was stirred for 90 minutes at room temperature. After this time, the reaction was quenched by the addition of a saturated aqueous NH_4Cl solution and Et_2O was added. After separation of both layers, the aqueous phase was extracted with Et_2O twice and the combined organic layers washed with brine, dried over anhydrous $MgSO_4$, filtered, and concentrated under reduced pressure. The resulting crude reaction was purified by flash-column chromatography (Silica gel, 20 % EtOAc in Hexanes) to obtain the desired silylether **277** (25.8 g, 80 %) as a light-yellow oil.

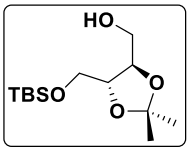

Physical aspect: light yellow oil.

Rf: 0.70 (silica gel, 40 % EtOAc in Hexanes).

^{1}H NMR (500 MHz, $CDCl_3$) δ (ppm): 4.03 – 3.95 (m, 1H), 3.92 – 3.84 (m, 2H), 3.78 (dt, J = 11.5, 4.5 Hz, 1H), 3.76 – 3.63 (m, 2H), 1.42 (s, 3H), 1.40 (s, 3H), 0.90 (s, 9H), 0.09 (s, 6H).

^{13}C NMR (126 MHz, $CDCl_3$) δ (ppm): δ 109.09, 80.14, 78.10, 63.68, 62.73, 27.01, 26.89, 25.84, 18.29, -5.50, -5.53.

7.2.18. Synthesis of compound 279

Swern oxidation of alcohol **277**

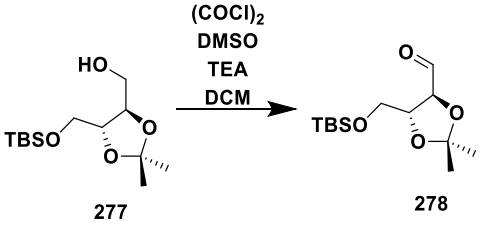

A solution of oxalyl chloride (4.41 mL, 50.68 mmol, 2.00 equiv.) in anhydrous CH_2Cl_2 (60 mL) was cooled to -78 ºC and DMSO (7.20 mL, 101.36 mmol, 4.00 equiv.) was added dropwise. After 10 minutes, a solution of alcohol **277** (7g, 25.34 mmol, 1.00 equiv.) in anhydrous CH_2Cl_2 (30 mL) was added. The resulting reaction mixture reaction was stirred at -78 ºC for 40 min. After this time, triethylamine (21.30 mL, 152.04 mmol, 6.00 equiv.) was added. After 10 minutes, the mixture was allowed at room temperature and then diluted with Et_2O and a saturated aqueous NH_4Cl solution. After separation of both layers, the aqueous phase was extracted, dried over anhydrous $MgSO_4$, filtered and concentrated under reduced pressure to obtain the desired aldehyde **278** as an orange oil which was used in the next step without any further purification.

Wittig reaction

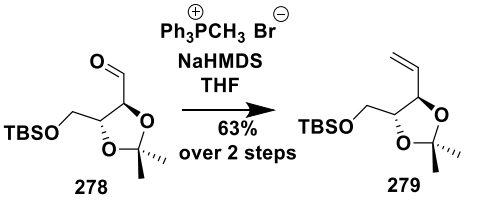

A solution of sodium bis(trimethylsilyl)amide (12 mL of 1 M solution in THF, 40.20 mmol, 3.00 equiv.) was added to a suspension of methyltriphenylphosphonium bromide (4 g, 40.20 mmol, 3.00 equiv.) in anhydrous THF (40 mL) at 0 ºC. The resulting yellow suspension mixture was stirred for 30 minutes. Then, a solution of aldehyde **278** (13.40 mmol, 1.00

equiv.) in anhydrous THF (20 mL) was added dropwise to the mixture reaction and it was stirred for 2 hours at room temperature. After this time, the crude was diluted with Et_2O and a saturated aqueous NH_4Cl solution. The aqueous phase was extracted, dried over anhydrous $MgSO_4$ and concentrated under reduced pressure. The resulting crude mixture was purified by flash-column chromatography (Silica gel, 5 % EtOAc in Hexanes) to obtain the desired alkene **279** (2.30 g, 63 % over 2 steps) as a light-yellow oil.

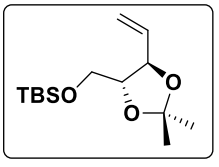

Physical aspect: light yellow oil.

Rf: 0.80 (silica gel, 10 % EtOAc in Hexanes).

^{1}H NMR (400 MHz, $CDCl_3$) δ (ppm): 5.86 (ddd, *J* = 17.2, 10.3, 6.9 Hz, 1H), 5.40 – 5.18 (m, 2H), 4.38 – 4.28 (m, 1H), 3.82 – 3.68 (m, 4H), 1.42 (s, 3H), 1.42 (s, 3H), 0.90 (s, 9H), 0.07 (s, 3H), 0.06 (s, 3H).

*7.2.19. **Synthesis of compound 280.** Deprotection reaction of silyl ether **279***

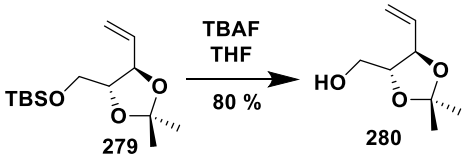

Tetra-n-butylammonium fluoride (18.35 mL, 22.02 mmol, 1.20 equiv.) was added dropwise to a stirred solution of alkene **279** (5g, 18.35 mmol, 1.00 equiv.) in THF (60 mL) at 0 ºC. The resulting mixture reaction was stirred for 1 hour at room temperature. After this time, a saturated aqueous NH_4Cl solution was added. The aqueous phase was extracted with Et_2O, dried over anhydrous $MgSO_4$, filtered and concentrated under reduced pressure. The resulting crude reaction was purified by flash-

column chromatography (Silica gel 40% EtOAc in Hexanes) to obtain the desired alcohol **280** (2.79 g, 80 %) as a colorless oil.

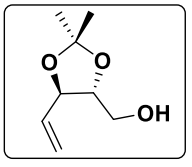

Physical aspect: colourless oil.

Rf: 0.10 (silica gel, 10 % EtOAc in Hexanes).

^{1}H NMR (500 MHz, $CDCl_3$) δ (ppm): 5.87 – 5.79 (m, 1H), 5.41 – 5.22 (m, 2H), 4.34 – 4.27 (m, 1H), 3.86 – 3.75 (m, 2H), 3.60 (dt, J = 11.2, 5.1 Hz, 1H), 1.44 (s, 3H), 1.43 (s, 3H).

^{13}C NMR (126 MHz, $CDCl_3$) δ (ppm): 135.06, 119.18, 109.30, 81.03, 78.36, 60.76, 27.02, 26.96.

7.2.20. Synthesis of compound 281

Swern oxidation of alcohol **72**

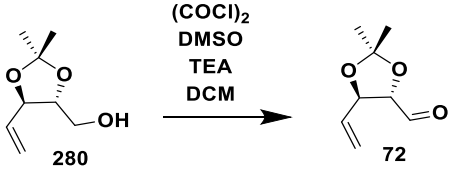

A solution of oxalyl chloride (2.76 mL, 31.6 mmol, 2.00 equiv.) in anhydrous CH_2Cl_2 (40 mL) was cooled to -78 ºC and DMSO (4.47 mL, 63.20 mmol, 4.00 equiv.) was added dropwise. After 10 minutes, a solution of alcohol **280** (2.50 g, 15.80 mmol, 1.00 equiv.) in anhydrous CH_2Cl_2 (30 mL) was added. The resulting reaction mixture reaction was stirred at -78 ºC for 40 min and then triethylamine (13 mL, 94.80 mmol, 6.00 equiv.) was added at this temperature. After 10 minutes, the mixture was allowed at room temperature and then diluted with Et_2O and a saturated aqueous NH_4Cl solution. After separation of both layers, the aqueous phase was extracted, dried over anhydrous $MgSO_4$, filtered and concentrated under

reduced pressure to obtain the desired aldehyde **72** as an orange oil which was used in the next step without any further purification.

Wittig reaction modified by Martin

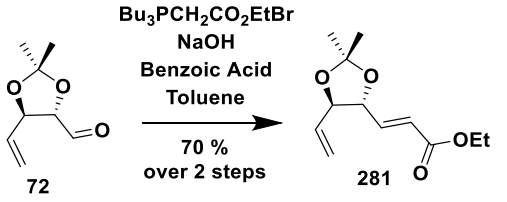

A solution of tributyl(ethoxycarbonylmethylene)phophonium bromide (7.20 g, 19.75 mmol, 1.25 equiv.) in CH_2Cl_2 (15 mL) was washed twice with 1.0 M aqueous NaOH solution (30 mL), dried over anhydrous $MgSO_4$ and diluted with toluene (20 mL). After removing CH_2Cl_2 under reduced pressure, the mixture was added to a stirred solution of the aldehyde **72** (15.80 mmol, 1.00 equiv.) and benzoic acid (0.40 g, 3.16 mmol, 0.20 equiv.) in toluene (40 mL). The resulting mixture reaction was heated at 90 ºC for 1 hour. After this time, solvent was removed under reduced pressure. The resulting crude was purified by flash-column chromatography (Silica gel, 10 % EtOAc in Hexanes) to obtain the derided α,β-unsaturated ester **281** (2.50 g, 70 % over 2 steps) as a colorless oil.

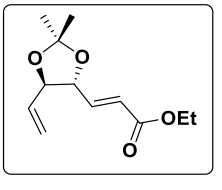

Physical aspect: colourless oil.

Rf: 0.10 (silica gel, 10 % EtOAc in Hexanes).

^{1}H NMR (500 MHz, $CDCl_3$) δ (ppm): 6.87 – 6.82 (m, 1H), 6.10 (d, J = 15.6 Hz, 1H), 5.85 – 5.76 (m, 1H), 5.41 – 5.23 (m, 2H), 4.24 – 4.16 (m, 2H), 4.15 – 4.05 (m, 2H), 1.44 (s, 3H), 1.42 (s, 3H), 1.28 – 1.25 (m, 3H).

^{13}C NMR (126 MHz, $CDCl_3$) δ (ppm): 165.94, 142.79, 133.57, 122.82, 119.77, 109.99, 82.05, 79.88, 60.59, 26.95, 26.71, 14.16.

7.2.21. Synthesis of compound 282. *Reduction reaction ester* ***281*** *with DIBAL-H*

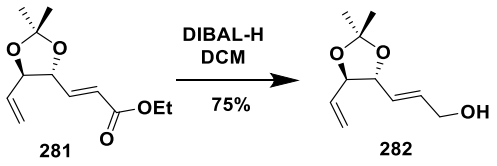

A solution of **281** (2.50 g, 11.04 mmol, 1.00 equiv.) in anhydrous CH_2Cl_2 was cooled to -78 ºC. Then, DIBAL-H (27.60 mL of 1 M solution in CH_2Cl_2, 27.60 mmol, 2.50 equiv.) was added dropwise at this temperature. After 30 minutes, the reaction was quenched by addition of EtOAc at -78 ºC and the mixture was allowed to reach room temperature and treated with a saturated aqueous Na^+/K^+ tartrate solution. The resulting mixture was vigorously stirred until a clear separation of both organic and aqueous phases. The aqueous phase was extracted, dried over anhydrous $MgSO_4$, filtered and concentrated under reduced pressure. The resulting crude reaction was purified by flash-column chromatography (Silica gel, 20 % EtOAc in Hexanes) to obtain the desired allylic alcohol **282** (1.50 g, 75 %) as a colourless oil.

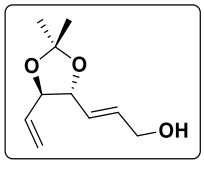

Physical aspect: colourless oil.

Rf: 0.10 (silica gel, 20 % EtOAc in Hexanes).

^{1}H NMR (500 MHz, $CDCl_3$) δ (ppm): 5.98 – 5.91 (m, 1H), 5.83 – 5.75 (m, 1H), 5.72 – 5.66 (m, 1H), 5.37 – 5.21 (m, 2H), 4.66 (s, 1H), 4.16 – 4.06 (m, 4H), 1.42 (s, 6H).

^{13}C NMR (126 MHz, $CDCl_3$) δ (ppm): 134.31, 134.00, 126.96, 126.45, 119.03, 109.16, 82.28, 81.33, 62.51, 26.99.

7.2.22. Synthesis of compound 73. *Sharpless AsymmetricEepoxidation (SAE)*

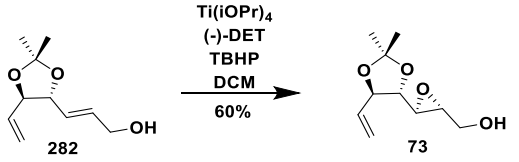

To a solution of titanium isopropoxide (0.74 mL, 2.49 mmol, 0.23 equiv.) in anhydrous CH_2Cl_2 (30 mL) was added *D*-(-)-DET (0.46 mL, 2.71 mmol, 0.25 equiv.) at -80 ºC. After 15 min at this temperature, a solution of allylic alcohol **282** (2 g, 10.85 mmol, 1.00 equiv.) in anhydrous CH_2Cl_2 (40 mL) was added dropwise, followed by the addition, after additional 30 min of a 5.5 M 1.1-Dimethyl hydroperoxide (TBHP) solution in decane (3 mL, 16.27 mmol, 1.50 equiv.) at the same temperature. After 8 h at this temperature, the reaction mixture was quenched with Me_2S (3.64 mL, 49.10 mmol, 4.60 equiv.) at 0 ºC, filtered off and the solvent was evaporated under reduced pressure. The resulting crude reaction was purified by flash-column chromatography (silica gel, 20 % EtOAc in Hexanes) to obtained the desired epoxy alcohol **73** (1.30 g, 60 %) as a colorless oil.

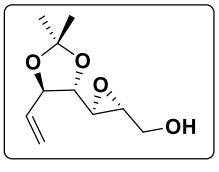

Physical aspect: colourless oil.

Rf: 0.59 (40% EtOAc in Hexanes).

^{1}H NMR (500 MHz, $CDCl_3$) δ (ppm): 5.88 – 5.80 (m, 1H), 5.45 – 5.28 (m, 2H), 4.53 (d, J = 6.8 Hz, 1H), 4.40 – 4.23 (m, 2H), 3.98 – 3.91 (m, 1H), 3.66 – 3.62 (m, 1H), 3.18 – 3.09 (m, 1H), 1.42 (s, 3H), 1.41 (s, 3H).

^{13}C NMR (126 MHz, $CDCl_3$) δ (ppm): 134.65, 119.61, 110.02, 79.98, 79.48, 60.62, 55.34, 53.52, 26.97, 26.55.

7.2.23. Synthesis of compound 283. Oxirane opening reaction

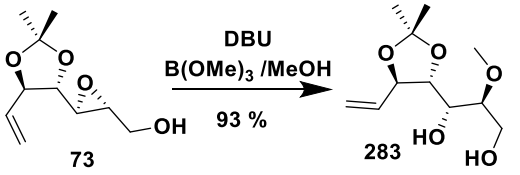

DBU (1.45 mL, 9.74 mmol, 1.50 equiv.) was added to a stirred solution of epoxy alcohol **73** (1.30 g, 6.49 mmol, 1.00 equiv.) in a mixture of MeOH:$B(OMe)_3$ (1:1, 60 mL). The resulting mixture was heated at 70 ºC for 12 h. After this time, the reaction mixture was allowed to room temperature, cooled to 0 ºC, and then treated with a saturated aqueous $NaHCO_3$ solution. After stirring 30 minutes at 0 ºC, EtOAc was added, and both phases were separated. The aqueous phase was extracted with EtOAc twice and the combined organic extracts were washed with water and brine, dried over anhydrous $MgSO_4$, filtered and concentrated in vacuo. The resulting crude mixture was purified by flash-column chromatography (Silica gel, 40 % EtOAc in Hexanes) to obtain the desired product **283** (1.40 g ,93 %) as a yellow oil.

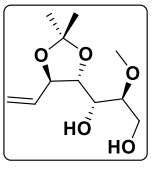

Physical aspect: yellow oil.

Rf: 0.58 (60 % EtOAc in Hexanes).

^{1}H NMR (500 MHz, $CDCl_3$) δ (ppm): 5.83 (ddd, J = 17.4, 10.3, 7.4 Hz, 1H), 5.46 – 5.23 (m, 2H), 4.52 (s, 1H), 4.44 (ddd, J = 8.5, 6.9, 1.0 Hz, 1H), 4.37 – 4.25 (m, 1H), 3.92 – 3.84 (m, 2H), 3.80 (d, J = 12.3 Hz, 1H), 3.66 – 3.56 (m, 1H), 3.43 (s, 3H), 3.18 (dt, J = 7.8, 3.8 Hz, 1H), 1.44 (s, 6H).

^{13}C NMR (126 MHz, $CDCl_3$) δ (ppm):134.75, 119.74, 109.45, 81.59, 79.40, 78.67, 67.66, 60.86, 57.99, 27.19, 26.86.

7.2.24. Synthesis of compound 284. Olefin Cross-Metathesis

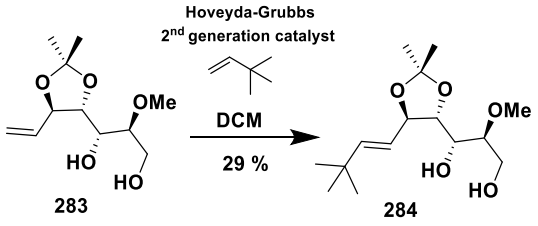

Olefin **283** (75 mg, 0.30 mmol, 1.00 equiv.) and Hoveyda-Grubbs 2nd generation catalyst (56 mg, 0.09 mmol, 0.30 equiv.) were dissolved in degassed CH_2Cl_2 (10 mL). Then, 3,3-dimethylbut-1-ene (10 mL) was added dropwise at room temperature. The resulting mixture reaction was heated at 40 ºC in a sealed tube for 12 h. After this time, solvents were concentrated in vacuo. The resulting crude reaction was purified by flash-column chromatography (Silica gel, 40% EtOAc in Hexanes) to obtain the desired alkene **284** (21 mg, 29 %) as a brown solid.

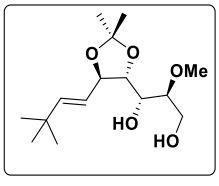

Physical aspect: brown solid.

Rf: 0.72 (silica gel, 60% EtOAc in Hexanes).

^{1}H NMR (500 MHz, $CDCl_3$) δ (ppm) 5.87 (d, J = 15.6 Hz, 1H), 5.33 (dd, J = 15.6, 8.2 Hz, 1H), 4.56 (d, J = 6.8 Hz, 2H), 4.40 (t, J = 8.4 Hz, 1H), 3.84 – 3.78 (m, 2H), 3.57 (t, J = 8.4 Hz, 1H), 3.45 (s, 3H), 3.19 (dt, J = 7.7, 4.0 Hz, 2H), 1.46 (s, 3H), 1.44 (s, 3H), 1.03 (s, 9H).

7.2.25. Synthesis of compound 286. *Coupling reaction between acid* ***283*** *and amine* ***267***

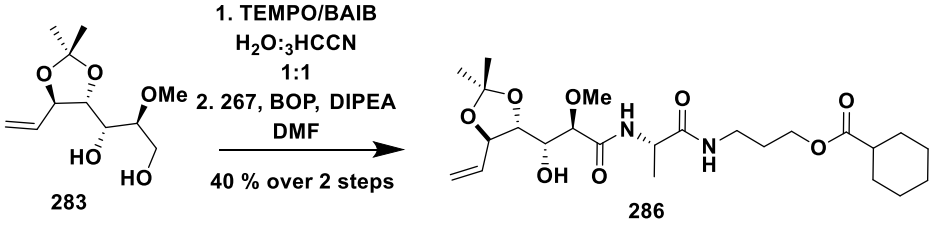

BAIB (2.60 g, 7.30 mmol, 6.00 equiv.) and TEMPO (0.113 g, 0.72 mmol, 0.60 equiv.) were added to a stirred solution of alkene **285** (0.30 g, 1.20 mmol, 1.00 equiv.) in a mixture of CH_3CN:H_2O (1:1, 6 mL) at room temperature. After 5 h, the crude mixture was diluted with EtOAc, quenched by the addition of a saturated aqueous $Na_2S_2O_3$ solution and, after separation of both layers, the aqueous phase was then extracted with EtOAc. The organic solution was washed again with a saturated aqueous $Na_2S_2O_3$ solution, then dried over anhydrous $MgSO_4$ and concentrated under reduced pressure. The crude acid was dissolved in DMF (18 mL) and treated with DIPEA (0.96 mL, 5.49 mmol, 3.30 equiv.), aminoacid derivative **267** (1.80 mmol, 1.50 equiv.) and BOP (1.16 g, 2.64 mmol, 2.20 equiv.) at room temperature for 48 h. After this time, the crude mixture was diluted with EtOAc and washed with a saturated aqueous NH_4Cl solution. The aqueous phase was extracted with EtOAc and the combined organic phases were washed with brine, dried over anhydrous MgSO4 and the solvent was removed under reduced pressure. The resulting crude reaction was purified by flash column-chromatography (silica gel, 80 % EtOAc in Hexanes) to obtain the desired coupling product **286** (230 mg, 40 % over 2 steps) as a light-yellow oil.

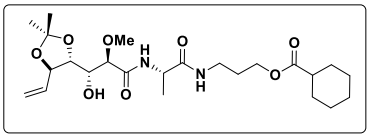

Physical aspect: yellow oil.

Rf: 0.48 (silica gel, 100 % EtOAc).

^{1}H NMR (500 MHz, $CDCl_3$) δ (ppm): 6.97 (d, J = 7.8 Hz, 1H), 6.77 (s, 1H), 5.88 (ddd, J = 17.1, 10.2, 7.5 Hz, 1H), 5.44 – 5.27 (m, 2H), 4.52 – 4.47 (m, 1H), 4.43 – 4.39 (m, 1H), 4.18 – 4.07 (m, 3H), 3.97 – 3.90 (m, 1H), 3.72 (s, 2H), 3.46 (s, 3H), 3.33 – 3.25 (m, 3H), 2.39 – 2.21 (m, 2H), 1.94 – 1.71 (m, 10H), 1.68 – 1.61 (m, 3H), 1.45 (s, 3H), 1.43 (s, 3H), 1.25 (s, 3H).

^{13}C NMR (126 MHz, $CDCl_3$) δ(ppm): 176.51, 171.79, 171.02, 135.14, 132.44, 130.08, 119.66, 109.57, 81.97, 79.31, 78.67, 70.78, 61.30, 59.21, 48.63, 43.23, 36.46, 36.24, 29.71, 29.05, 28.59, 27.16, 26.89, 25.71, 25.67, 25.41, 25.38, 17.88.

*7.2.26. **Synthesis of precursor 289.** Olefin Cross-Metathesis*

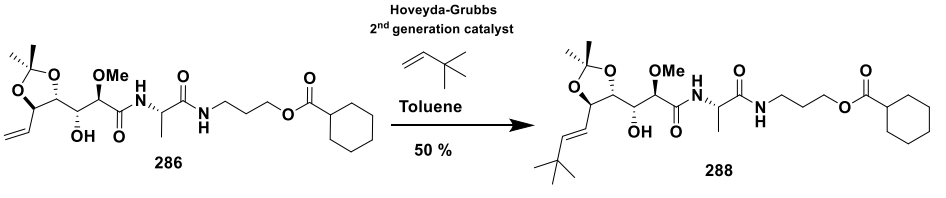

Olefin **286** (230 mg, 0.47 mmol, 1.00 equiv.) and 2nd generation Hoveyda-Grubbs catalyst (58.9 mg, 0.09 mmol, 0.20 equiv.) were dissolved in de-gassed toluene (20 mL). Then, 3,3-dimethylbut-1-ene (20 mL) was added dropwise at room temperature. The resulting mixture reaction was heated at 80 ^{o}C in a sealed tube for 12 h. After this time, the crude mixture was concentrated in vacuo and purified by flash column chromatography

(Silica gel, 60 % EtOAc in hexanes) to obtain the desired precursor **288** (129 mg, 50 %) as a brown solid.

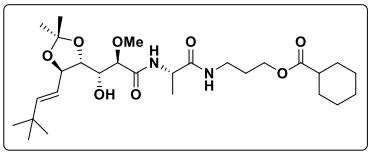

Physical aspect: brown solid.

Rf: 0.60 (silica gel, 100 % EtOAc).

^{1}H NMR (500 MHz, $CDCl_3$) δ (ppm): 6.91 (d, J = 8.0 Hz, 1H), 6.77 (t, J = 5.7 Hz, 1H), 5.78 (d, J = 15.5 Hz, 1H), 5.33 (dd, J = 15.6, 8.3 Hz, 1H), 4.42 (p, J = 7.2 Hz, 1H), 4.29 (t, J = 8.3 Hz, 1H), 4.04 (t, J = 6.2 Hz, 2H), 3.84 (dd, J = 8.4, 3.8 Hz, 1H), 3.68 – 3.59 (m, 2H), 3.38 (s, 3H), 3.21 (dt, J = 10.6, 6.6 Hz, 2H), 2.27 – 2.18 (m, 2H), 1.87 – 1.64 (m, 9H), 1.61 – 1.54 (m, 2H), 1.40 – 1.34 (m, 9H), 0.96 (s, 9H).

^{13}C NMR (126 MHz, $CDCl_3$): δ 176.40, 171.70, 170.67, 148.44, 121.64, 108.97, 81.78, 79.34, 79.09, 71.09, 61.36, 59.10, 48.56, 43.20, 36.20, 29.26, 29.03, 28.61, 27.26, 26.91, 25.71, 25.40, 18.00.

7.2.27. Synthesis of bengamide analogue 145. Acidic hydrolysis of precusor 288

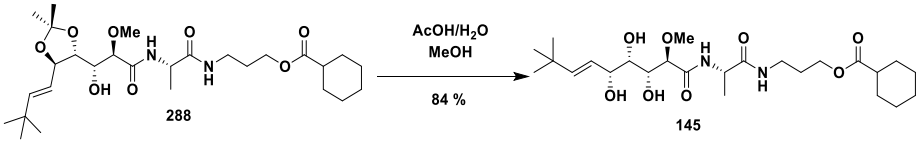

A 70 % aqueous AcOH solution (19.50 mL) was added to a stirred solution of precusor **288** (90 mg, 0.17 mmol, 1.00 equiv.) in MeOH (6 mL) at room temperature. The reaction was heated at 70 ^{o}C and was stirred for 3 h. After this time, the crude reaction was allowed to room temperature and solvents were removed under reduced pressure. The resulting crude

reaction was purified by flash-column chromatography (Silica gel, 10 % MeOH in CH_2Cl_2) to yield the desired bengamide analogue **145** (70 mg, 84 %) as a colourless oil.

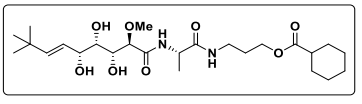

Physical aspect: colourless oil.

Rf: 0.10 (silica gel,10 % MeOH in CH_2Cl_2).

^{1}H NMR (500 MHz, $CDCl_3$) δ (ppm): 7.13 (s, 1H), 6.79 (s, 1H), 5.84 (d, *J* = 15.7 Hz, 1H), 5.49 (dd, *J* = 15.6, 6.4 Hz, 1H), 4.55 – 4.40 (m, 2H), 4.27 – 4.18 (m, 1H), 4.10 (t, *J* = 6.5 Hz, 2H), 4.00 (s, 1H), 3.83 (d, *J* = 4.2 Hz, 1H), 3.69 (s, 1H), 3.50 (s, 3 H), 3.40 – 3.26 (m, 2H), 3.18 (dt, *J* = 13.5, 6.2 Hz, 1H), 2.35 – 2.24 (m, 2H), 1.95 – 1.70 (m, 8H), 1.45 (d, *J* = 7.2 Hz, 3H), 1.25 (s, 4H), 1.03 (s, *J* = 0.9 Hz, 9H).

^{13}C NMR (126 MHz, $CDCl_3$) δ (ppm) : 176.90, 171.95, 171.37, 145.50, 141.01, 134.97, 130.20, 123.39, 82.53, 74.80, 73.29, 72.92, 61.69, 59.13, 48.82, 43.21, 36.19, 33.04, 29.44, 29.03, 28.46, 25.70, 25.40, 21.08, 17.85, 17.66.

7.2.28. Synthesis of compound 294

Protection reaction of *L*-azetidine.

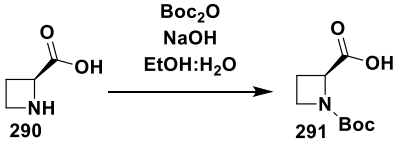

Boc_2O (2.40 g, 10.95 mmol, 1.25 equiv.) was added to a stirred solution of *L*-azetidine **290** (0.50 g, 8.76 mmol, 1.00 equiv.) in a mixture of EtOH:H_2O (2:1, 15 mL) at room temperature. Then, NaOH (0.37 g, 9.20

mmol, 1.05 equiv.) was added at 0 ºC and the mixture reaction was stirred for 12 h at room temperature. After this time, solvents were removed under reduced pressure and water (10 mL) and HCl 1 M was added to obtain pH 3. The crude was diluted with EtOAc, after separation of both phases, the aqueous phase was extracted, dried over anhydrous $MgSO_4$ and concentrated under reduced pressure to obtain the desired compound **291** as a colourless oil which was used in the next step without any further purification.

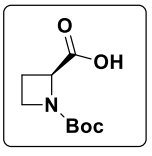

Physical aspect: colourless oil.

Rf: 0.10 (silica gel, 100 % EtOAc)

^{1}H RMN (500 MHz, $CDCl_3$) δ (ppm): 4.79 (s, 1H), 3.99 – 3.80 (m, 2H), 2.62 – 2.38 (m, 2H), 1.52 (s, 9H).

Boc desprotection of **292**

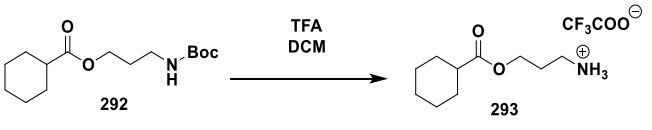

Trifluoracetic acid (2.5 mL, 32.50 mmol, 65 equiv.) was added dropwise to a stirred mixture of intermediate **292** (0.14 g, 0.50 mmol, 1.00 equiv.) in CH_2Cl_2 (13 mL) at 0 ºC. The resulting reaction mixture was stirred at room temperature for 3 h. After this time, solvents were concentrated in vacuo to obtain the desired compound **293** which was used in the next step without any further purification.

Coupling between amine **293** and acid of Boc-*L*-azetidine **291**

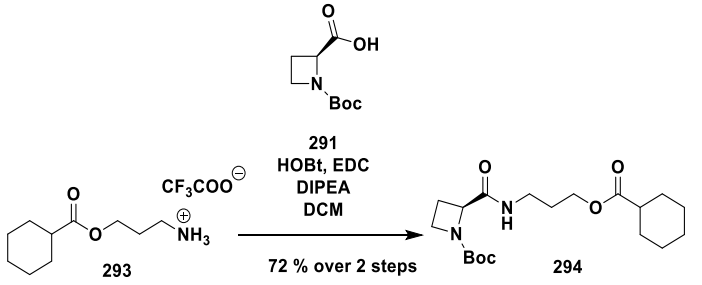

A solution of ester **293** (0.50 mmol, 1.00 equiv.) in CH_2Cl_2 (5 mL) was added dropwise to a stirred mixture of Boc-*L*-azetidine **291** (0.10 g, 0.5 mmol, 1.00 equiv.), HOBt (0.08 g, 0.60 mmol 1.20 equiv.), EDC (0.12 g, 0.60 mmol, 1.20 equiv.) and DIPEA (0.30 mL, 1.80 mmol, 3.60 equiv.) in CH_2Cl_2 (6 mL) dropwise at 0 ºC. The mixture was stirred for 12 h at room temperature. After this time, the reaction mixture was diluted with EtOAc. The organic layer was washed with brine, dried over anhydrous $MgSO_4$, filtered and concentrated under reduced pressure. The resulting crude was purified by flash-column chromatography (silica gel, 80 % EtOAc in Hexanes) to obtain the desired amino acid derivative **294** (2.33 g, 72 % over 2 steps) as a colourless oil.

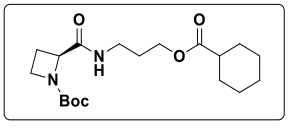

Physical aspect: colourless oil.

Rf: 0.40 (100 % EtOAc).

^{1}H RMN (500 MHz, $CDCl_3$) δ (ppm): 4.62 (t, *J* = 8.1 Hz, 1H), 4.12 (q, *J* = 5.9 Hz, 2H), 3.94 – 3.75 (m, 2H), 3.44 – 3.28 (m, 2H), 2.30 (tt, *J* = 11.3, 3.6 Hz, 1H), 1.95 – 1.49 (m, 9H), 1.45 (s, 9H), 1.33 – 1.16 (m, 5H).

^{13}C NMR (126 MHz, $CDCl_3$) δ (ppm): 176.16, 171.83, 80.98, 61.77, 61.42, 43.22, 43.17, 36.04, 29.71, 29.09, 29.04, 29.03, 28.77, 28.41, 28.33, 28.30, 28.27, 25.76, 25.74, 25.44.

7.2.29. Synthesis of compound 296

Boc deprotection of **294**

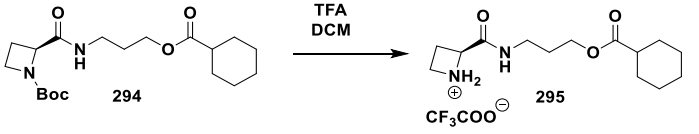

Trifluoracetic acid (2.7 mL, 27.3 mmol, 64 equiv.) was added dropwise to a stirred mixture of **294** (154 mg, 0.42 mmol, 1.00 equiv.) in CH_2Cl_2 (13 mL) at 0 ºC. The resulting reaction mixture was stirred at room temperature for 3 h. After this time, solvents were concentrated in vacuo to yield amino acid derivative **295** which was used in the next step without any further purification.

Coupling reaction between acid **285** and *L*-azetidine derivative **295**

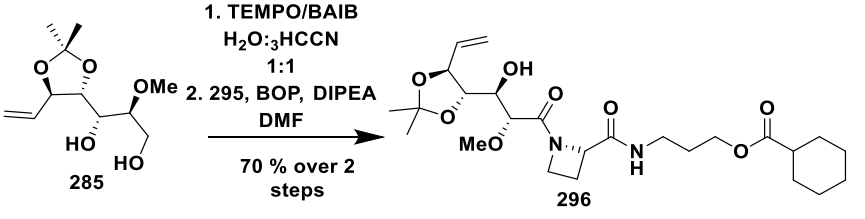

BAIB (549 mg, 1.70 mmol, 6.00 equiv.) and TEMPO (26.30 mg, 0.16 mmol,0.60 equiv.) were added to a stirred solution of alkene **285** (70 mg, 0.28 mmol, 1.00 equiv.) in a mixture of CH_3CN:H_2O (1:1, 1.4 mL) at room temperature. After 5 h, the crude mixture was diluted with EtOAc, quenched by the addition of a saturated aqueous $Na_2S_2O_3$ solution and, after separation of both layers, the aqueous phase was then extracted with EtOAc. The organic solution was washed again with a saturated aqueous $Na_2S_2O_3$ solution, then dried over anhydrous MgSO4 and the solvent was evaporated under reduced pressure. The crude acid was dissolved in DMF (3 mL) and treated with DIPEA (170 µL, 0.92 mmol, 3.30 equiv.), *L*-azetidine derivative **295** (0.42 mmol, 1.50 equiv.) and BOP (297 mg, 442.28 mmol, 2.40 equiv.) at room temperature. After being stirred at this temperature overnight, the crude mixture was diluted with EtOAc

and washed with a saturated aqueous NH_4Cl solution. The aqueous phase was extracted with EtOAc and the combined organic phases were washed with brine, dried over anhydrous $MgSO_4$ and the solvent was concentrated under reduced pressure. The resulting crude reaction was purified by flash column-chromatography (silica gel, 80 % EtOAc in Hexanes) to obtain amide precursor **296** (95 mg, 70 % over 2 steps) as a light-yellow oil.

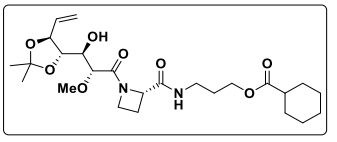

Physical aspect: colourless oil.

Rf: 0.65 (100 % EtOAc).

^{1}H RMN (500 MHz, $CDCl_3$) δ (ppm): 6.92 (s, 1H), 5.76 (ddd, J = 17.4, 10.3, 7.3 Hz, 1H), 5.39 – 5.20 (m, 2H), 4.44 – 4.37 (m, 1H), 4.21 (t, J = 8.0 Hz, 2H), 4.08 – 3.97 (m, 3H), 3.82 – 3.69 (m, 3H), 3.32 (s, 3H), 3.28 – 3.22 (m, 2H), 2.26 – 2.19 (m, 1H), 1.85 – 1.75 (m, 5H), 1.69 – 1.61 (m, 5H), 1.39 (s, 6H).

^{13}C NMR (125 MHz, $CDCl_3$) δ (ppm): 172.55, 167.78, 147.05, 146.54, 132.46, 130.89, 128.81, 120.35, 98.74, 82.60, 78.46, 70.16, 70.10, 68.17, 38.74, 30.37, 29.71, 29.33, 28.93, 25.69, 25.63, 23.75, 22.99, 14.06, 10.97.

7.2.30. Synthesis of precursor 297. Olefin-Cross Metathesis

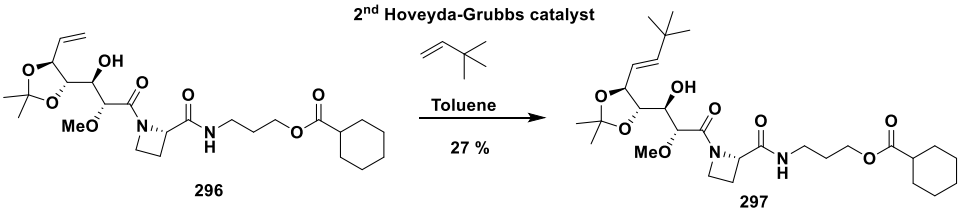

Olefin **296** (95 mg, 0.20 mmol, 1.00 equiv.) and Hoveyda-Grubbs 2nd generation catalyst (25 mg, 0.04 mmol, 0.20 equiv.) were dissolved in degassed toluene (10 mL). Then, 3,3-dimethylbut-1-ene (10 mL) was added dropwise at room temperature. The resulting mixture reaction was heated at 80 ºC in a sealed tube for 12 h. After this time, the crude mixture was concentrated in vacuo and purified by flash column chromatography (Silica gel, 60 % EtOAc in Hexanes) to obtain the desired precursor **297** (30 mg, 27 %) as a brown solid.

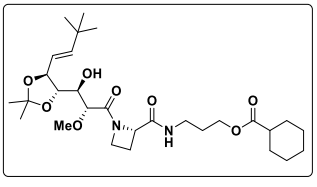

Physical aspect: Brown solid.

Rf: 0.80 (100% EtOAc).

^{1}H RMN (500 MHz, $CDCl_3$) δ (ppm): δ 5.94 (d, J = 15.9, 1H), 5.77 (d, J = 15.8 Hz, 1H), 5.52 (dd, J = 15.8, 7.6 Hz, 1H), 5.38 (dd, J = 15.8, 6.5 Hz, 1H), 4.56 – 4.49 (m, 3H), 4.46 (t, J = 2.8 Hz, 4H), 4.45 – 4.43 (m, 2H), 4.42 (d, J = 2.1 Hz, 1H), 4.39 (dd, J = 4.5, 2.8 Hz, 1H), 4.15 (qd, J = 10.9, 5.9 4Hz, 4H), 4.08 – 4.01 (m, 4H), 3.63 (s, 3H), 3.60 (s, 1H), 2.41 – 2.25 (m, 6H), 1.80 (dqd, J = 15.2, 2.5, 1.3 Hz, 4H), 1.61 (td, J = 12.3, 6.2 Hz, 5H), 1.32 – 1.22 (m, 12H), 0.97 (s, 9H).

^{13}C NMR (125 MHz, CDCl3) δ (ppm): 172.55, 167.78, 147.05, 146.54, 132.46, 130.89, 128.81, 120.35, 98.74, 82.60, 78.46, 70.16, 70.10, 68.17, 59.32, 38.74, 30.37, 29.71, 29.33, 28.93, 25.69, 25.63, 23.75, 22.99, 14.06, 10.97, 1.03.

7.2.31. Synthesis of bengamide analogue 289. *Acidic hydrolysis of precursor* ***297***

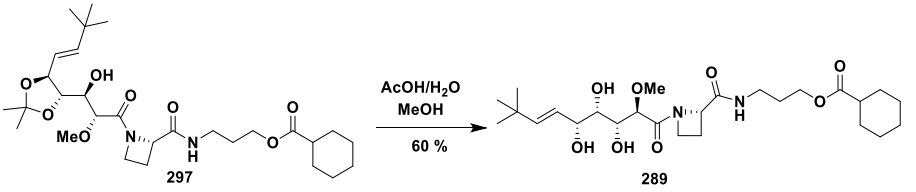

A 70% aqueous AcOH solution (0.70 mL) was added to a stirred solution of precursor **297** (10 mg, 0.02 mmol, 1.00 equiv.) in MeOH (0.3 mL) at room temperature. The reaction was heated at 70 ºC and it was stirred for 3 h. After this time, the crude reaction was allowed to room temperature and solvents were removed under reduced pressure. The resulting crude reaction was purified by flash column chromatography (Silica gel, 4 % MeOH in DCM) to obtain the desired **bengamide analogue 289** (6 mg, 60%) as a colourless oil.

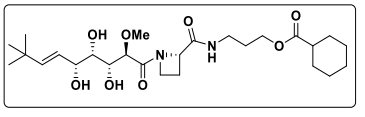

Physical aspect: colourless oil.

Rf: 0.80 (silica gel, 10 % MeOH in DCM).

^{1}H NMR (400 MHz, $CDCl_3$) δ (ppm): δ 6.94 (s, 1H), 5.94 (dd, J = 15.8, 1.2 Hz, 1H), 5.38 (dd, J = 15.8, 6.5 Hz, 1H), 4.57 – 4.49 (m, 2H), 4.49 – 4.43 (m, 2H), 4.44 – 4.43 (m, 1H), 3.63 (s, 3H), 2.44 – 2.32 (m, 3H), 1.80 (dqd, J = 15.1, 2.5, 1.3 Hz, 2H), 1.61 (h, J = 6.1 Hz, 2H), 1.43 (d, J = 6.1 Hz, 1H), 1.39 – 1.32 (m, 4H), 1.26 – 1.22 (m, 10H), 0.97 (s, 9H).

^{13}C NMR (125 MHz, $CDCl_3$) δ (ppm): 172.54, 167.78, 146.54, 132.46, 130.90, 128.81, 120.34, 82.61, 78.47, 70.78, 68.31, 68.17, 59.32, 38.74, 30.37, 29.71, 29.33, 28.94, 23.75, 22.99, 14.06, 10.97.

7.2.32. Synthesis of compound 306. *Opening reaction of lactone* ***254*** *with L-alanine amide hydrochloride*

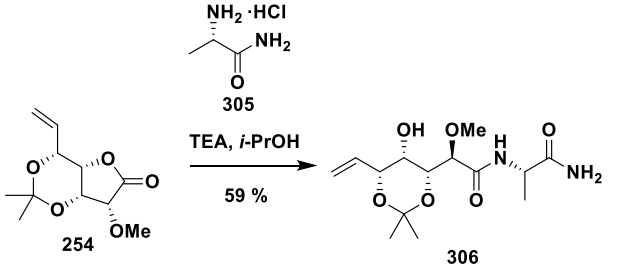

Triethylamine (TEA) (0.14 mL, 1.00 mmol, 2.50 equiv.) was added to a stirred solution of lactone **254** (183 mg, 0.80 mmol, 2.00 equiv.) and *L*-alanine amide hydrochloride **305** (50 mg, 0.40 mmol, 1.00 equiv.) in *i*-propanol (2 mL) at room temperature. Then, the reaction was stirred for 24 hours at reflux. After this time, the solvent was removed under reduced pressure. The resulting crude reaction was purified by flash-column chromatography (Silica gel, 20 % MeOH in DCM) to obtain the desired compound **306** (75 mg, 59 %) as a yellow oil.

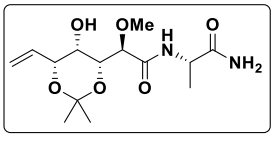

Physical aspect: yellow oil.

Rf: 0.80 (silica gel, 10 % MeOH in CH_2Cl_2).

^{1}H NMR (400 MHz, MeOD) δ (ppm): 5.93 (ddd, J = 17.4, 10.6, 5.7 Hz, 1H), 5.37 – 5.30 (m, 1H), 5.23 – 5.18 (m, 1H), 4.46 – 4.41 (m, 2H), 4.05 (dd, J = 8.4, 1.4 Hz, 1H), 3.89 (d, J = 8.4 Hz, 1H), 3.53 (t, J = 1.4 Hz, 1H), 3.40 (d, J = 6.0 Hz, 1H), 3.38 (s, 3H), 1.43 (s, 3H), 1.40 – 1.36 (m, 6H).

^{13}C NMR (125 MHz, MeOD) δ (ppm): 177.22, 173.28, 137.04, 116.95, 100.60, 81.00, 75.22, 74.26, 65.77, 58.42, 49.94, 29.62, 19.43, 18.31.

7.2.33. Synthesis of compound 307. *Acidic hydrolysis of precursor* ***306***

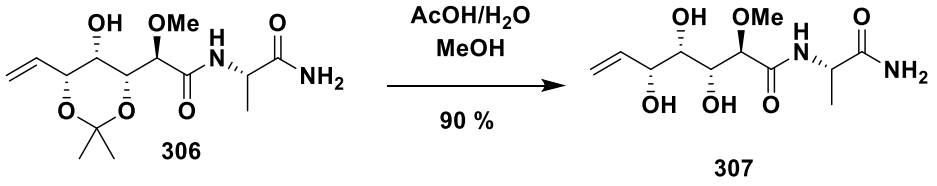

A 70 % aqueous AcOH solution (8.97 mL) was added dropwise to a stirred solution of **298** (50 mg, 0.16 mmol, 1.00 equiv.) in MeOH (3.90 mL). The resulting reaction mixture was heated at 70 ^{o}C for 2 h. After this time, the crude reaction was diluted with EtOAc and the excess of AcOH was quenched by a saturated aqueous $NaHCO_3$ solution. The aqueous phase was extracted with EtOAc and the combined organic layers were washed with brine, dried over anhydrous $MgSO_4$, filtered and solvents were concentrates under reduced pressure. The resulting crude reaction was purified by flash-column chromatography (Silica gel, 40 % MeOH in CH_2Cl_2) to obtain the desired product **307** (20.54 mg, 43 %) as a colourless oil.

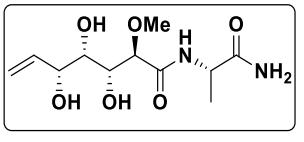

Physical aspect: colourless oil.

Rf: 0.50 (silica gel, 10% MeOH in CH_2Cl_2).

^{1}H NMR (400 MHz, MeOD) δ (ppm): 5.92 (ddd, J = 17.1, 10.5, 6.5 Hz, 1H), 5.34 (ddd, J = 17.1, 1.9, 1.2 Hz, 1H), 5.19 (ddd, J = 10.5, 1.9, 1.2 Hz, 1H), 4.42 (q, J = 7.2 Hz, 1H), 4.22 (tt, J = 6.4, 1.2 Hz, 1H), 3.84 (d, J = 1.4 Hz, 2H), 3.59 (dt, J = 6.0, 1.4 Hz, 1H), 3.39 (s, 3H), 1.41 (d, J = 7.2 Hz, 3H).

^{13}C (125 MHz, MeOD) δ (ppm): 177.55, 173.63, 139.10, 117.07, 83.52, 75.07, 74.12, 72.96, 58.52, 49.88, 18.10.

7.2.34. Synthesis of compound 310

Fmoc-Gly-OH loaded 2-Chlorotrityl Chloride Resin

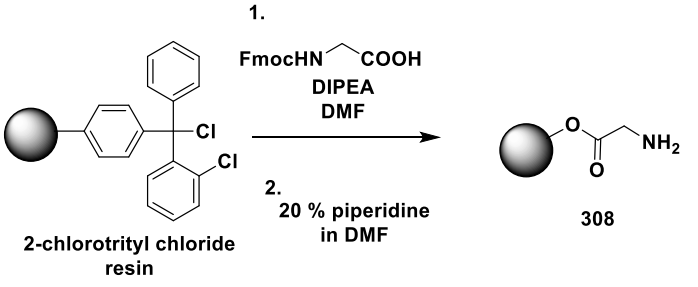

A 5 mL polypropylene syringe fitted with porous polyethylene disk charged with 2-chlorotrityl chloride resin (197 mg, L = 1.22 mmol/g, 0.244 mmol, 1.00 equiv.), was loaded with a solution of Fmoc-Gly-OH (228 mg, 0.723 mmol, 3.00 equiv.) and DIPEA (152 µL, 0.85 mmol, 3.50 equiv.) in dry DMF (3 mL). The resulting suspension was shaken at 280 rpm for 30 h, the solution was unloaded, and the resin was washed by shaking with dry DMF (5 x 3 mL). The resulting swelled resin was used in the next step. To a 5 mL polypropylene syringe fitted with a porous polyethylene disk and loaded with the Fmoc-Gly-OH (197 mg, L = 1.22 mmol/g, 0.244 mmol, 1.00 equiv.) was added a solution of 20 % piperidine in DMF (3 x 3 mL, 10 min.), and the mixture was shaken at 280 rpm. After the last run, the resin was washed with dry DMF (5 x 3 mL).

Opening lactone **254** reaction in solid phase

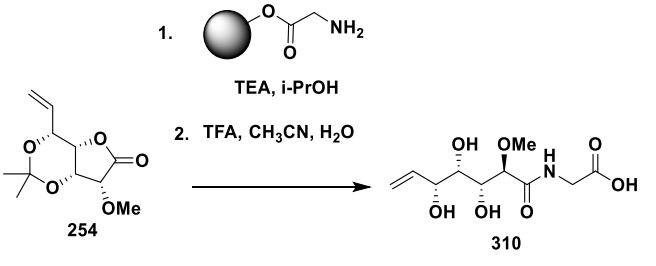

To a 5 mL polypropylene syringe fitted with a porous polyethylene disk and loaded with the resin **308** (197 mg, L = 1.22 mmol/g, 0.244 mmol,

1.00 equiv.) the resin was washed with dry DMF (5 x 3 mL) and treated with a solution of the lactone **254** (83 mg, 0.37 mmol, 1.50 equiv.) and triethylamine (162 mg, 0.976 mmol, 4.00 equiv.) in anhydrous *i*-PrOH (3 mL) and the mixture was stirred at reflux for 24 hours. Once the solution was unloaded, the resin was washed with DMF (4 x 3 mL) and DCM (4 x 3 mL). The resulting resin was dissolved in mixture CH_3CN and water (1:1, 2 mL) and treated with TFA (3 mL) for 3 h at room temperature. After that, the solution was collected, and the resin washed with DCM (2 x 3 mL). All the collected organic solvents were evaporated under reduced pressure to obtain to obtain an epimer mixture of **310.**

Opening lactone **254** reaction in solid phase

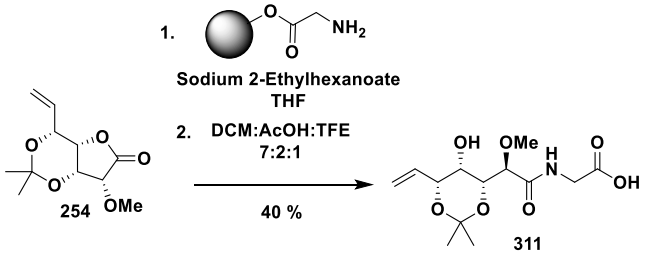

To a 5 mL polypropylene syringe fitted with a polyethylene porous disk and loaded with the resin **308** (197 mg, L = 1.22 mmol/g, 0.244 mmol, 1.00 equiv.) was added a solution of 20% piperidine in DMF (3 x 3 mL, 10 min.), and the mixture was shaken at 280 rpm. After the last run, the resin was washed with dry DMF (5 x 3 mL) and treated with a solution of the lactone **254** (83 mg, 0.37 mmol, 1.50 equiv.) and sodium 2-ethylhexanoate (162 mg, 0.976 mmol, 4.00 equiv.) in dry THF (3 mL) and the mixture was stirred at room temperature for 48 hours. Once the solution was unloaded, the resin was washed with DCM (4 x 4 mL). The resulting resin was treated with a solution of DCM/AcOH/TFE (7:2:1, 3 mL) for 30 min. After that, the solution was collected, and the resin washed with DCM (2 x 3 mL). All the collected organic solvents were evaporated under reduced pressure to obtain de desired compound **311** (30 mg, 40 %) as a yellow oil.

Opening lactone **254** reaction in solid phase

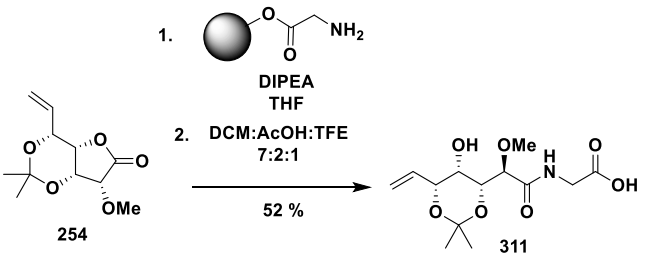

To a 5 mL polypropylene syringe fitted with a polyethylene porous disk and loaded with the resin 308 (197 mg, L = 1.22 mmol/g, 0.244 mmol, 1.00 equiv.) was added a solution of 20 % piperidine in DMF (3 x 3 mL, 10 min.), and the mixture was shaken at 280 rpm. After the last run, the resin was washed with dry DMF (5 x 3 mL) and treated with a solution of the lactone **254** (83.54 mg, 0.37 mmol, 1.50 equiv.) and DIPEA (118 µL, 0.732 mmol, 3.00 equiv.) in dry THF (3 mL) and the mixture was stirred at 50 ºC for 48 hours. Once the solution was unloaded, the resin was washed with DCM (4 x 4 mL). The resin was treated with a solution of DCM/AcOH/TFE (7:2:1, 3 mL) for 30 min. After that, the solution was collected, and the resin washed with DCM (2 x 3 mL). All the collected organic solvents were evaporated under reduced pressure to obtain the desired compound **311** (15.3 mg, 20 %) as a yellow oil.

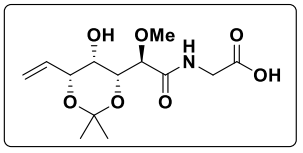

Physical aspect: yellow oil.

Rf: 0.80 (silica gel, 10 % MeOH in DCM).

^{1}H NMR (400 MHz, $CDCl_3$) δ (ppm): 5.86 (ddd, J = 17.4, 10.2, 7.4 Hz, 1H), 5.44 – 5.21 (m, 2H), 4.67 – 4.59 (m, 1H), 4.41 (t, J = 7.9 Hz, 1H), 4.10 (d, J = 5.7 Hz, 1H), 4.06 (d, J = 5.7 Hz, 1H), 3.96 – 3.90 (m, 2H), 3.87 (d, J = 5.0 Hz, 1H), 3.72 (s, 3H), 1.43 (s, 6H),

^{13}C NMR (100 MHz, $CDCl_3$) δ (ppm): 171.67, 134.83, 119.65, 109.58, 82.22, 79.10, 78.39, 69.15, 59.73, 47.95, 29.71, 27.22, 26.74.

7.2.35. Synthesis of precursor compound 312

Fmoc-*L*-Ala-OH Loaded in 2-Chlorotrityl Chloride Resin

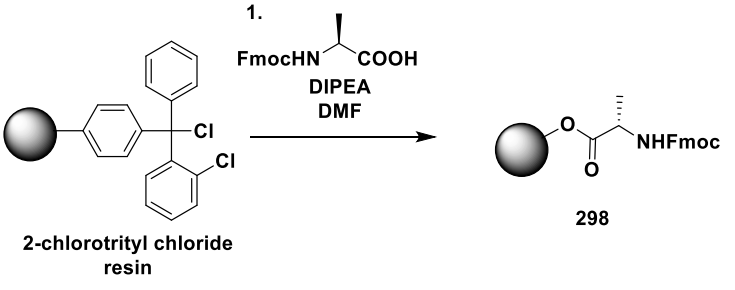

A 5 mL polypropylene syringe fitted with polyethylene porous disk charged with 2-chlorotrityl chloride resin (100 mg, L = 1.22 mmol/g, 0.16 mmol, 1.00 equiv.), was loaded with a solution of Fmoc-*L*-Ala-OH (150 mg, 0.48 mmol, 3.00 equiv.) and DIPEA (90 µL, 0.56 mmol, 3.50 equiv.) in dry DMF (3 mL). The resulting suspension was shaken at 280 rpm for 30 h, the solution was unloaded, and the resin was washed by shaking with dry DMF (5 x 3 mL). The resulting swelled resin was used in the next step.

Oxidation with TEMPO/BAIB

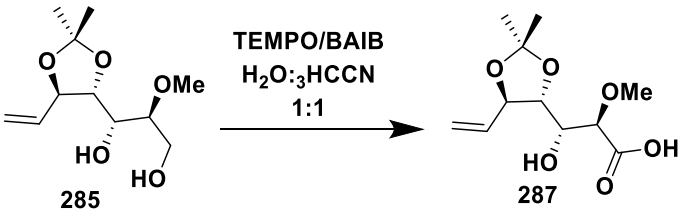

BAIB (618 mg, 1.92 mmol, 6.00 equiv.) and TEMPO (29.7 mg, 0.19 mmol, 0.60 equiv.) were added to a stirred solution of alkene **285** (78.80 mg, 0.32 mmol, 1.00 equiv.) in a 1:1 mixture of CH_3CN:H_2O (1.4 mL) at room temperature. After 5 h, the crude mixture was diluted with EtOAc, quenched by the addition of a saturated aqueous $Na_2S_2O_3$ solution and, after separation of both layers, the aqueous phase was then extracted with EtOAc. The organic solution was washed again with a saturated aqueous $Na_2S_2O_3$ solution, then dried over anhydrous MgSO4 and the solvent was evaporated under reduced pressure.

Coupling reaction between acid **287** and *resin **298***

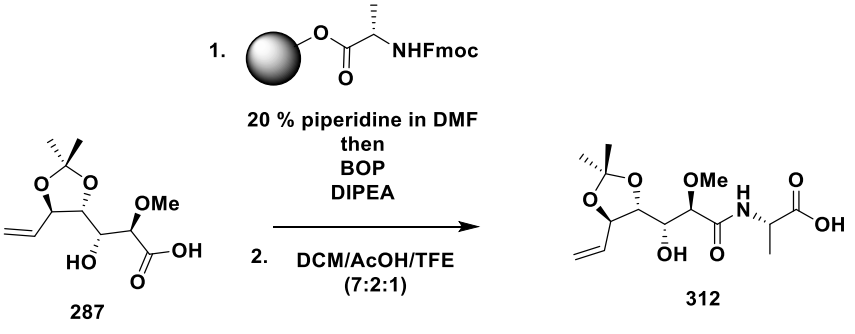

To a 5 mL polypropylene syringe fitted with a polyethylene porous disk and loaded with the Fmoc-*L*-Ala-resin **298** (100 mg, L = 1.22 mmol/g, 0.16 mmol, 1.00 equiv.) was added a solution of 20 % piperidine in DMF (3 x 3 mL, 10 min.), and the mixture was shaken at 280 rpm. After the last run, the resin was washed with dry DMF (5 x 3 mL) and treated with a solution of the acid **287** (0.36 mmol, 2.00 equiv.), BOP (170 mg, 0.38 mmol, 2.4 equiv.) and DIPEA (94 µL, 0.53 mmol, 3.3 equiv.) in dry DMF (2 mL) and

the mixture was stirred at room temperature for 48 hours. Once the solution was unloaded, the resin was washed with DMF 4 x 4 mL) and it was used in the next step without any further purification. The resin was treated with a solution of DCM/AcOH/TFE (7:2:1, 3 mL) for 30 min. After that, the solution was collected, and the resin washed with DCM (2 x 3 mL). All the collected organic solvents were evaporated under reduced pressure to obtain the desired compound **312** (40 mg, 52 %) as a yellow oil.

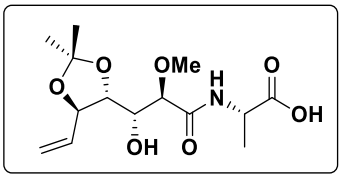

Physical aspect: yellow oil.

Rf: 0.80 (silica gel, 10 % MeOH in DCM).

^{1}H NMR (400 MHz, $CDCl_3$) δ (ppm): 8.03 (s, 1H), 7.19 (s, 1H), 7.15 (d, J = 7.9 Hz, 1H), 5.87 (ddd, J = 17.5, 10.3, 7.5 Hz, 1H), 5.46 – 5.27 (m, 2H), 4.66 – 4.59 (m, 1H), 4.42 (t, J = 7.9 Hz, 1H), 4.19 – 4.02 (m, 2H), 4.02 – 3.92 (m, 2H), 3.77 – 3.69 (m, 2H), 3.46 (s, 3H), 1.44 (s, 6H), 1.26 (s, 3H).

7.2.36. Synthesis of precursor compound 315

Coupling reaction between resin **298** and Fmoc-*L*-Alanine-OH

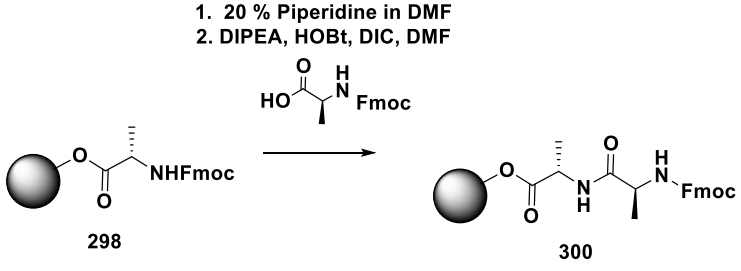

The polypropylene syringe loaded with the swelled resin **298** (100 mg, L = 1.22 mmol/g, 0.16 mmol, 1.00 equiv.) was treated with 20 % piperidine in DMF (3 x 3 mL, 10 min). After the last run, the resin was washed with dry DMF (5 x 3 mL) and loaded with a solution of Fmoc-*L*-Ala-OH (100

mg, 0.32 mmol, 2.00 equiv.), HOBt (40 mg, 0.32 mmol, 2.00 equiv.) and DIC (60 µL, 0.73 mmol. 2.50 equiv.) in dry DMF (3 mL). The resulting suspension was shaken at 280 rpm for 24 h, and then, the solution was unloaded and the resin washed with dry DMF (5 x 3 mL). The resulting swelled resin was used in the next step.

Oxidation with TEMPO/BAIB

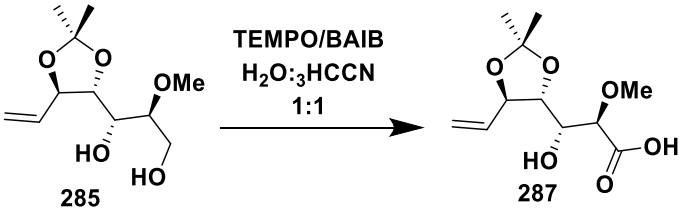

BAIB (618 mg, 1.92 mmol, 6.00 equiv.) and TEMPO (29.7 mg, 0.19 mmol, 0.60 equiv.) were added to a stirred solution of Alkene **285** (78.80 mg, 0.32 mmol, 1.00 equiv.) in a 1:1 mixture of CH_3CN:H_2O (1.4 mL) at room temperature. After 5 h, the crude mixture was diluted with EtOAc, quenched by the addition of a saturated aqueous $Na_2S_2O_3$ solution and, after separation of both layers, the aqueous phase was then extracted with EtOAc. The organic solution was washed again with a saturated aqueous $Na_2S_2O_3$ solution, then dried over anhydrous MgSO4 and the solvent was evaporated under reduced pressure to obtain the desired acid 287 which was used in the next step without any further purification.

Coupling reaction between acid **300** and dipeptide **313**

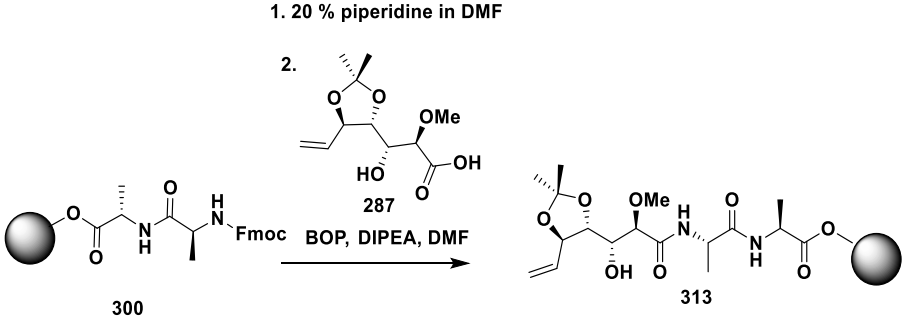

To a 5 mL polypropylene syringe fitted with a polyethylene porous disk and loaded with the resin **300** (100 mg, L = 1.22 mmol/g, 0.16 mmol, 1.00 equiv.) was added a solution of 20 % piperidine in DMF (3 x 3 mL, 10 min.), and the mixture was shaken at 280 rpm. After the last run, the resin was washed with dry DMF (5 x 3 mL) and treated with a solution of the acid **287** (0.36 mmol, 2.00 equiv.), BOP (170 mg, 0.38 mmol, 2.40 equiv.) and DIPEA (94 µL, 0.53 mmol, 3.30 equiv.) in dry DMF (2 mL) and the mixture was stirred at room temperature for 48 hours. Once the solution was unloaded, the resin was washed with DMF (4 x 4 mL) and it was used in the next step without any further purification.

Olefin Cross-Metathesis

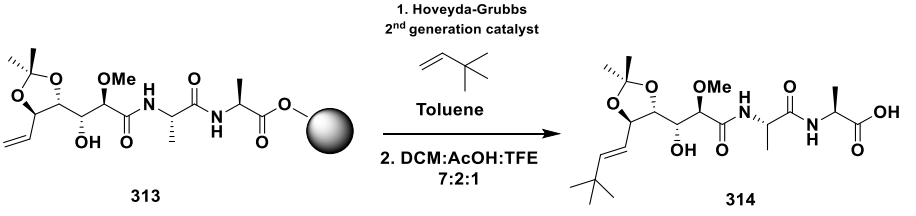

Resin **313** (100 mg, 0.16 mmol, 1.00 equiv.) and Hoveyda-Grubbs 2nd generation catalyst (20 mg, 0.032 mmol, 0.20 equiv.) were dissolved in degassed toluene (10 mL). Then, 3,3-dimethylbut-1-ene (10 mL) was added dropwise at room temperature. The resulting mixture reaction was heated at 60 ^{o}C in a sealed tube for 12 h. Once the solution was unloaded, the resin was washed with DCM (4 x 4 mL). The resin was treated with a solution of DCM:AcOH:TFE (7:2:1, 3 mL) for 30 min at room temperature. After that, the solution was collected, and the resin washed with DCM (2 x 3 mL). All the collected organic solvents were evaporated under reduced pressure and the crude was purified by flash- column chromatography (Silica Gel, 20 % MeOH in DCM) to obtain the desired precursor **313** (40 mg, 21 % over 3 steps) as a brown oil.

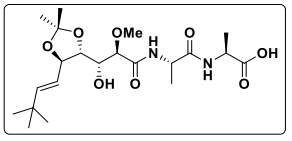

Physical aspect: Brown solid.

Rf: 0.43 (10 % MeOH in DCM).

^{1}H RMN (500 MHz, MeOD) δ (ppm): 5.70 (d, *J* = 15.9 Hz, 1H), 5.45 (dd, *J* = 15.9, 6.7 Hz, 1H), 4.50 – 4.37 (m, 2H), 4.32 – 4.20 (m, 3H), 3.97 – 3.86 (m, 3H), 3.79 (d, *J* = 8.6 Hz, 1H), 3.28 (s, 3H), 1.34 – 1.27 (m, 8H), 1.19 (s, 6H), 0.94 (s, 9H).

^{13}C NMR (125 MHz, MeOD) δ (ppm): 144.16, 141.17, 128.18, 128.06, 128.03, 125.63, 122.27, 99.13, 79.41, 74.18, 72.74, 64.84, 62.91, 57.10, 33.67, 32.39, 31.67, 31.59, 29.35, 29.07, 28.40, 28.30, 22.33, 18.12, 16.81.

*7.2.37. Synthesis of bengamide analogue **315**. Acidic hydrolysis of precursor **314***

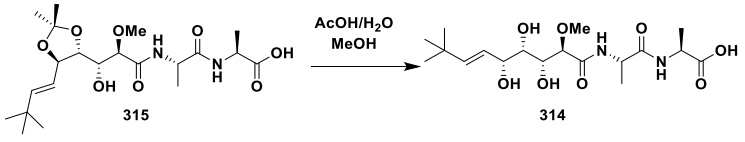

315 314

A 70 % aqueous AcOH solution (0.70 mL) was added to a stirred solution of precursor **315** (10 mg, 0.02 mmol, 1.00 equiv.) in MeOH (0.3 mL) at room temperature. The reaction was heated at 70 ºC and it was stirred for 3 h. After this time, the crude reaction was allowed to room temperature and solvents were removed under reduced pressure. The resulting crude reaction was purified by flash column chromatography (Silica gel, 4 % MeOH in DCM) to obtain the desired analogue **314** (6 mg, 60 %) as a colourless oil.

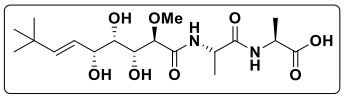

Physical aspect: colourless oil.

Rf: 0.80 (silica gel, 10% MeOH in DCM).

^{1}H NMR (500 MHz, MeOD) δ (ppm): 5.70 (d, *J* = 15.9 Hz, 1H), 5.45 (dd, *J* = 15.9, 6.7 Hz, 1H), 4.50 – 4.37 (m, 2H), 4.32 – 4.20 (m, 3H), 3.97 – 3.86 (m, 3H), 3.79 (d, *J* = 8.6 Hz, 1H), 3.28 (s, 3H), 1.34 – 1.27 (m, 8H), 0.94 (s, 9H).

^{13}C NMR (126 MHz, MeOD) δ (ppm): 178.06, 178.04, 172.11, 171.83, 140.98, 127.19, 74.27, 74.08, 72.99, 58.70, 50.16, 49.35, 33.51, 29.74, 29.70, 18.12, 18.01, 18.00.

7.2.38. Synthesis of bengamide analogue 316

Fmoc-β-Alanine-OH Loaded 2-Chlorotrityl Chloride Resin

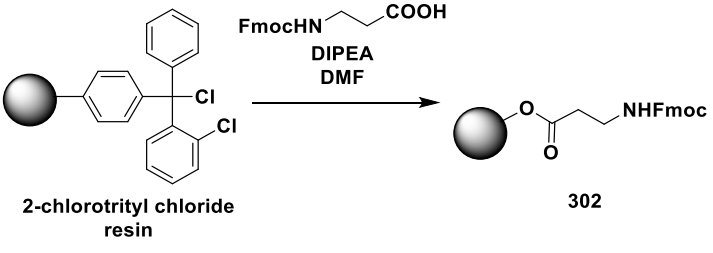

2-chlorotrityl chloride resin

302

A 5 mL polypropylene syringe fitted with polyethylene porous disk charged with 2-chlorotrityl chloride resin (100 mg, L = 1.22 mmol/g, 0.16 mmol, 1.00 equiv.), was loaded with a solution of Fmoc-β-Ala-OH (150 mg, 0.48 mmol, 3.00 equiv.) and DIPEA (90 µL, 0.56 mmol, 3.50 equiv.) in dry DMF (3 mL). The resulting suspension was shaken at 280 rpm for 30 h, the solution was unloaded, and the resin was washed by shaking with dry DMF (5 x 3 mL). The resulting swelled resin was used in the next step.

Coupling reaction between resin **302** and Fmoc-*L*-Alanine-OH

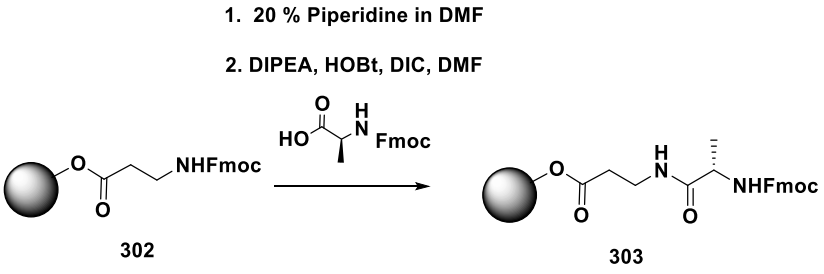

The polypropylene syringe loaded with the swelled resin **302** (100 mg, L = 1.22 mmol/g, 0.16 mmol, 1.00 equiv.) was treated with 20 % piperidine in DMF (3 x 3 mL, 10 min). After the last run, the resin was washed with dry DMF (5 x 3 mL) and loaded with a solution of Fmoc-*L*-Ala-OH (100 mg, 0.32 mmol, 2.00 equiv.), HOBt (40 mg, 0.32 mmol, 2.00 equiv.) and DIC (60 µL, 0.73 mmol. 2.50 equiv.) in dry DMF (3 mL). The resulting suspension was shaken at 280 rpm for 24 h, and then, the solution was unloaded and the resin washed with dry DMF (5 x 3 mL). The resulting swelled resin was used in the next step.

Coupling reaction between acid **287** and dipeptide **303**

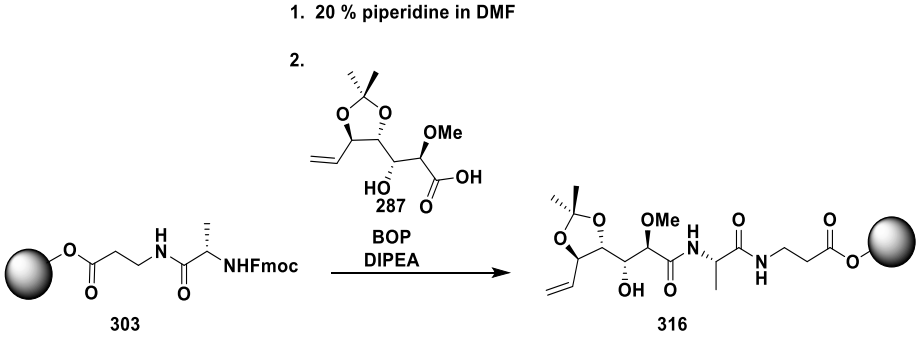

To a 5 mL polypropylene syringe fitted with a polyethylene porous disk and loaded with the resin **303** (100 mg, L = 1.22 mmol/g, 0.16 mmol, 1.00 equiv.) was added a solution of 20 % piperidine in DMF (3 x 3 mL, 10 min.), and the mixture was shaken at 280 rpm. After the last run, the resin was washed with dry DMF (5 x 3 mL) and treated with a solution of the acid **287** (0.36 mmol, 2.00 equiv.), BOP (170 mg, 0.38 mmol, 2.4 equiv.)

and Diisopropylamine (DIPEA) (94 µL, 0.53 mmol, 3.3 equiv.) in dry DMF (2 mL) and the mixture was stirred at room temperature for 48 hours. Once the solution was unloaded, the resin was washed with DMF (4 x 4 mL) and it was used in the next step without any further purification.

Olefin cross metathesis

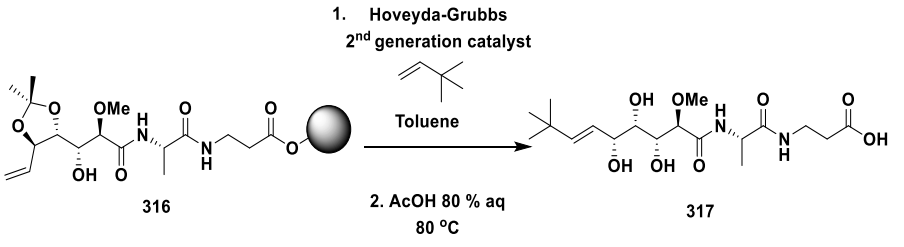

Resin **316** (25 mg, 0.09 mmol, 1.00 equiv.) and Hoveyda-Grubbs 2nd generation catalyst (5 mg, 0.018 mmol, 0.20 equiv.) were dissolved in degassed toluene (5 mL). Then, 3,3-dimethylbut-1-ene (5 mL) was added dropwise at room temperature. The resulting mixture reaction was heated at 60ºC in a sealed tube for 12 h. Once the solution was unloaded, the resin was washed with DCM (4 x 4 mL). The resulting resin was treated with a solution of aqueous 80 % AcOH solution (3 mL) for 30 min at 80 ºC. After that, the solution was collected, and the resin washed with DCM (2 x 3 mL). All the collected organic solvents were evaporated under reduced pressure and the crude was purified by flash- column chromatography (Silica Gel, 20 % MeOH in DCM) to obtain the desired analogue **317** (11 mg, 25 % over 4 steps) as a brown oil.

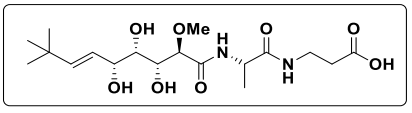

Physical aspect: colourless oil.

Rf: 0.80 (silica gel, 10% MeOH in DCM).

^{1}H NMR (500 MHz, $CDCl_3$) δ (ppm): 5.70 (d, J = 15.7 Hz, 1H), 5.45 (dd, J = 15.8, 6.8 Hz, 1H), 4.37 (q, J = 7.0 Hz, 2H), 4.26 (d, J = 6.8 Hz, 1H), 4.15 (d, J = 7.9 Hz, 1H), 3.89 (dd, J = 8.7, 1.4 Hz, 1H), 3.78 (d, J = 8.7 Hz, 1H), 3.28 (s, 3H), 1.32 (s, 3H), 1.30 (s, 5H), 1.28 (s, 3H), 1.27 (s, 2H), 0.94 (s, 9H).

^{13}C NMR (125 MHz, MeOD) δ (ppm): 174.67, 144.92, 129.47, 129.39, 127.22, 125.60, 121.35, 83.46, 79.43, 70.03, 67.84, 32.40, 31.67, 29.35, 28.43, 26.72, 25.51, 22.33, 13.03.

7.3. Experimental for nanoparticles systems

7.3.1. Characterization

The prepared NPs were characterized to determinate physical, chemical and morphology properties. Thus, the obtained data were analysed to search an optimized synthesis. The characterization techniques employed will be detailed bellow.

UV–vis spectroscopy

The absorption spectra of the different obtained NPs were recorded with an Agilent 8453 UV-vis spectrophotometer. The measure was taken using a 1 cm quartz cell in a range between 300-900 nm. Moreover, these measures allow to monitor the encapsulation and release of the active drug into the NPs and make the corresponding calibrated lines.

Dynamic Light Scattering (DLS)

Through the technique of dynamic light scattering and potential Z was determined the size of NPs, Dh, the dispersion of the sample and the superficial charge. DLS measurements were carried out in a Zetasizer Nano S from Malvern Instruments, at a detection angle of Θ= 173º and at a scattering q vector Θ = 0.0264 nm^{-1}. Moreover, to carried out the analysis different temperature and pH values were employed to determinate the size and the charge under different conditions.

Hydrodynamic ratio

The diluted samples were irradiated with a laser He-Ne of 4 mW in a wavelength of 633 nm with the objective of detecting the fluctuations that the intensity of light suffers due to collision with the particles, which are in constant movement determined by the Brownian movement. Thus, relating the intensity fluctuations with the translational diffusion coefficient and with the diameter of the particle by means of the Stokes-Einstein equation, the average hydrodynamic radius of the particle is determined.

Using this technique, the lowest critical phase transition temperature in solution (LCST) of a thermosensitive polymer can be determined, that is, the temperature at which the polymer goes from being in a collapsed state to a sllowen state.

Z potential

To measure the charge on the surface, the sample of NPs is placed in a cuvette equipped with metal electrodes located at both ends of a transparent plastic capillary. When the capillary cell is subjected to an electric field, the NPs present move in the direction of the field or in the opposite direction to it, with a speed proportional to their surface charge. Through data processing by the team, the Z potential of the nanoparticles is obtained, which depends on the ionic charge and the pH of the medium.

Transmission electron microscopy

For TEM imaging a JEOL JEM1400 TEM microscope operated at 100 kV was employed. 10 µL of each colloidal solution were dropped on 100 mesh copper TEM grids and left to dry. In order to obtain better resolution, Talos F200X was used which operated at 80 kV.

The samples were prepared by placing a 10 µL drop of NPs dispersed, depending on their nature, in toluene or water, on copper grids with a carbon substrate. The NPs, once allowed to dry on the grids, were visualized for analysis.

Raman spectroscopy

The Raman spectra were acquired using a near-infrared (NIR) diode laser at 785 nm (Renishaw inVia Raman spectroscope). A small portion of *p*NIPAM system sample was placed on a glass slide. Adsorption analyses were carried out in a XGT-5000W (Horiba) spectrometer.

7.3.2. Materials

The materials used during the synthesis of the polymeric nanoparticle systems were: *N*-isopropylacrylamide (NIPAM, 97 %), 3-butenoic acid (3-BA), acrylic acid (AA), allylamine (AA), *N,N'*-methylbisacrylamide (BIS, 95 %) and 2,2'-azobis(2-methylpropionamide) (V50, 97%). All these products were supplied by Sigma-Aldrich and were employed without any further purification. All the experiments were carried out using Mili-Q water.

7.3.3. Preparation pNIPAM nanoparticles (pNIPAM@)

Polymerization reaction was carried out in a three-neck round bottom flask (25 mL). Under Ar, a mixture of *N*-isoprpylacrylamide and *N,N'*-methylenebisacrylamide, according to

Table 23, in degassed H_2O (20 mL) was heated at 70 ºC under medium magnetic stirring. After observing a homogeneous medium, the radical initiator V50 (100 mM in H_2O, 0.150 mL) was added. After 10 min, the solution became turbid, which means that the polymerisation process is occurring. Then, the resulting mixture was stirred for 2 h at 70 ºC. After this time, the resulting crude reaction was allowed to cool down at room temperature under stirring and then it was transferred to centrifuge tubes and centrifuged at 8000 rpm for 1 h. After that, the supernatant was removed, and the pellet was washed with H_2O (20 mL) to produce a clear colloidal dispersion. This centrifugation process was repeated 4 times. An aliquot was taken and lyophilised for analyses. This sample was kept at 5 ºC and protected from light.

Table 23. Conditions for the polymerization of *p*NIPAM@

	***p*NIPAM**	***N*-isopropylacrylamide**		***N,N´*-Methylenbisacrylamide**		
Entry	**nM**	**mmol**	**g**	**mmol**	**g**	**% mol**
1	50	1.0	0.113	0.1	0.015	10
2	75	1.5	0.170	0.15	0.023	10
3	100	2.0	0.226	0.2	0.031	10
4	150	3.0	0.339	0	0	0
5	150	3.0	0.339	0.075	0.015	2.5
6	150	3.0	0.339	0.15	0.023	5
7	150	3.0	0.339	0.21	0.032	7.5
8	150	3.0	0.339	0.3	0.046	10
9	200	4.0	0.453	0.4	0.062	10
10	250	5.0	0.566	0.5	0.077	10

7.3.4. Preparation of pNIPAM-co-3BA@, pNIPAM-co-AA@ and pNIPAM-co-AA@ co-polymeric nanoparticles

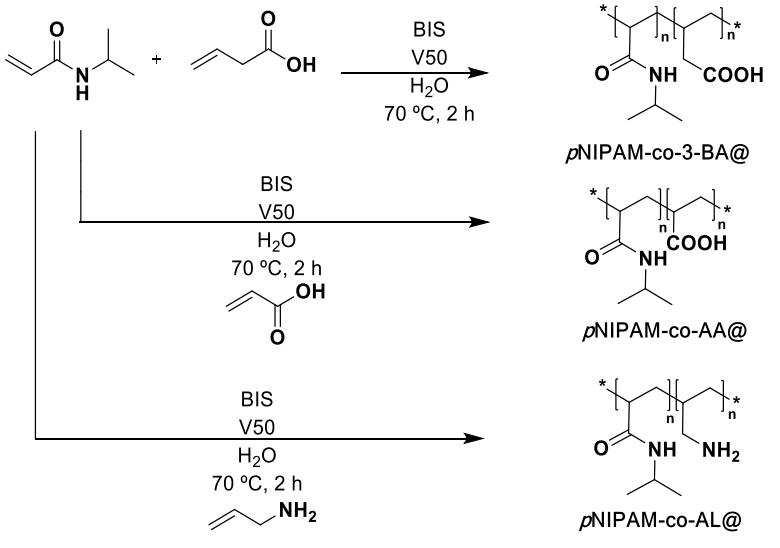

A mixture of *N*-isoprpylacrylamide (3 mmol, 0.339 g) and *N,N'*-methylenebisacrylamide (0.3 mmol, 0.046 g) in degassed H_2O (20 mL, Ar) was

heated at 70 ºC and the corresponding co-monomer: 3-butenoic acid (0.35 mmol, 0.03 g, 0.03 mL), acrylic acid (0.30 mmol, 0.046 g) or allylamine hydrochloride in H_2O (50 mM, 1 mL), was added. Then, the radical initiator V50 (100 mM in H_2O, 0.150 mL) was added, and the mixture was stirred for 2 h at 70 ºC. The purification of these nanoparticles was carried out as in 7.3.2.1.

7.3.5. Preparation of magnetic nanoparticles (@Fe_3O_4). Co-precipitation method

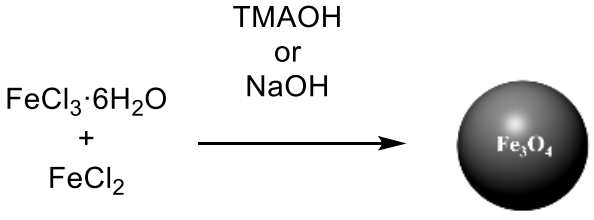

7.3.6. *Coprecipitation with TMAOH in 25 % MeOH or H2O*

TMAOH (25 % in MeOH, or 25% in H_2O, 10.5 mL) in water (22 mL) was heated at 70 ºC in a three-neck round bottom flask. Then, a solution of $FeCl_3 \cdot 6H_2O$ (4 mmol, 1083 mg) and $FeCl_2$ (1.97 mmol, 250 mg) in H_2O (3 mL) was added dropwise, when it finished a black precipitated was observed at the bottom of the flask. The mixture was stirred for 30 min at 70 ºC. After this time, the mixture was allowed cool down to room temperature and, to remove the excess of TMAOH, a magnetic decantation using a neodimium magnet was caried out. Decantation was not observed when water was used as a solvent, and the nanoparticles were isolated by centrifugation (8000 rpm, 1h). The supernatant was discarded, and the the pellet was washed with MiliQ H_2O (3x10 mL). An aliquot of the dispersion (1mL) was used to calculate the dry residue,

which was obtained by introducing the sample in an oven at 80 ºC, resulting 7.2 mg/mL.

7.3.7. Coprecipitation with NaOH

A solution of NaOH in water (0.4 M, 20 mL) was added to a stirred solution of $FeCl_2$ (1.07 mmol, 250 mg) and $FeCl_3 \cdot 6H_2O$ (4 mmol, 1083 mg) in water (200 mL) at 50 ºC the pH value of the solution was 11. The mixture reaction was stirred at this temperature for 2 h. After this time, the mixture was allowed to cool at room temperature. The purification process of nanoparticles was carried out a section 7.3.3.1. The dry residue in this case was 4.4 mg/mL.

7.3.8. Functionalization of magnetic nanoparticles with 3-butenoic acid (@Fe_3O_4-3BA) or acrylic acid (@Fe_3O_4-AA)

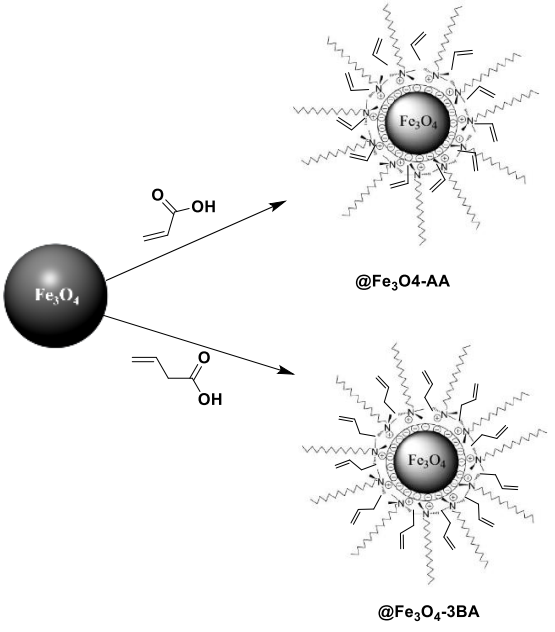

In a three-neck round bottom flask (250 mL), the acid derivative (Acrylic acid (9.4 mmol, 0.678 g, 0.645 mL) or 3-butenoic acid (9.40 mmol, 0.81 g, 0.80 mL)) was added to a stirred solution of @Fe_3O_4 (25 mg) in H_2O (100 mL) at room temperature. Then, the reaction was heated at 70 ºC

and was sonicated for 1 h. After this time, the mixture reaction was allowed to cool at room temperature and a solution of hexadecyl trimethyl ammonium bromide (CTAB) in water (200 mM, 2 mL) was added. The mixture was stirred for 5 min more. Finally, NPs dispersion was centrifuged (1 h, 8000 rpm). Then, the supernatant was removed and the pelled was redispersed in H_2O (100 mL) containing CTAB (5 mM, 1.25 mL) to obtain @Fe_3O_4-3BA or @Fe_3O_4-AA.

7.3.9. *Synthesis of hybrid pNIPAM magnetic systems: pNIPAM@Fe_3O_4-3BA, pNIPAM@Fe_3O_4-AA and pNIPAM-co-AL@Fe_3O_4-AA*

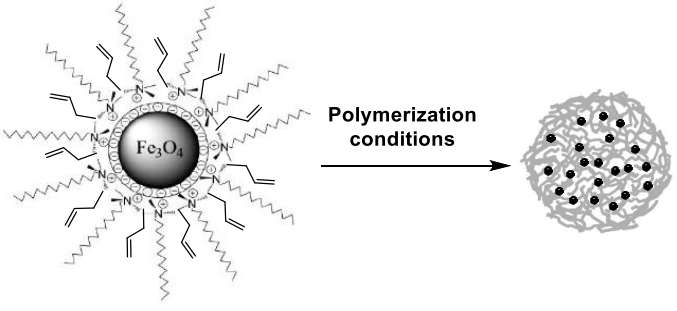

Hybrid colloidal nanoparticles were prepared by using the previously synthesised @Fe_3O_4-3BA and @Fe_3O_4-AA nanoparticles as seeds during *p*NIPAM polymerisation. In a three-neck round bottom flask (25 mL), a mixture of *N*-isopropylacrylamide (3 mmol, 0.339 g), *N,N'*-methylenebisacrylamide (0.30 mmol, 0.046 g) and @Fe_3O_4-3BA or @Fe_3O_4-AA (1:1, Fe_3O_4:H_2O, 20 mL) was heated at 70 ºC and degassed with a flux of Ar for 10 min. Then, the polymerization initiator V50 (100 mM in H_2O, 0.150 mL) was added. For *p*NIPAM-co-AL@Fe_3O_4-AA system, allylamine (50 mM, 1 mL) was added at this moment. After the sample became turbid (around 10 min), the flask was sealed, and the mixture reaction was stirred for 2 h at 70 ºC. After this time, the mixture was allowed to cool down at room temperature and magnetic decantation using a neodymium magnet was carried out to remove the excess of *p*NIPAM microgels. The supernatant was discarded, and the pellet was washed with

H_2O (3 x 20 mL). The polymeric-magnetic systems were lyophilised and kept at 5 ºC protected from light.

7.3.10. *Functionalization of hybrid nanoparticles pNIPAM-co-Al@Fe_3O_4-AA with fluorescein isothiocyanate (FITC)*

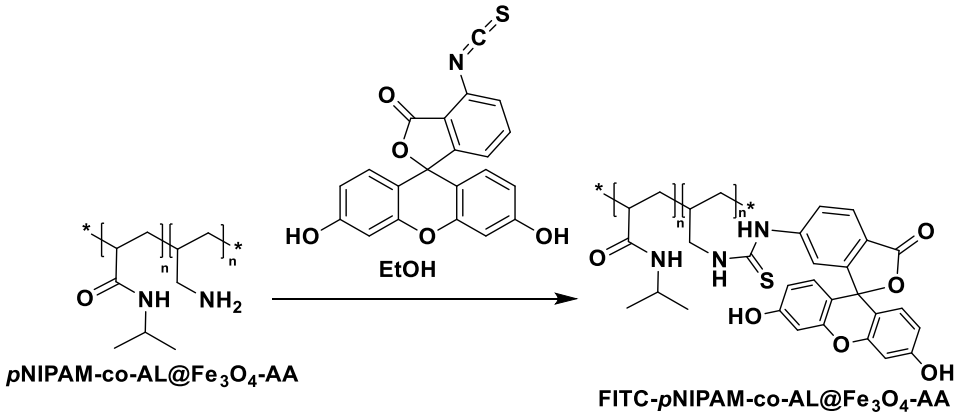

In a round bottom flask (10 mL), FITC (Fluorescein isothiocyanate) (2 mg) was added to a stirred solution of *p*NIPAM-co-AL@Fe_3O_4-AA (4.80 mg) in EtOH (4.80 mL). The reaction mixture was stirred for 24 h protected light at room temperature. After this time, the mixture was centrifugated (40 min, 8000 rpm), the supernatant was removed and the pelled was washed with H_2O (4 mL) and centrifugated. This process was repeated three times, and finally, the pellet was redispersed in MiliQ H_2O (4 mL) to obtain FITC-*p*NIPAM-co-Al- @Fe_3O_4-AA.

7.4. Experimental for drug encapsulation

7.4.1. General process of encapsulation drugs.

The encapsulation of different drugs has been carried out using of the nanoparticles. Thus, the drug loading was carried out at 20 ºC cause this temperature the *p*NIPAM remains in an expanded state and the drug can be include inside the system. On the other hand, the drug encapsulation efficiency (EE %) has been calculate by UV spectrometry analysis of the supernatant after centrifugation.

$$EE\% = \frac{D_L - D_F}{D_F}\ x\ 100$$

where D_L is the initial added concentration of drug and D_F is the concentration of the free drug after centrifugation.

Specifically, the systems used for encapsulation of drugs were: *p*NIPAM@, *p*NIPAM@Fe_3O_4-3BA, FITC-pNIPAM-co-Al@Fe_3O_4-AA. To carry out this encapsulation process, the nanoparticle system selected is dissolved in water (10 mL) and the drug (5-fluorouracil, oxaliplatin, bengamide analogue X or hidroxytirosol analogues X, X and X) were added. Then, the resulting mixture was stirred for 48 h at 20 ºC. After this time, the mixture was centrifugated (8000 rpm, 1h). The supernatant was discarded, and the pellet was washed with water. The supernatant was kept to determinate the EE % in an indirect way, i.e., the amount of non-encapsulate drug was quantified by UV spectroscopy.

7.4.2. General process of in vitro release.

To carry out the in vitro drug release study was used a sample of lyophilised NPs loading the drug (*p*NIPAM-derivative system) suspended in PBS (10 mL) and a cellulose dialysis bag placed in an Erlenmeyer. Thus, PBS buffer was used as solvent in this experiment to maintain the pH of the solution in 7.4 (stationary phase) and at constant stirring of 100 rpm.

Drug release analysed were carried out at 4, 20 and 40 ºC to observe the influence of the temperature. Thus, different aliquots of 3 mL were collected at intervals of 10 min during the first 60 min and every 12h for 48 h.

7.4.3. Synthesis tyrosol analogues

Synthesis of compound 328. Protection reaction with benzyl bromide

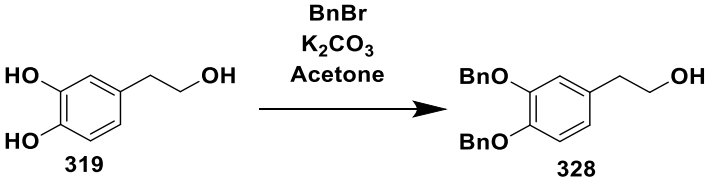

Benzyl bromide (1.72 mL, 14.60 mmol, 2.30 equiv.) and K_2CO_3 (1.70 g, 25.84 mmol, 4.00 equiv.) were added to a stirred solution of hydroxytirosol **319** (1.00 g, 6.46 mmol, 1.00 equiv.) in acetone (30 mL). Then, the mixture was heated at reflux for 24 hours. After this time crude was filtered off and concentrated under reduced pressure to obtain the desired compound **328**, which was used in the next step without any further purification.

Synthesis of precursors 329, 330 and 331. *Substitution reaction.*

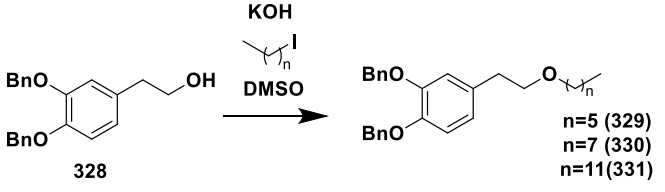

KOH (50.3 mg, 0.89 mmol, 6.00 equiv.) and the corresponding alkyl Iodine (0.45 mmol, 3.00 equiv.) were added to a stirred solution of Benzyl derivate **328** (50 mg, 0.15 mmol, 1.00 equiv.) in dimethylsulfoxide (5mL). Then, the mixture was stirred for 12 hours at room temperature. After this time, HCl 3 M was added. The crude was diluted with Et_2O and a saturated aqueous $Na_2S_2O_3$ solution. After separation of both layers, the

organic was extracted, dried over anhydrous $MgSO_4$ and concentrated under reduced pressure. The resulting crude mixture was purified by flash-column chromatography (Silica gel, 10 % EtOAc in Hexanes) to obtain **329** (45.2 mg, 72 %), **330** (46.2 mg, 69 %) and **331** (44.4 mg, 59 %).

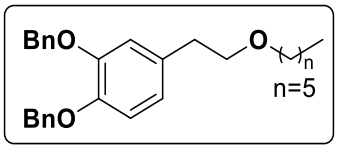

Physical aspect: white solid.

Rf: 0.80 (silica gel, 20 % EtOAc in Hexanes).

^{1}H NMR (400 MHz, $CDCl_3$) δ (ppm): 7.49 – 7.43 (m, 5H), 7.40 – 7.35 (m, 5H), 6.88 (s, 1H), 6.75 (d, *J* = 2.0 Hz, 1H), 6.73 (d, *J* = 2.0 Hz, 1H), 5.15 (s, 2H), 5.14 (s, 2H), 3.64 (t, *J* = 7.0 Hz, 1H), 3.56 (t, *J* = 7.2 Hz, 2H), 3.41 (t, *J* = 6.7 Hz, 2H), 2.85 (d, *J* = 7.0 Hz, 1H), 2.79 (t, *J* = 7.2 Hz, 2H), 1.33 – 1.29 (m, 10H), 0.92 – 0.87 (m, 3H).

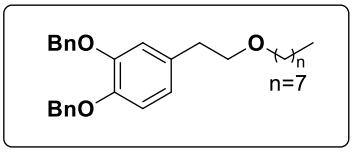

Physical aspect: white solid.

Rf: 0.85 (silica gel, 20 % EtOAc in Hexanes).

^{1}H NMR (400 MHz, $CDCl_3$) δ (ppm): δ 7.48 – 7.43 (m, 4H), 7.38 – 7.34 (m, 4H), 7.33 – 7.29 (m, 2H), 6.85 (s, 1H), 6.75 (d, *J* = 2.0 Hz, 1H), 5.15 (s, 1H), 5.13 (s, 2H), 3.56 (t, *J* = 7.3 Hz, 2H), 3.41 (t, *J* = 6.7 Hz, 2H), 2.79 (t, *J* = 7.2 Hz, 2H), 1.83 (p, *J* = 7.1 Hz, 2H), 1.65 – 1.50 (m, 5H), 1.47 – 1.37 (m, 7H), 1.01 – 0.75 (m, 3H).

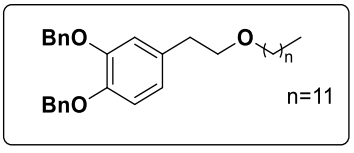

Physical aspect: white solid.

Rf: 0.95 (silica gel 20 % EtOAc in Hexanes).

^{1}H NMR (400 MHz, $CDCl_3$) δ (ppm): δ 7.48 – 7.43 (m, 4H), 7.38 – 7.34 (m, 4H), 7.33 – 7.29 (m, 2H), 6.85 (s, 1H), 6.75 (d, *J* = 2.0 Hz, 1H), 5.15 (s, 1H), 5.13 (s, 2H), 3.56 (t, *J* = 7.3 Hz, 2H), 3.41 (t, *J* = 6.7 Hz, 2H), 2.79 (t, *J* = 7.2 Hz, 2H), 1.83 (p, *J* = 7.1 Hz, 2H), 1.65 – 1.50 (m, 5H), 1.47 – 1.37 (m, 17H), 1.01 – 0.75 (m, 3H).

Synthesis of compounds 325, 326 and 327. *Reduction reaction.*

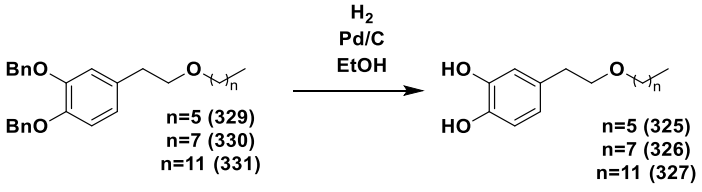

The corresponding compound (**329**-**331**) (0.05 mmol) was dissolved in EtOH (2 mL) and the system was purged with Ar. Then, 10% Pd/C (10 wt %) was added to a Flask and the system was sealed with a septum. After two vacuum/H_2 cycles to replace the air inside with hydrogen, the mixture was vigorously stirred at room temperature under ordinary hydrogen pressure (balloon) for 24 h. The reaction mixture was filtered, and the filtrate was concentrated. The crude was purified by flash-column chromatography (Silica gel, 40 % EtOAc in Hexanes) to obtain the desired analogues **325** (7.1 mg, 60 %), **326** (6.4 mg, 51 %) and **327** (11.3 mg, 70 %).

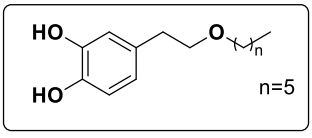

Physical aspect: white solid.

Rf: 0.50 (silica gel, 40% EtOAc in Hexanes).

^{1}H NMR (400 MHz, $CDCl_3$) δ (ppm): 6.73 (d, *J* = 8.0 Hz, 1H), 6.67 (d, *J* = 2.0 Hz, 1H), 6.60 (dd, *J* = 8.0, 2.0 Hz, 1H), 3.63 (t, *J* = 7.1 Hz, 2H), 3.48 (t, *J* = 6.9 Hz, 2H), 2.76 (t, *J* = 7.2 Hz, 2H), 1.65 – 1.52 (m, 2H), 1.37 – 1.20 (m, 7H), 0.93 – 0.83 (m, 3H).

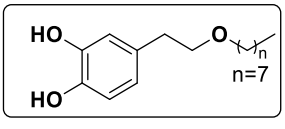

Physical aspect: white solid.

Rf: 0.54 (silica gel, 40% EtOAc in Hexanes).

^{1}H NMR (400 MHz, $CDCl_3$) δ (ppm): 6.73 (d, J = 8.0 Hz, 1H), 6.67 (d, J = 2.0 Hz, 1H), 6.60 (dd, J = 8.0, 2.0 Hz, 1H), 3.64 (t, J = 7.2 Hz, 2H), 3.48 (t, J = 6.9 Hz, 2H), 2.77 (t, J = 7.1 Hz, 2H), 1.63 – 1.53 (m, 2H), 1.32 – 1.23 (m, 12H), 0.90 – 0.86 (m, 3H).

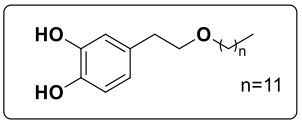

Physical aspect: white solid.

Rf: 0.50 (silica gel, 40% EtOAc in Hexanes).

^{1}H NMR (400 MHz, $CDCl_3$) δ (ppm): 6.74 (d, J = 8.0 Hz, 1H), 6.68 (d, J = 2.0 Hz, 1H), 6.61 (dd, J = 8.1, 2.0 Hz, 1H), 3.63 (t, J = 7.1 Hz, 2H), 3.47 (t, J = 6.8 Hz, 2H), 2.77 (t, J = 7.1 Hz, 2H), 1.65 – 1.46 (m, 2H), 1.41 – 1.26 (m, 20H), 0.94 – 0.85 (m, 4H).

Resumen Tesis: ***Synthesis of new bengamide analogues and encapsulation into thermo-responsive magnetic nanoparticles.***

Estudiante de doctorado: Cristina Porras Alcalá.

Después de las enfermedades cardiovasculares, el cáncer se trata de una de las principales causas de muerte en el mundo desarrollado por lo que resulta una máxima prioridad la investigación dirigida a la búsqueda de fármacos que puedan curar dicha enfermedad. Se debe tener en cuenta que el cáncer representa un conjunto de enfermedades con la característica común de presentar células aberrantes con un crecimiento descontrolado que invade el organismo del enfermo rápidamente, lo cual es un gran problema. A pesar del gran arsenal de agentes antitumorales actualmente existentes, todavía es necesario continuar la búsqueda y desarrollo de nuevos agentes que permita hacer frente a ciertos tumores que resultan intratables o que presenten menor toxicidad que los fármacos empleados en quimioterapia.

Sin duda, el avance en el conocimiento de las bases moleculares de dicha enfermedad ha permitido el desarrollo de nuevos agentes terapéuticos dirigidos hacia dianas muy específicas presentes en las células tumorales y que la diferencia de las células normales. En concreto, se han desarrollado una serie de fármacos dirigidos sobre todo hacia el ataque del crecimiento de dichas células tumorales, inhibiendo quinasas implicadas en el desarrollo celular o activando el sistema inmunológico mediante la actuación sobre antígenos tumorales (inmunoterapias) o actuando sobre oncogenes. Por tanto, en los últimos años hemos sido testigos de importantes avances en el tratamiento del cáncer, pero los efectos secundarios de dichos fármacos limitan su uso. De esta manera, se desarrolla paralelamente un campo de investigación para la búsqueda de terapias alternativas eficaces, fármacos basados en productos naturales bioactivos puesto que se tratan de una de las fuentes esencial de

nuevas terapias, lo que se demuestra con agentes como el taxol, vinblastina, doxorubicina o ectenaiscidina, entre otros productos naturales.

La síntesis de compuestos bioactivos inspirados en productos naturales representa una estrategia importante y válida para el desarrollo de nuevos fármacos, que combinado con la liberación controlada de fármacos mediante la inclusión de estos compuestos en nanopartículas, podría dar lugar a un nuevo tratamiento contra el cáncer menos invasivo y más efectivo. Así, esta Tesis Doctoral estudia la síntesis y desarrollo de productos naturales bioactivos, el diseño de nuevos nanosistemas híbridos e inclusión de distintos fármacos anticancerígenos en dichas nanopartículas, los cuales son un prometedor tratamiento del cáncer de colon. En concreto, esta investigación se centra en la familia de las bengamidas, productos naturales antitumorales extraídos de la esponja Jaspidae. Además, las bengamidas ocupan un lugar preferente en la investigación farmacéutica debido a la propiedades antitumorales, antibióticas y antihelmínticas que presentan, siendo particularmente importantes sus propiedades antiproliferativas. Así, la actividad de estos compuestos se debe a la interacción de la bengamida y la metionina aminopeptidasa (MetAPs), que es una enzima implicada en el crecimiento del tumor. Para ello, en esta Tesis Doctoral se estudia una relación estructura-actividad (SAR) con el objetivo de incrementar la actividad antitumoral de estos compuestos, así como la solubilidad en agua. Por lo tanto, la investigación para obtener una mejor interacción entre bengamidas y MetAPs se recoge en esta tesis. Para lograr este objetivo, se ha realizado un profundo estudio hacia la síntesis de estos compuestos activos.

Centrándonos, por tanto, en ellas, la estructura general de estos productos naturales se caracteriza por poseer un esqueleto de 10 átomos de carbonos, denominada cadena lateral que contiene tres grupos hidroxilos, un metoxilo contiguo y una olefina disustituida *trans*. Dicha cadena C-10 se une a un anillo de caprolactama (**Figura 1**) a través de una unión

amida. En función de dicho anillo y de la cadena lateral C-10 se clasifican las diferentes bengamidas.

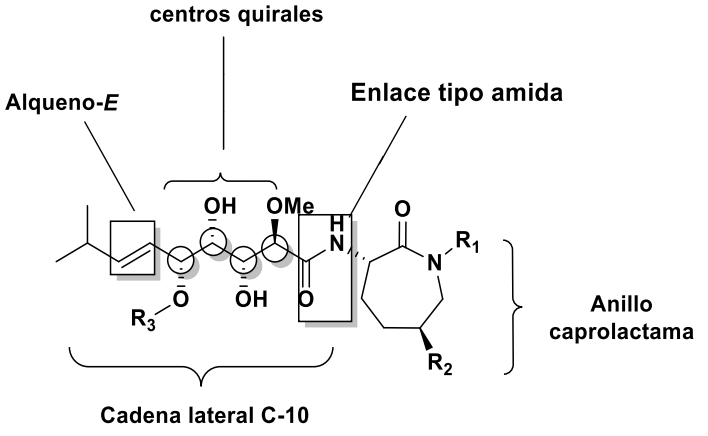

Figura 1. *Estructura general de las bengamidas.*

En primer lugar, se ha modificado el anillo de caprolactama para estudiar el efecto de este fragmento en cuanto la actividad del compuesto. Para ello, se ha realizado la síntesis total del análogo de bengamida E (**1**) y el análogo de bengamida (**2**) y se han comparado sus actividades biológicas, presentando este segundo análogo una más potente actividad. Por ello, se concluyó que modificando este fragmento de la molécula se podría incrementar la interacción entre la bengamida y MetAPs. De hecho, el análogo **2** despertó tanto interés que fue preparada en las cantidades necesarias para realizar estudios *in vivo*.

En segundo lugar, se decidió profundizar en la modificación en el anillo de caprolactama y en concreto se decidió realizar la síntesis de un análogo que mantuviese la estructura de **2,** pero en lugar de presentar un residuo de *L*-alanina en su estructura que presentara un residuo de *L*-azetidina (**compuesto 3**), con el objetivo de que el aminoácido cíclico aportarse una mayor rigidez a la estructura y así, la bengamida encajase de una manera más compacta en el sitio activo de la MetAPs, dando lugar a una mayor actividad antitumoral. Desafortunadamente, la actividad que presentó este compuesto fue mucho menor que la del

compuesto de referencia **2**, por lo que se decidió mantener el residuo de *L*-alanina en las siguientes modificaciones.

En último lugar, la metodología de síntesis en fase sólida como estrategia eficaz para obtener una nueva biblioteca de análogos de bengamidas. Se desarrolló así una nueva metodología para la preparación de nuevos análogos que podrían presentar mayor actividad y mejores propiedades de solubilidad en agua. En concreto, se prepararon dos nuevos análogos de bengamida a través de esta estrategia sintética, manteniendo tal y como se comentó en residuo de *L*-alanina y añadiendo otro aminoácido más a la estructura: *L*-alanina y *β*-alanina (compuestos **4** y **5**).

En conclusión, en cuanto a la síntesis de nuevos análogos de bengamidas, en la presente tesis doctoral se ha desarrollado:

- Síntesis de los análogos **1** y **2**, para realizar estudios in vitro e in vivo.
- Síntesis de un nuevo análogo de bengamida **3**.
- Desarrollo de una nueva metodología hacia las bengamidas y preparación de dos nuevos (**4** y **5**) análogos a través de dicha estrategia.

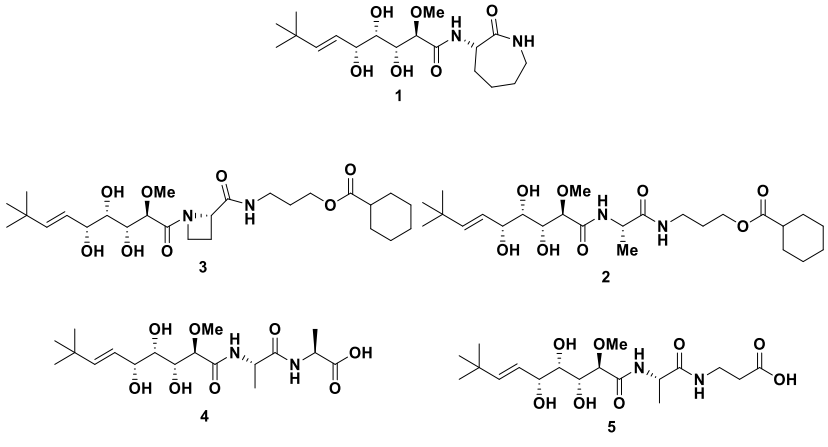

Figura 2. *Resumen de las bengamidas sintetizadas durante la presente Tesis Doctoral.*

Por otro lado, este trabajo de investigación también está enfocado al campo de la nanomedicina debido a las características generales que presentan las nanopartículas:

- Pequeño tamaño, en el rango de nanómetros, que permite la entrada al tumor.
- Dichas nanopartículas puedan responder a una estimulación externa (luz, temperatura o campo magnético) o interna (pH, reacciones redox o actividad enzimática) que se convierten en un sistema de liberación de fármaco más selectivo y la biocompatible.
- Existe una alta relación superficie-volumen que permite el transporte efectivo de compuestos activos en su interior.
- Posibilidad de vectorización hacia el tumor de dichos sistemas.

Así, entre todo tipo de nanopartículas, esta Tesis Doctoral se centra en el desarrollo en un nanosistema híbrido que presente un centro magnético (Fe_3O_4) y esté envuelto por un microgel polimérico (*p*NIPAM), el cual es termosensible. Así, este nanosistema podría dirigirse al tumor con la aplicación de un campo magnético externo, con el objetivo de evitar efectos secundarios derivados de la quimioterapia tradicional, desarrollando un potente híbrido de nanopartículas.

Es importante señalar la termosensibilidad del polímero *p*NIPAM, ya que es una de las principales características por las que se utiliza en el campo de la biomedicina. Así, la respuesta de las variaciones de temperatura por parte de este polímero se entiende teniendo en cuenta las interacciones del mismo consigo mismo o con el disolvente. A temperatura menor de 32 ºC el *p*NIPAM es soluble en agua, ya que la red polimérica forma enlaces de hidrogeno con las moléculas de agua, estando la nanopartícula en un estado expandido. Mientras que, a temperaturas mayores de 32 ºC dichos enlaces de hidrogeno se rompen y la interacción entre polímero-polimero son mayores, la nanopartícula en este momento se encuentra en un estado colapsado, liberando el fármaco que reside en su interior (**Figura 3**).

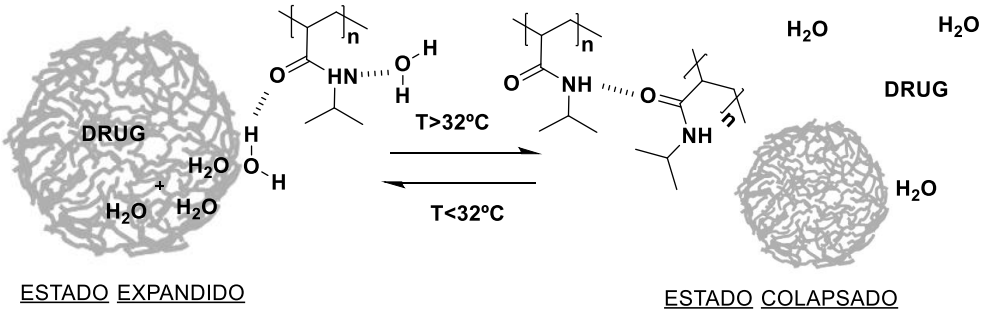

Figura 3. *Estados del pNIPAM en función de la temperatura.*

En primer lugar, en esta Tesis Doctoral se ha optimizado la síntesis de las nanopartículas macizas de *p*NIPAM@, concluyendo que las mejores condiciones para obtener un tamaño de nanopartícula óptimo para su aplicación como sistema de liberación de fármaco y una monodispersidad adecuada fueron en las que el monómero NIPAM se añadía en una concentración 150 nM, 5 % del entrecruzante *N,N'*-metilbisacrilamida con respecto al monómero y una concentración del iniciador radical V50 (**Esquema 1**).

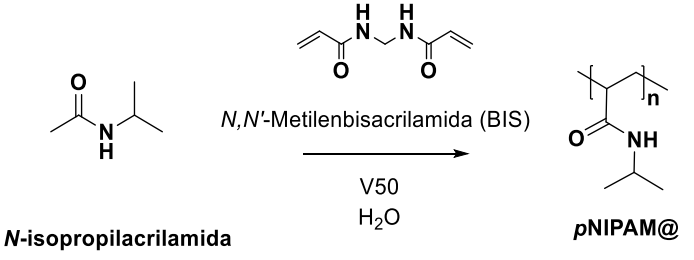

Esquema 1. *Reacción de polimerización para la obtención de pNIPAM@.*

En segundo lugar, tras optimizar la síntesis de *p*NIPAM@, se procedió a preparar estos nanosistemas con distintos comonómeros: ácido 3-butenoico (-3BA), ácido acrílico (-AA) y alilamina (-AL). Así se obtuvieron los nanosistemas deseados: *pNIPAM-co-3BA@, pNIPAM-co-AA@ y pNIPAM-co-AL@* (**Figura 4**). Tras, el análisis de TEM y confirmar que el grupo del ácido carboxílico (-COOH) en los nanosistemas *pNIPAM-co-3BA@ y pNIPAM-co-AA@* y el grupo amino (-NH_2) en el nanosistema estaban presentes a través de ZP análisis, se pudo concluir que la

morfología de la nanopartícula no se veía afectada al cambiar la composición química, obteniéndose unas nanopartículas en un rango de entre 519 ± 3.0 nm y 540 ± 5.5 nm.

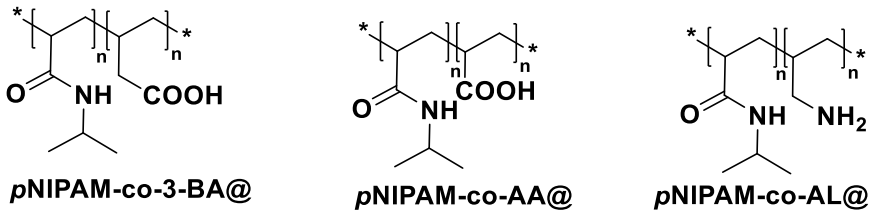

Figura 4. *Estructura química de p*NIPAM-co-3-BA@, *p*NIPAM-co-AA@ and *p*NIPAM-co-AL@.

Tras el control de la síntesis de las nanopartículas poliméricas, se procedió a la preparación del centro magnético para desarrollar el sistema híbrido de nanopartícula magnética-polimérica. Así, se preparó el centro magnético de ferrita a través del método de precipitación de iones férricos y ferrosos en una proporción molar de 2:1 ((Fe(III):Fe(II)) en medio básico.

$$Fe^{2+} + 2Fe^{3+} + 8OH^- \leftrightarrow Fe(OH)_2 + Fe(OH)_3 \rightarrow Fe_3O_4\downarrow + 4H_2O$$

El medio básico fue aportado por TMAOH al 25 % en agua, obteniéndose un residuo seco de 8.66 mg/mL.

Así, tras la obtención del núcleo magnético, se procedió a la funcionalización de este con ácido 3-butenoico y ácido acrílico, con el objetivo de aumentar la compatibilidad de dicho centro con el polímero con el cual se pretendía envolver (*p*NIPAM) y evitar la agregación entre las nanopartículas magnéticas, obteniéndose los centros magnéticos deseados *p*NIPAM@Fe_3O_4-AA y *p*NIPAM@Fe_3O_4-3BA (**Esquema 2**).

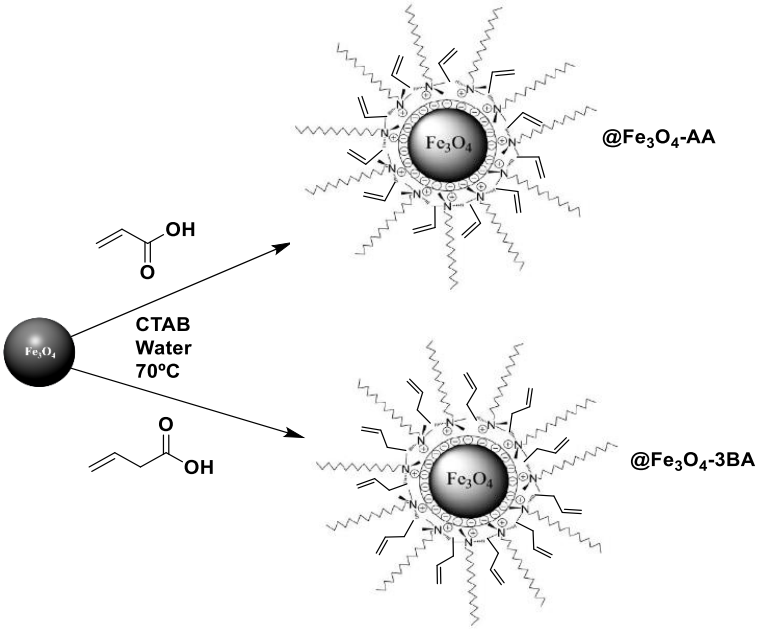

Esquema 2. *Modificación de las nanopartículas magnéticas.*

Tras obtener el centro magnético funcionalizado (@Fe_3O_4-3BA y @Fe_3O_4-AA) se procedió al crecimiento del polímero *p*NIPAM alrededor de dicho centro. Para ello se optimizaron los distintos parámetros de la reacción de polimerización tales como: concentración de monómero y concentración de entrecruzante, concluyendo que las condiciones óptimas de síntesis son las reflejadas en el **esquema 3**.

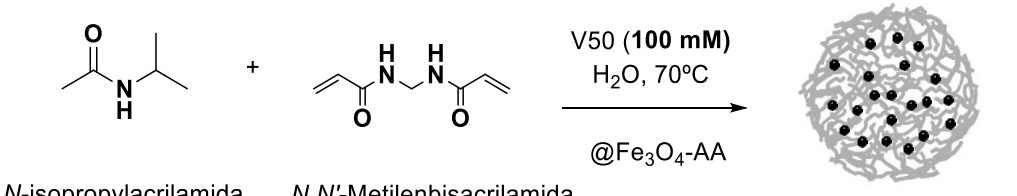

N-isopropylacrilamida (NIPAM) **50 mM**

N,N'-Metilenbisacrilamida (BIS) **5%**

***p*NIPAM@Fe_3O_4-AA**

Esquema 3*. Condiciones óptimas para la síntesis de nanopartículas pNIPAM@Fe_3O_4 (255 nm de diámetro).*

En este punto de estudio en cuanto la síntesis de nanopartículas, se decidió utilizar las condiciones de crecimiento de polímero alrededor del centro magnético utilizando como comonómero alilamina para obtener las nanopartículas *p*NIPAM-co-Al@Fe_3O_4 (**Esquema 4).**

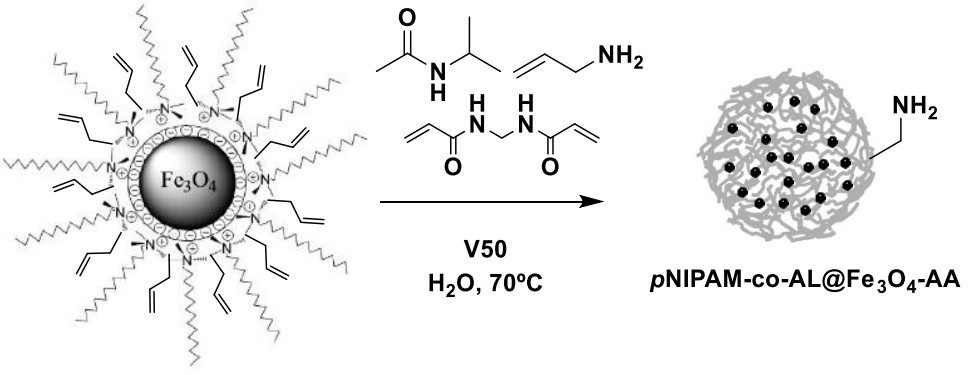

Esquema 4. *Proceso de polimerización alrededor del centro magnético empleado p*NIPAM-co-Al@Fe_3O_4

Por último, se empleó el nanosistema *p*NIPAM-co-AL@Fe_3O_4-AA para funcionalizar dicha nanopartícula con moléculas fluorescentes para poder visualizar dichos sistemas híbridos por microscopio confocal y seguir la internalización de las nanopartículas en medios biológicos. Así, *p*NIPAM-co-AL@Fe_3O_4-AA fue funcionalizado con isotiociando de fluoriseína (FITC). Esta funcionalización fue obtenida a través de la reacción entre los grupos aminos libres presentes en la red polimérica y el grupo isotiocianato del FITC, para rendir un grupo tiourea, dando lugar a FITC-*p*NIPAM-co-AL@Fe_3O_4-AA (**Esquema 5**).

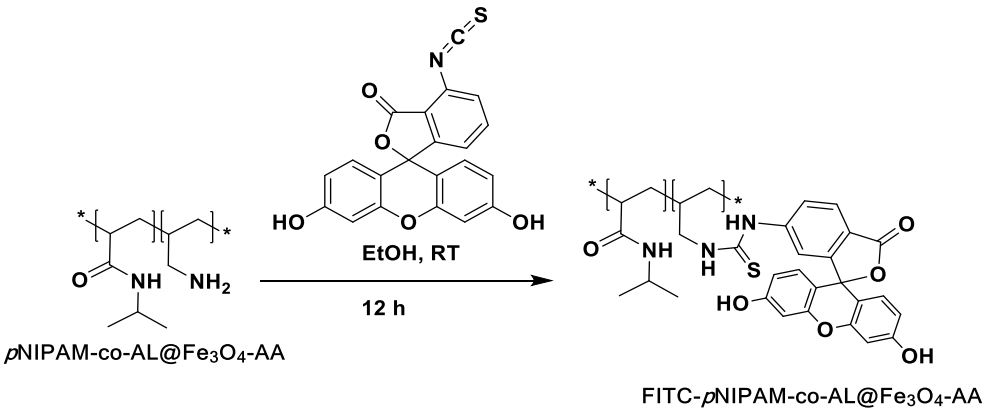

***Esquema 5**. Marcaje fluorescente con FITC de pNIPAM-co-Al@Fe_3O_4-AA.*

La incorporación de este cromóforo fue confirmada a través de microscopia fluorescente confocoal, excitando la muestra a una longitud de onda de 429 nm y emitiendo en 518 nm.

En conclusión, en esta Tesis Doctoral se han preparado los siguientes nanosistemas:

- Nanopartículas poliméricas sólidas (*p*NIPAM@, *p*NIPAM-co-3-BA@, *p*NIPAM-co-AA@ y *p*NIPAM-co-AL@).

- Nanopartículas híbridas *p*NIPAM@Fe_3O_4 (*p*NIPAM@Fe_3O_4-AA, *p*NIPAM@Fe_3O_4-3BA y *p*NIPAM-co-AL@Fe_3O_4-AA).

- Nanopartículas fluorescentes FITC-*p*NIPAM-co-AA@Fe_3O_4-AA.

Finalmente, para unir los dos campos de conocimiento, la síntesis orgánica y la nanomedicina, se han encapsulado en el nanosistema y estudiado biológicamente diferentes fármacos.

Así, en primer lugar, se procedió a realizar la encapsulación de dos fármacos anticancerígenos comerciales: 5-FU y OXA, con el objetivo de mejorar las propiedades de especificidad y selectividad de dichos fármacos, así como de evitar la rápida metabolización de dichos fármacos (**Figura 5**).

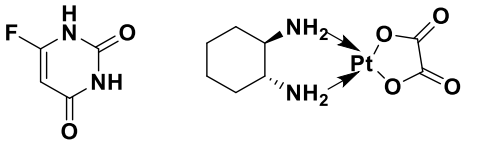

5-FU OXA

***Figura 5**. Estructura fármacos 5-FU y OXA.*

Así, la encapsulación de 5-FU se realizó en los siguientes nanosistemas: *p*NIPAM@, *p*NIPAM@Fe_3O_4-3BA y *p*NIPAM-co-AL@Fe_3O_4-AA. Mientras que OXA fue incluido en los nanosistemas: *p*NIPAM@ y *p*NIPAM@Fe_3O_4-3BA. Ambos fármacos fueron encapsulados en los nanosistemas a una temperatura de 20 ºC, a la que el polímero se encuentra en un estado expandido y las moléculas se incluyen dentro de este, en un periodo de 48 h.

Así, tras realizar el proceso de encapsulación se midió la eficiencia de encapsulamiento (EE %):

$$EE\ \% = \frac{D_L - D_F}{D_L} \cdot 100$$

Donde D_L es la concentración inicial de fármaco y D_F era la concentración de fármaco libre obtenida tras el proceso de encapsulación.

Así, la concentración de fármaco libre fue medida mediante espectroscopia UV-Vis, midiendo las muestras en un espectrofotómetro UV-Vis a longitudes de ondas de 257 y 248 nm, respectivamente para 5-FU y OXA (**tabla 1**).

Tabla 1. Encapsulación de 5-FU en distintas NPs

	Fármaco (mg)	*p*NIPAM NPs (mg)	EE (%)
1	5-FU (20)	*p*NIPAM@ (10)	36.3
2	5-FU (20)	*p*NIPAM@Fe_3O_4-3BA (10)	60.7
3	5-FU (3)	FITC-*p*NIPAM-co-AL-@Fe_3O_4-AA (6)	60
4	5-FU (6)	*p*NIPAM-co-AL@Fe_3O_4-AA (17)	65
5	OXA (10)	*p*NIPAM@(10)	38.5
6	OXA (10)	*p*NIPAM@Fe_3O_4-3BA (10)	77.5
7	OXA (10)	*p*NIPAM-co-AL@Fe_3O_4-AA (10)	73.5

En general, los EE% obtenidos para todos los nanosistemas fueron muy altos. Sin embargo, el valor más bajo fue el obtenido para las nanopartículas macizas *p*NIPAM@. Mientras que los mejores valores de EE% fueron obtenidos para los sistemas híbridos, *p*NIPAM@Fe_3O_4, debido al mayor tamaño de estos nanosistemas. Por otro lado, si son comparados los valores obtenidos entre los distintos fármacos, 5-FU presenta EE% más bajo que OXA. Este hecho se puede explicar porque la solubilidad del 5-FU es mayor en agua y tiende a quedarse disuelto en la fase acuosa.

Tras realizar el proceso de encapsulación, se decidió realizar un estudio de liberación in vitro empleando una membrana de diálisis, dicho estudio se llevó a cabo a distintas temperaturas: 4, 20 y 40 ºC. Observándose una liberación acumulada de 2.5 % a temperaturas de 4 y 20 ºC mientras que a 40 ºC la liberación acumulada del fármaco era del 42 % durante los primeros 60 minutos y 81 % tras 48 horas, demostrando que a la temperatura corporal el nanosistema liberaría el fármaco.

Una vez estudiada la encapsulación de dichos fármacos comerciales, se procedió a introducir el análogo de bengamida **1** en los siguientes nanosistemas: *p*NIPAM@, *p*NIPAM@Fe_3O_4-3BA, FITC-*p*NIPAM-co-AL@Fe_3O_4-AA. Sin embargo, el EE% no se midió por medio de

espectroscopia UV-Vis, debido a que no se detectó absorción de este compuesto, por lo que se decidió calcular dicho valor por medio de pesada del fármaco libre (**tabla 2**).

Tabla 2. Encapsulación de bengamida **1** en distintas NPs

Experiemento	bengamida (mg)	*p*NIPAM NPs (mg)	EE (%)
1	5	pNIPAM@ (10)	21
2	5	*p*NIPAM@Fe_3O_4-3BA (10)	28.3
3	5	FITC-*p*NIPAM-co-AL-@Fe_3O_4-AA (6)	32.1
4	5	*p*NIPAM-co-AL@Fe_3O_4-AA (17)	22

Desafortunadamente, los valores de EE % obtenidos fueron más bajos que los que se obtuvieron al encapsular 5-FU y OXA. Así, esto se puede explicar debido a que el tamaño molecular de la bengamida es alrededor del doble que el de dichos fármacos, siendo más difícil la inclusión de dichos fármacos en los nanosistemas.

A.

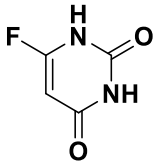

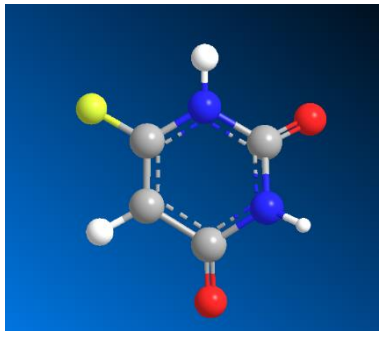

B.

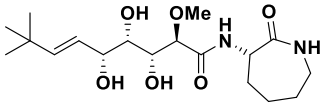

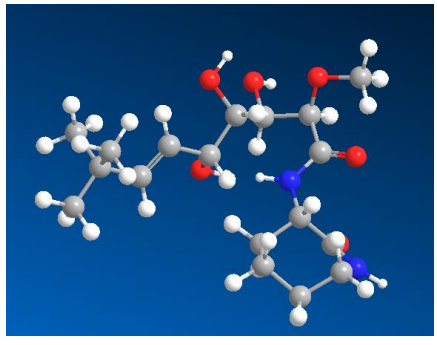

Figure 6. *Estructura 3D de (a) 5-FU and (b) bengamida* ***1****.*

Para mejorar estos resultados, el proceso de encapsulación se decidió llevar a más bajas temperaturas, intentando así que el tamaño del nano-sistema sea mayor (**tabla 3**).

Tabla 3. Encapsulación de bengamida **1** en distintas NPs

Experimento	Bengamida (mg)	*p*NIPAM NPs (mg)	EE (%)
1	5	*p*NIPAM@(10)	15
2	5	*p*NIPAM@Fe_3O_4-3BA (10)	32.2
3	5	FITC-*p*NIPAM-co-AL @Fe_3O_4-AA(6)	44
4	5	*p*NIPAM-co-AL@Fe_3O_4-AA (17)	26

Así, tal y como se puede observar en la tabla, los EE % aumentaron con respecto al realizar el experimento a 20 ºC. Por otro lado, los valores fueron mayores para las nanopartículas hibridas, ya que el tamaño de dichas nanopartículas es mayor y la inclusión de la bengamida **1**, es más fácil.

Por último, en esta tesis también se ha realizado la síntesis de otros compuestos de interés bioactivo derivados del tirosol e hidroxtirosol, dos compuestos fenólicos extraídos del aceite de oliva, con actividad anticancerígena. En concreto, los análogos preparados se recogen en la **figura 7**.

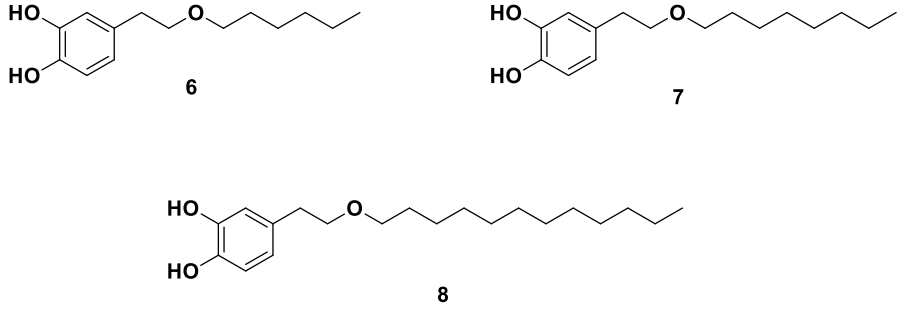

Figura 7. *Estructura molecular de los análogos de hidroxitirosol preparados durante la presente Tesis Doctoral.*

Tras la evaluación biológica de dichos análogos, realizando ensayos de MTT para calcular el IC_{50} de dichos fármacos, se obtuvieron valores parecidos para los análogos **6** y **7** (IC_{50} = 3.99 y 3.55). Mientras que, para el análogo **8** se obtuvo un valor más alto del esperado (IC_{50}= 7.55). Este resultado se asoció a la baja solubilidad en medio acuoso de dicho análogo, por lo que se decidió realizar la encapsulación de dicho compuesto en nanopartículas *p*NIPAM@, obteniéndose un porcentaje de eficiencia de encapsulación del 63 %.

En resumen, se ha estudiado la encapsulación de 5-FU y OXA en los nanosistemas previamente preparados, se ha incluido por primera vez un análogo de bengamida en dichos nanosistemas, estudiando la manera de incrementar la eficiencia de encapsulación y, por último, se ha realizado la síntesis de análogos del hidroxitirosol, se ha estudiado su actividad biológica y se ha incluido en los nanosistemas poliméricos de *p*NIPAM@.

De esta Tesis Doctoral se pueden extraer una serie de conclusiones:

- La evaluación biológica de los análogos **1** y **2** de las bengamidas ha demostrado el potencial de estos compuestos como nuevos fármacos contra el cáncer.
- El análogo de bengamida **2** ha sido preparado en la cantidad necesaria para realizar ensayos *in vivo*, siendo estos principalmente satisfactorios.
- Desde un punto de vista sintético, se han obtenido con éxito tres nuevos análogos de bengamidas (**3**, **4** y **5**).
- Se ha desarrollado una nueva metodología para análogos de peptidil bengamidas basada en la estrategia de síntesis en fase sólida, que proporciona métodos rápidos y efectivos para una nueva biblioteca de bengamidas.
- Se han preparado diferentes sistemas de nanopartículas poliméricas de *p*NIPAM@.

- Estos sistemas *p*NIPAM han sido co-polimerizadas con diferentes comonómeros (3-BA, AA y AL).
- Se han sintetizado nanopartículas magnéticas *p*NIPAM (*p*NIPAM@Fe_3O_4).
- Las nanopartículas *p*NIPAM-co-Al@Fe_3O_4 han sido marcadas con fluorescencia con isotiocianato de fluoresceína (FITC).
- Se han encapsulado fármacos comerciales (5-fluorouracilo y oxaliplatino) en diferentes sistemas *p*NIPAM y se ha estudiado su liberación en una membrana de diálisis.
- Desde un punto de vista biológico, estas nanoformulaciones mostraron una gran biocompatibilidad, lo que sugiere estos sistemas de nanopartículas como tratamiento contra el cáncer. Además, los híbridos de nanosistemas que contienen un núcleo magnético (*p*NIPAM@Fe_3O_4) podrían dirigirse directamente al tumor a través de un campo magnético externo evitando los efectos secundarios de la quimioterapia.
- El análogo de bengamida **1** ha sido encapsulada en diferentes nanosistemas *p*NIPAM@.
- Se han preparado otras moléculas bioactivas (análogos de hidroxi-tirosol) y encapsulado en nanopartículas de *p*NIPAM@.

ANNEXES.
NMR SPECTRA

Spectra 1: ^{1}H-NMR (400 MHz, $CDCl_3$) of compound **255**

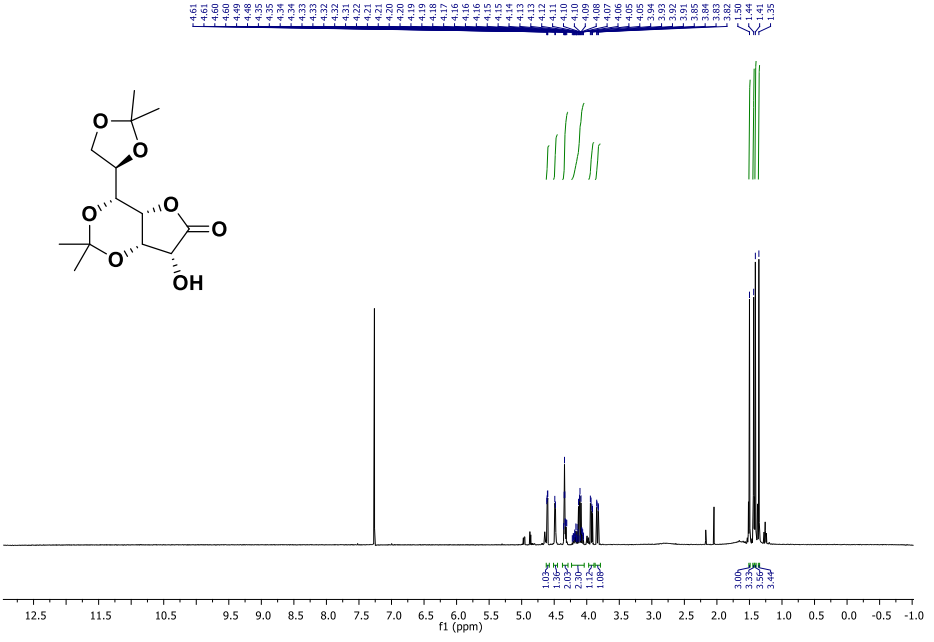

Spectra 2: ^{13}C-NMR (100 MHz, $CDCl_3$) of compound **255**

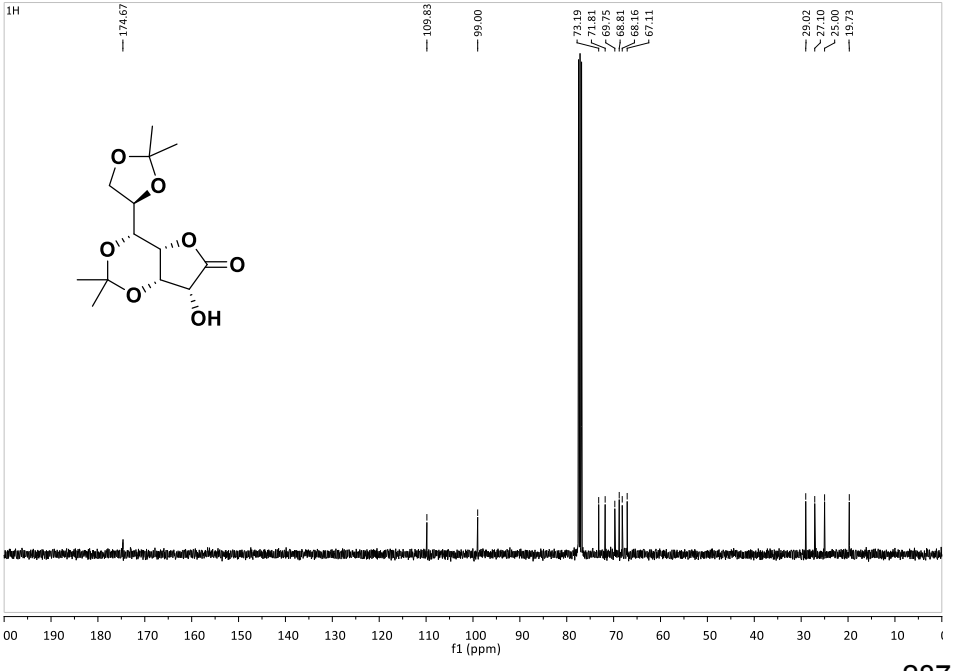

Spectra 3: ^{1}H-NMR (400 MHz, $CDCl_3$) of compound **256**

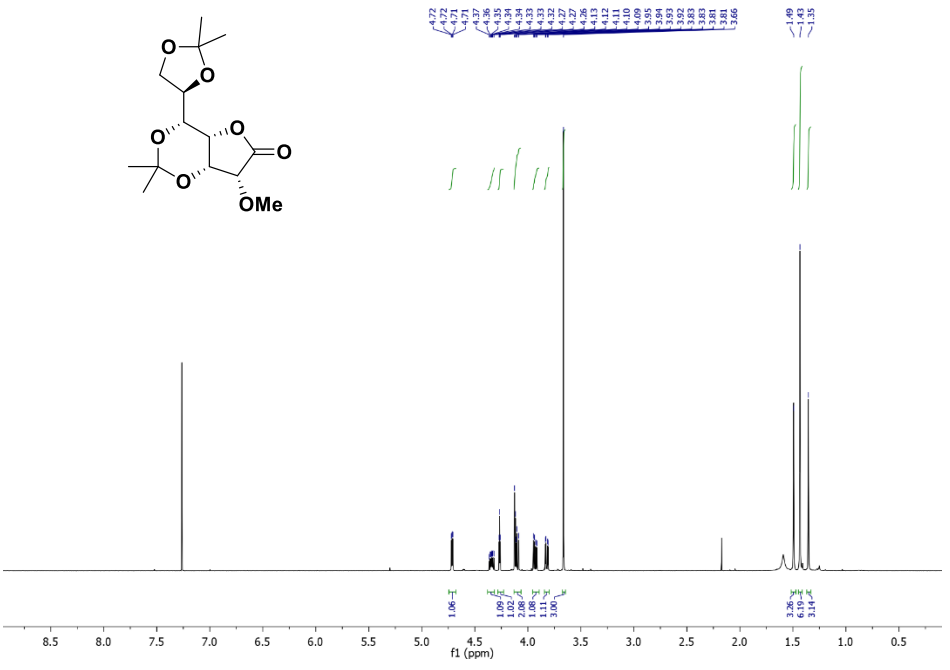

Spectra 4: ^{13}C-NMR (100 MHz, $CDCl_3$) of compound **256**

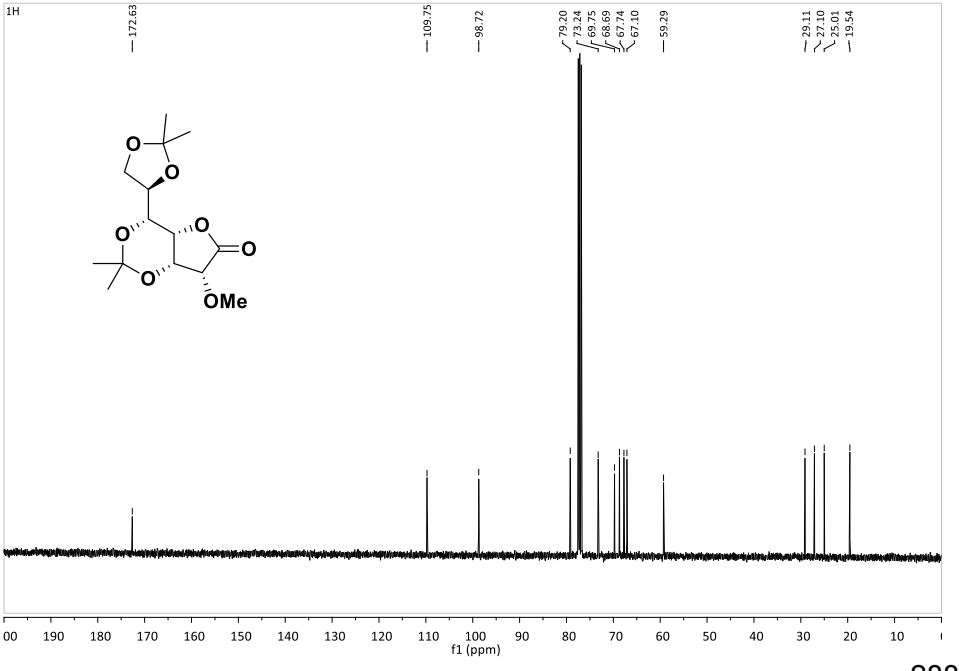

Spectra 5: ^{1}H-NMR (400 MHz, MeOD) of compound **257**

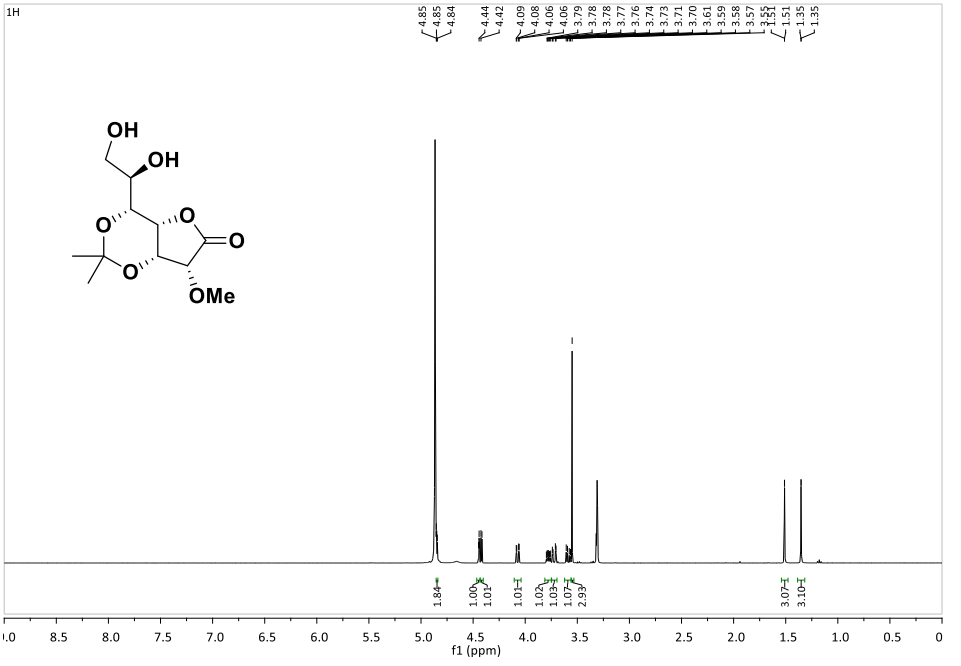

Spectra 6: ^{13}C-NMR (100 MHz, MeOD) of compound **257**

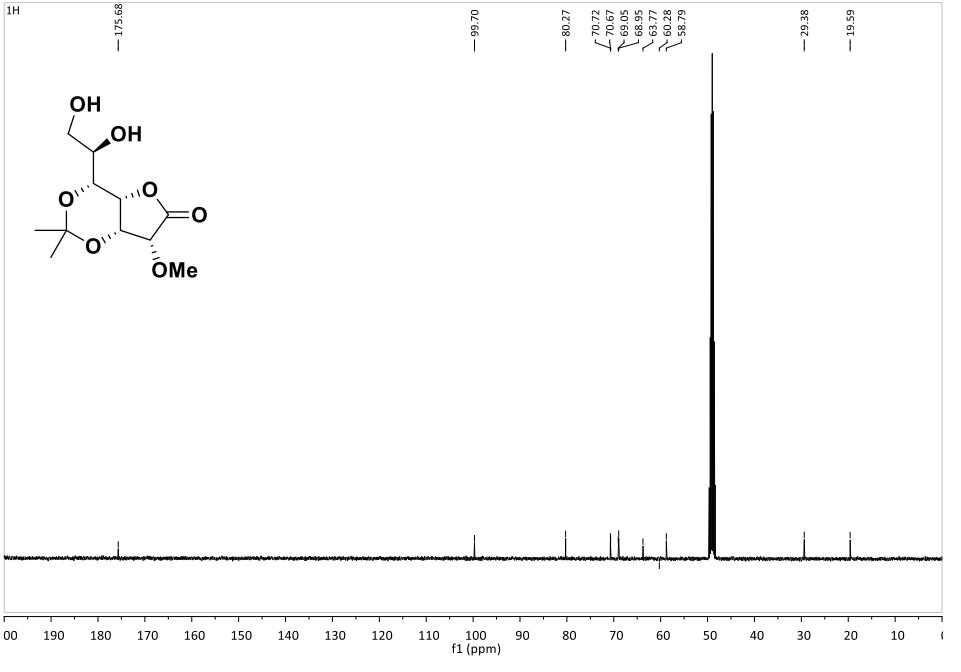

Spectra 7: ^{1}H-NMR (400 MHz, $CDCl_3$) of compound **259**

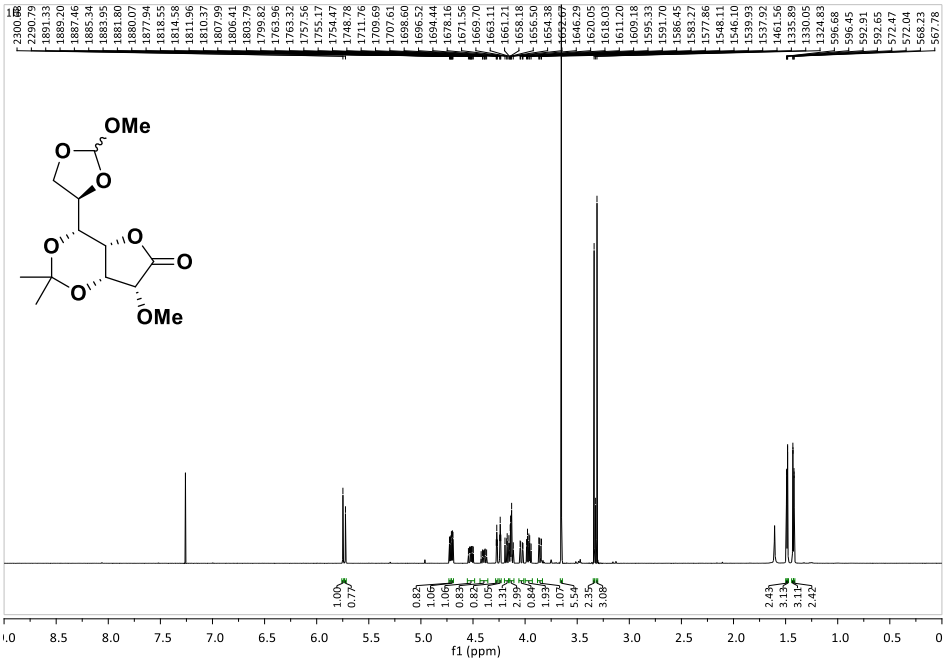

Spectra 8: ^{13}C-NMR (100 MHz, $CDCl_3$) of compound **259**

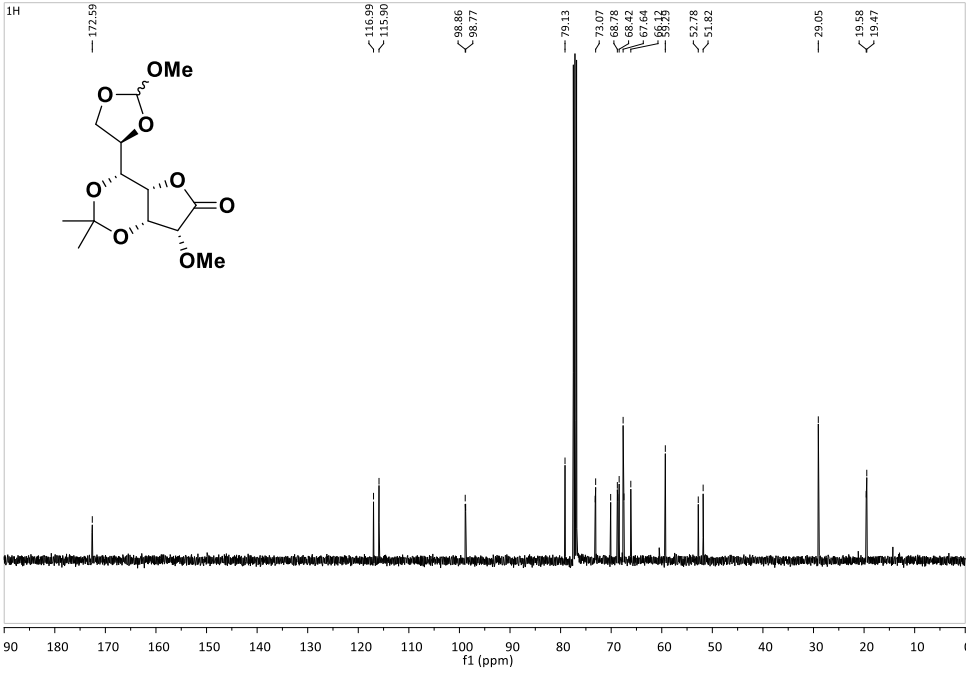

Spectra 9: ^{1}H-NMR (400 MHz, $CDCl_3$) of compound **254**

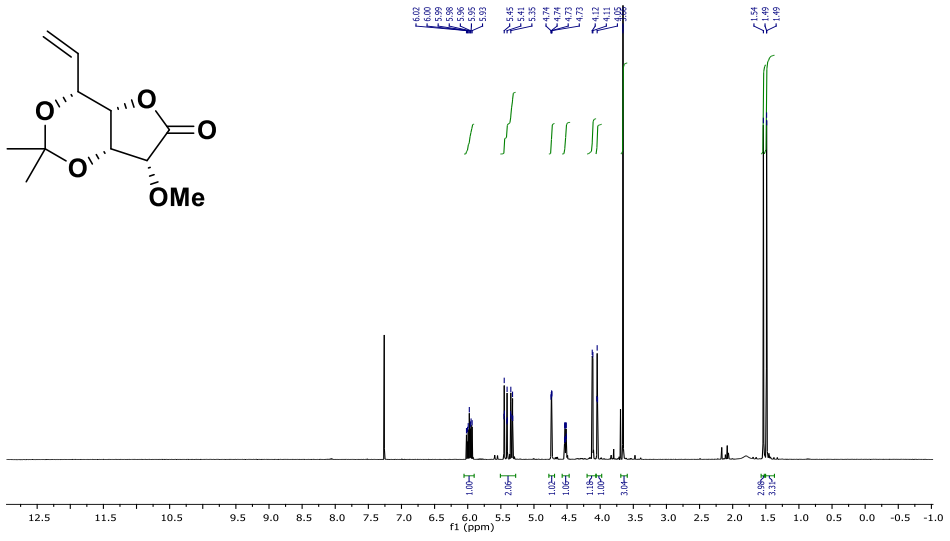

Spectra 10: ^{13}C-NMR (100 MHz, $CDCl_3$) of compound **259**

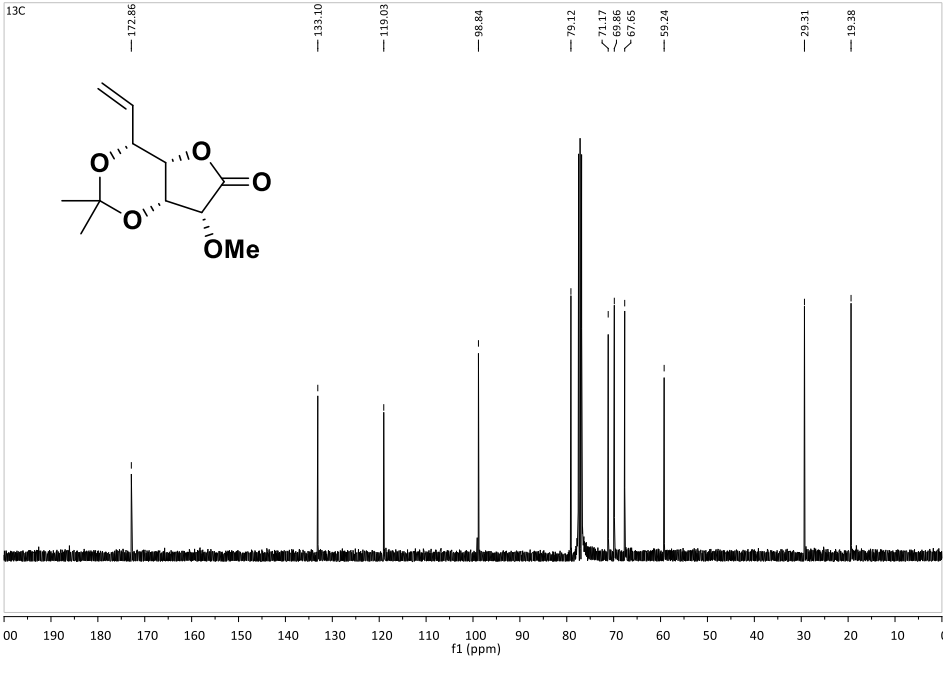

Spectra 11: ^{1}H-NMR (400 MHz, $CDCl_3$) of compound **90**

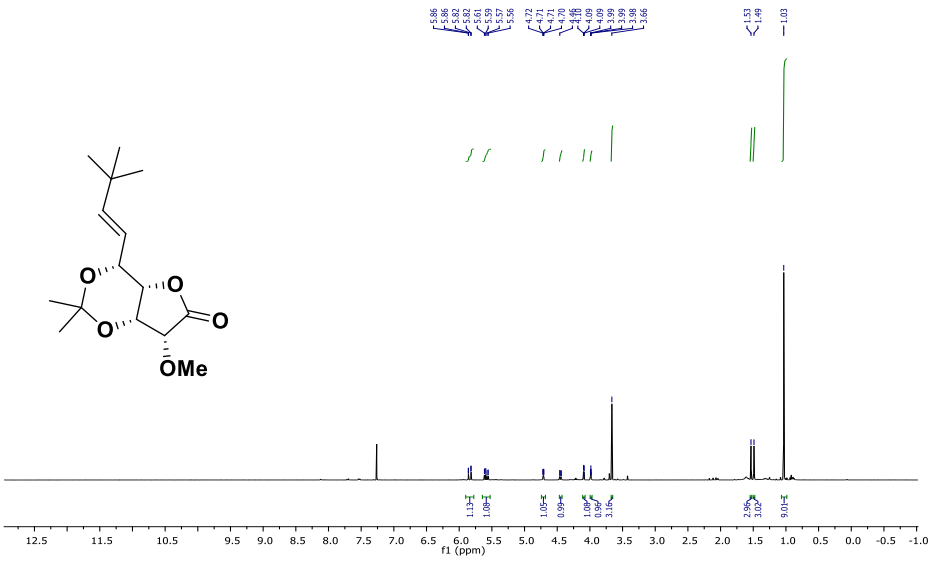

Spectra 12: ^{13}C-NMR (100 MHz, $CDCl_3$) of compound **90**

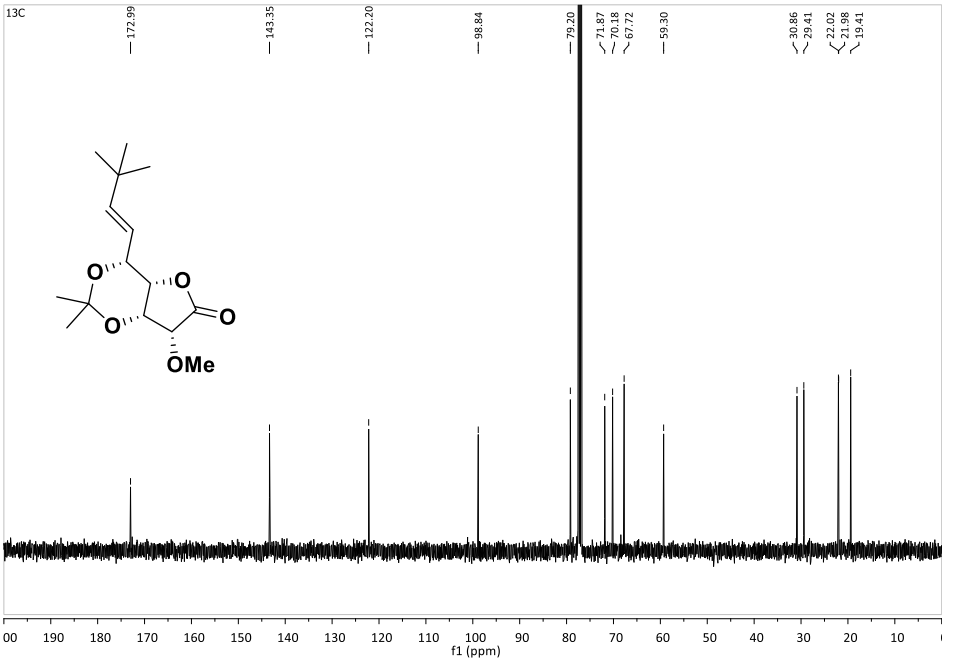

Spectra 13: ^{1}H-NMR (400 MHz, $CDCl_3$) of compound **261**

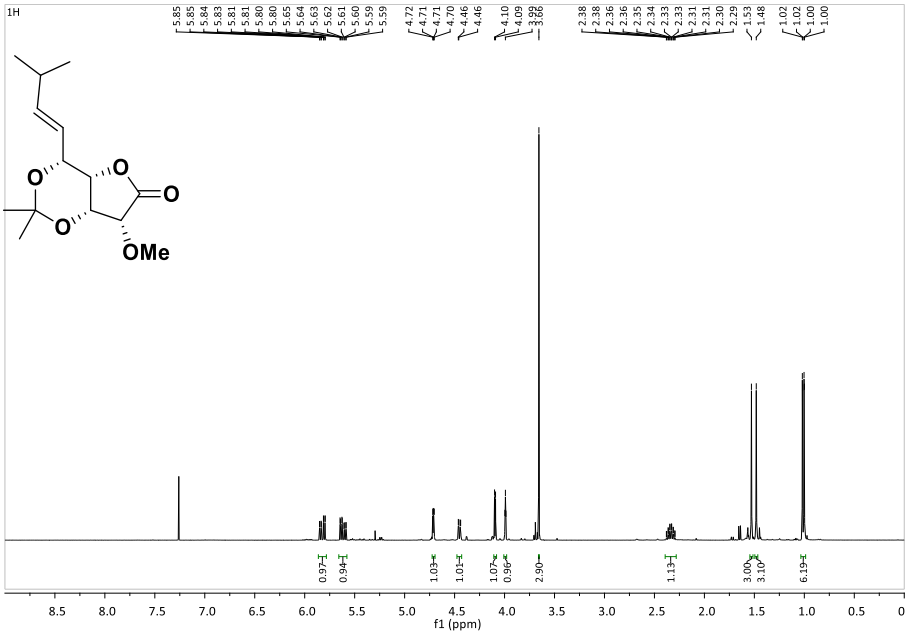

Spectra 14: ^{1}H-NMR (400 MHz, $CDCl_3$) of compound **262**

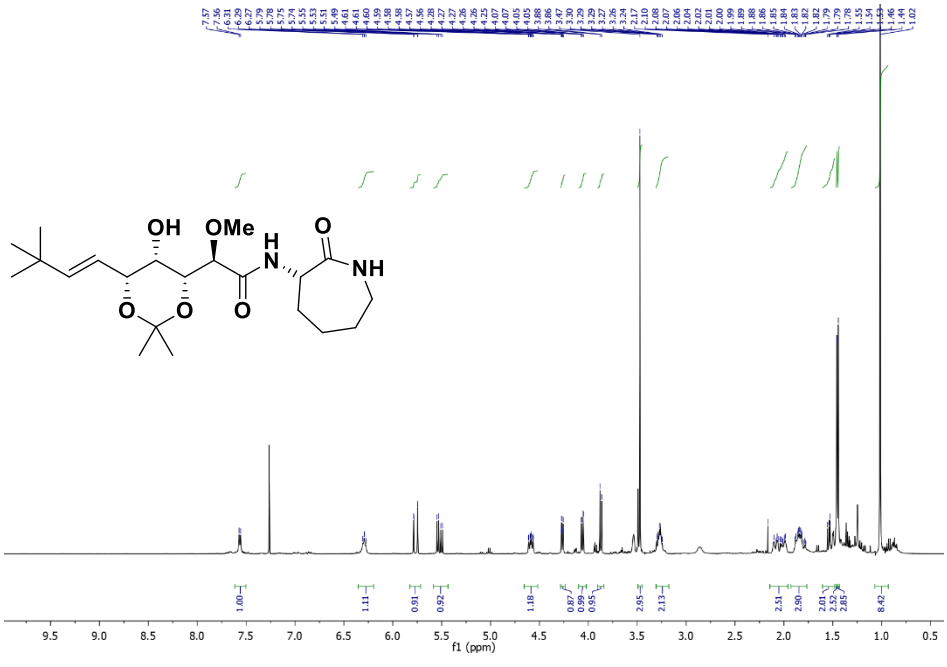

Spectra 15: ^{1}H-NMR (400 MHz, $CDCl_3$) of compound **172**

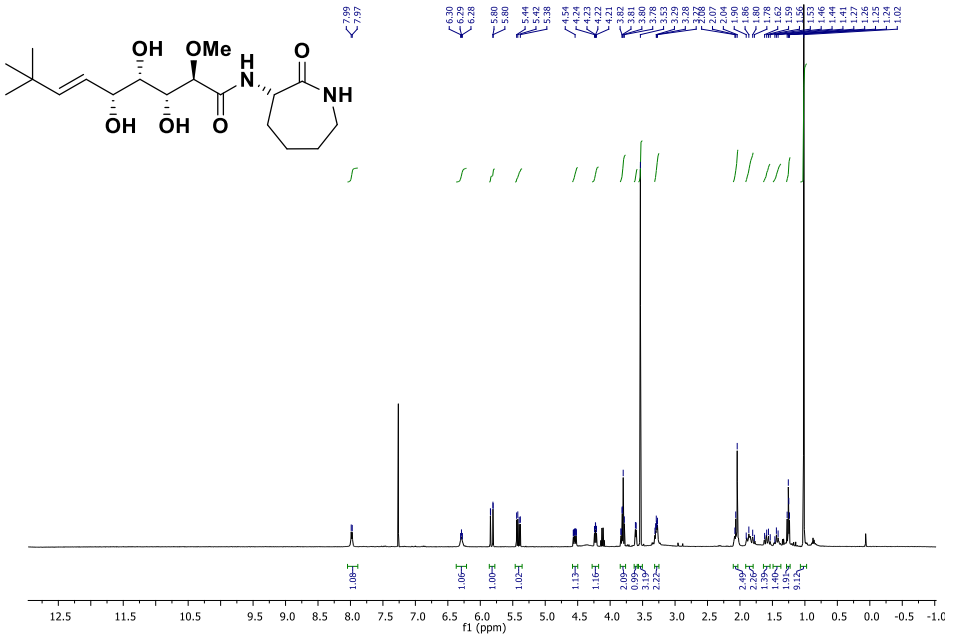

Spectra 16: ^{13}C-NMR (100 MHz, $CDCl_3$) of compound **172**

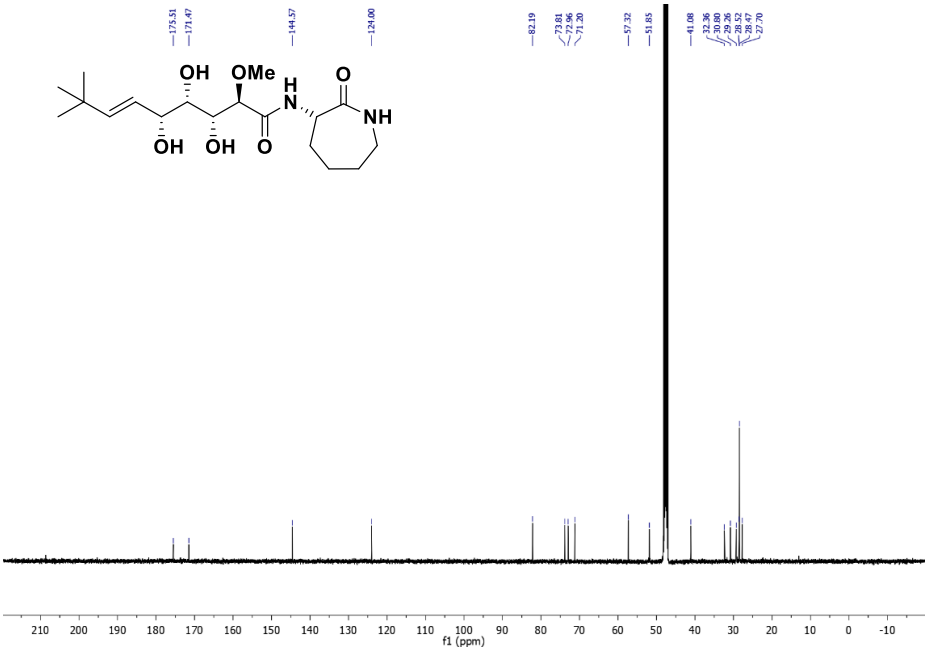

Spectra 17: ^{1}H-NMR (400 MHz, $CDCl_3$) of compound **266**

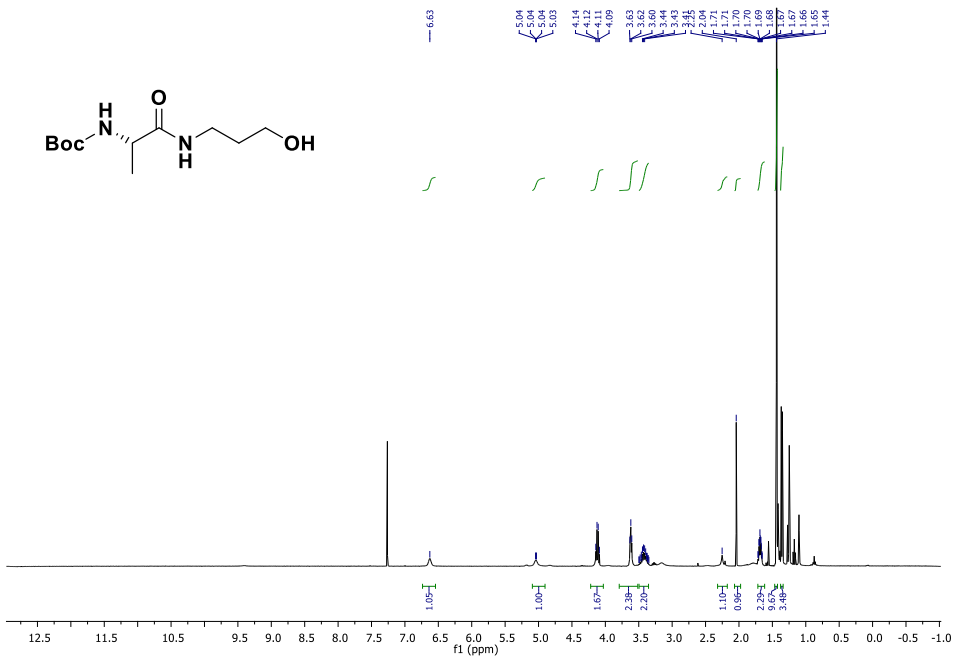

Spectra 18: ^{1}H-NMR (400 MHz, $CDCl_3$) of compound **266**

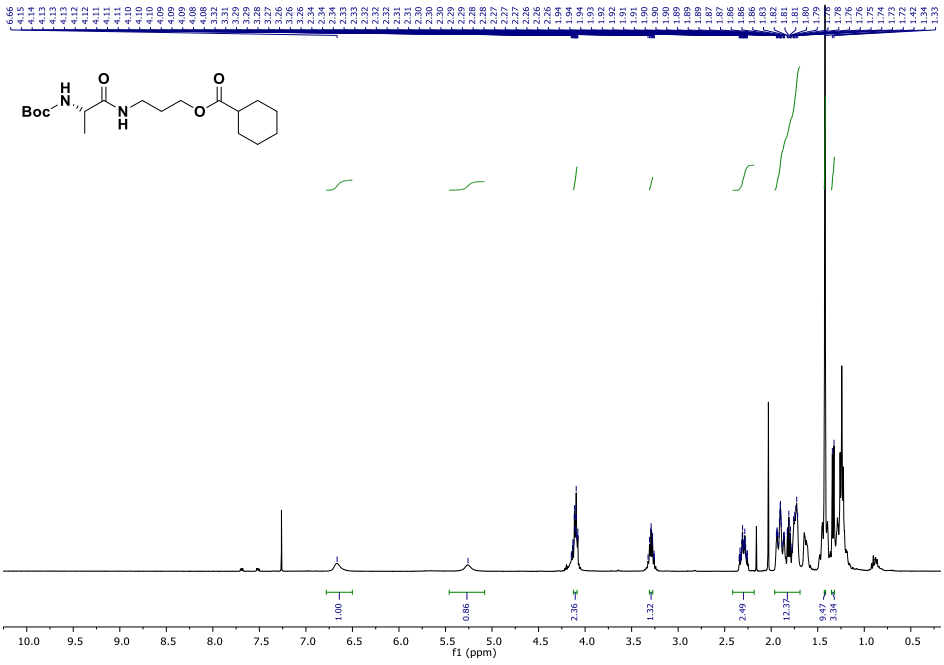

Spectra 13: ^{13}C-NMR (100 MHz, $CDCl_3$) of compound **261**

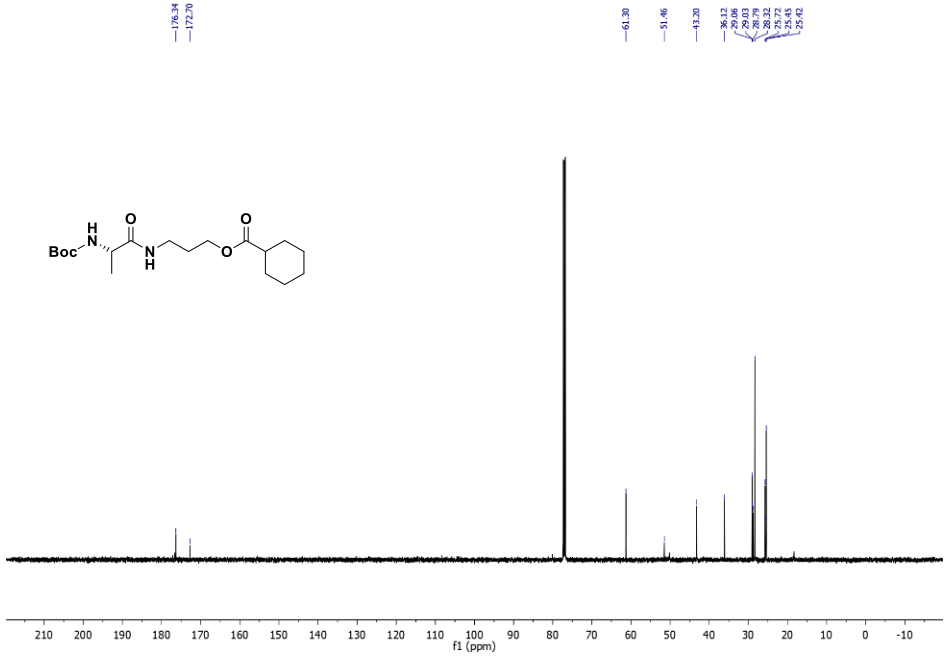

Spectra 14: ^{1}H-NMR (400 MHz, $CDCl_3$) of compound **268**

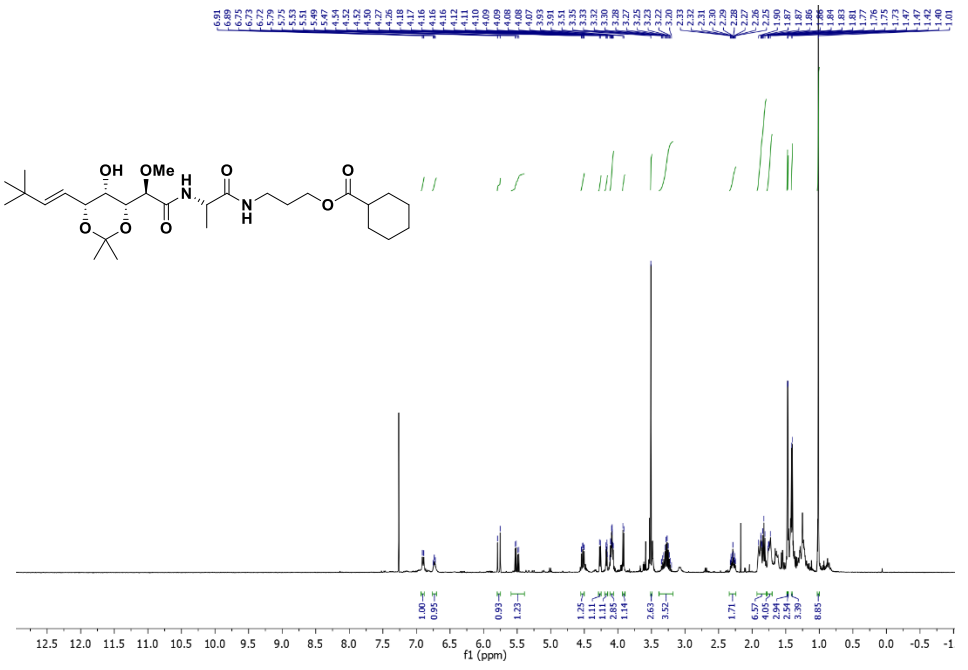

Spectra 15: ^{13}C-NMR (400 MHz, $CDCl_3$) of compound **268**

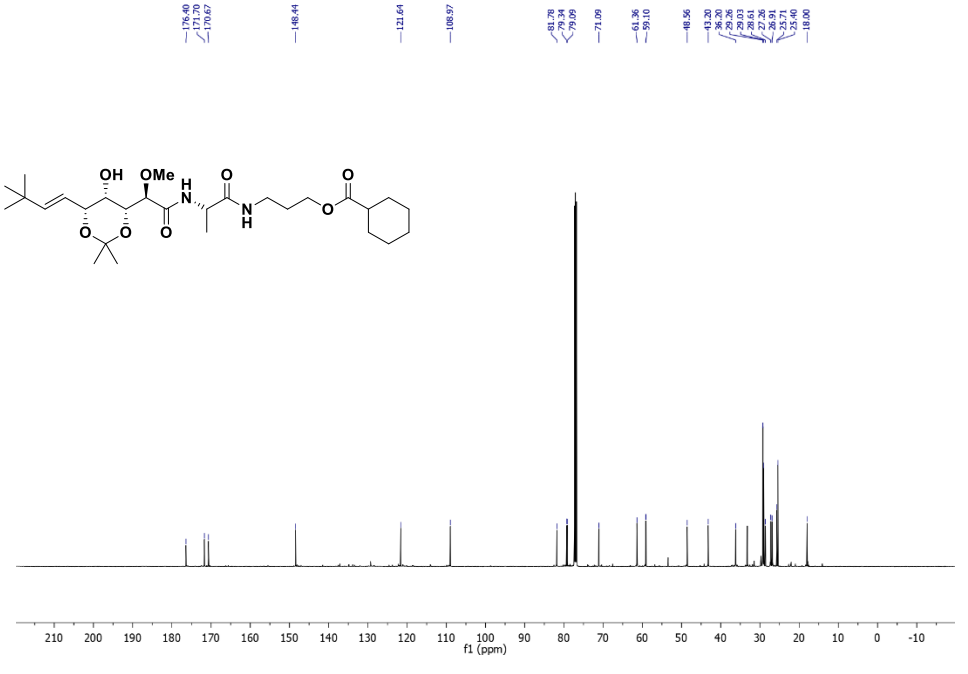

Spectra 16: ^{1}H-NMR (400 MHz, $CDCl_3$) of compound **145**

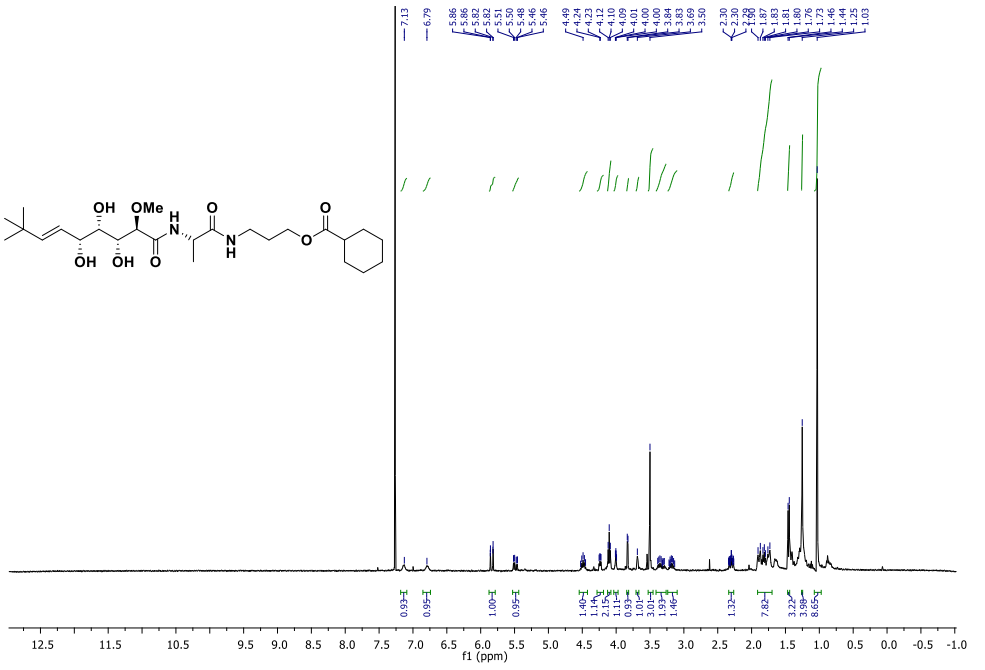

Spectra 17: ^{13}C-NMR (100 MHz, $CDCl_3$) of compound **268**

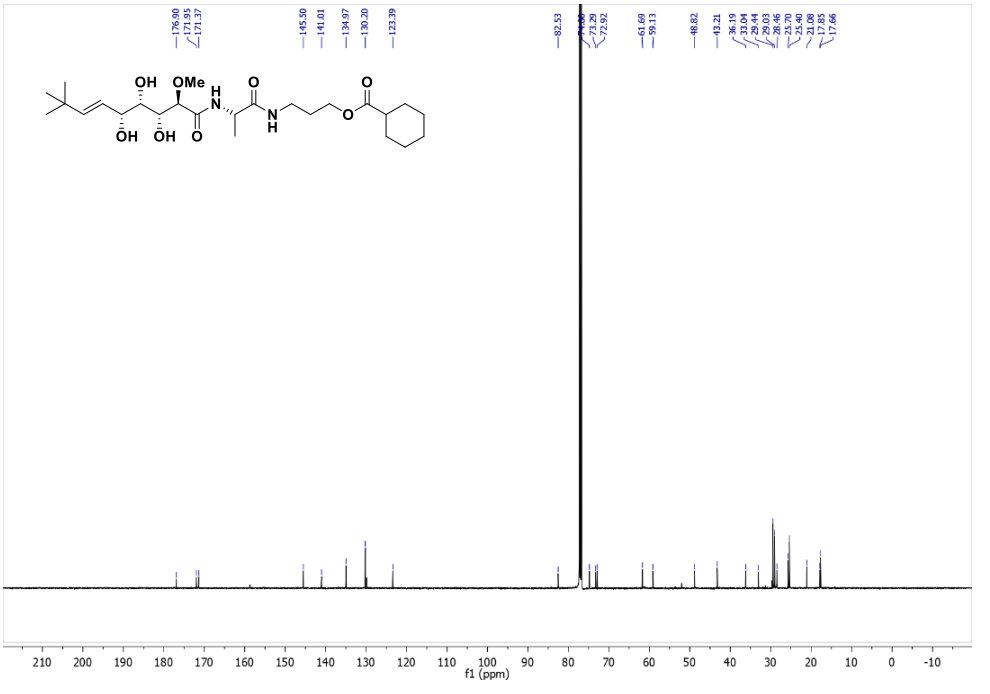

Spectra 18: ^{1}H-NMR (400 MHz, $CDCl_3$) of compound **271**

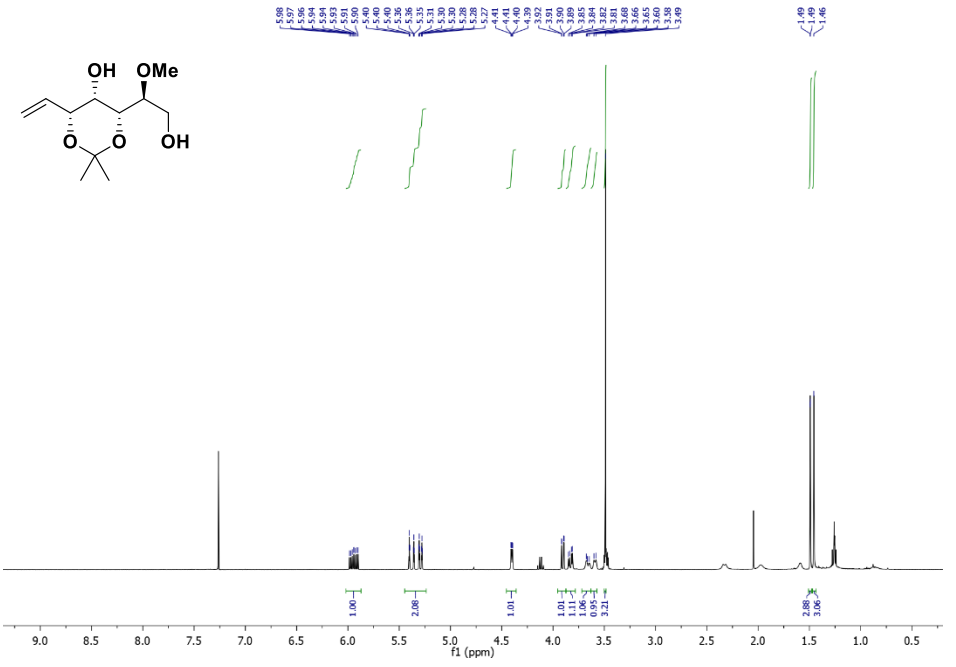

Spectra 19: ^{13}C-NMR (100 MHz, $CDCl_3$) of compound **271**

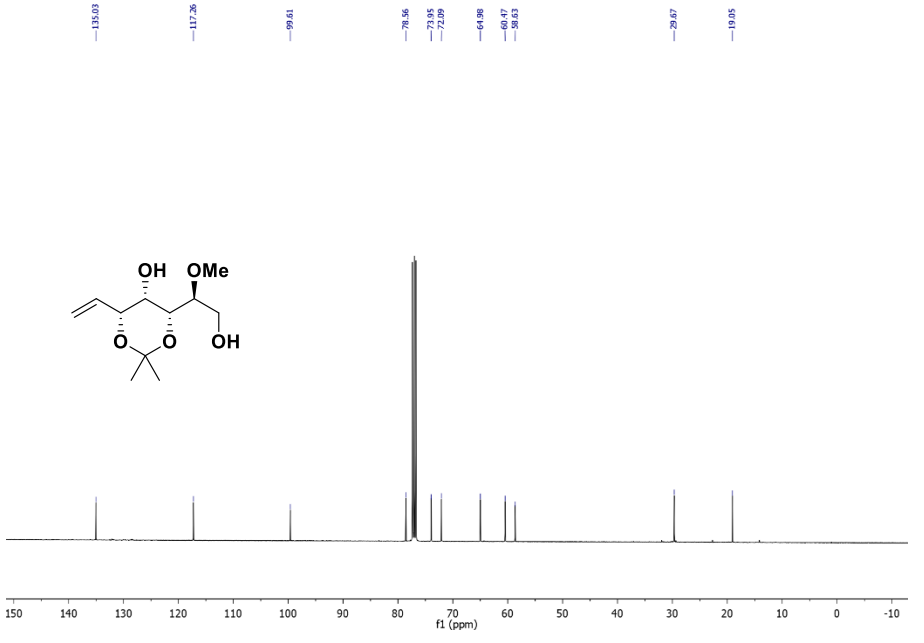

Spectra 20: ^{1}H-NMR (500 MHz, $CDCl_3$) of compound **274**

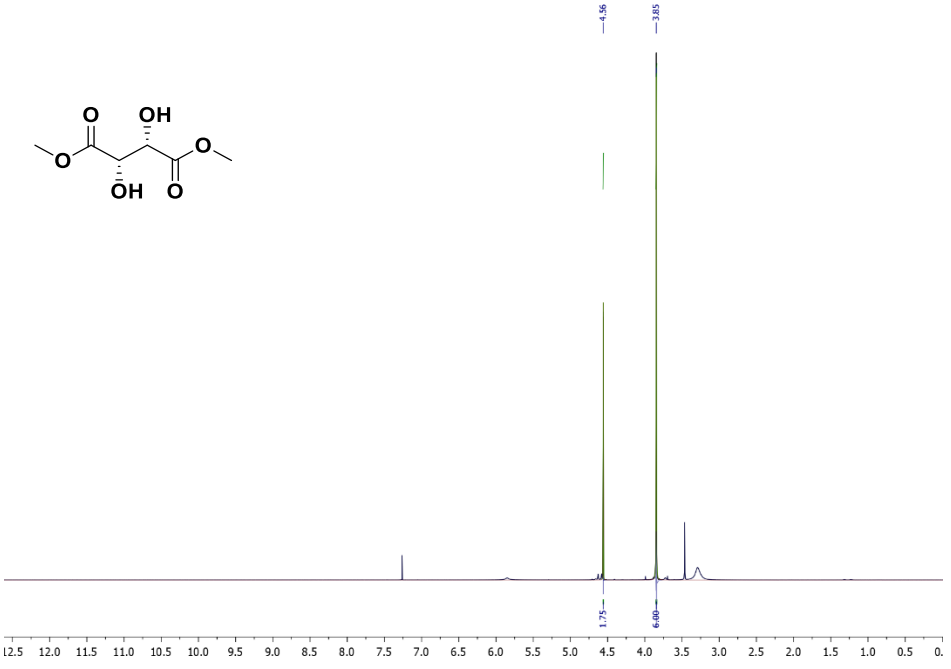

Spectra 21: ^{1}H-NMR (500 MHz, $CDCl_3$) of compound **275**

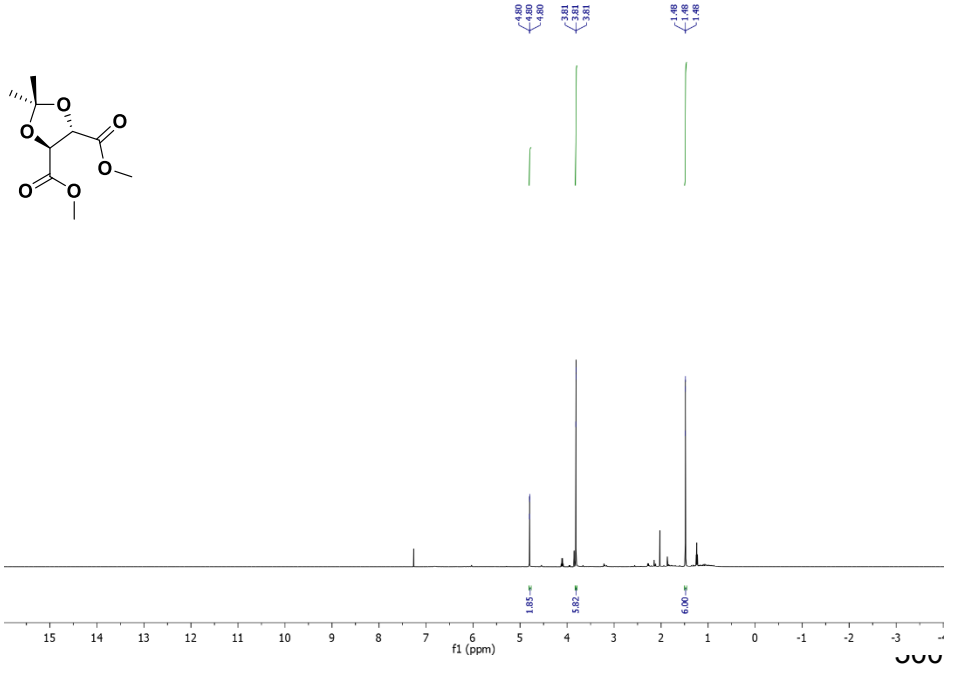

Spectra 22: ^{1}H-NMR (500 MHz, $CDCl_3$) of compound **276**

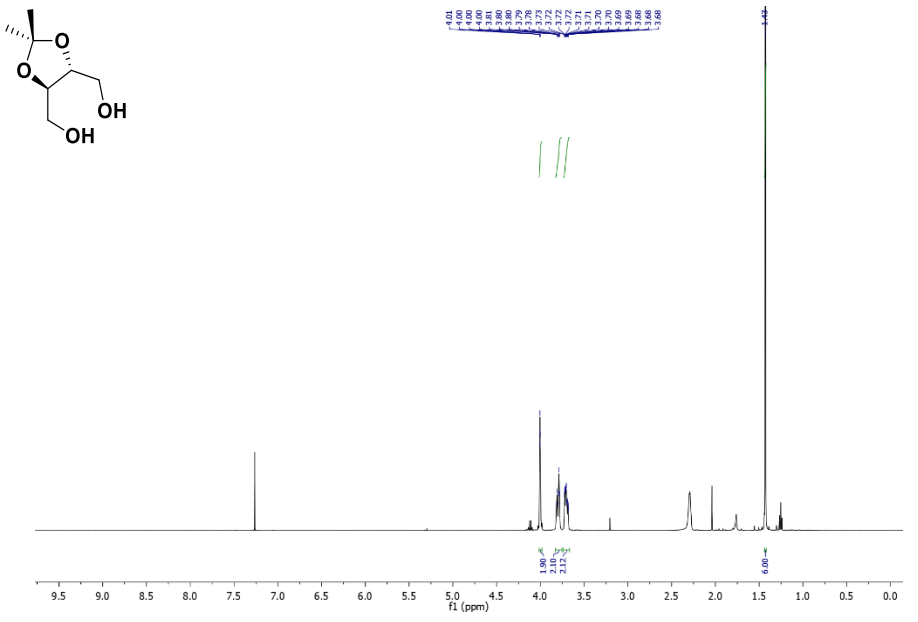

Spectra 23: ^{1}H-NMR (500 MHz, $CDCl_3$) of compound **277**

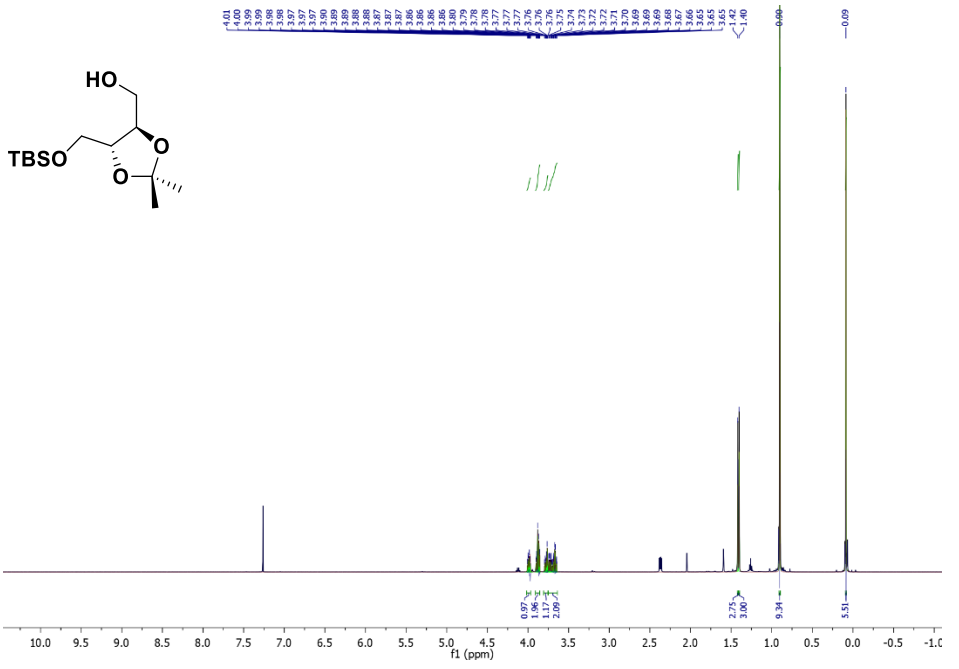

Spectra 24: ^{13}C-NMR (125 MHz, $CDCl_3$) of compound **277**

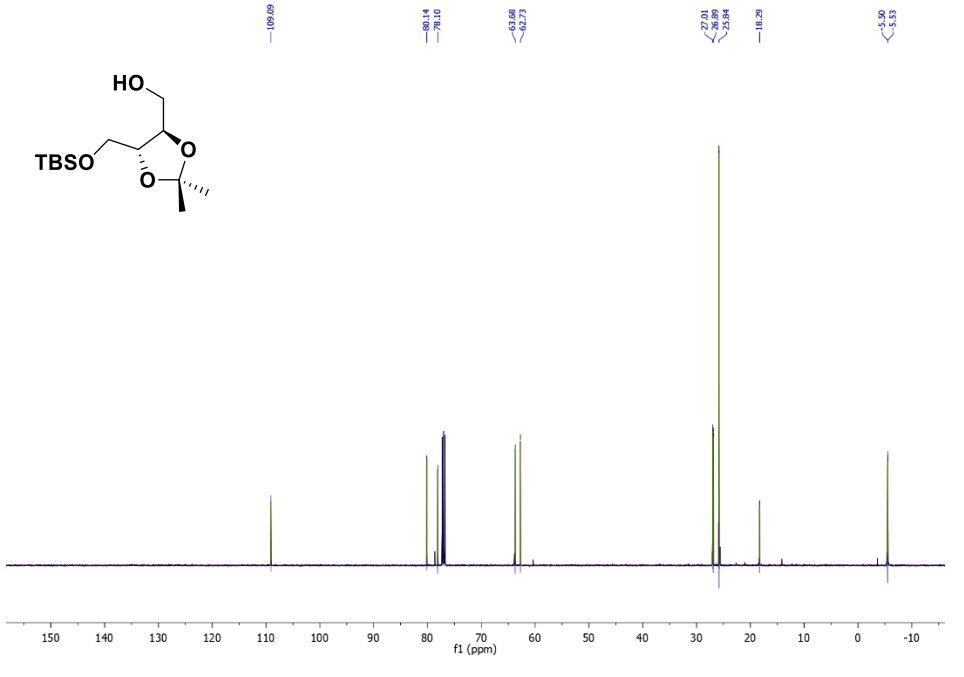

Spectra 25: ^{1}H-NMR (500 MHz, $CDCl_3$) of compound **278**

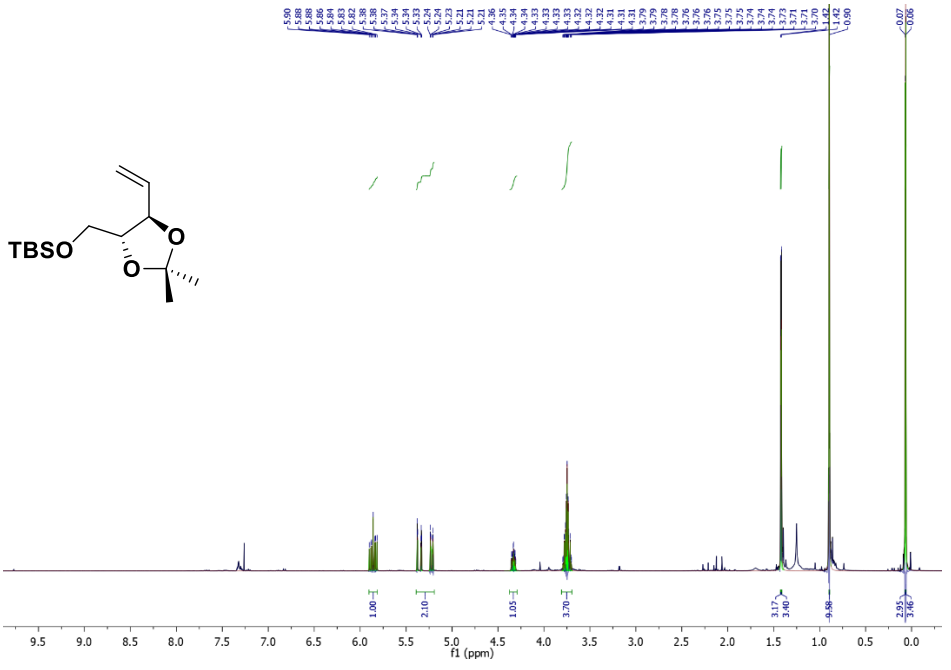

Spectra 26: ^{1}H-NMR (500 MHz, $CDCl_3$) of compound **280**

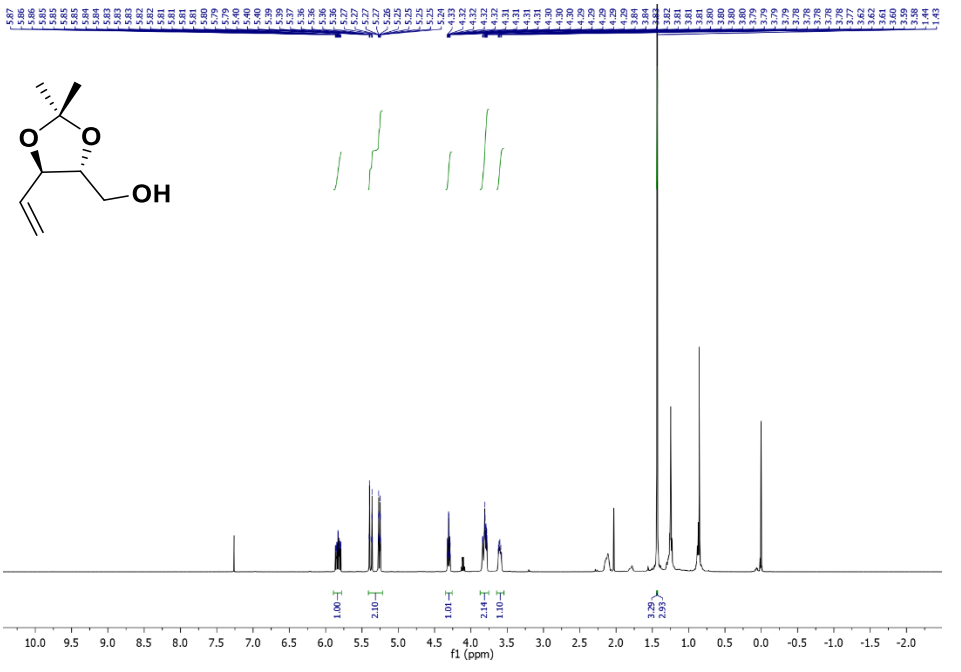

Spectra 27: ^{13}C-NMR (100 MHz, $CDCl_3$) of compound **280**

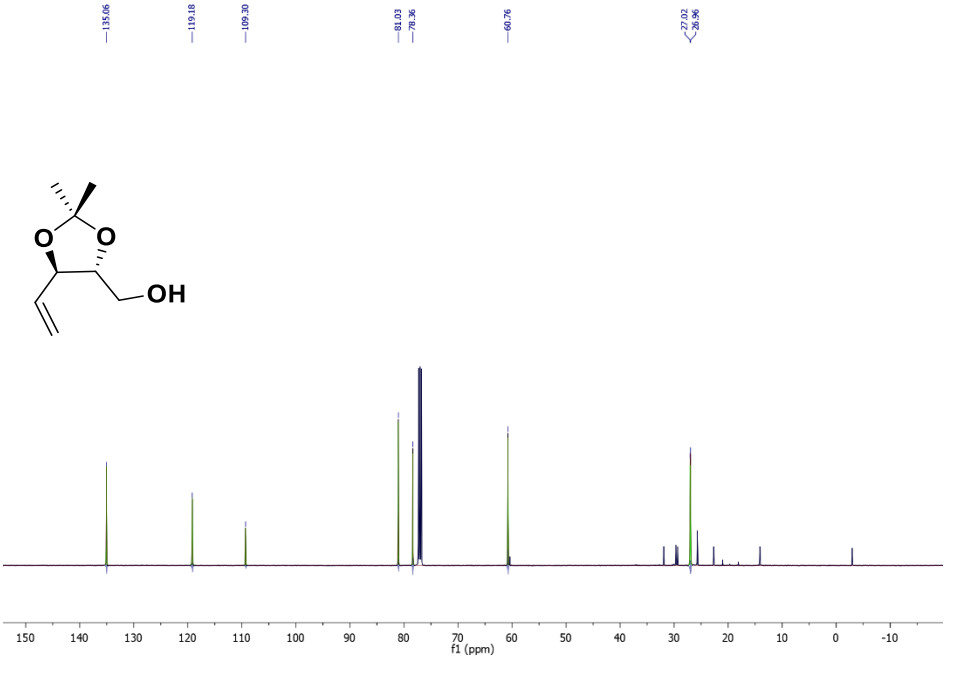

Spectra 28: ^{1}H-NMR (500 MHz, $CDCl_3$) of compound **281**

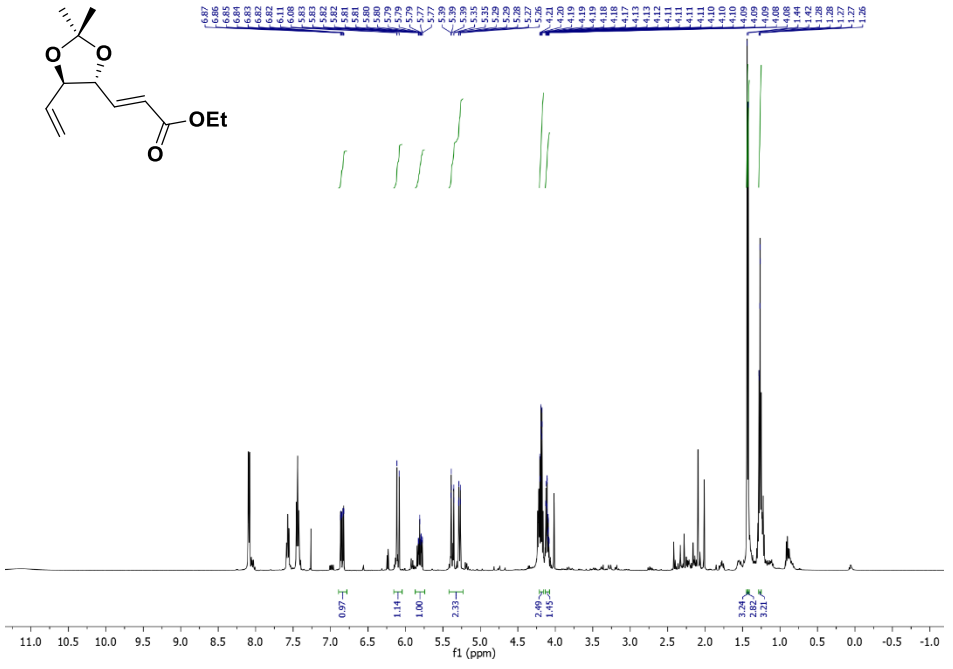

Spectra 29: ^{13}C-NMR (125 MHz, $CDCl_3$) of compound **281**

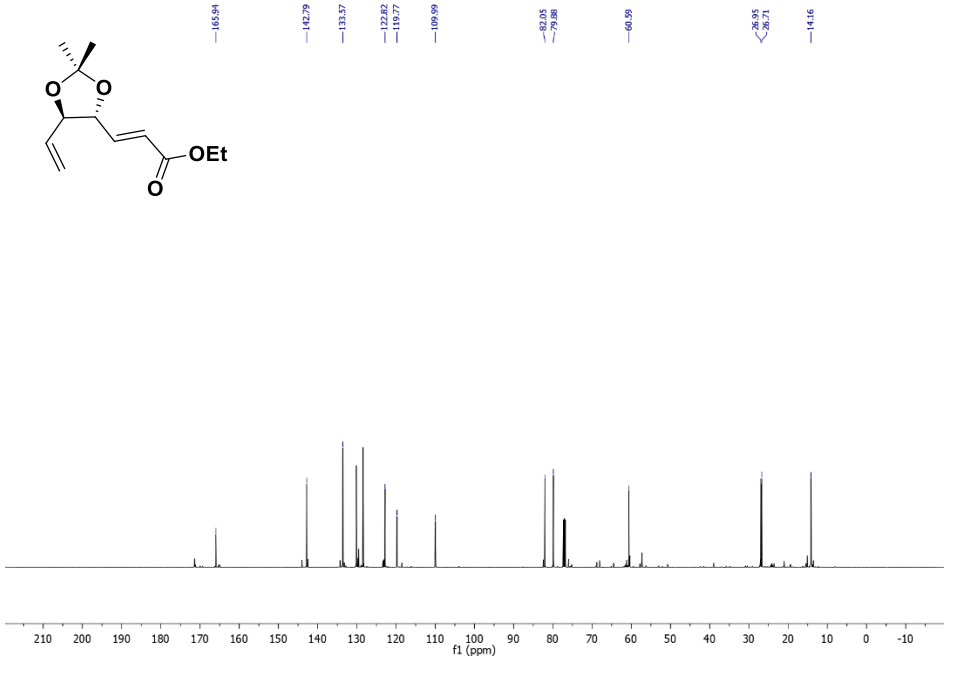

Spectra 30: ^{1}H-NMR (500 MHz, $CDCl_3$) of compound **282**

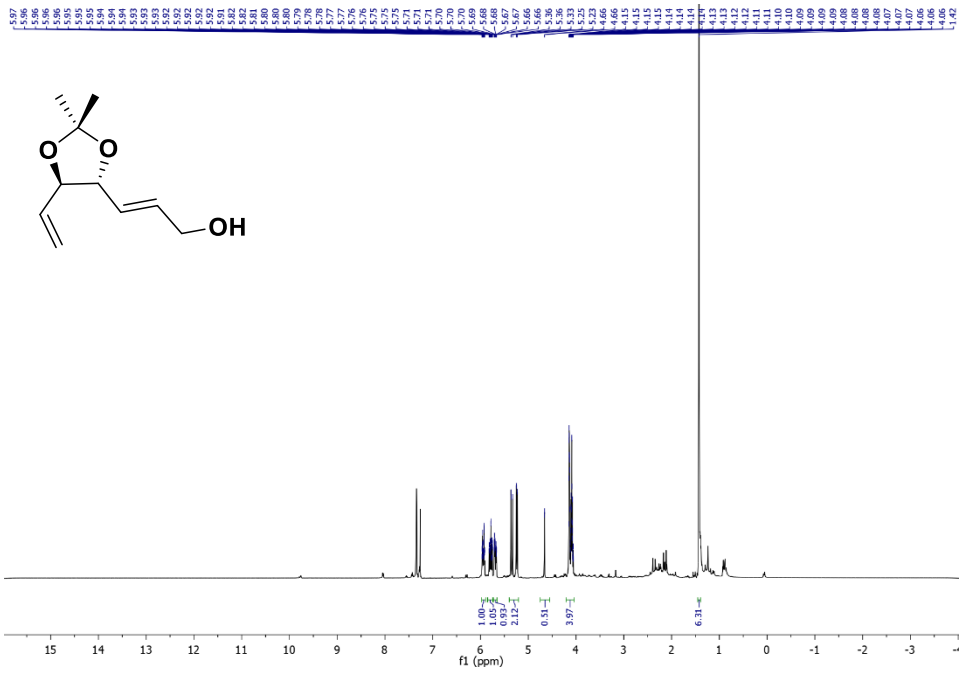

Spectra 31: ^{13}C-NMR (125 MHz, $CDCl_3$) of compound **282**

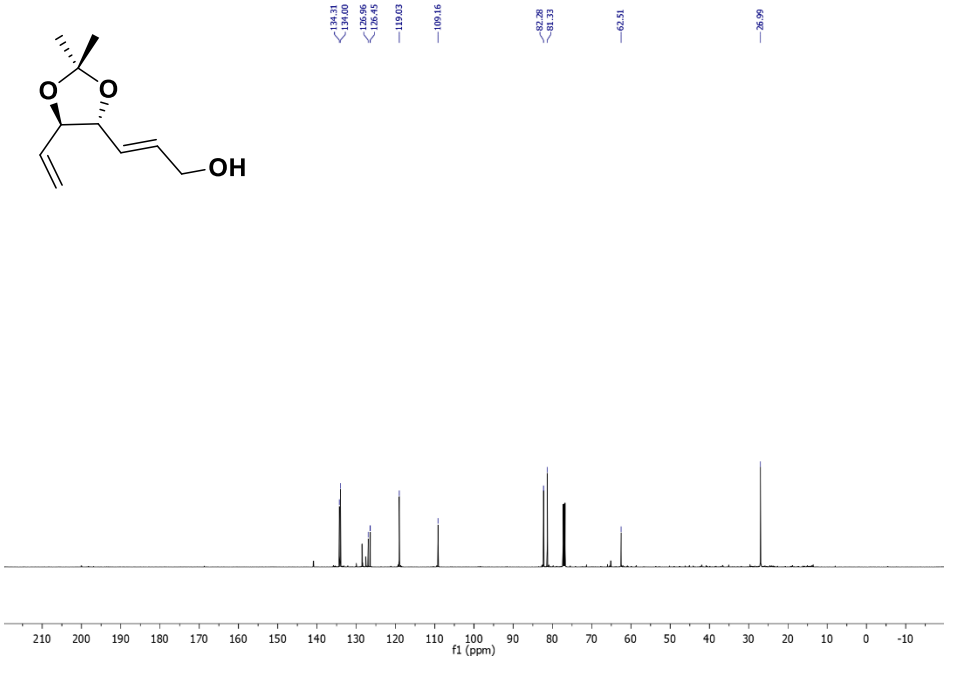

Spectra 32: ^{1}H-NMR (500 MHz, $CDCl_3$) of compound **73**

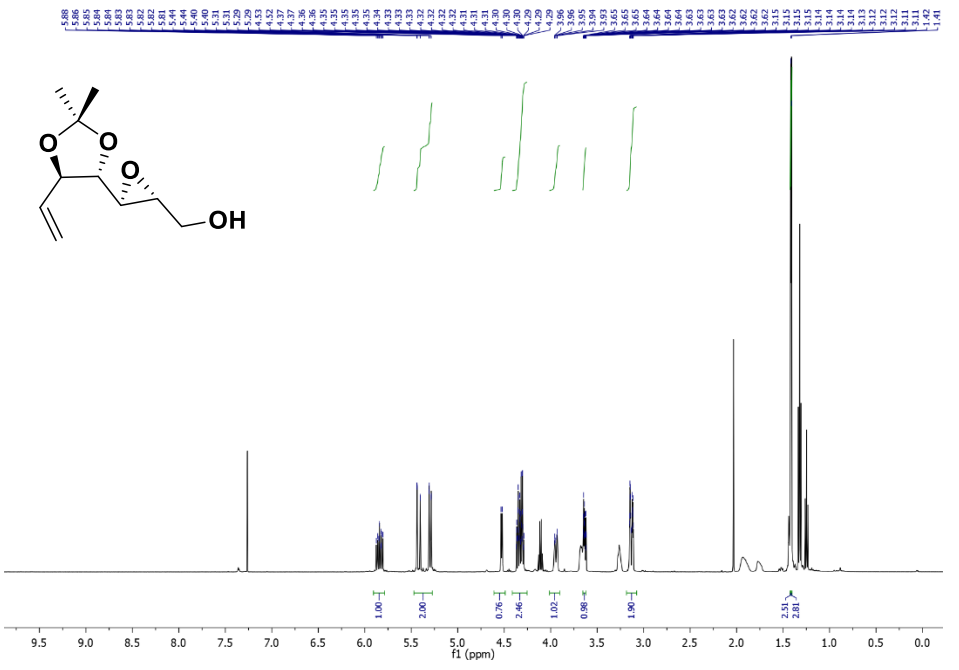

Spectra 33: ^{13}C-NMR (125 MHz, $CDCl_3$) of compound **73**

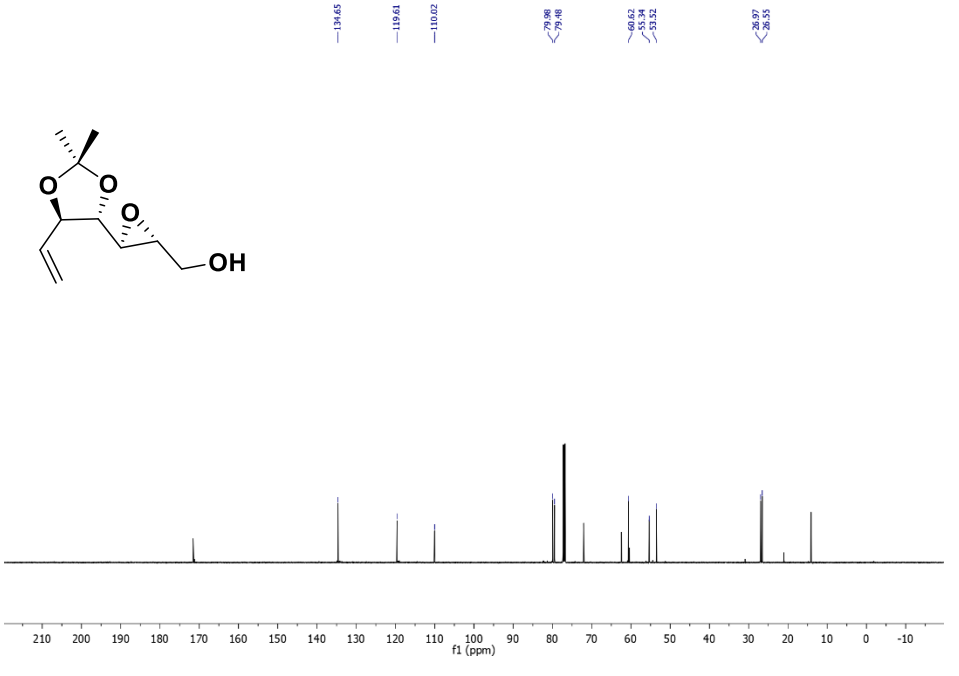

Spectra 34: ^{1}H-NMR (500 MHz, $CDCl_3$) of compound **283**

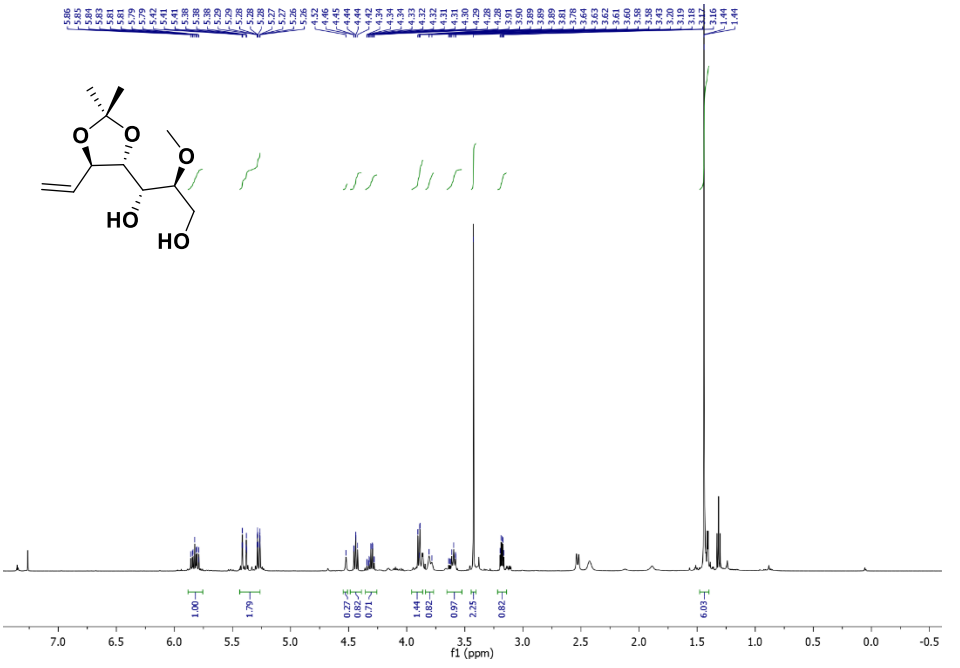

Spectra 35: ^{13}C-NMR (125 MHz, $CDCl_3$) of compound **283**

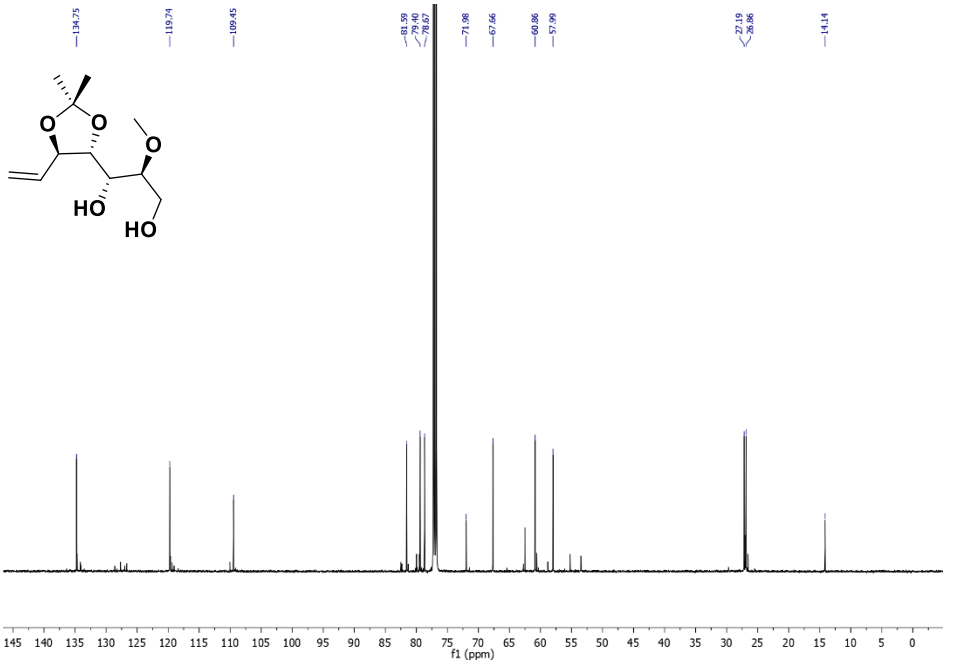

Spectra 35: ^{1}H-NMR (500 MHz, $CDCl_3$) of compound **284**

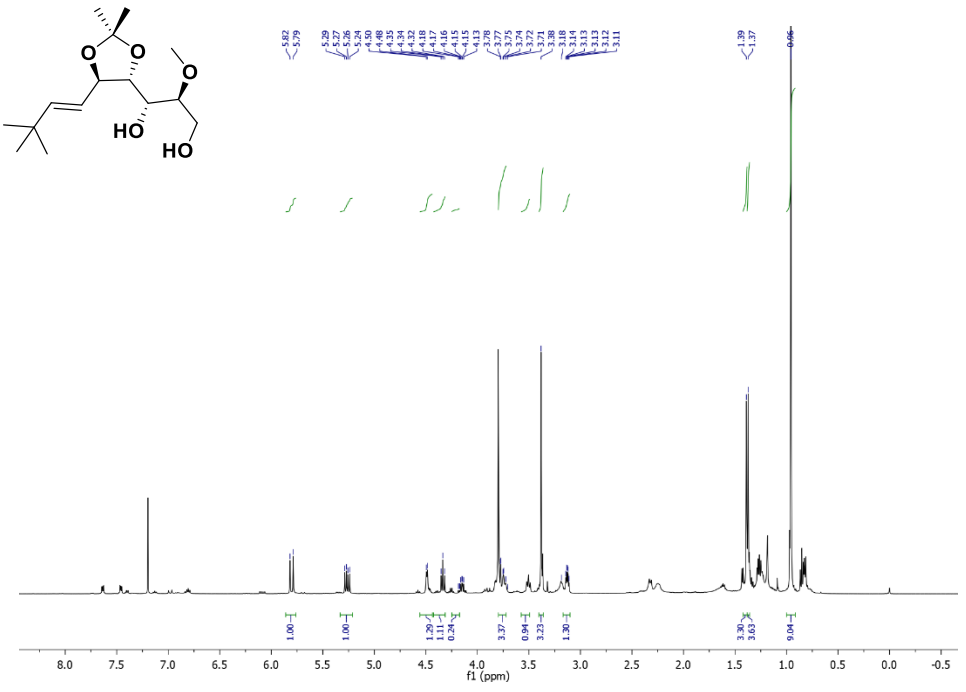

Spectra 36: ^{1}H-NMR (500 MHz, $CDCl_3$) of compound **286**

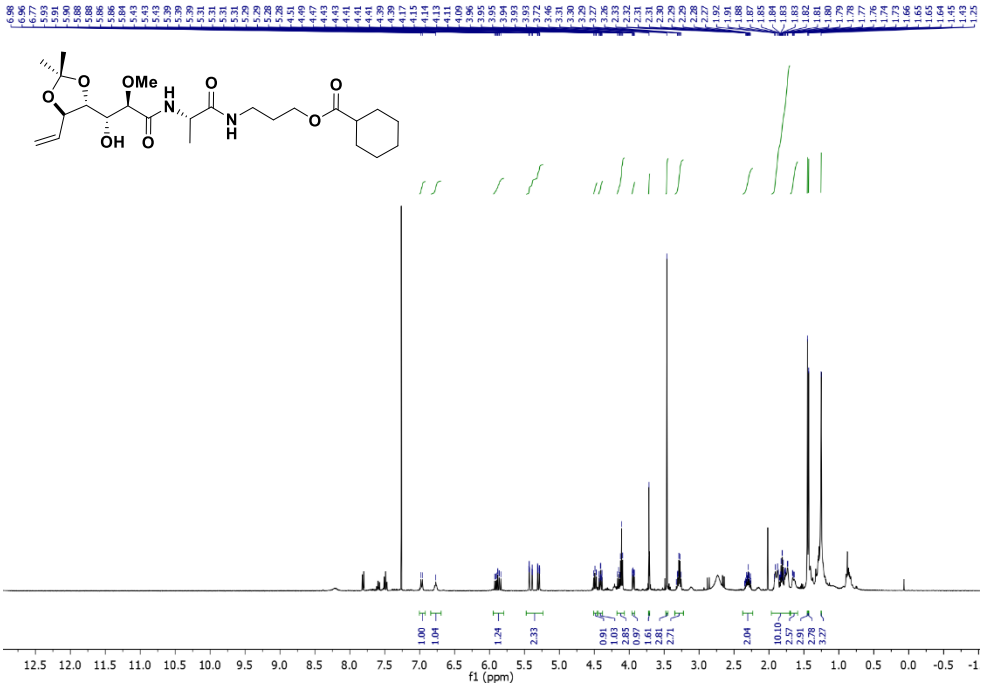

Spectra 37: ^{13}C-NMR (125 MHz, $CDCl_3$) of compound **286**

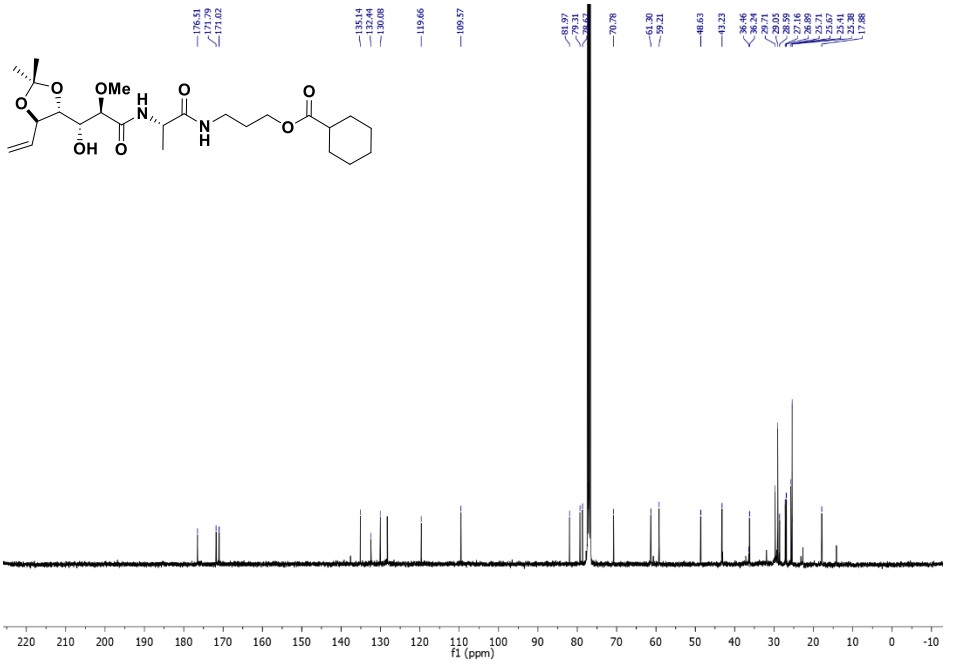

Spectra 38: ^{1}H-NMR (500 MHz, $CDCl_3$) of compound **288**

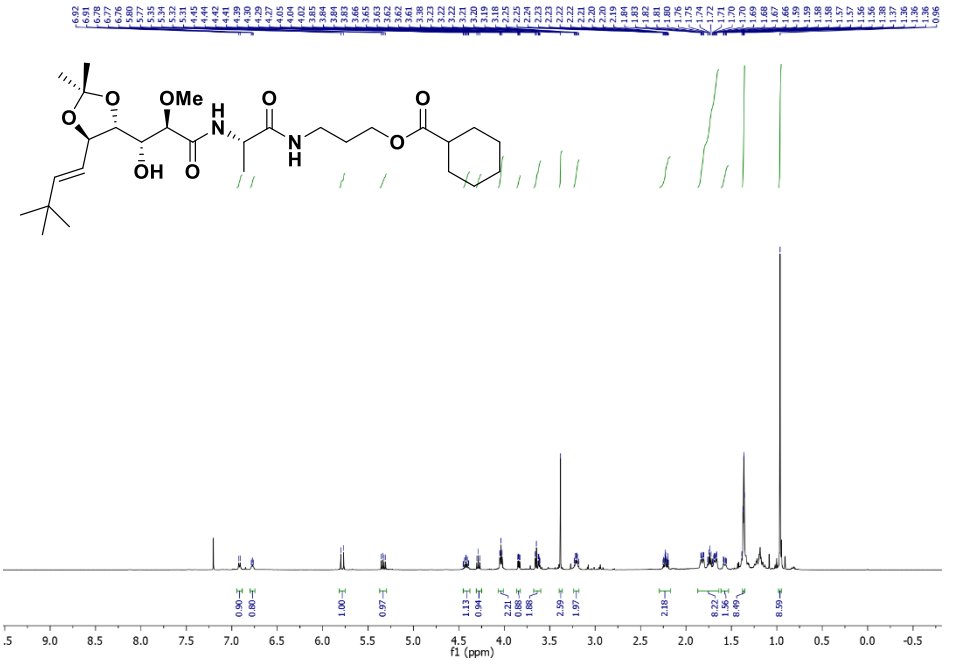

Spectra 39: ^{13}C-NMR (125 MHz, $CDCl_3$) of compound **288**

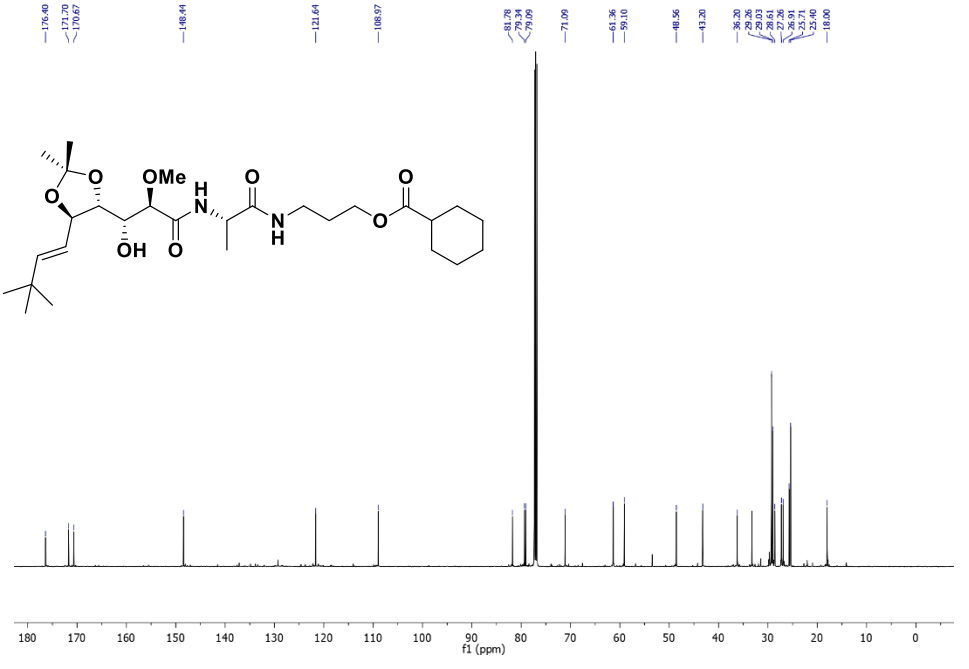

Spectra 40: ^{1}H-NMR (500 MHz, $CDCl_3$) of compound **294**

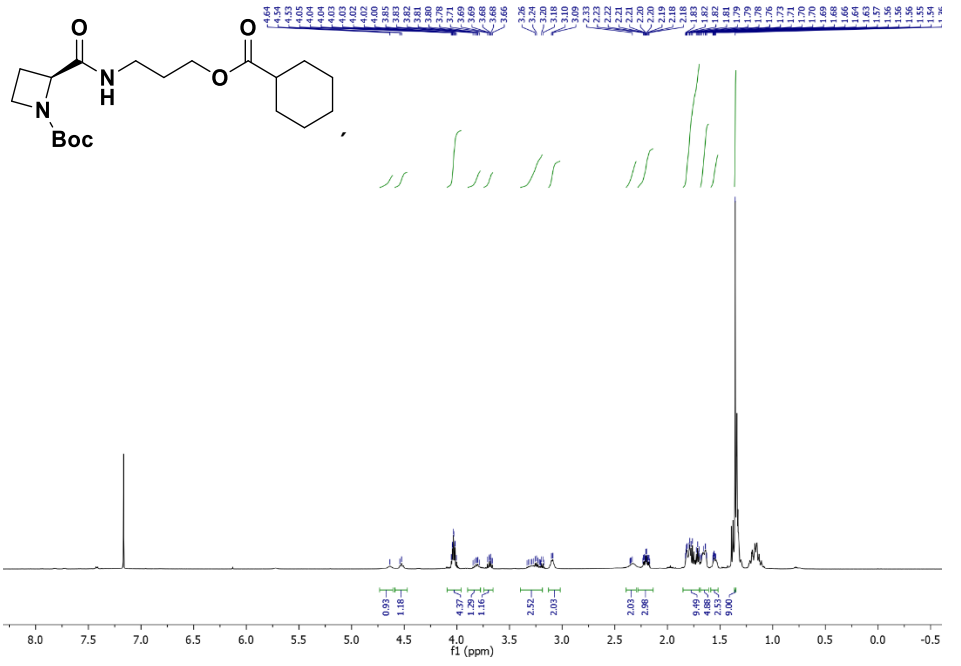

Spectra 41: ^{13}C-NMR (125 MHz, $CDCl_3$) of compound **294**

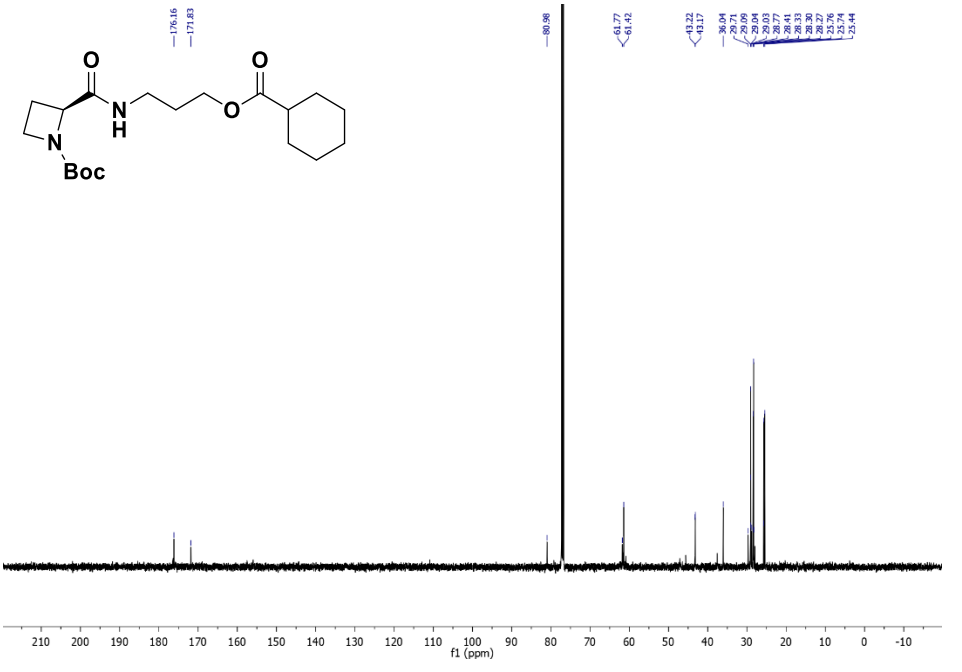

Spectra 42: ^{1}H-NMR (500 MHz, $CDCl_3$) of compound **296**

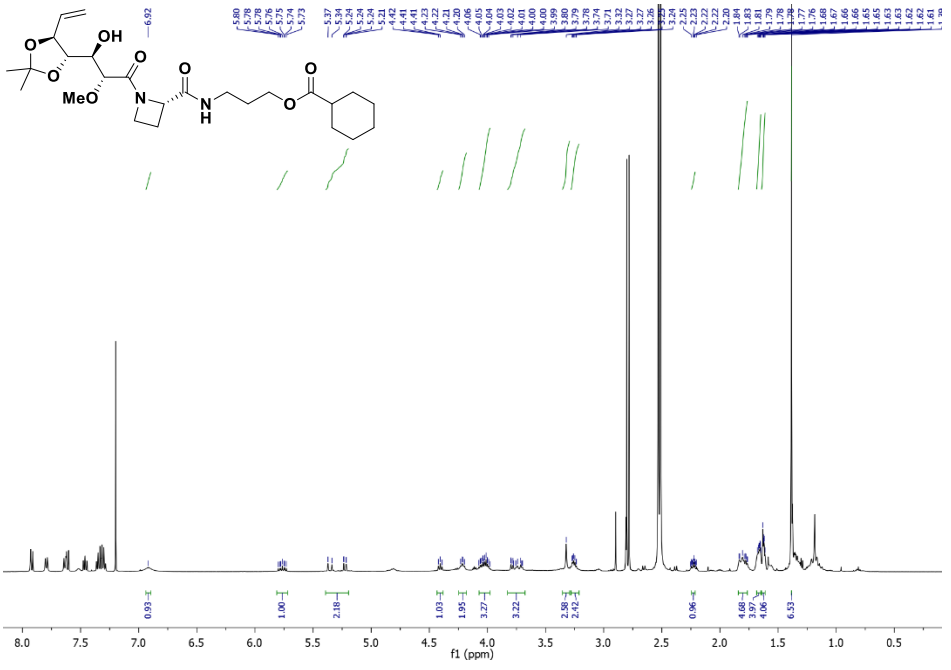

Spectra 43: ^{13}C-NMR (125 MHz, $CDCl_3$) of compound **296**

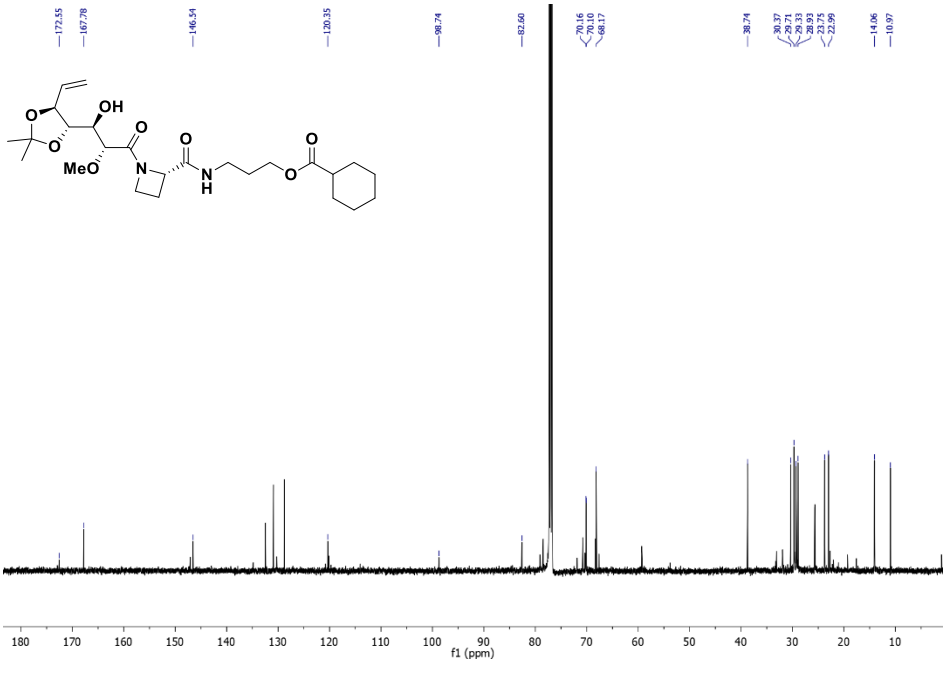

Spectra 44: ^{1}H-NMR (500 MHz, $CDCl_3$) of compound **297**

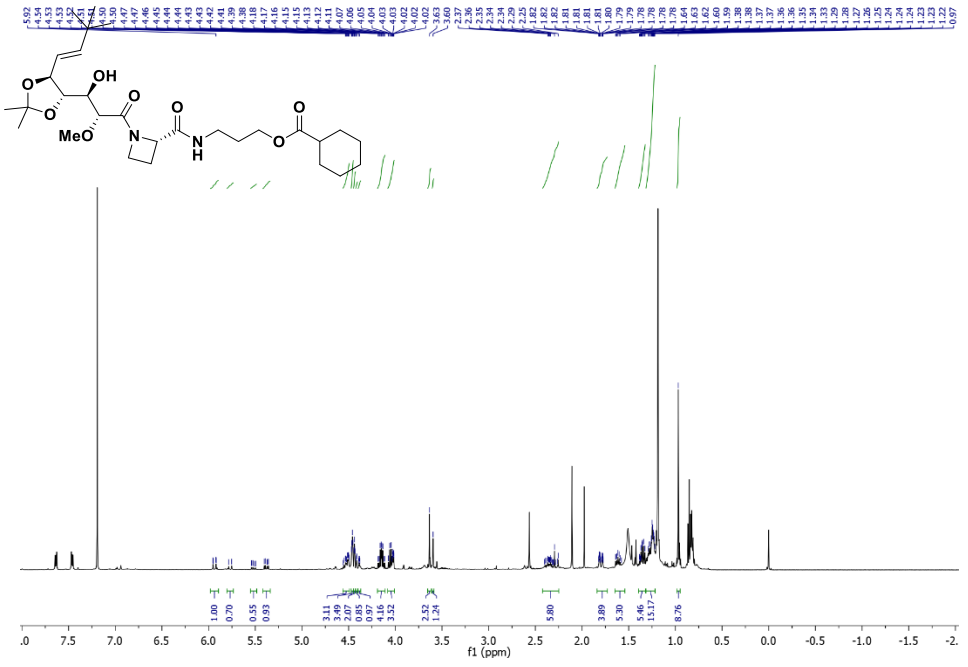

Spectra 45: ^{1}H-NMR (500 MHz, $CDCl_3$) of compound **289**

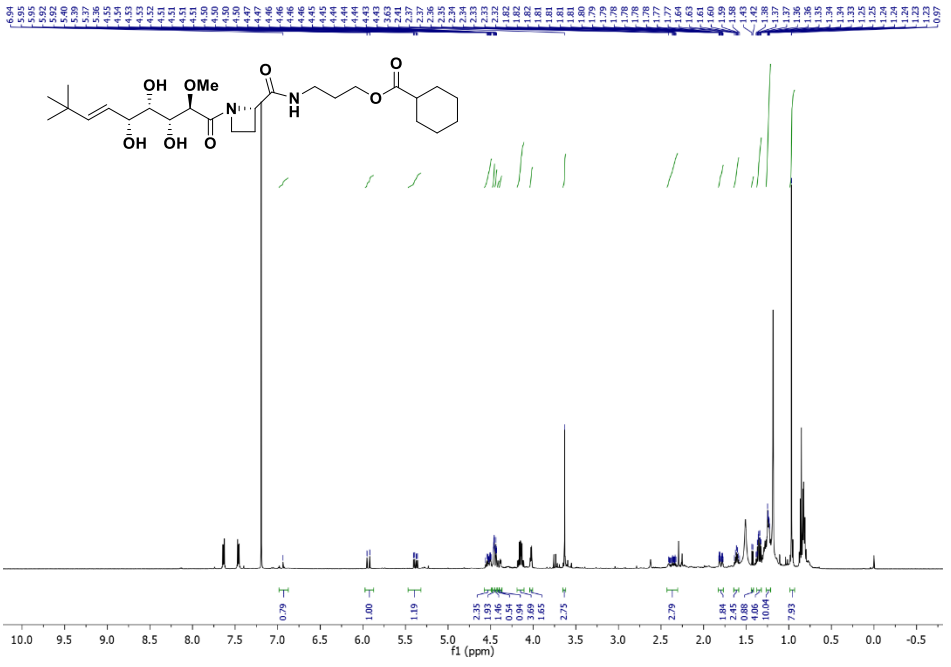

Spectra 46: ^{13}C-NMR (125 MHz, $CDCl_3$) of compound **289**

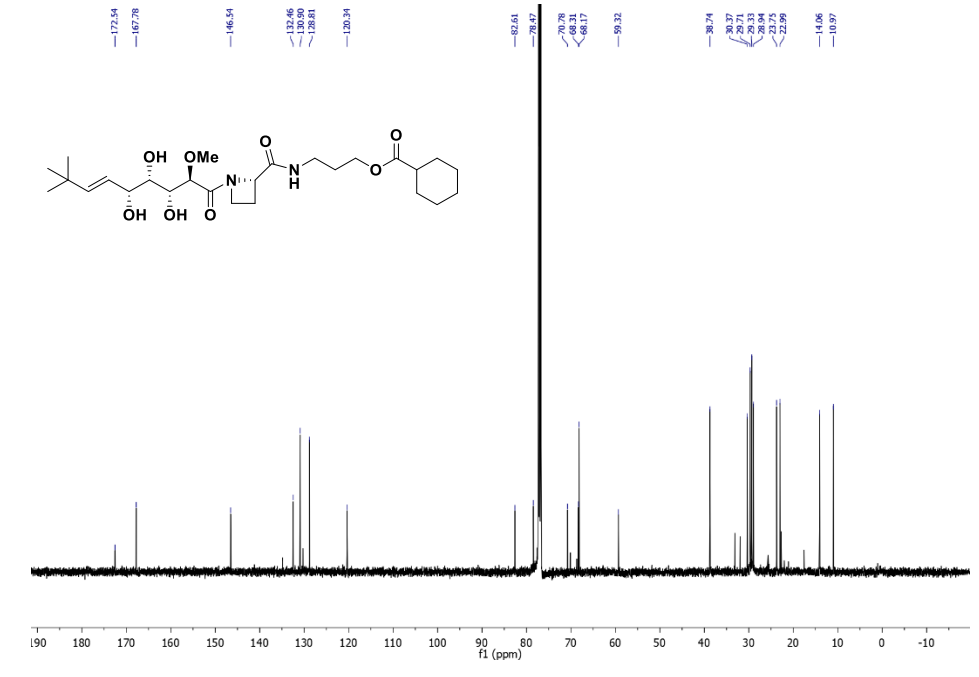

Spectra 47: ^{1}H-NMR (400 MHz, MeOD) of compound **306**

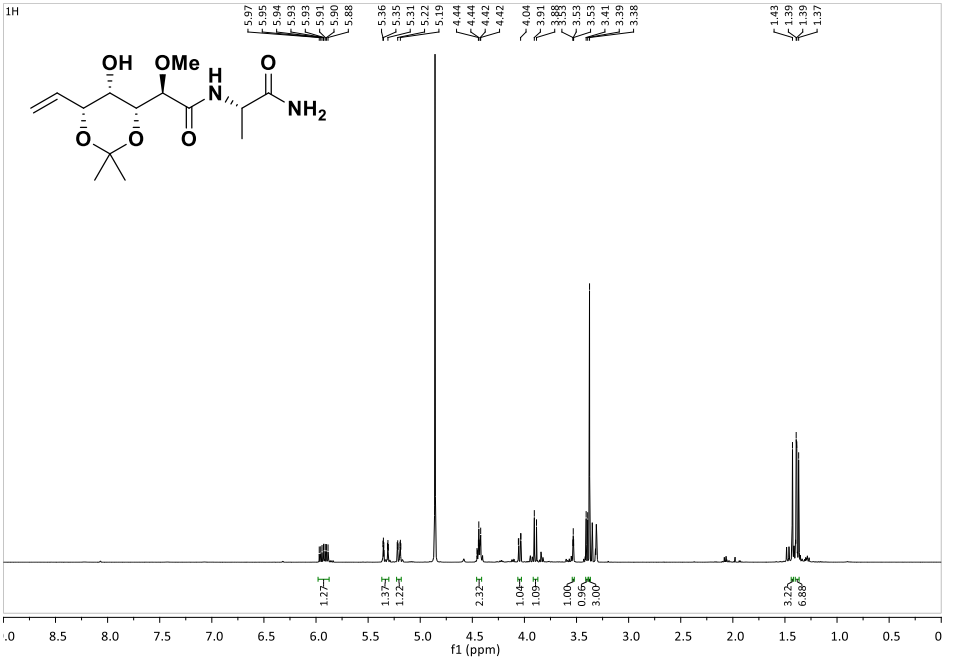

Spectra 48: ^{13}C-NMR (100 MHz, MeOD) of compound **306**

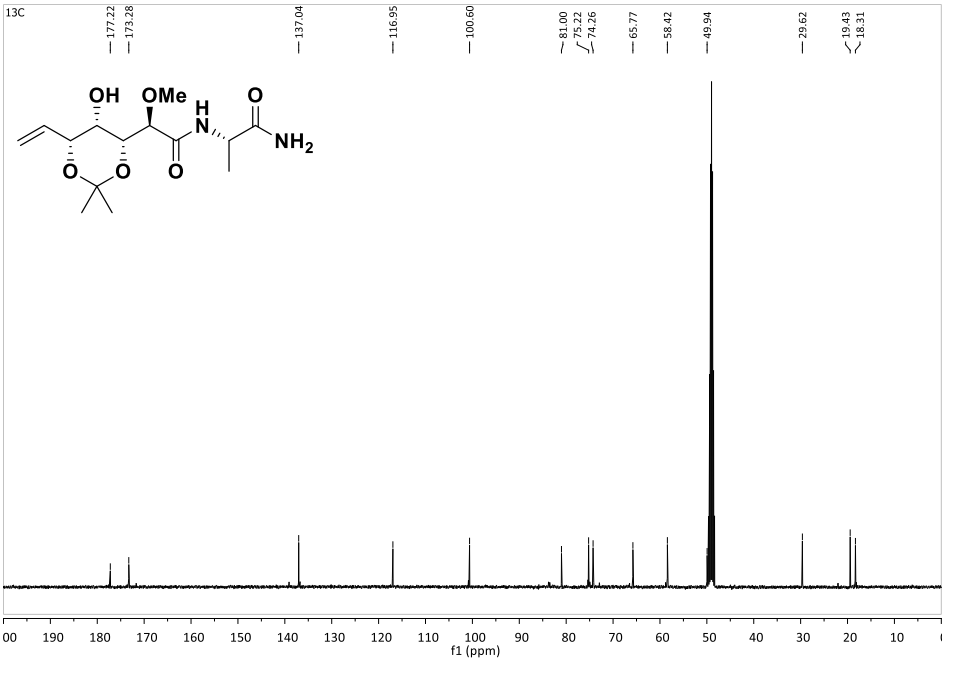

Spectra 49: ^{1}H-NMR (400 MHz, MeOD) of compound **307**

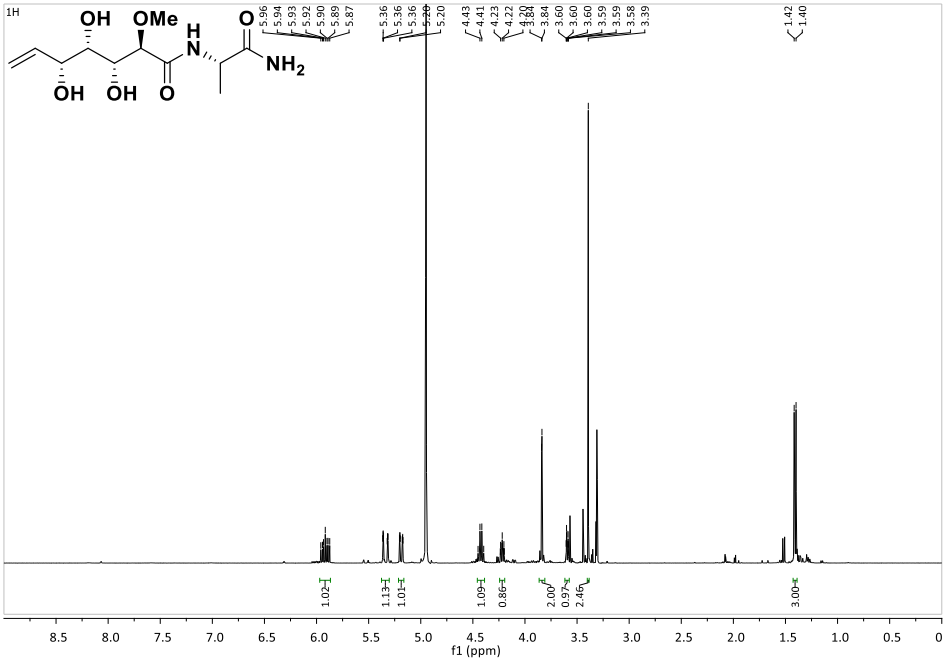

Spectra 50: ^{13}C-NMR (100 MHz, MeOD) of compound **307**

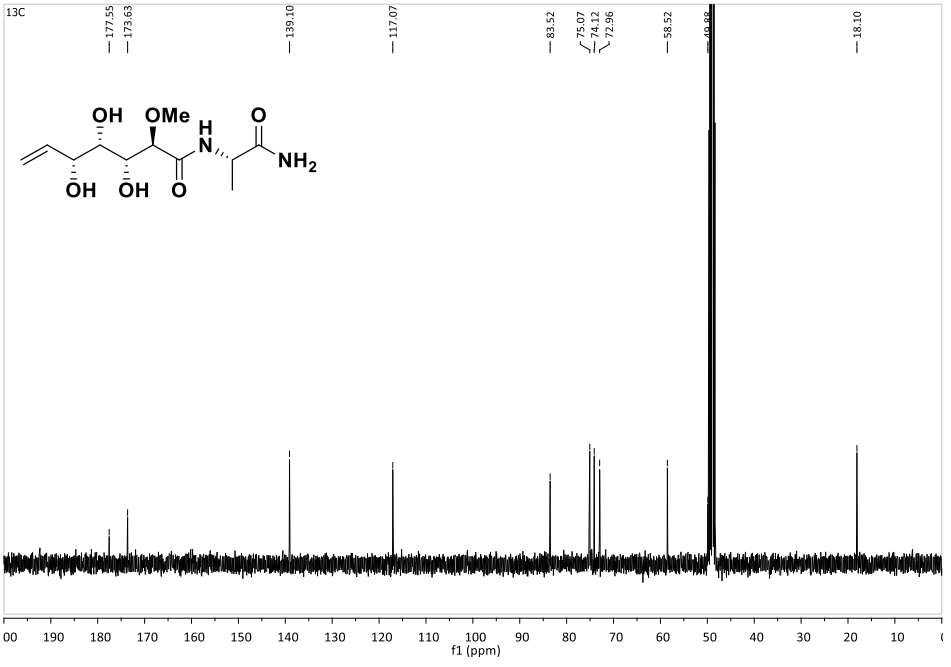

Spectra 51: ^{1}H-NMR (400 MHz, $CDCl_3$) of compound **311**

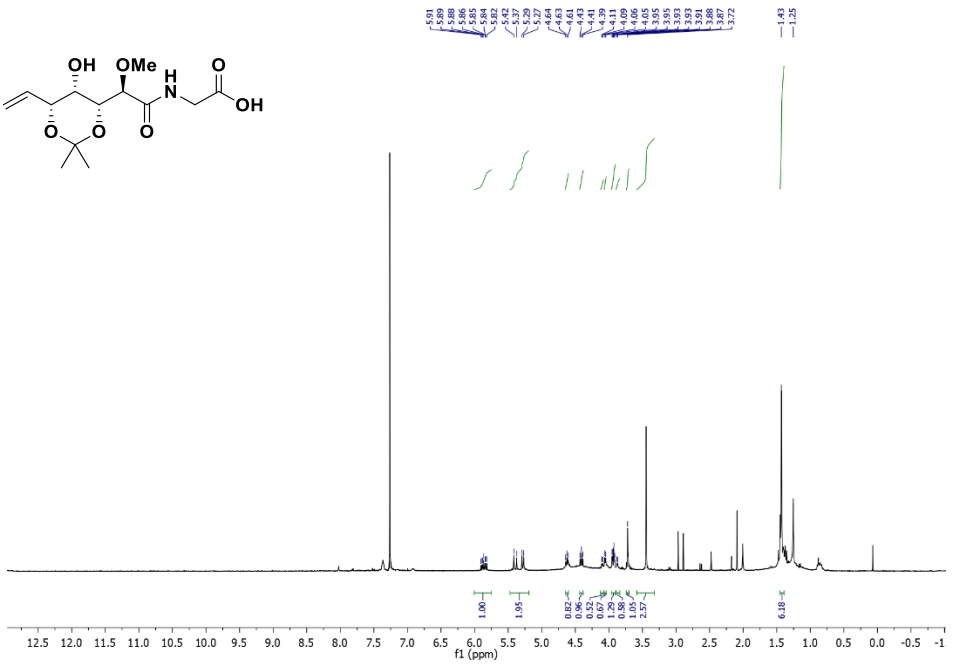

Spectra 52: ^{1}H-NMR (400 MHz, $CDCl_3$) of compound **312**

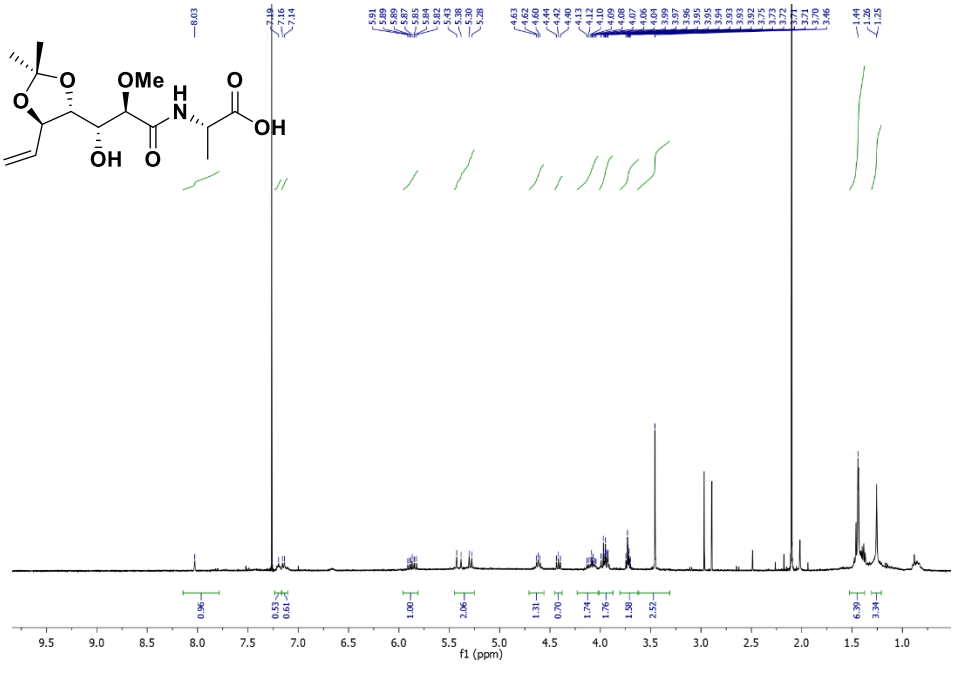

Spectra 53: ^{1}H-NMR (500 MHz, $CDCl_3$) of compound **314**

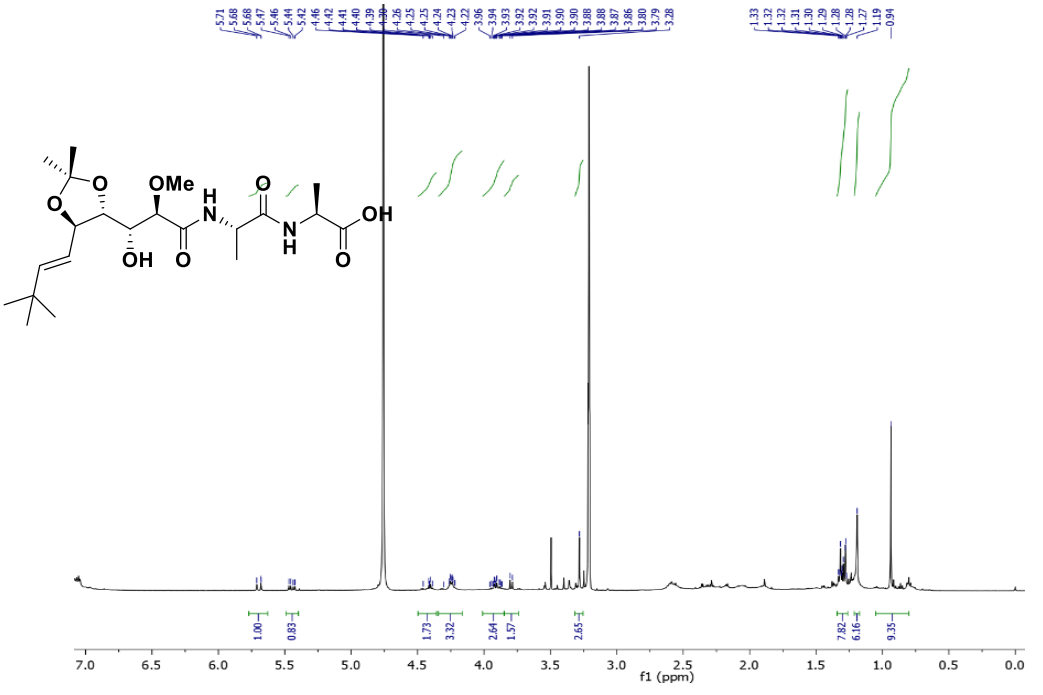

Spectra 54: ^{13}C-NMR (100 MHz, $CDCl_3$) of compound **314**

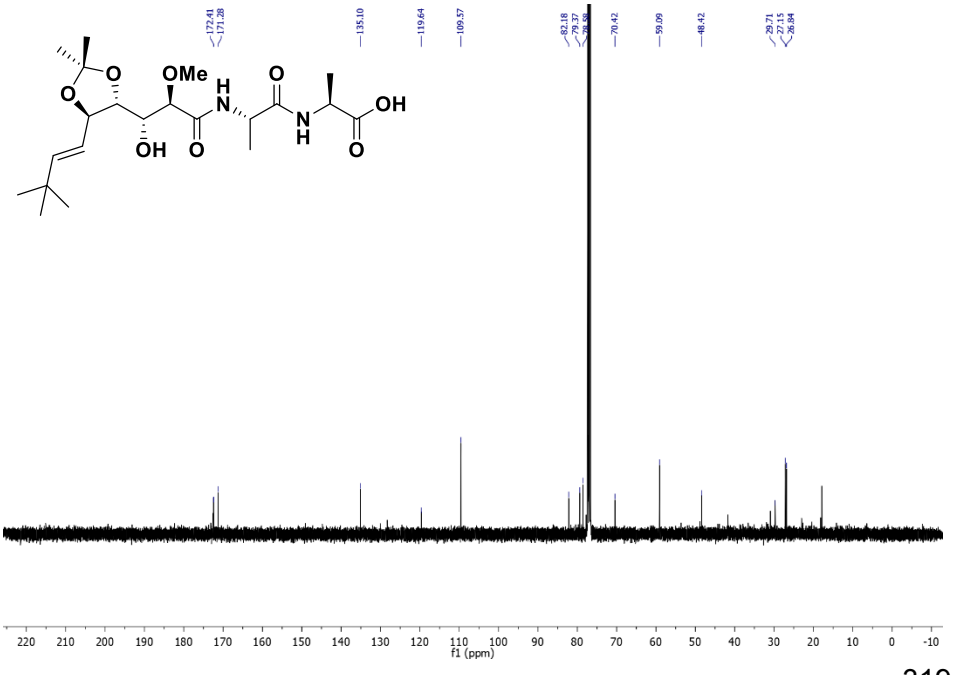

Spectra 55: ^{1}H-NMR (500 MHz, MeOD) of compound **315**

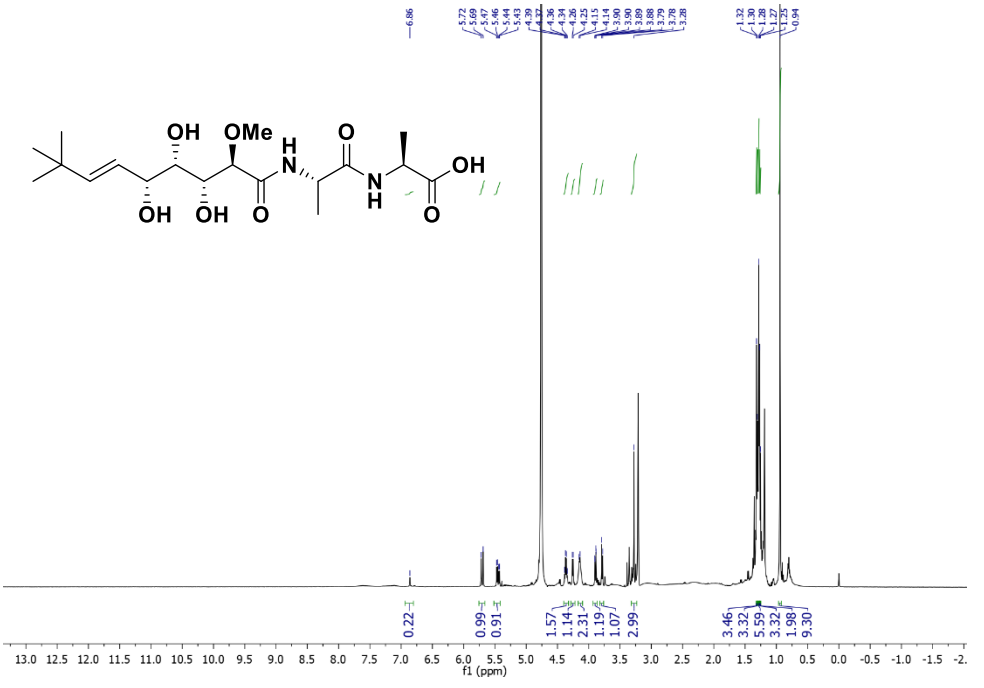

Spectra 56: ^{13}C-NMR (125 MHz, MeOD) of compound **315**

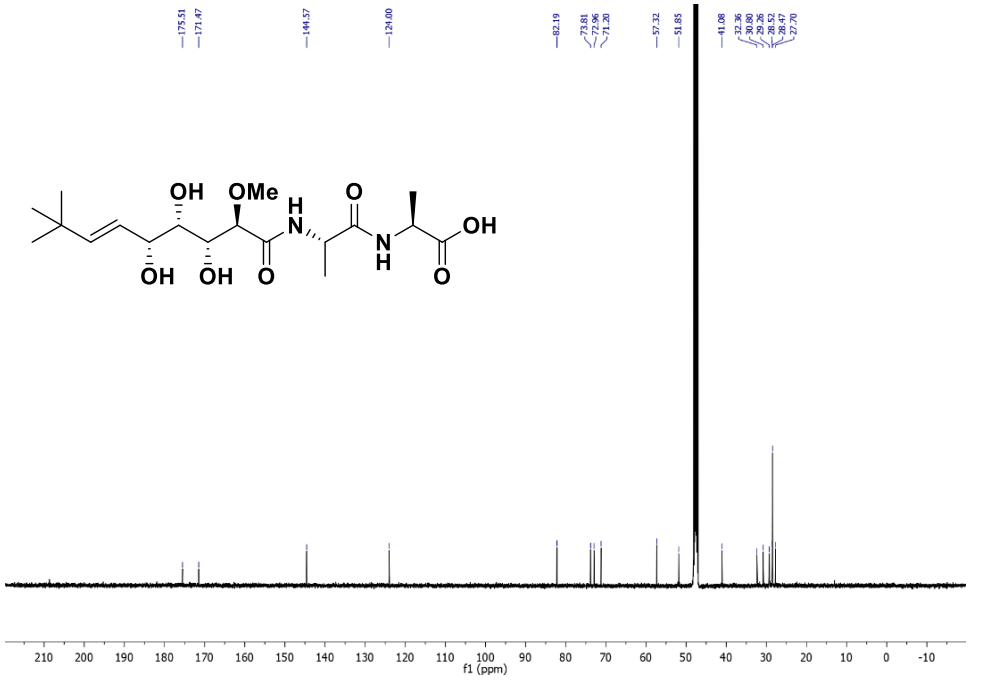

Spectra 57: ^{1}H-NMR (500 MHz, MeOD) of compound **317**

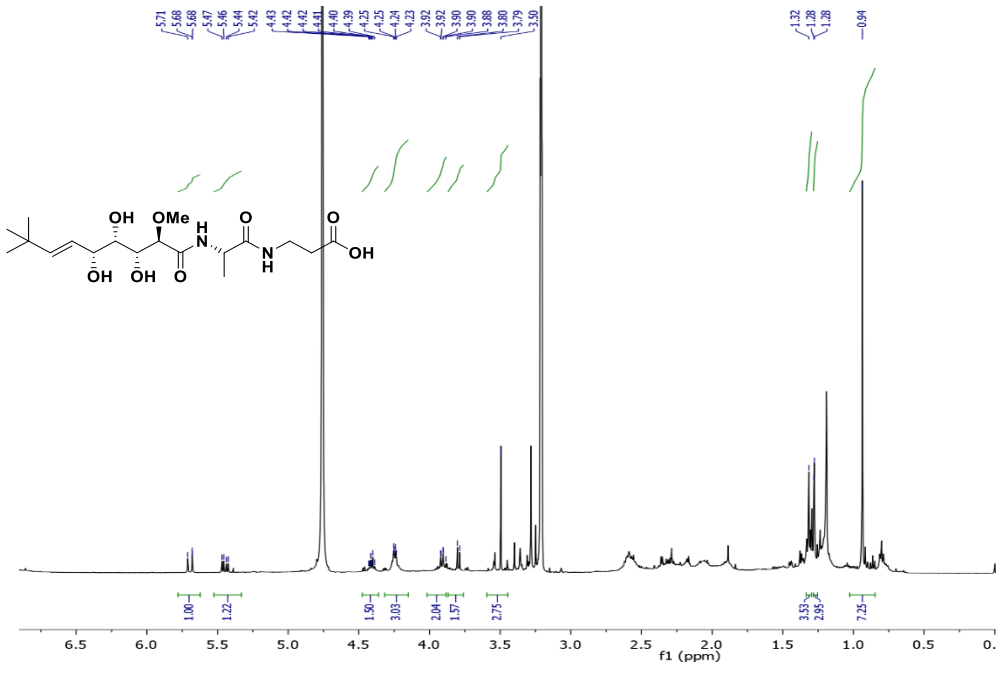

Spectra 58: ^{13}C-NMR (125 MHz, MeOD) of compound **317**

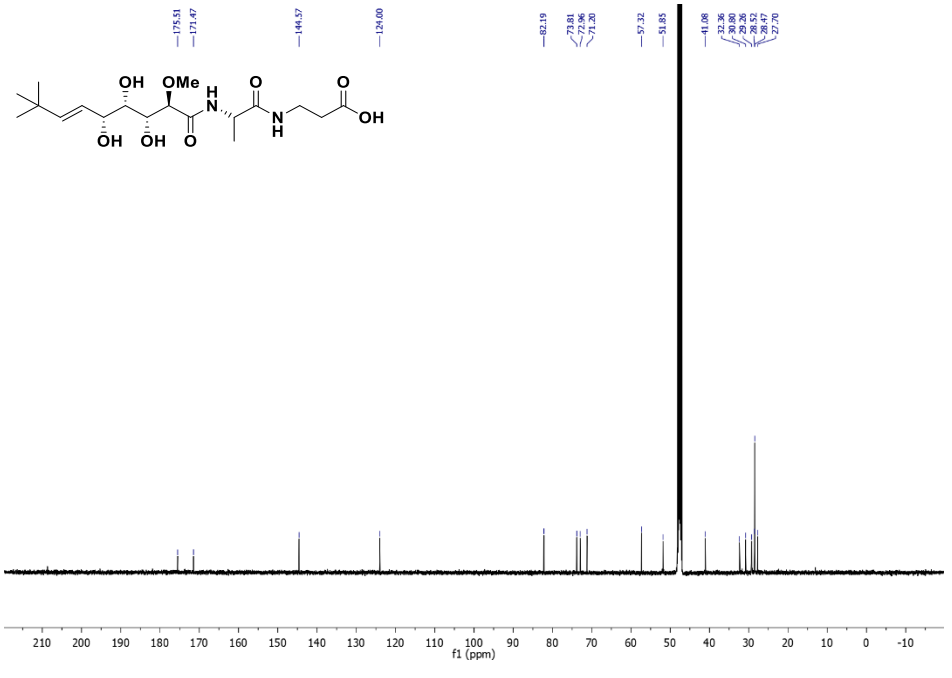

Spectra 59: ^{1}H-NMR (500 MHz, $CDCl_3$) of compound **329**

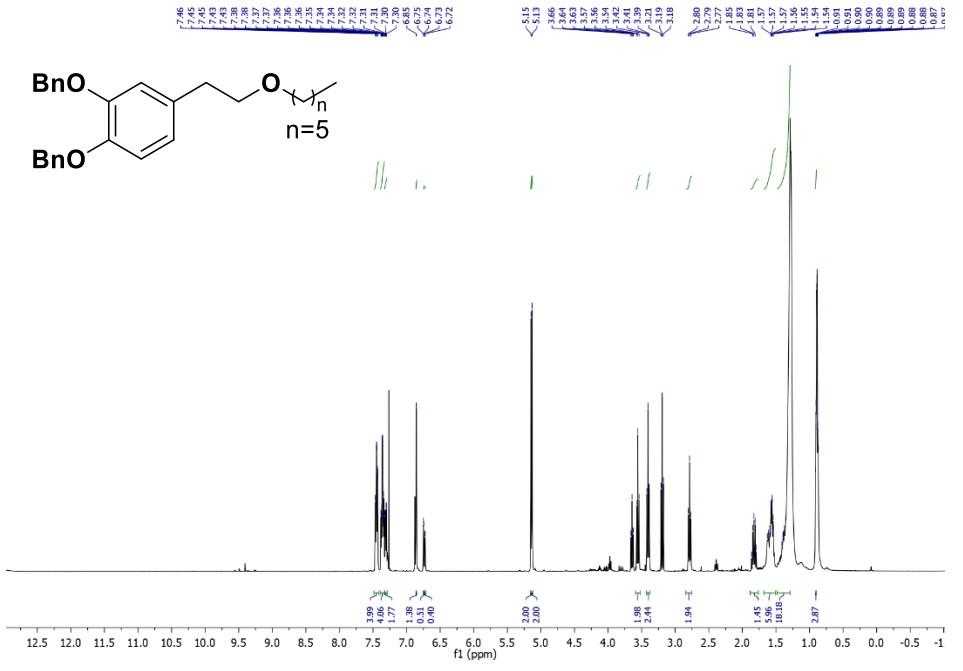

Spectra 60: ^{1}H-NMR (500 MHz, $CDCl_3$) of compound **330**

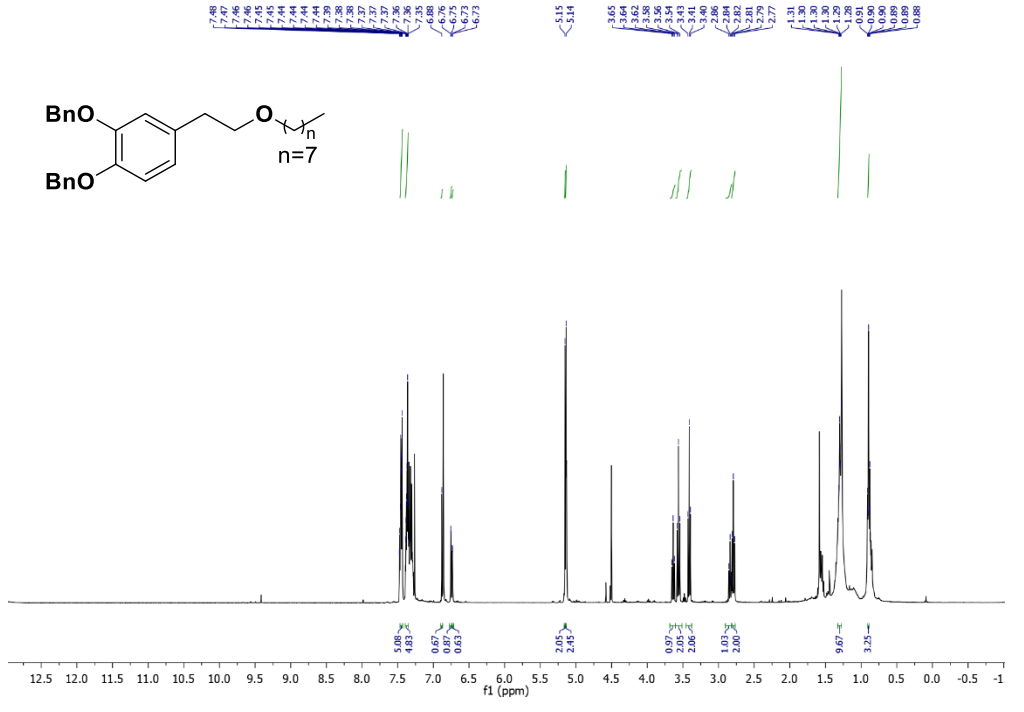

Spectra 61: ^{1}H-NMR (500 MHz, $CDCl_3$) of compound **331**

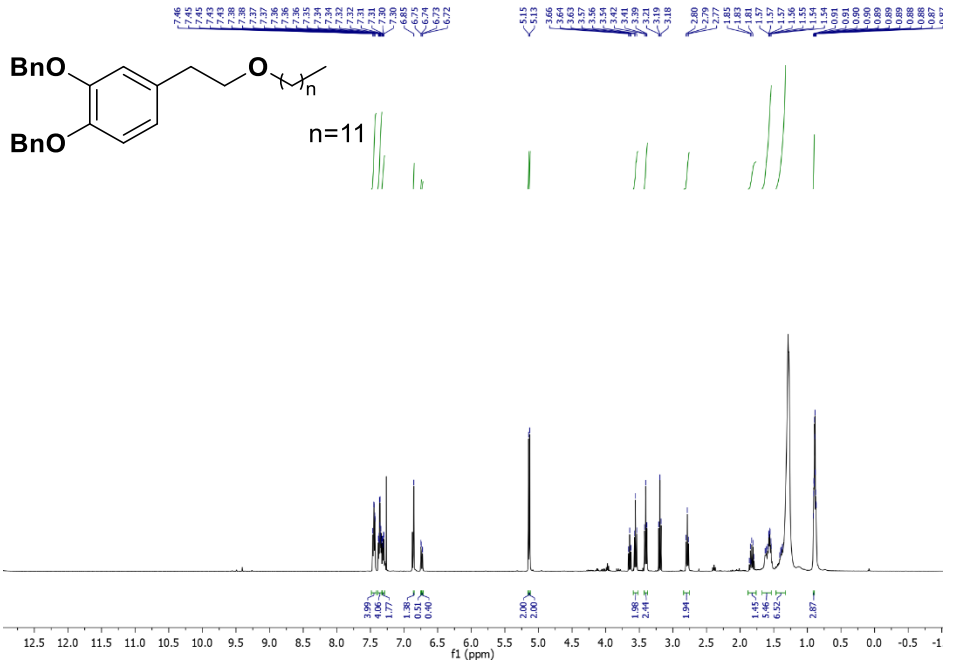

Spectra 62: ^{1}H-NMR (500 MHz, $CDCl_3$) of compound **325**

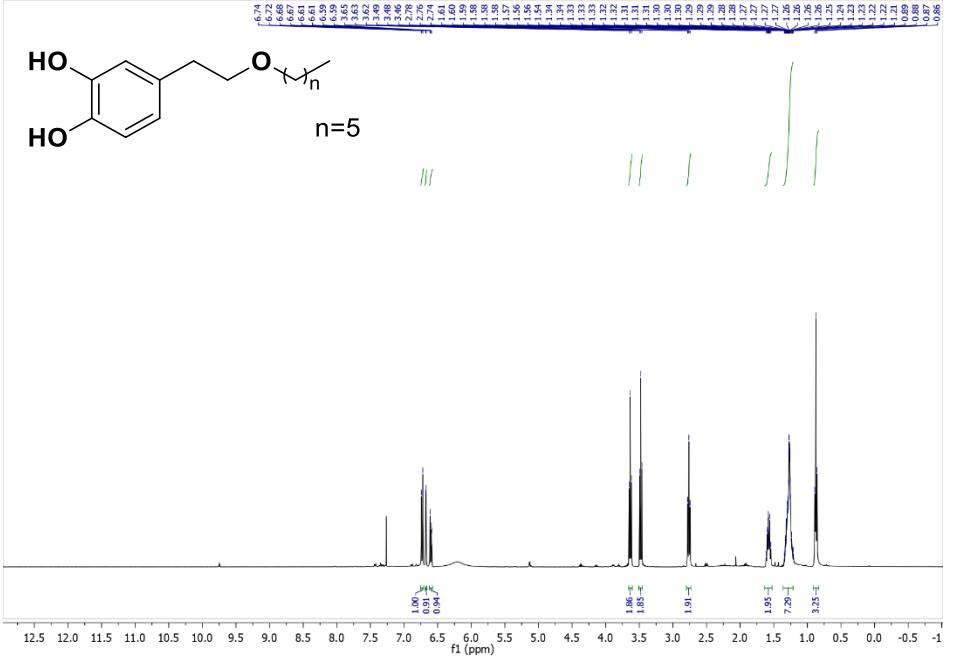

Spectra 63: ^{1}H-NMR (500 MHz, $CDCl_3$) of compound **326**

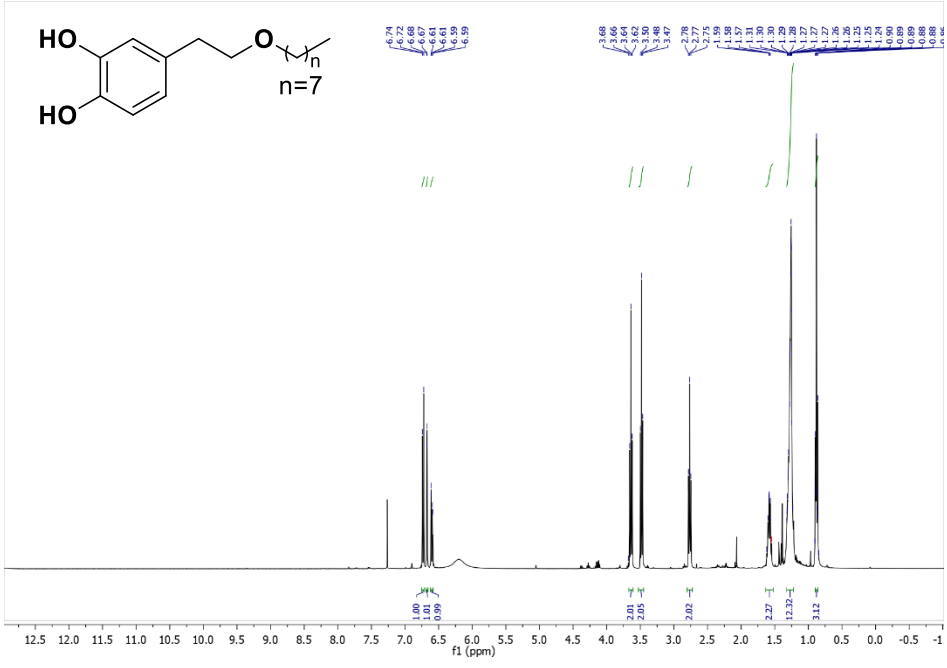

Spectra 64: ^{1}H-NMR (500 MHz, $CDCl_3$) of compound **327**

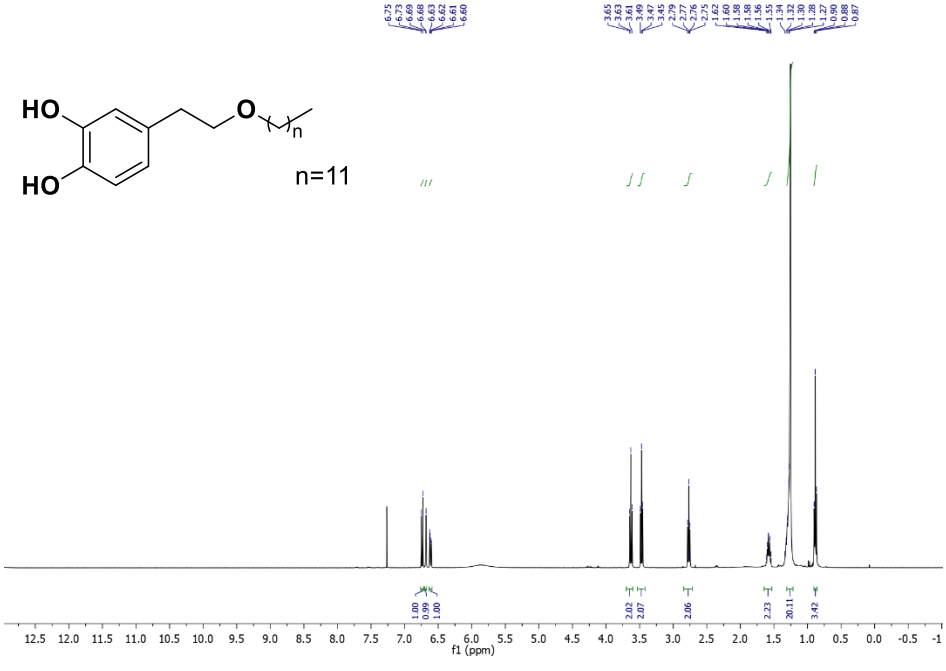

BIBLIOGRAPHY

(1) Siegel, R. L.; Miller, K. D.; Jemal, A. Cancer Statistics, 2018. *CA Cancer J Clin* **2018**, *68* (1), 7–30. https://doi.org/10.3322/caac.21442.

(2) Sept, O. *GLOBOCAN 2018: Counting the Toll of Cancer*; 2018; Vol. 392. http://gco.iarc.fr.

(3) Seeber, A.; Gastl, G. Targeted Therapy of Colorectal Cancer. *Oncology Research and Treatment*. S. Karger AG November 1, 2016, pp 796–802. https://doi.org/10.1159/000453027.

(4) Fernández Montes, A.; Martínez Lago, N.; Covela Rúa, M.; de la Cámara Gómez, J.; González Villaroel, P.; Méndez Méndez, J. C.; Jorge Fernández, M.; Salgado Fernández, M.; Reboredo López, M.; Quintero Aldana, G.; Luz Pellón Augusto, M.; Graña Suárez, B.; García Gómez, J. Efficacy and Safety of FOLFIRI/Aflibercept in Second-Line Treatment of Metastatic Colorectal Cancer in a Real-World Population: Prognostic and Predictive Markers. *Cancer Med* **2019**, *8* (3), 882–889. https://doi.org/10.1002/cam4.1903.

(5) Bray, F.; Ferlay, J.; Soerjomataram, I.; Siegel, R. L.; Torre, L. A.; Jemal, A. Global Cancer Statistics 2018: GLOBOCAN Estimates of Incidence and Mortality Worldwide for 36 Cancers in 185 Countries. *CA Cancer J Clin* **2018**, *68* (6), 394–424. https://doi.org/10.3322/caac.21492.

(6) Gallego-Jara, J.; Lozano-Terol, G.; Sola-Martínez, R. A.; Cánovas-Díaz, M.; de Diego Puente, T. A Compressive Review about Taxol®: History and Future Challenges. *Molecules* **2020**, *25* (24), 5986. https://doi.org/10.3390/molecules25245986.

(7) Quinoa, E.; Adamczeski, M.; Crews, P.; Bakus, G. J. Bengamides, Heterocyclic Anthelmintics from a Jaspidae Marine Sponge. *J Org Chem* **1986**, *51* (23), 4494–4497. https://doi.org/10.1021/jo00373a036.

(8) Groweiss, A.; Newcomer, J. J.; O'Keefe, B. R.; Blackman, A.; Boyd, M. R. Cytotoxic Metabolites from an Australian Collection of the Sponge *Jaspis* Species. *J Nat Prod* **1999**, *62* (12), 1691–1693. https://doi.org/10.1021/np9902688.

(9) Crews, P.; Manes, L. V; Boehler, M. Jasplakinolide, a Cyclodepsipeptide from the Marine Sponge, SP. *Tetrahedron Lett* **1986**, *27* (25), 2797–2800. https://doi.org/10.1016/S0040-4039(00)84645-6.

(10) Kobayashi, J.; Yuasa, K.; Kobayashi, T.; Sasaki, T.; Tsuda, M. Jaspiferals A ~ G, New Cytotoxic Isomalabaricane-Type Nortriterpenoids from Okinawan Marine Sponge Jaspis Stellifera. *Tetrahedron* **1996**, *52* (16), 5745–5750. https://doi.org/10.1016/0040-4020(96)00206-2.

(11) Tsuda, M.; Ishibashi, M.; Agemi, K.; Sasaki, T.; Kobayashi, J. Stelliferins A–F, New Antineoplastic Isomalabaricane Triterpenes from the Okinawan Marine Sponge Jaspis Stellifera. *Tetrahedron* **1991**, *47* (12–13), 2181–2194. https://doi.org/10.1016/S0040-4020(01)96129-0.

(12) Adamczeski, M.; Quinoa, E.; Crews, P. Novel Sponge-Derived Amino Acids. 5. Structures, Stereochemistry, and Synthesis of Several New Heterocycles. *J Am Chem Soc* **1989**, *111* (2), 647–654. https://doi.org/10.1021/ja00184a037.

(13) Thale, Z.; Kinder, F. R.; Bair, K. W.; Bontempo, J.; Czuchta, A. M.; Versace, R. W.; Phillips, P. E.; Sanders, M. L.; Wattanasin, S.; Crews, P. Bengamides Revisited: New Structures and Antitumor Studies. *J Org Chem* **2001**, *66* (5), 1733–1741. https://doi.org/10.1021/jo001380+.

(14) D'Auria, M. V.; Giannini, C.; Minale, L.; Zampella, A.; Debitus, C.; Frostin, M. Bengamides and Related New Amino Acid Derivatives

from the New Caledonian Marine Sponge *Jaspis Carteri*. *J Nat Prod* **1997**, *60* (8), 814–816. https://doi.org/10.1021/np970050q.

(15) Rudi, A.; Kashman, Y.; Benayahu, Y.; Schleyer, M. Amino Acid Derivatives from the Marine Sponge Jaspis Digonoxea. *J Nat Prod* **1994**, *57* (6), 829–832. https://doi.org/10.1021/np50108a023.

(16) Ebada, S.; Wray, V.; De Voogd, N.; Deng, Z.; Lin, W.; Proksch, P. Two New Jaspamide Derivatives from the Marine Sponge Jaspis Splendens. *Mar Drugs* **2009**, *7* (3), 435–444. https://doi.org/10.3390/md7030435.

(17) Braekman, J. C.; Daloze, D.; Moussiaux, B.; Riccio, R. Jaspamide from the Marine Sponge Jaspis Johnstoni. *J Nat Prod* **1987**, *50* (5), 994–995. https://doi.org/10.1021/np50053a048.

(18) Molinski, T. F. Developments in Marine Natural Products. Receptor-Specific Bioactive Compounds. *J Nat Prod* **1993**, *56* (1), 1–8. https://doi.org/10.1021/np50091a001.

(19) Kobayashi, J.; Murata, O.; Shigemori, H.; Sasaki, T. Jaspisamides A-C, New Cytotoxic Macrolides from the Okinawan Sponge Jaspis Sp. *J Nat Prod* **1993**, *56* (5), 787–791. https://doi.org/10.1021/np50095a021.

(20) Tsukamoto, S.; Kato, H.; Hirota, H.; Fusetani, N. Narains: N, N-Dimethylguanidinium Styryl Sulfates, Metamorphosis Inducers of Ascidian Larvae from a Marine Sponge Jaspis Sp. *Tetrahedron Lett* **1994**, *35* (32), 5873–5874. https://doi.org/10.1016/S0040-4039(00)78206-2.

(21) Ohta, S.; Kobayashi, H.; Ikegami, S. Isojaspisin: A Novel Styryl Sulfate from a Marine Sponge, Jaspis Sp., That Inhibits Hatching of Sea Urchin Embryos. *Tetrahedron Lett* **1994**, *35* (26), 4579–4580. https://doi.org/10.1016/S0040-4039(00)60734-7.

(22) Searle, P. A.; Richter, R. K.; Molinski, T. F. Bengazoles C−G from the Sponge *Jaspis* Sp. Synthesis of the Side Chain and Determination of Absolute Configuration. *J Org Chem* **1996**, *61* (12), 4073–4079. https://doi.org/10.1021/jo952261a.

(23) Ledroit, V.; Debitus, C.; Lavaud, C.; Massiot, G. Jaspines A and B: Two New Cytotoxic Sphingosine Derivatives from the Marine Sponge Jaspis Sp. *Tetrahedron Lett* **2003**, *44* (2), 225–228. https://doi.org/10.1016/S0040-4039(02)02541-8.

(24) Chevallier, C.; Richardson, A. D.; Edler, M. C.; Hamel, E.; Harper, M. K.; Ireland, C. M. A New Cytotoxic and Tubulin-Interactive Milnamide Derivative from a Marine Sponge *Cymbastela* Sp. *Org Lett* **2003**, *5* (20), 3737–3739. https://doi.org/10.1021/ol035476c.

(25) Ovenden, S. P. B.; Nielson, J. L.; Liptrot, C. H.; Willis, R. H.; Tapiolas, D. M.; Wright, A. D.; Motti, C. A. A New Diketopiperazine, Cyclo-(4-S-Hydroxy-R-Proline-R-Isoleucine), from an Australian Specimen of the Sponge Stelletta Sp. *Mar Drugs* **2011**, *9* (11), 2469–2478. https://doi.org/10.3390/md9112469.

(26) Johnson, T. A.; Sohn, J.; Vaske, Y. M.; White, K. N.; Cohen, T. L.; Vervoort, H. C.; Tenney, K.; Valeriote, F. A.; Bjeldanes, L. F.; Crews, P. Myxobacteria versus Sponge-Derived Alkaloids: The Bengamide Family Identified as Potent Immune Modulating Agents by Scrutiny of LC–MS/ELSD Libraries. *Bioorg Med Chem* **2012**, *20* (14), 4348–4355. https://doi.org/10.1016/j.bmc.2012.05.043.

(27) Fernández, R.; Dherbomez, M.; Letourneux, Y.; Nabil, M.; Verbist, J. F.; Biard, J. F. Antifungal Metabolites from the Marine Sponge *Pachastrissa* Sp.: New Bengamide and Bengazole Derivatives. *J Nat Prod* **1999**, *62* (5), 678–680. https://doi.org/10.1021/np980330l.

(28) Tanaka, N.; Momose, R.; Shibazaki, A.; Gonoi, T.; Fromont, J.; Kobayashi, J. Stelliferins J–N, Isomalabaricane-Type Triterpenoids from Okinawan Marine Sponge Rhabdastrella Cf. Globostellata. *Tetrahedron* **2011**, *67* (35), 6689–6696. https://doi.org/10.1016/j.tet.2011.04.095.

(29) Oku, N.; Matsunaga, S.; Wada, S.; Watabe, S.; Fusetani, N. New Isomalabaricane Triterpenes from the Marine Sponge *Stelletta Globostellata* That Induce Morphological Changes in Rat Fibroblasts. *J Nat Prod* **2000**, *63* (2), 205–209. https://doi.org/10.1021/np990333d.

(30) Tabudravu, J. N.; Jaspars, M. Stelliferin Riboside, a Triterpene Monosaccharide Isolated from the Fijian Sponge *Geodia g Lobostellifera*. *J Nat Prod* **2001**, *64* (6), 813–815. https://doi.org/10.1021/np010019v.

(31) Dhand, V.; Chang, S.; Britton, R. Total Synthesis of the Cytotoxic Anhydrophytosphingosine Pachastrissamine (Jaspine B). *J Org Chem* **2013**, *78* (16), 8208–8213. https://doi.org/10.1021/jo4013223.

(32) Adamczeski, Madeline.; Quinoa, Emilio.; Crews, Phillip. Unusual Anthelminthic Oxazoles from a Marine Sponge. *J Am Chem Soc* **1988**, *110* (5), 1598–1602. https://doi.org/10.1021/ja00213a037.

(33) Sarabia, F.; Martín-Gálvez, F.; Chammaa, S.; Martín-Ortiz, L.; Sánchez-Ruiz, A. Chiral Sulfur Ylides for the Synthesis of Bengamide E and Analogues. *J Org Chem* **2010**, *75* (16), 5526–5532. https://doi.org/10.1021/jo100696w.

(34) Adamczeski, M.; Quinoa, E.; Crews, P. Novel Sponge-Derived Amino Acids. 11. The Entire Absolute Stereochemistry of the Bengamides. *J Org Chem* **1990**, *55* (1), 240–242. https://doi.org/10.1021/jo00288a039.

(35) Dale, J. A.; Mosher, H. S. Nuclear Magnetic Resonance Enantiomer Regents. Configurational Correlations via Nuclear Magnetic Resonance Chemical Shifts of Diastereomeric Mandelate, O-Methylmandelate, and .Alpha.-Methoxy-.Alpha.-Trifluoromethylphenylacetate (MTPA) Esters. *J Am Chem Soc* **1973**, *95* (2), 512–519. https://doi.org/10.1021/ja00783a034.

(36) Chida, N.; Tobe, T.; Okada, S.; Ogawa, S. Total Synthesis and Absolute Configuration of Bengamide A. *J Chem Soc Chem Commun* **1992**, No. 15, 1064. https://doi.org/10.1039/c39920001064.

(37) Broka, C. A.; Ehrler, J. Enantioselective Total Syntheses of Bengamides B and E. *Tetrahedron Lett* **1991**, *32* (42), 5907–5910. https://doi.org/10.1016/S0040-4039(00)79423-8.

(38) Chida, N.; Tobe, T.; Ogawa, S. Total Synthesis of Bengamide E. *Tetrahedron Lett* **1991**, *32* (8), 1063–1066. https://doi.org/10.1016/S0040-4039(00)74488-1.

(39) Carballeira, N.; Thompson, J. E.; Ayanoglu, E.; Djerassi, C. Biosynthetic Studies of Marine Lipids. 5. The Biosynthesis of Long-Chain Branched Fatty Acids in Marine Sponges. *J Org Chem* **1986**, *51* (14), 2751–2756. https://doi.org/10.1021/jo00364a024.

(40) Wenzel, S. C.; Hoffmann, H.; Zhang, J.; Debussche, L.; Haag-Richter, S.; Kurz, M.; Nardi, F.; Lukat, P.; Kochems, I.; Tietgen, H.; Schummer, D.; Nicolas, J.; Calvet, L.; Czepczor, V.; Vrignaud, P.; Mühlenweg, A.; Pelzer, S.; Müller, R.; Brönstrup, M. Production of the Bengamide Class of Marine Natural Products in Myxobacteria: Biosynthesis and Structure–Activity Relationships. *Angewandte Chemie International Edition* **2015**, *54* (51), 15560–15564. https://doi.org/10.1002/anie.201508277.

(41) Acquah, K. S.; Beukes, D. R.; Seldon, R.; Jordaan, A.; Sunassee, S. N.; Warner, D. F.; Gammon, D. W. Identification of Antimycobacterial Natural Products from a Library of Marine Invertebrate

Extracts. *Medicines* **2022**, *9* (2), 9. https://doi.org/10.3390/medicines9020009.

(42) García-Ruiz, C.; Sarabia, F. Chemistry and Biology of Bengamides and Bengazoles, Bioactive Natural Products from Jaspis Sponges. *Mar Drugs* **2014**, *12* (3), 1580–1622. https://doi.org/10.3390/md12031580.

(43) Kinder, , Frederick R.; Wattanasin, S.; Versace, R. W.; Bair, K. W.; Bontempo, J.; Green, M. A.; Lu, Y. J.; Marepalli, H. R.; Phillips, P. E.; Roche, D.; Tran, L. D.; Wang, R.; Waykole, L.; Xu, D. D.; Zabludoff, S. Total Syntheses of Bengamides B and E. *J Org Chem* **2001**, *66* (6), 2118–2122. https://doi.org/10.1021/jo0017133.

(44) Phillips, P. E. ; B. K. W. ; B. j. ; C. P. ; C. M. ; K. F. R. ; V. R. W. ; W. B. ; W. J. ; W. A. ; Z. S. Bengamide E Arrests Cells at the G1/S Restriction Point and within the G2/M Phase of the Cell Cycle. *Proc. Am. Assoc. Cancer Res.* **2000**, *41*, 59.

(45) Towbin, H.; Bair, K. W.; DeCaprio, J. A.; Eck, M. J.; Kim, S.; Kinder, F. R.; Morollo, A.; Mueller, D. R.; Schindler, P.; Song, H. K.; van Oostrum, J.; Versace, R. W.; Voshol, H.; Wood, J.; Zabludoff, S.; Phillips, P. E. Proteomics-Based Target Identification: Bengamides as a New Class of Methionine Aminopeptidase Inhibitors. *J Biol Chem* **2003**, *278* (52), 52964–52971. https://doi.org/10.1074/jbc.M309039200.

(46) Xu, D. D.; Waykole, L.; Calienni, J. V.; Ciszewski, L.; Lee, G. T.; Liu, W.; Szewczyk, J.; Vargas, K.; Prasad, K.; Repič, O.; Blacklock, T. J. An Expedient Synthesis of LAF389, a Bengamide B Analogue. *Org Process Res Dev* **2003**, *7* (6), 856–865. https://doi.org/10.1021/op0341162.

(47) Griffith, E. C.; Su, Z.; Niwayama, S.; Ramsay, C. A.; Chang, Y. H.; Liu, J. O. Molecular Recognition of Angiogenesis Inhibitors Fumagillin and Ovalicin by Methionine Aminopeptidase 2. *Proc Natl*

Acad Sci U S A **1998**, *95* (26), 15183–15188. https://doi.org/10.1073/pnas.95.26.15183.

(48) Griffith, E. C.; Su, Z.; Turk, B. E.; Chen, S.; Chang, Y. H.; Wu, Z.; Biemann, K.; Liu, J. O. Methionine Aminopeptidase (Type 2) Is the Common Target for Angiogenesis Inhibitors AGM-1470 and Ovalicin. *Chem Biol* **1997**, *4* (6), 461–471. https://doi.org/10.1016/s1074-5521(97)90198-8.

(49) Sashidhara, K. V.; White, K. N.; Crews, P. A Selective Account of Effective Paradigms and Significant Outcomes in the Discovery of Inspirational Marine Natural Products. *J Nat Prod* **2009**, *72* (3), 588–603. https://doi.org/10.1021/np800817y.

(50) Lowther, W. T.; Matthews, B. W. Structure and Function of the Methionine Aminopeptidases. *Biochim Biophys Acta* **2000**, *1477* (1–2), 157–167. https://doi.org/10.1016/s0167-4838(99)00271-x.

(51) Giglione, C.; Boularot, A.; Meinnel, T. Protein N-Terminal Methionine Excision. *Cell Mol Life Sci* **2004**, *61* (12), 1455–1474. https://doi.org/10.1007/s00018-004-3466-8.

(52) Ben-Bassat, A.; Bauer, K.; Chang, S. Y.; Myambo, K.; Boosman, A.; Chang, S. Processing of the Initiation Methionine from Proteins: Properties of the Escherichia Coli Methionine Aminopeptidase and Its Gene Structure. *J Bacteriol* **1987**, *169* (2), 751–757. https://doi.org/10.1128/jb.169.2.751-757.1987.

(53) Levine, A. J. P53, the Cellular Gatekeeper for Growth and Division. *Cell* **1997**, *88* (3), 323–331. https://doi.org/10.1016/S0092-8674(00)81871-1.

(54) Ingber, D.; Fujita, T.; Kishimoto, S.; Sudo, K.; Kanamaru, T.; Brem, H.; Folkman, J. Synthetic Analogues of Fumagillin That Inhibit Angiogenesis and Suppress Tumour Growth. *Nature* **1990**, *348* (6301), 555–557. https://doi.org/10.1038/348555a0.

(55) Sato, Y. Role of Aminopeptidase in Angiogenesis. *Biol Pharm Bull* **2004**, *27* (6), 772–776. https://doi.org/10.1248/bpb.27.772.

(56) Xu, W.; Lu, J.-P.; Ye, Q.-Z. Structural Analysis of Bengamide Derivatives as Inhibitors of Methionine Aminopeptidases. *J Med Chem* **2012**, *55* (18), 8021–8027. https://doi.org/10.1021/jm3008695.

(57) Kim, S.; LaMontagne, K.; Sabio, M.; Sharma, S.; Versace, R. W.; Yusuff, N.; Phillips, P. E. Depletion of Methionine Aminopeptidase 2 Does Not Alter Cell Response to Fumagillin or Bengamides. *Cancer Res* **2004**, *64* (9), 2984–2987. https://doi.org/10.1158/0008-5472.CAN-04-0019.

(58) Liu, S.; Widom, J.; Kemp, C. W.; Crews, C. M.; Clardy, J. Structure of Human Methionine Aminopeptidase-2 Complexed with Fumagillin. *Science (1979)* **1998**, *282* (5392), 1324–1327. https://doi.org/10.1126/science.282.5392.1324.

(59) Bernier, S. G.; Taghizadeh, N.; Thompson, C. D.; Westlin, W. F.; Hannig, G. Methionine Aminopeptidases Type I and Type II Are Essential to Control Cell Proliferation. *J Cell Biochem* **2005**, *95* (6), 1191–1203. https://doi.org/10.1002/jcb.20493.

(60) Porras-Alcalá, C.; Moya-Utrera, F.; García-Castro, M.; Sánchez-Ruiz, A.; López-Romero, J. M.; Pino-González, M. S.; Díaz-Morilla, A.; Kitamura, S.; Wolan, D. W.; Prados, J.; Melguizo, C.; Cheng-Sánchez, I.; Sarabia, F. The Development of the Bengamides as New Antibiotics against Drug-Resistant Bacteria. *Mar Drugs* **2022**, *20* (6), 373. https://doi.org/10.3390/md20060373.

(61) Chang, S. Y.; McGary, E. C.; Chang, S. Methionine Aminopeptidase Gene of Escherichia Coli Is Essential for Cell Growth. *J Bacteriol* **1989**, *171* (7), 4071–4072. https://doi.org/10.1128/jb.171.7.4071-4072.1989.

(62) Lu, J.-P.; Yuan, X.-H.; Ye, Q.-Z. Structural Analysis of Inhibition of Mycobacterium Tuberculosis Methionine Aminopeptidase by Bengamide Derivatives. *Eur J Med Chem* **2012**, *47*, 479–484. https://doi.org/10.1016/j.ejmech.2011.11.017.

(63) Lu, J.-P.; Yuan, X.-H.; Yuan, H.; Wang, W.-L.; Wan, B.; Franzblau, S. G.; Ye, Q.-Z. Inhibition of Mycobacterium Tuberculosis Methionine Aminopeptidases by Bengamide Derivatives. *ChemMedChem* **2011**, *6* (6), 1041–1048. https://doi.org/10.1002/cmdc.201100003.

(64) Luo, Q.-L.; Li, J.-Y.; Liu, Z.-Y.; Chen, L.-L.; Li, J.; Qian, Z.; Shen, Q.; Li, Y.; Lushington, G. H.; Ye, Q.-Z.; Nan, F.-J. Discovery and Structural Modification of Inhibitors of Methionine Aminopeptidases from *Escherichia c Oli* and *Saccharomyces c Erevisiae*. *J Med Chem* **2003**, *46* (13), 2631–2640. https://doi.org/10.1021/jm0300532.

(65) Quan, D. H.; Nagalingam, G.; Luck, I.; Proschogo, N.; Pillalamarri, V.; Addlagatta, A.; Martinez, E.; Sintchenko, V.; Rutledge, P. J.; Triccas, J. A. Bengamides Display Potent Activity against Drug-Resistant Mycobacterium Tuberculosis. *Sci Rep* **2019**, *9* (1), 14396. https://doi.org/10.1038/s41598-019-50748-2.

(66) Gogineni, V.; Schinazi, R. F.; Hamann, M. T. Role of Marine Natural Products in the Genesis of Antiviral Agents. *Chem Rev* **2015**, *115* (18), 9655–9706. https://doi.org/10.1021/cr4006318.

(67) Jamison, M.; Wang, X.; Cheng, T.; Molinski, T. Synergistic Anti-Candida Activity of Bengazole A in the Presence of Bengamide A. *Mar Drugs* **2019**, *17* (2), 102. https://doi.org/10.3390/md17020102.

(68) Tietjen, I.; Williams, D. E.; Read, S.; Kuang, X. T.; Mwimanzi, P.; Wilhelm, E.; Markle, T.; Kinloch, N. N.; Naphen, C. N.; Tenney, K.; Mesplède, T.; Wainberg, M. A.; Crews, P.; Bell, B.; Andersen, R. J.; Brumme, Z. L.; Brockman, M. A. Inhibition of NF-KB-Dependent

HIV-1 Replication by the Marine Natural Product Bengamide A. *Antiviral Res* **2018**, *152*, 94–103. https://doi.org/10.1016/j.antiviral.2018.02.017.

(69) Roco, M. C. The Long View of Nanotechnology Development: The National Nanotechnology Initiative at 10 Years. In *Nanotechnology Research Directions for Societal Needs in 2020*; Springer Netherlands: Dordrecht, 2011; pp 1–28. https://doi.org/10.1007/978-94-007-1168-6_1.

(70) Bhushan, B. Introduction to Nanotechnology; 2017; pp 1–19. https://doi.org/10.1007/978-3-662-54357-3_1.

(71) Rwei, S.-P.; Anh, T.; Chiang, W.-Y.; Way, T.-F.; Hsu, Y.-J. Synthesis and Drug Delivery Application of Thermo- and PH-Sensitive Hydrogels: Poly(β-CD-Co-N-Isopropylacrylamide-Co-IAM). *Materials* **2016**, *9* (12), 1003. https://doi.org/10.3390/ma9121003.

(72) Sevastre, A. S.; Horescu, C.; Baloi, S. C.; Cioc, C. E.; Vatu, B. I.; Tuta, C.; Artene, S. A.; Danciulescu, M. M.; Tudorache, S.; Dricu, A. Benefits of Nanomedicine for Therapeutic Intervention in Malignant Diseases. *Coatings*. MDPI AG October 1, 2019. https://doi.org/10.3390/coatings9100628.

(73) Nakamura, Y.; Mochida, A.; Choyke, P. L.; Kobayashi, H. Nanodrug Delivery: Is the Enhanced Permeability and Retention Effect Sufficient for Curing Cancer? *Bioconjug Chem* **2016**, *27* (10), 2225–2238. https://doi.org/10.1021/acs.bioconjchem.6b00437.

(74) Wu, W.; Pu, Y.; Shi, J. Nanomedicine-Enabled Chemotherapy-Based Synergetic Cancer Treatments. *J Nanobiotechnology* **2022**, *20* (1), 4. https://doi.org/10.1186/s12951-021-01181-z.

(75) Saleem, K.; Khursheed, Z.; Hano, C.; Anjum, I.; Anjum, S. Applications of Nanomaterials in Leishmaniasis: A Focus on Recent

Advances and Challenges. *Nanomaterials* **2019**, *9* (12), 1749. https://doi.org/10.3390/nano9121749.

(76) Bolotin, E. M.; Cohen, R.; Bar, L. K.; Emanuel, N.; Ninio, S.; Barenholz, Y.; Lasic, D. D. Ammonium Sulfate Gradients for Efficient and Stable Remote Loading of Amphipathic Weak Bases into Liposomes and Ligandoliposomes. *J Liposome Res* **1994**, *4* (1), 455–479. https://doi.org/10.3109/08982109409037057.

(77) Kaushik, N.; Borkar, S. B.; Nandanwar, S. K.; Panda, P. K.; Choi, E. H.; Kaushik, N. K. Nanocarrier Cancer Therapeutics with Functional Stimuli-Responsive Mechanisms. *Journal of Nanobiotechnology*. BioMed Central Ltd December 1, 2022. https://doi.org/10.1186/s12951-022-01364-2.

(78) Wang, Q.; Alshaker, H.; Böhler, T.; Srivats, S.; Chao, Y.; Cooper, C.; Pchejetski, D. Core Shell Lipid-Polymer Hybrid Nanoparticles with Combined Docetaxel and Molecular Targeted Therapy for the Treatment of Metastatic Prostate Cancer. *Sci Rep* **2017**, *7* (1), 5901. https://doi.org/10.1038/s41598-017-06142-x.

(79) Chen, Y.; Zhu, X.; Zhang, X.; Liu, B.; Huang, L. Nanoparticles Modified With Tumor-Targeting ScFv Deliver SiRNA and MiRNA for Cancer Therapy. *Molecular Therapy* **2010**, *18* (9), 1650–1656. https://doi.org/10.1038/mt.2010.136.

(80) García-Pinel, B.; Porras-Alcalá, C.; Ortega-Rodríguez, A.; Sarabia, F.; Prados, J.; Melguizo, C.; López-Romero, J. M. Lipid-Based Nanoparticles: Application and Recent Advances in Cancer Treatment. *Nanomaterials* **2019**, *9* (4), 638. https://doi.org/10.3390/nano9040638.

(81) Oliveira, R. R.; Carrião, M. S.; Pacheco, M. T.; Branquinho, L. C.; de Souza, A. L. R.; Bakuzis, A. F.; Lima, E. M. Triggered Release of Paclitaxel from Magnetic Solid Lipid Nanoparticles by Magnetic

Hyperthermia. *Materials Science and Engineering: C* **2018**, *92*, 547–553. https://doi.org/10.1016/j.msec.2018.07.011.

(82) Haron, A. S.; Syed Alwi, S. S.; Saiful Yazan, L.; Abd Razak, R.; Ong, Y. S.; Zakarial Ansar, F. H.; Roshini Alexander, H. Cytotoxic Effect of Thymoquinone-Loaded Nanostructured Lipid Carrier (TQ-NLC) on Liver Cancer Cell Integrated with Hepatitis B Genome, Hep3B. *Evidence-Based Complementary and Alternative Medicine* **2018**, *2018*, 1–13. https://doi.org/10.1155/2018/1549805.

(83) Silva, C. O.; Pinho, J. O.; Lopes, J. M.; Almeida, A. J.; Gaspar, M. M.; Reis, C. Current Trends in Cancer Nanotheranostics: Metallic, Polymeric, and Lipid-Based Systems. *Pharmaceutics* **2019**, *11* (1), 22. https://doi.org/10.3390/pharmaceutics11010022.

(84) Abdellatif, F. H. H.; Abdellatif, M. M. Utilization of Sustainable Biopolymers in Textile Processing. In *Green Chemistry for Sustainable Textiles*; Elsevier, 2021; pp 453–469. https://doi.org/10.1016/B978-0-323-85204-3.00013-0.

(85) Păduraru, D. N.; Niculescu, A.-G.; Bolocan, A.; Andronic, O.; Grumezescu, A. M.; Bîrlă, R. An Updated Overview of Cyclodextrin-Based Drug Delivery Systems for Cancer Therapy. *Pharmaceutics* **2022**, *14* (8), 1748. https://doi.org/10.3390/pharmaceutics14081748.

(86) Yadav, H. K. S.; Almokdad, A. A.; shaluf, S. I. M.; Debe, M. S. Polymer-Based Nanomaterials for Drug-Delivery Carriers. In *Nanocarriers for Drug Delivery*; Elsevier, 2019; pp 531–556. https://doi.org/10.1016/B978-0-12-814033-8.00017-5.

(87) Ueno, T.; Endo, K.; Hori, K.; Ozaki, N.; Tsuji, A.; Kondo, S.; Wakisaka, N.; Murono, S.; Kataoka, K.; Kato, Y.; Yoshizaki, T. Assessment of Antitumor Activity and Acute Peripheral Neuropathy of 1,2-Diaminocyclohexane Platinum (II)-Incorporating Micelles

(NC-4016). *Int J Nanomedicine* **2014**, 3005. https://doi.org/10.2147/IJN.S60564.

(88) Scarano, W.; de Souza, P.; Stenzel, M. H. Dual-Drug Delivery of Curcumin and Platinum Drugs in Polymeric Micelles Enhances the Synergistic Effects: A Double Act for the Treatment of Multidrug-Resistant Cancer. *Biomater Sci* **2015**, *3* (1), 163–174. https://doi.org/10.1039/C4BM00272E.

(89) Thipparaboina, R.; Chavan, R. B.; Kumar, D.; Modugula, S.; Shastri, N. R. Micellar Carriers for the Delivery of Multiple Therapeutic Agents. *Colloids Surf B Biointerfaces* **2015**, *135*, 291–308. https://doi.org/10.1016/j.colsurfb.2015.07.046.

(90) Parveen, S.; Sahoo, S. K. Polymeric Nanoparticles for Cancer Therapy. *J Drug Target* **2008**, *16* (2), 108–123. https://doi.org/10.1080/10611860701794353.

(91) Oh, J. K.; Drumright, R.; Siegwart, D. J.; Matyjaszewski, K. The Development of Microgels/Nanogels for Drug Delivery Applications. *Prog Polym Sci* **2008**, *33* (4), 448–477. https://doi.org/10.1016/j.progpolymsci.2008.01.002.

(92) Mendoza-Munoz, N.; Quintanar-Guerrero, D.; Allemann, E. The Impact of the Salting-Out Technique on the Preparation of Colloidal Particulate Systems for Pharmaceutical Applications. *Recent Pat Drug Deliv Formul* **2012**, *6* (3), 236–249. https://doi.org/10.2174/187221112802652688.

(93) LANGER, R.; FOLKMAN, J. Polymers for the Sustained Release of Proteins and Other Macromolecules. *Nature* **1976**, *263* (5580), 797–800. https://doi.org/10.1038/263797a0.

(94) Palma, E.; Pasqua, A.; Gagliardi, A.; Britti, D.; Fresta, M.; Cosco, D. Antileishmanial Activity of Amphotericin B-Loaded-PLGA

Nanoparticles: An Overview. *Materials* **2018**, *11* (7), 1167. https://doi.org/10.3390/ma11071167.

(95) Abbasi, E.; Aval, S. F.; Akbarzadeh, A.; Milani, M.; Nasrabadi, H. T.; Joo, S. W.; Hanifehpour, Y.; Nejati-Koshki, K.; Pashaei-Asl, R. Dendrimers: Synthesis, Applications, and Properties. *Nanoscale Res Lett* **2014**, *9* (1), 247. https://doi.org/10.1186/1556-276X-9-247.

(96) Kamal, M. A.; Jabir NR, N.; Tabrez; Ashraf; Shakil; Damanhouri. Nanotechnology-Based Approaches in Anticancer Research. *Int J Nanomedicine* **2012**, 4391. https://doi.org/10.2147/IJN.S33838.

(97) She, W.; Pan, D.; Luo, K.; He, B.; Cheng, G.; Zhang, C.; Gu, Z. PEGylated Dendrimer-Doxorubicin Cojugates as PH-Sensitive Drug Delivery Systems: Synthesis and <I>In Vitro</I> Characterization. *J Biomed Nanotechnol* **2015**, *11* (6), 964–978. https://doi.org/10.1166/jbn.2015.1865.

(98) Kesavan, A.; Ilaiyaraja, P.; Sofi Beaula, W.; Veena Kumari, V.; Sugin Lal, J.; Arunkumar, C.; Anjana, G.; Srinivas, S.; Ramesh, A.; Rayala, S. K.; Ponraju, D.; Venkatraman, G. Tumor Targeting Using Polyamidoamine Dendrimer–Cisplatin Nanoparticles Functionalized with Diglycolamic Acid and Herceptin. *European Journal of Pharmaceutics and Biopharmaceutics* **2015**, *96*, 255–263. https://doi.org/10.1016/j.ejpb.2015.08.001.

(99) Hutter, E.; Fendler, J. H. Exploitation of Localized Surface Plasmon Resonance. *Advanced Materials* **2004**, *16* (19), 1685–1706. https://doi.org/10.1002/adma.200400271.

(100) Huang, X.; Jain, P. K.; El-Sayed, I. H.; El-Sayed, M. A. Gold Nanoparticles: Interesting Optical Properties and Recent Applications in Cancer Diagnostics and Therapy. *Nanomedicine* **2007**, *2* (5), 681–693. https://doi.org/10.2217/17435889.2.5.681.

(101) Ali, H. R.; Selim, S. A.; Aili, D. Effects of Macrophage Polarization on Gold Nanoparticle-Assisted Plasmonic Photothermal Therapy. *RSC Adv* **2021**, *11* (40), 25047–25056. https://doi.org/10.1039/D1RA03671H.

(102) Tao, Y.; Chan, H. F.; Shi, B.; Li, M.; Leong, K. W. Light: A Magical Tool for Controlled Drug Delivery. *Adv Funct Mater* **2020**, *30* (49), 2005029. https://doi.org/10.1002/adfm.202005029.

(103) Molaei, M. J. Carbon Quantum Dots and Their Biomedical and Therapeutic Applications: A Review. *RSC Adv* **2019**, *9* (12), 6460–6481. https://doi.org/10.1039/C8RA08088G.

(104) Ghanbari, N.; Salehi, Z.; Khodadadi, A. A.; Shokrgozar, M. A.; Sabouri, A. A. Glucosamine-Conjugated Graphene Quantum Dots as Versatile and PH-Sensitive Nanocarriers for Enhanced Delivery of Curcumin Targeting to Breast Cancer. *Materials Science and Engineering: C* **2021**, *121*, 111809. https://doi.org/10.1016/j.msec.2020.111809.

(105) Deatsch, A. E.; Evans, B. A. Heating Efficiency in Magnetic Nanoparticle Hyperthermia. *J Magn Magn Mater* **2014**, *354*, 163–172. https://doi.org/10.1016/j.jmmm.2013.11.006.

(106) Arami, H.; Khandhar, A.; Liggitt, D.; Krishnan, K. M. In Vivo Delivery, Pharmacokinetics, Biodistribution and Toxicity of Iron Oxide Nanoparticles. *Chem Soc Rev* **2015**, *44* (23), 8576–8607. https://doi.org/10.1039/C5CS00541H.

(107) Odom, T. W.; Huang, J.-L.; Kim, P.; Lieber, C. M. Atomic Structure and Electronic Properties of Single-Walled Carbon Nanotubes. *Nature* **1998**, *391* (6662), 62–64. https://doi.org/10.1038/34145.

(108) Anbarasan, B.; Babu, S. V.; Elango, K.; Shriya, B.; Ramaprabhu, S. PH Responsive Release of Doxorubicin to the Cancer Cells by Functionalized Multi-Walled Carbon Nanotubes. *J Nanosci*

Nanotechnol **2015**, *15* (7), 4799–4805. https://doi.org/10.1166/jnn.2015.9817.

(109) Naderi, N.; Madani, S. Y.; Mosahebi, A.; Seifalian, A. M. Octa-Ammonium POSS-Conjugated Single-Walled Carbon Nanotubes as Vehicles for Targeted Delivery of Paclitaxel. *Nano Rev* **2015**, *6* (1), 28297. https://doi.org/10.3402/nano.v6.28297.

(110) Arora, S.; Kumar, R.; Kaur, H.; Rayat, C. S.; Kaur, I.; Arora, S. K.; Srivastava, J.; Bharadwaj, L. M. Translocation and Toxicity of Docetaxel Multi-Walled Carbon Nanotube Conjugates in Mammalian Breast Cancer Cells. *J Biomed Nanotechnol* **2014**, *10* (12), 3601–3609. https://doi.org/10.1166/jbn.2014.1875.

(111) Wu, L.; Man, C.; Wang, H.; Lu, X.; Ma, Q.; Cai, Y.; Ma, W. PEGylated Multi-Walled Carbon Nanotubes for Encapsulation and Sustained Release of Oxaliplatin. *Pharm Res* **2013**, *30* (2), 412–423. https://doi.org/10.1007/s11095-012-0883-5.

(112) Figarol, A.; Pourchez, J.; Boudard, D.; Forest, V.; Tulliani, J.-M.; Lecompte, J.-P.; Cottier, M.; Bernache-Assollant, D.; Grosseau, P. Biological Response to Purification and Acid Functionalization of Carbon Nanotubes. *Journal of Nanoparticle Research* **2014**, *16* (7), 2507. https://doi.org/10.1007/s11051-014-2507-y.

(113) BAZAK, R.; HOURI, M.; ACHY, S. EL; HUSSEIN, W.; REFAAT, T. Passive Targeting of Nanoparticles to Cancer: A Comprehensive Review of the Literature. *Mol Clin Oncol* **2014**, *2* (6), 904–908. https://doi.org/10.3892/mco.2014.356.

(114) Suk, J. S.; Xu, Q.; Kim, N.; Hanes, J.; Ensign, L. M. PEGylation as a Strategy for Improving Nanoparticle-Based Drug and Gene Delivery. *Adv Drug Deliv Rev* **2016**, *99*, 28–51. https://doi.org/10.1016/j.addr.2015.09.012.

(115) Rosenblum, D.; Joshi, N.; Tao, W.; Karp, J. M.; Peer, D. Progress and Challenges towards Targeted Delivery of Cancer Therapeutics. *Nat Commun* **2018**, *9* (1), 1410. https://doi.org/10.1038/s41467-018-03705-y.

(116) Sanità, G.; Carrese, B.; Lamberti, A. Nanoparticle Surface Functionalization: How to Improve Biocompatibility and Cellular Internalization. *Front Mol Biosci* **2020**, *7*. https://doi.org/10.3389/fmolb.2020.587012.

(117) Rana, S.; Gallo, A.; Srivastava, R. S.; Misra, R. D. K. On the Suitability of Nanocrystalline Ferrites as a Magnetic Carrier for Drug Delivery: Functionalization, Conjugation and Drug Release Kinetics. *Acta Biomater* **2007**, *3* (2), 233–242. https://doi.org/10.1016/j.actbio.2006.10.006.

(118) Panja, S.; Maji, S.; Maiti, T. K.; Chattopadhyay, S. A Smart Magnetically Active Nanovehicle for On-Demand Targeted Drug Delivery: Where van Der Waals Force Balances the Magnetic Interaction. *ACS Appl Mater Interfaces* **2015**, *7* (43), 24229–24241. https://doi.org/10.1021/acsami.5b07706.

(119) Jia, Y.; Jiang, Y.; He, Y.; Zhang, W.; Zou, J.; Magar, K. T.; Boucetta, H.; Teng, C.; He, W. Approved Nanomedicine against Diseases. *Pharmaceutics* **2023**, *15* (3), 774. https://doi.org/10.3390/pharmaceutics15030774.

(120) Gurjar, M. K.; Srinivas, N. R. An Ehantiospecific Approach towards the C10 Side-Chain of Bengamides. *Tetrahedron Lett* **1991**, *32* (28), 3409–3412. https://doi.org/10.1016/S0040-4039(00)92722-9.

(121) Kishimoto, H.; Ohrui, H.; Meguro, H. An Enantioselective Synthesis of Bengamide E. *J Org Chem* **1992**, *57* (18), 5042–5044. https://doi.org/10.1021/jo00044a053.

(122) Marshall, J. A.; Luke, G. P. Stereoselective Total Synthesis of Bengamide E from Glyceraldehyde Acetonide and a Nonracemic .Gamma.-Alkoxy Allylic Stannane. *J Org Chem* **1993**, *58* (23), 6229–6234. https://doi.org/10.1021/jo00075a017.

(123) Mukai, C.; Kataoka, O.; Hanaoka, M. A Cobalt-Complexed Propyanl in Organic Synthesis: A Highly Stereoselective Total Synthesis of Bengamide E. *Tetrahedron Lett* **1994**, *35* (37), 6899–6902. https://doi.org/10.1016/0040-4039(94)85036-4.

(124) Chida, N.; Tobe, T.; Murai, K.; Yamazaki, K.; Ogawa, S. Stereoselective Conversion of L-Quebrachitol into a Novel Hydroxylated Caprolactam: Total Synthesis of Bengamide B. *Heterocycles* **1994**, *38* (11), 2383. https://doi.org/10.3987/COM-94-6869.

(125) Banwell, M. G.; McRae, K. J. A Chemoenzymatic Total Synthesis of *Ent* -Bengamide E. *J Org Chem* **2001**, *66* (20), 6768–6774. https://doi.org/10.1021/jo0159486.

(126) Liu, W.; Szewczyk, J. M.; Waykole, L.; Repič, O.; Blacklock, T. J. Total Synthesis of Bengamide E. *Tetrahedron Lett* **2002**, *43* (8), 1373–1375. https://doi.org/10.1016/S0040-4039(02)00022-9.

(127) Annunziata, R.; Cinquini, M.; Cozzi, F.; Lombardi Borgia, A. Diastereoselective Synthesis of Anti and Syn .Alpha.,.Beta.-Dihydroxy Thioesters by Titanium Enolate Aldol Condensation. *J Org Chem* **1992**, *57* (23), 6339–6342. https://doi.org/10.1021/jo00049a053.

(128) Boeckman, , Robert K.; Clark, T. J.; Shook, B. C. A Practical Enantioselective Total Synthesis of the Bengamides B, E, and Z. *Org Lett* **2002**, *4* (12), 2109–2112. https://doi.org/10.1021/ol026101e.

(129) Boeckman, Jr. , R. K.; Clark, T. J.; Shook, B. C. The Development of a Convergent and Efficient Enantioselective Synthesis of the Bengamides via a Common Polyol Intermediate. *Helv Chim Acta*

2002, *85* (12), 4532–4560. https://doi.org/10.1002/hlca.200290026.

(130) Sarabia, F.; Sánchez-Ruiz, A. A Diversity-Oriented Synthetic Approach to Bengamides. *Tetrahedron Lett* **2005**, *46* (7), 1131–1135. https://doi.org/10.1016/j.tetlet.2004.12.096.

(131) Sarabia, F.; Vivar-García, C.; García-Castro, M.; García-Ruiz, C.; Martín-Gálvez, F.; Sánchez-Ruiz, A.; Chammaa, S. A Highly Stereoselective Synthesis of Glycidic Amides Based on a New Class of Chiral Sulfonium Salts: Applications in Asymmetric Synthesis. *Chemistry - A European Journal* **2012**, *18* (47), 15190–15201. https://doi.org/10.1002/chem.201201332.

(132) Sasaki, M.; Tanino, K.; Hirai, A.; Miyashita, M. The C2 Selective Nucleophilic Substitution Reactions of 2,3-Epoxy Alcohols Mediated by Trialkyl Borates: The First *Endo* -Mode Epoxide-Opening Reaction through an Intramolecular Metal Chelate. *Org Lett* **2003**, *5* (10), 1789–1791. https://doi.org/10.1021/ol034455f.

(133) Zhang, W.; Liang, Q.; Li, H.; Meng, X.; Li, Z. Concise Synthesis and Antitumor Activity of Bengamide E and Its Analogs. *Tetrahedron* **2013**, *69* (2), 664–672. https://doi.org/10.1016/j.tet.2012.11.004.

(134) Dondoni, A.; Fantin, G.; Fogagnolo, M.; Medici, A.; Pedrini, P. Iterative, Stereoselective Homologation of Chiral Polyalkoxy Aldehydes Employing 2-(Trimethylsilyl)Thiazole as a Formyl Anion Equivalent. The Thiazole Route to Higher Carbohydrates. *J Org Chem* **1989**, *54* (3), 693–702. https://doi.org/10.1021/jo00264a035.

(135) Prasad, K. R.; Gholap, S. L. Stereoselective Total Synthesis of (+)-Cardiobutanolide. *J Org Chem* **2008**, *73* (7), 2916–2919. https://doi.org/10.1021/jo7025614.

(136) Metri, P. K.; Schiess, R.; Prasad, K. R. Enantiospecific Total Synthesis of (−)-Bengamide E. *Chem Asian J* **2013**, *8* (2), 488–493. https://doi.org/10.1002/asia.201200999.

(137) Chida, N.; Tobe, T.; Ogawa, S. Total Synthesis of Bengamide E. *Tetrahedron Lett* **1991**, *32* (8), 1063–1066. https://doi.org/10.1016/S0040-4039(00)74488-1.

(138) Broka, C. A.; Ehrler, J. Enantioselective Total Syntheses of Bengamides B and E. *Tetrahedron Lett* **1991**, *32* (42), 5907–5910. https://doi.org/10.1016/S0040-4039(00)79423-8.

(139) Mukai, C.; Kataoka, O.; Hanaoka, M. An Efficient Method for the Optical Resolution of 3-Hydroxy-2-Substituted-4-Alkynoates: A Highly Stereoselective Total Synthesis of (+)-Bengamide E1. *J Org Chem* **1995**, *60* (18), 5910–5918. https://doi.org/10.1021/jo00123a030.

(140) Sarabia, F.; Sánchez-Ruiz, A. Total Synthesis of Bengamide E and Analogues by Modification at C-2 and at Terminal Olefinic Positions. *J Org Chem* **2005**, *70* (23), 9514–9520. https://doi.org/10.1021/jo0516032.

(141) Kinder, , Frederick R.; Versace, R. W.; Bair, K. W.; Bontempo, J. M.; Cesarz, D.; Chen, S.; Crews, P.; Czuchta, A. M.; Jagoe, C. T.; Mou, Y.; Nemzek, R.; Phillips, P. E.; Tran, L. D.; Wang, R.; Weltchek, S.; Zabludoff, S. Synthesis and Antitumor Activity of Ester-Modified Analogues of Bengamide B. *J Med Chem* **2001**, *44* (22), 3692–3699. https://doi.org/10.1021/jm010188c.

(142) Friedrich, E. C.; Falling, S. N.; Lyons, D. E. A Convenient Synthesis of Ethylidine Iodide. *Synth Commun* **1975**, *5* (1), 33–36. https://doi.org/10.1080/00397917508063512.

(143) Dumez, H.; Gall, H.; Capdeville, R.; Dutreix, C.; van Oosterom, A. T.; Giaccone, G. A Phase I and Pharmacokinetic Study of LAF389

Administered to Patients with Advanced Cancer. *Anticancer Drugs* **2007**, *18* (2), 219–225. https://doi.org/10.1097/CAD.0b013e328010ef5b.

(144) Liu, G.; Tai, W.-Y.; Li, Y.-L.; Nan, F.-J. Facile Synthesis of Versatile Functionalized Amino Caprolactams Using RCM Reactions of α-Amino Acrylamide. *Tetrahedron Lett* **2006**, *47* (19), 3295–3298. https://doi.org/10.1016/j.tetlet.2006.03.022.

(145) Liu, G.; Ma, Y.-M.; Tai, W.-Y.; Xie, C.-M.; Li, Y.-L.; Li, J.; Nan, F.-J. Design, Synthesis, and Biological Evaluation of Caprolactam-Modified Bengamide Analogues. *ChemMedChem* **2008**, *3* (1), 74–78. https://doi.org/10.1002/cmdc.200700214.

(146) Tai, W.-Y.; Zhang, R.-T.; Ma, Y.-M.; Gu, M.; Liu, G.; Li, J.; Nan, F.-J. Design, Synthesis, and Biological Evaluation of Ring-Opened Bengamide Analogues. *ChemMedChem* **2011**, *6* (9), 1555–1558. https://doi.org/10.1002/cmdc.201100164.

(147) Liu, Q. J.; Li, H.; Chen, S. P.; Zhou, G. C. Synthesis of (3S,4R)-Bengamide E. *Chinese Chemical Letters* **2011**, *22* (5), 505–507. https://doi.org/10.1016/j.cclet.2010.11.023.

(148) Sarabia, F.; Martín-Gálvez, F.; García-Ruiz, C.; Sánchez-Ruiz, A.; Vivar-García, C. *Epi* -, Epoxy-, and C2-Modified Bengamides: Synthesis and Biological Evaluation. *J Org Chem* **2013**, *78* (11), 5239–5253. https://doi.org/10.1021/jo4003272.

(149) Martín-Gálvez, F.; García-Ruiz, C.; Sánchez-Ruiz, A.; Valeriote, F. A.; Sarabia, F. An Array of Bengamide E Analogues Modified at the Terminal Olefinic Position: Synthesis and Antitumor Properties. *ChemMedChem* **2013**, *8* (5), 819–831. https://doi.org/10.1002/cmdc.201300033.

(150) Nicolaou, K. C.; Bulger, P. G.; Sarlah, D. Palladium-Catalyzed Cross-Coupling Reactions in Total Synthesis. *Angewandte*

Chemie International Edition **2005**, *44* (29), 4442–4489. https://doi.org/10.1002/anie.200500368.

(151) Sonogashira, K.; Tohda, Y.; Hagihara, N. A Convenient Synthesis of Acetylenes: Catalytic Substitutions of Acetylenic Hydrogen with Bromoalkenes, Iodoarenes and Bromopyridines. *Tetrahedron Lett* **1975**, *16* (50), 4467–4470. https://doi.org/10.1016/S0040-4039(00)91094-3.

(152) Zeng, X.; Hu, Q.; Qian, M.; Negishi, E. Clean Inversion of Configuration in the Pd-Catalyzed Cross-Coupling of 2-Bromo-1,3-Dienes. *J Am Chem Soc* **2003**, *125* (45), 13636–13637. https://doi.org/10.1021/ja0304392.

(153) Phi, T. D.; Doan Thi Mai, H.; Tran, V. H.; Truong, B. N.; Tran, T. A.; Vu, V. L.; Chau, V. M.; Pham, V. C. Design, Synthesis and Cytotoxicity of Bengamide Analogues and Their Epimers. *Medchemcomm* **2017**, *8* (2), 445–451. https://doi.org/10.1039/C6MD00587J.

(154) Phi, T. D.; Mai, H. D. T.; Tran, V. H.; Vu, V. L.; Truong, B. N.; Tran, T. A.; Chau, V. M.; Pham, V. C. Synthesis of Bengamide E Analogues and Their Cytotoxic Activity. *Tetrahedron Lett* **2017**, *58* (19), 1830–1833. https://doi.org/10.1016/j.tetlet.2017.03.077.

(155) Kong, X.; Wei, B.; Yu, C.; Guan, X.; Ma, W.; Liu, G.; Yang, C.; Nan, F. Design, Synthesis and Biological Evaluation of Bengamide Analogues as <scp>ClpP</Scp> Activators. *Chin J Chem* **2020**, *38* (10), 1111–1115. https://doi.org/10.1002/cjoc.202000133.

(156) Zhang, J.; Ye, F.; Lan, L.; Jiang, H.; Luo, C.; Yang, C.-G. Structural Switching of Staphylococcus Aureus Clp Protease. *Journal of Biological Chemistry* **2011**, *286* (43), 37590–37601. https://doi.org/10.1074/jbc.M111.277848.

(157) Yu, C.; Wei, B.; Kong, X.; Yang, C.; Nan, F. Synthesis and <scp>Structure-Activity</Scp> Relationships of <scp>Ring-Opened</Scp> Bengamide Analogues against <scp>Methicillin-Resistant</Scp> *Staphylococcus Aureus* †. *Chin J Chem* **2021**, *39* (3), 671–676. https://doi.org/10.1002/cjoc.202000502.

(158) Wang, Z. *Comprehensive Organic Name Reactions and Reagents*; Wiley, 2010. https://doi.org/10.1002/9780470638859.

(159) Alam, S.; Dhimane, H. A Concise Synthesis of Bengamide E and Analogues via E-Selective Cross-Metathesis Olefination. *Synlett* **2010**, *2010* (19), 2923–2927. https://doi.org/10.1055/s-0030-1259015.

(160) García-Pinel, B.; Porras-Alcalá, C.; Cabeza, L.; Ortiz, R.; Prados, J.; Melguizo, C.; Cheng-Sánchez, I.; López-Romero, J. M.; Sarabia, F. Bengamide Analogues Show a Potent Antitumor Activity against Colon Cancer Cells: A Preliminary Study. *Mar Drugs* **2020**, *18* (5). https://doi.org/10.3390/md18050240.

(161) Mukai, C.; Moharram, S. M.; Kataoka, O.; Hanaoka, M. Highly Stereocontrolled Total Synthesis of (+)-Bengamide E. *J Chem Soc Perkin 1* **1995**, No. 22, 2849. https://doi.org/10.1039/p19950002849.

(162) Mancuso, A. J.; Huang, S.-L.; Swern, D. Oxidation of Long-Chain and Related Alcohols to Carbonyls by Dimethyl Sulfoxide "Activated" by Oxalyl Chloride. *J Org Chem* **1978**, *43* (12), 2480–2482. https://doi.org/10.1021/jo00406a041.

(163) Nicolaou, K. C.; Härter, M. W.; Gunzner, J. L.; Nadin, A. The Wittig and Related Reactions in Natural Product Synthesis. *Liebigs Annalen* **1997**, *1997* (7), 1283–1301. https://doi.org/10.1002/jlac.199719970704.

(164) Chen, J.; Marx, J. N. A Stereoselective Total Synthesis of (−)-Rishitin. *Tetrahedron Lett* **1997**, *38* (11), 1889–1892. https://doi.org/10.1016/S0040-4039(97)00228-1.

(165) Harcken, C.; Martin, S. F. Improved E-Selectivity in the Wittig Reaction of Stabilized Ylides with r-Alkoxyaldehydes and Sugar Lactols. **2001**. https://doi.org/10.1021/ol016729.

(166) Katsuki, T.; Sharpless, K. B. The First Practical Method for Asymmetric Epoxidation. *J Am Chem Soc* **1980**, *102* (18), 5974–5976. https://doi.org/10.1021/ja00538a077.

(167) Cheng-Sánchez, I.; Sarabia, F. Recent Advances in Total Synthesis via Metathesis Reactions. *Synthesis (Stuttg)* **2018**, *50* (19), 3749–3786. https://doi.org/10.1055/s-0037-1610206.

(168) Nicolaou, K. C.; Bulger, P. G.; Sarlah, D. Metathesis Reactions in Total Synthesis. *Angewandte Chemie International Edition* **2005**, *44* (29), 4490–4527. https://doi.org/10.1002/anie.200500369.

(169) Epp, J. B.; Widlanski, T. S. Facile Preparation of Nucleoside-5'-Carboxylic Acids. *J Org Chem* **1999**, *64* (1), 293–295. https://doi.org/10.1021/jo981316g.

(170) Ortigosa-Palomo, A.; Porras-Alcalá, C.; Quiñonero, F.; Moya-Utrera, F.; Ortiz, R.; López-Romero, J. M.; Melguizo, C.; Sarabia, F.; Prados, J. Antitumor Activity of Bengamide Ii in a Panel of Human and Murine Tumor Cell Lines: In Vitro and in Vivo Determination of Effectiveness against Lung Cancer. *Biomedicine & Pharmacotherapy* **2023**, *168*, 115789. https://doi.org/10.1016/j.biopha.2023.115789.

(171) Sarabia, F.; Chammaa, S.; García-Ruiz, C. Solid Phase Synthesis of Globomycin and SF-1902 A $_5$. *J Org Chem* **2011**, *76* (7), 2132–2144. https://doi.org/10.1021/jo1025145.

(172) Tannert, R.; Milroy, L.-G.; Ellinger, B.; Hu, T.-S.; Arndt, H.-D.; Waldmann, H. Synthesis and Structure−Activity Correlation of Natural-Product Inspired Cyclodepsipeptides Stabilizing F-Actin. *J Am Chem Soc* **2010**, *132* (9), 3063–3077. https://doi.org/10.1021/ja9095126.

(173) Bionda, N.; Stawikowski, M.; Stawikowska, R.; Cudic, M.; López-Vallejo, F.; Treitl, D.; Medina-Franco, J.; Cudic, P. Effects of Cyclic Lipodepsipeptide Structural Modulation on Stability, Antibacterial Activity, and Human Cell Toxicity. *ChemMedChem* **2012**, *7* (5), 871–882. https://doi.org/10.1002/cmdc.201200016.

(174) Rubio-Retama, J.; Zafeiropoulos, N. E.; Serafinelli, C.; Rojas-Reyna, R.; Voit, B.; Lopez Cabarcos, E.; Stamm, M. Synthesis and Characterization of Thermosensitive PNIPAM Microgels Covered with Superparamagnetic γ-Fe $_2$ O $_3$ Nanoparticles. *Langmuir* **2007**, *23* (20), 10280–10285. https://doi.org/10.1021/la7009594.

(175) Pelton, R. H.; Chibante, P. Preparation of Aqueous Latices with N-Isopropylacrylamide. *Colloids and Surfaces* **1986**, *20* (3), 247–256. https://doi.org/10.1016/0166-6622(86)80274-8.

(176) Jańczewski, D.; Tomczak, N.; Han, M.-Y.; Vancso, G. J. Stimulus Responsive PNIPAM/QD Hybrid Microspheres by Copolymerization with Surface Engineered QDs. *Macromolecules* **2009**, *42* (6), 1801–1804. https://doi.org/10.1021/ma802521a.

(177) Tzounis, L.; Doña, M.; Lopez-Romero, J. M.; Fery, A.; Contreras-Caceres, R. Temperature-Controlled Catalysis by Core–Shell–Satellite AuAg@pNIPAM@Ag Hybrid Microgels: A Highly Efficient Catalytic Thermoresponsive Nanoreactor. *ACS Appl Mater Interfaces* **2019**, *11* (32), 29360–29372. https://doi.org/10.1021/acsami.9b10773.

(178) Doña, M.; Ortega-Rodriguez, A.; Alarcón-Fernández, C.; López-Romero, J. M.; Contreras-Cáceres, R. Effect of the Cross-Linking

Density on the Gold Core Oxidation in Hybrid Core@shell Au@pNIPAM and Janus Au@p4VP Systems. *Colloids Surf A Physicochem Eng Asp* **2020**, *584*, 124014. https://doi.org/10.1016/j.colsurfa.2019.124014.

(179) Rejinold, N. S.; Baby, T.; Chennazhi, K. P.; Jayakumar, R. Dual Drug Encapsulated Thermo-Sensitive Fibrinogen-Graft-Poly (N-Isopropyl Acrylamide) Nanogels for Breast Cancer Therapy. *Colloids Surf B Biointerfaces* **2014**, *114*, 209–217. https://doi.org/10.1016/j.colsurfb.2013.10.015.

(180) Blanco, M. D.; Guerrero, S.; Benito, M.; Fernández, A.; Teijón, C.; Olmo, R.; Katime, I.; Teijón, J. M. In Vitro and In Vivo Evaluation of a Folate-Targeted Copolymeric Submicrohydrogel Based on N-Isopropylacrylamide as 5-Fluorouracil Delivery System. *Polymers (Basel)* **2011**, *3* (3), 1107–1125. https://doi.org/10.3390/polym3031107.

(181) Peng, J.; Qi, T.; Liao, J.; Chu, B.; Yang, Q.; Li, W.; Qu, Y.; Luo, F.; Qian, Z. Controlled Release of Cisplatin from PH-Thermal Dual Responsive Nanogels. *Biomaterials* **2013**, *34* (34), 8726–8740. https://doi.org/10.1016/j.biomaterials.2013.07.092.

(182) Patil, A. S.; Gadad, A. P.; Hiremath, R. D.; Joshi, S. D. Biocompatible Tumor Micro-Environment Responsive CS-g-PNIPAAm Co-Polymeric Nanoparticles for Targeted Oxaliplatin Delivery. *Journal of Polymer Research* **2018**, *25* (3), 77. https://doi.org/10.1007/s10965-018-1453-2.

(183) Patil, A. S.; Gadad, A. P. Development and Evaluation of High Oxaliplatin Loaded CS-g-PNIPAAm Co-Polymeric Nanoparticles for Thermo and PH Responsive Delivery. *Indian Journal of Pharmaceutical Education and Research* **2018**, *52* (1), 62–70. https://doi.org/10.5530/ijper.52.1.7.

(184) Jun, Y.; Choi, J.; Cheon, J. Heterostructured Magnetic Nanoparticles: Their Versatility and High Performance Capabilities. *Chem. Commun.* **2007**, No. 12, 1203–1214. https://doi.org/10.1039/B614735F.

(185) Kittel, C. Theory of the Structure of Ferromagnetic Domains in Films and Small Particles. *Physical Review* **1946**, *70* (11–12), 965–971. https://doi.org/10.1103/PhysRev.70.965.

(186) Garcia-Pinel, B.; Ortega-Rodríguez, A.; Porras-Alcalá, C.; Cabeza, L.; Contreras-Cáceres, R.; Ortiz, R.; Díaz, A.; Moscoso, A.; Sarabia, F.; Prados, J.; López-Romero, J. M.; Melguizo, C. Magnetically Active PNIPAM Nanosystems as Temperature-Sensitive Biocompatible Structures for Controlled Drug Delivery. *Artif Cells Nanomed Biotechnol* **2020**, *48* (1), 1022–1035. https://doi.org/10.1080/21691401.2020.1773488.

(187) Kim, H.; Jo, A.; Baek, S.; Lim, D.; Park, S.-Y.; Cho, S. K.; Chung, J. W.; Yoon, J. Synergistically Enhanced Selective Intracellular Uptake of Anticancer Drug Carrier Comprising Folic Acid-Conjugated Hydrogels Containing Magnetite Nanoparticles. *Sci Rep* **2017**, *7* (1), 41090. https://doi.org/10.1038/srep41090.

(188) Shen, B.; Ma, Y.; Yu, S.; Ji, C. Smart Multifunctional Magnetic Nanoparticle-Based Drug Delivery System for Cancer Thermo-Chemotherapy and Intracellular Imaging. *ACS Appl Mater Interfaces* **2016**, *8* (37), 24502–24508. https://doi.org/10.1021/acsami.6b09772.

(189) Zhang, Q.; Yang, Y.; Yan, H.; Liu, J. Deformable Bi-Compartmental Particles and Their Application in Controlling Electric Conductivity. *Mater Adv* **2022**, *3* (20), 7508–7512. https://doi.org/10.1039/D2MA00837H.

(190) Faraji, A. H.; Wipf, P. Nanoparticles in Cellular Drug Delivery. *Bioorg Med Chem* **2009**, *17* (8), 2950–2962. https://doi.org/10.1016/j.bmc.2009.02.043.

(191) de Barros, A.; Tsourkas, A.; Saboury, B.; Cardoso, V.; Alavi, A. Emerging Role of Radiolabeled Nanoparticles as an Effective Diagnostic Technique. *EJNMMI Res* **2012**, *2* (1), 39. https://doi.org/10.1186/2191-219X-2-39.

(192) Elias, D. R.; Poloukhtine, A.; Popik, V.; Tsourkas, A. Effect of Ligand Density, Receptor Density, and Nanoparticle Size on Cell Targeting. *Nanomedicine* **2013**, *9* (2), 194–201. https://doi.org/10.1016/j.nano.2012.05.015.

(193) Peretz, V.; Motiei, M.; Sukenik, C. N.; Popovtzer, R. The Effect of Nanoparticle Size on Cellular Binding Probability. *J At Mol Opt Phys* **2012**, *2012*, 1–7. https://doi.org/10.1155/2012/404536.

(194) Huang, J.; Bu, L.; Xie, J.; Chen, K.; Cheng, Z.; Li, X.; Chen, X. Effects of Nanoparticle Size on Cellular Uptake and Liver MRI with Polyvinylpyrrolidone-Coated Iron Oxide Nanoparticles. *ACS Nano* **2010**, *4* (12), 7151–7160. https://doi.org/10.1021/nn101643u.

(195) Albanese, A.; Tang, P. S.; Chan, W. C. W. The Effect of Nanoparticle Size, Shape, and Surface Chemistry on Biological Systems. *Annu Rev Biomed Eng* **2012**, *14* (1), 1–16. https://doi.org/10.1146/annurev-bioeng-071811-150124.

(196) Hoshyar, N.; Gray, S.; Han, H.; Bao, G. The Effect of Nanoparticle Size on *in Vivo* Pharmacokinetics and Cellular Interaction. *Nanomedicine* **2016**, *11* (6), 673–692. https://doi.org/10.2217/nnm.16.5.

(197) Moghimi, S. M.; Hunter, A. C.; Andresen, T. L. Factors Controlling Nanoparticle Pharmacokinetics: An Integrated Analysis and Perspective. *Annu Rev Pharmacol Toxicol* **2012**, *52* (1), 481–503. https://doi.org/10.1146/annurev-pharmtox-010611-134623.

(198) Laurenti, M.; Guardia, P.; Contreras-Cáceres, R.; Pérez-Juste, J.; Fernandez-Barbero, A.; Lopez-Cabarcos, E.; Rubio-Retama, J. Synthesis of Thermosensitive Microgels with a Tunable Magnetic Core. *Langmuir* **2011**, *27* (17), 10484–10491. https://doi.org/10.1021/la201723a.

(199) Contreras-Cáceres, R.; Abalde-Cela, S.; Guardia-Girós, P.; Fernández-Barbero, A.; Pérez-Juste, J.; Alvarez-Puebla, R. A.; Liz-Marzán, L. M. Multifunctional Microgel Magnetic/Optical Traps for SERS Ultradetection. *Langmuir* **2011**, *27* (8), 4520–4525. https://doi.org/10.1021/la200266e.

(200) Wu, W.; He, Q.; Jiang, C. Magnetic Iron Oxide Nanoparticles: Synthesis and Surface Functionalization Strategies. *Nanoscale Res Lett* **2008**, *3* (11), 397. https://doi.org/10.1007/s11671-008-9174-9.

(201) Vikesland, P. J.; Rebodos, R. L.; Bottero, J. Y.; Rose, J.; Masion, A. Aggregation and Sedimentation of Magnetite Nanoparticle Clusters. *Environ Sci Nano* **2016**, *3* (3), 567–577. https://doi.org/10.1039/C5EN00155B.

(202) Zhang, N.; Yin, Y.; Xu, S.-J.; Chen, W.-S. 5-Fluorouracil: Mechanisms of Resistance and Reversal Strategies. *Molecules* **2008**, *13* (8), 1551–1569. https://doi.org/10.3390/molecules13081551.

(203) Apetoh, L.; Ghiringhelli, F. Enhancing the Anticancer Effects of 5-Fluorouracil: Current Challenges and Future Perspectives. *Biomed J* **2015**, *38* (2), 111. https://doi.org/10.4103/2319-4170.130923.

(204) Griffith, K. A.; Zhu, S.; Johantgen, M.; Kessler, M. D.; Renn, C.; Beutler, A. S.; Kanwar, R.; Ambulos, N.; Cavaletti, G.; Bruna, J.; Briani, C.; Argyriou, A. A.; Kalofonos, H. P.; Yerges-Armstrong, L. M.; Dorsey, S. G. Oxaliplatin-Induced Peripheral Neuropathy and Identification of Unique Severity Groups in Colorectal Cancer. *J Pain Symptom Manage* **2017**, *54* (5), 701-706.e1. https://doi.org/10.1016/j.jpainsymman.2017.07.033.

(205) CASALE, F. Plasma Concentrations of 5-Fluorouracil and Its Metabolites in Colon Cancer Patients. *Pharmacol Res* **2004**, *50* (2), 173–179. https://doi.org/10.1016/j.phrs.2004.01.006.

(206) Fortes, C.; García-Vilas, J. A.; Quesada, A. R.; Medina, M. Á. Evaluation of the Anti-Angiogenic Potential of Hydroxytyrosol and Tyrosol, Two Bio-Active Phenolic Compounds of Extra Virgin Olive Oil, in Endothelial Cell Cultures. *Food Chem* **2012**, *134* (1), 134–140. https://doi.org/10.1016/j.foodchem.2012.02.079.

(207) López-Jiménez, A.; Gallardo, E.; Espartero, J. L.; Madrona, A.; Quesada, A. R.; Medina, M. Á. Comparison of the Anti-Angiogenic Potential of Hydroxytyrosol and Five Derivatives. *Food Funct* **2018**, *9* (8), 4310–4316. https://doi.org/10.1039/C8FO01140K.

(208) Marrero, A. D.; Castilla, L.; Espartero, J. L.; Madrona, A.; R. Quesada, A.; Medina, M. Á.; Martínez-Poveda, B. A Comparative Study of the Antiangiogenic Activity of Hydroxytyrosyl Alkyl Ethers. *Food Chem* **2020**, *333*, 127476. https://doi.org/10.1016/j.foodchem.2020.127476.

(209) Winikoff, S. E.; Zeh, H. J.; DeMarco, R.; Lotze, M. T. Cytolytic Assays. In *Measuring Immunity*; Elsevier, 2005; pp 343–349. https://doi.org/10.1016/B978-012455900-4/50291-9.